

Evaluating Groundwater Inflow and Nutrient Transport to Texas Coastal Embayments

Final Report

GLO Contract No. 14-081-000-7949
August 2015

Prepared by:
Dorina Murgulet, Principal Investigator

and

Michael S. Wetz, Co-Principal Investigator
Audrey Douglas, Graduate Research Assistant
William McBee, Graduate Research Assistant
Nicholas Spalt, Graduate Research Assistant
Karen Linares, Undergraduate Research Assistant

Texas A&M University-Corpus Christi
6300 Ocean Dr., Unit 5850
Corpus Christi, Texas 78412
Phone: 361-825-2309
Email: Dorina.murgulet@tamucc.edu

Submitted to:
Texas General Land Office
1700 Congress Ave.
Austin, TX 78701-1495

A report submitted to the Texas Land Commissioner pursuant to National Oceanic and Atmospheric Administration Award No. NA13NOS4190113



Contents

EXECUTIVE SUMMARY	4
INTRODUCTION.....	6
Background Information.....	6
Study area	9
Physiographic Aspects.....	9
Soils	12
Hydrogeology	12
METHODS.....	13
Sampling Design	13
Resistivity Imaging.....	16
Data collection	16
Salinity Mass Balance and Submarine Groundwater Discharge Flux Calculations.....	18
Radiogenic Isotopes.....	20
Sampling and lab measurements.....	20
Submarine groundwater flux calculations	21
Residence time of water mass	22
Major Ions and Stable Isotope Sampling.....	23
Nutrient and Chlorophyll-α Sampling	24
Statistical Analyses	25
RESULTS AND DISCUSSION	27
Continuous Resistivity Profiles	27
Time-Lapse Resistivity Profiling and Resistivity-Derived SGD rates	28
Radiogenic Isotope Concentrations.....	32
Radon-derived SGD rates	34
Major Ion and Stable Isotopes	37
Major Ions	37
Stable Isotopes	41

Spatial-temporal Distribution of Phytoplankton and Nutrients.....	44
Organic Matter Distributions.....	47
Nutrient Fluxes	48
Spatial and Temporal Extent of Hypoxia	49
Seasonal Trend Analyses Using SAS	50
SUMMARY.....	54
REFERENCES.....	58
TABLE LEGEND.....	64
FIGURE LEGEND	66
APPENDIX LEGEND	103

EXECUTIVE SUMMARY

Submarine groundwater discharge (SGD) has been recognized as an important component of the hydrologic and biogeochemical systems that link terrestrial waters to marine environments. A key aspect of this study was to better understand potential sources of nutrients that fuel phytoplankton growth in southeastern Corpus Christi Bay and the upper Laguna Madre, as well as potential sources of organic matter fueling hypoxia in southeastern Corpus Christi Bay. This study indicates that SGD may have a large impact on biogeochemical cycles of the Corpus Christi Bay system, including Upper Laguna Madre. Nutrient, major ion, stable and radiogenic isotopes and electrical resistivity (ER) measurements were acquired between January (winter) to December (late fall), 2014 at twenty-nine stations throughout the Corpus Christi bay and Upper Laguna Madre. SGD rates were monitored during summer and fall 2014 at three locations selected based on preliminary observations. Average groundwater fluxes, measured using time-lapse ER measurements and continuous Radon-222, ranged from 1.1 to 5.7 m³/m.d in summer and from 1.5 to 9.7 m³/m.d in fall. Average concentrations of nutrients in porewater samples collected were as follows: 1,549.3 µmol/L dissolved organic carbon (DOC), 325.5 µmol/L total dissolved nitrogen (TDN), 761.1 µmol/L ammonium (NH(4)), 0.15 µmol/L nitrate + nitrite (N+N as N), 0.6 µmol/L nitrite (NO(2)), 19.89 µmol/L orthophosphate (PO(4)), and 335.8 µmol/L silica in summer; and 3778 µmol/L dissolved organic carbon (DOC), 2345.2 µmol/L total dissolved nitrogen (TDN), 1716.6 µmol/L ammonium (NH(4)), 0.15 µmol/L nitrate + nitrite (N+N as N), 0.57 µmol/L nitrite (NO(2)), 34.71 µmol/L orthophosphate (PO(4)), and 566.42 µmol/L silica in fall. Levels of NH(4), DOC, and silica were significantly higher in samples from SGD sites than in seawater. Measured SGD rates and nutrient concentrations were used to calculate nutrient loads discharged into the study area. The estimates suggest that SGD delivers a

dissolved inorganic nitrogen (DIN) load of 1.326 moles (M)/day, 5.5 M/day of DOC, 1.329 M/day TDN, 1.4 m/day silicate, and a 0.09 M/day load of PO(4) per meter of bottom sediment into the Bay of Corpus Christi during summer. By late fall the estimated nutrient loads increase by an order of magnitude and are as follows: (DIN) load of 16.22 mol/day, 32.48 mol/day of DOC, 22.02 mol/day TDN, 5.03 mol/day silicate, and a 0.3 mol/day load of PO(4) per meter of bottom sediment. The identified potential SGD sites correlate well with the location of the hypoxia occurrence in the Corpus Christi Bay. Thus, it is likely that the influence of porewaters on water column nutrient concentrations and microbial respiration, although patchy, is significant in these systems under the environmental conditions in which our sampling regime took place. Because the ER and stable and radiogenic isotopes show high hydrogeologic and hydrologic “heterogeneity” in the investigated systems, further investigations are necessary to better characterize the system to project input loads to the entire Corpus Christi Bay system. This research shows that the Upper Laguna Madre is significantly influenced by groundwater discharge which could potentially trigger the brown tide outbreaks.

INTRODUCTION

Background Information

Corpus Christi Bay and the Laguna Madre, located on the South Texas Gulf coast, provide essential nursery habitat for numerous commercially and recreationally important fish and shellfish species, marine mammals, reptiles, resident birds, shorebirds, and other avian species. There is emerging concern that the ecological health of these vital habitats are threatened by water quality degradation, specifically pertaining to hypoxia formation ($O_2 < 2 \text{ mg- l}$ that are detrimental to aquatic organisms; Corpus Christi Bay), red tide (Corpus Christi Bay & Laguna Madre) and brown tide (Laguna Madre) outbreaks. Given the rapidly expanding human populations and land use change in south Texas coastal regions, it is likely that nutrient and organic matter loading from both point and non-point sources play a role in this water quality degradation. These symptoms tend to occur during summer through fall, a time of year when surface freshwater inflows (i.e., riverine) are at annual lows, hinting at the importance of non-riverine sources of nutrients and organic matter.

Submarine groundwater discharge (SGD) and coastal groundwater discharge are important components of the hydrologic and biogeochemical systems that link terrestrial waters to marine environments (Moore, 1996; Burnett et al., 2003; Cardenas et al., 2010). Submarine groundwater discharge enables the flow and transport of fluids and solutes from terrestrial groundwater sources into offshore coastal embayments (i.e. bays, estuaries, oceans, etc.) whereby coastal groundwater discharge occurs from offshore to inland environments (i.e. wetlands, marshes, etc.). Coastal groundwater discharge (CGD) and saltwater intrusion are similar in their definition and mechanisms of fluid transport; however, CGD assumes that saline groundwater from seawater intrusion will eventually discharge into adjacent surface waters depending upon the

hydrogeologic conditions. Bays and estuaries rely on a specific range of salinity and nutrient levels to maintain optimal productivity and ecosystem services (Palmer et al., 2011). Inflows from riverine and groundwater resources to estuaries are the dominant source of freshwater inflows that can affect coastal ecosystem structure indirectly by changing salinity regimes, hydrology, and transport of nutrients and contaminants. Groundwater, which can accumulate exceptionally high concentrations of nutrients and organic matter, has been shown to contribute to water quality degradation in many coastal systems worldwide (Church, 1996). Organic matter-contaminated groundwater discharging to the bays may fuel bacterial respiration, leading to hypoxia formation. It has also been demonstrated that nutrient-contaminated groundwater can fuel growth of phytoplankton and algae in coastal systems. Given the arid nature of south Texas, it is conceivable that groundwater represents a significant source of freshwater, nutrients and organic matter and plays a major role in ecosystem health. However, groundwater contribution is entirely unknown for this area as well as for most of the Texas coastal zone.

Commonly, analyses of groundwater discharge to surface water has been conducted using elemental and isotopic geochemistry (Moore, 1996; Grossman et al., 2002; Burnett et al., 2003; Cable et al., 2004; Ni et al., 2011; Dimova et al., 2013) as well as density-dependent flow and transport simulation codes (Guo and Langevin, 2002; Murgulet and Tick, 2015). Statistical methods such as analysis of variance (ANOVA), multivariate linear regression (MLR) and Factor analysis on environmental data have also produced valuable models that aid in identifying variations in water quality and contamination sources in various hydrologic systems (Morell et al., 1996; Voudouris et al., 2000; Morehead et al., 2008; Palmer et al., 2011; Thareja et al., 2011; Hae-Cheol and Montagna, 2012; Khan and Kumar, 2012). Recently, subsurface imaging techniques such as direct current electrical resistivity (ER) surveys have been increasingly used

to delineate and quantify groundwater flow paths and discharge rates into surface water bodies (White, 1988; Greenwood et al., 2006; Green et al, 2008; Nyquist et al, 2008; Cardenas et al., 2010; Dimova et al., 2012). Consecutive/continuous ER images acquired along the same survey lines over time periods of hours or during different environmental conditions are used to locate potential groundwater discharge seepage faces and estimate changes in discharge rates over time (Nyquist et al., 2008; Dimova et al., 2012; Johnson et al., 2012).

In south Texas, severe drought conditions caused depletion of freshwater inflows from riverine sources leading to increased salinity contents in surface waters (Schmidt and Garland, 2012). Most studies in south Texas show that impaired waterways are the result of high levels of bacteria or other microbes, dissolved oxygen (DO) depletion, and increasing salinity levels (Montagna and Ritter, 2006; Palmer et al., 2011). Reoccurring formations of hypoxia have cyclically surfaced during the late spring through the fall months in Corpus Christi Bay (Nelson & Montagna, 2009). Various coastal systems around the world have experienced and recorded water quality degradation due to nutrient loading from groundwater that can fuel phytoplankton growth as well as bacterial respiration aiding in hypoxic episodes (Church, 1996). Although monitoring efforts have been extensive, limited efforts were directed towards identifying the quality and quantity of freshwater inputs to Texas coastal embayments. Recent efforts to regulate freshwater inflows for optimal salinity ranges to promote ecosystem health of bays and estuaries along the Texas Gulf Coast do not include groundwater inputs (Alexander and Dunton, 2006; Kim and Montagna, 2012). This study shows that groundwater may have a significant role in delivering nutrients to estuaries in south Texas therefore requiring the incorporation of groundwater inflows for proper evaluation of freshwater and nutrient budgets. Corpus Christi Bay's water column and sediments have been extensively monitored and sampled but little data

has been collected in regards to groundwater contributions. Corpus Christi Bay plays an important role both environmentally and economically to the surrounding area, and despite the importance of groundwater discharge to the nutrient budget and overall vitality of the surrounding coastal waters, this hydrologic cycle component has been overlooked for decades.

The main objectives of this study are to improve understanding of groundwater contributions to water quality and habitat degradation in relevant embayments of the South Texas coast. Objectives are: 1) map groundwater discharge and groundwater-surface water interaction zones, 2) quantify the spatial-temporal distribution of groundwater contaminant (nutrients, organic matter) transport and discharge, 3) evaluate the role of groundwater nutrients in system-wide nutrient budgets (i.e., inputs-outputs), and 4) evaluate hypoxia and phytoplankton (red & brown tide) trends in relation to groundwater flow and nutrient discharge. To fulfill these objectives, we have quantified groundwater discharge on a seasonal basis to South Texas embayments and have evaluated the potential groundwater contaminants that may contribute to water quality degradation. The resulting data products will be used for the development of decision support products and educational materials that will better equip resource managers and other end users to analyze, detect, and identify potential threats to freshwater resources (e.g., groundwater) and the health of environmentally sensitive ecosystems such as those of Corpus Christi Bay and Laguna Madre.

Study area

Physiographic Aspects

Study area, located in south Texas, includes the south side of Corpus Christi Bay and the upper portion of upper Laguna Madre (Figure 1) which are predominantly shielded from the Gulf of Mexico by North Padre Island. The surface area of Corpus Christi Bay is roughly 445 km² and

represents approximately 7.1% of the overall Texas estuary network (USEPA, 1999). Corpus Christi Bay is a shallow (~3.2 m; Orlando et al. 1991), almost enclosed bay with a level bottom (Montagna and Kalke 1992; Martin and Montagna 1995; Ritter and Montagna 1999) and a total open water surface area of 432.9 km². Given the microtidal (small tidal range) characteristic, this bay is sensitive to meteorological forcing such as temperature, precipitation and wind. Average monthly wind speeds range from 17 km/h to 28 km/h. Two principle wind regimes dominate the Corpus Christi Bay: persistent, southeasterly winds from March through September and north-northeasterly winds from October through March (Behrens and Watson 1973; Brown et al. 1976). Corpus Christi Bay is connected with several bodies of water including Oso Bay, Nueces Bay, Aransas Bay and the Gulf of Mexico due to dredged ship channels and canals and natural hydrological process. These secondary bays and the Gulf provide the system with fresh and saline water as well as an influx of nutrients; however, Oso Bay is assumed to be the primary nutrient input into Corpus Christi Bay because of the large discharges from municipal wastewater treatment plants. The mean depth of Corpus Christi Bay is 2.4 m whereas the Upper Laguna Madre the mean depth is 1.2 m. Prevailing southeastern winds drive the shallow waters, resulting in a generally well-mixed water column during the fall and winter and a more stratified water column during the late-spring and summer months.

A key aspect of this study was to better understand potential sources of nutrients that fuel phytoplankton growth in southeastern Corpus Christi Bay and the upper Laguna Madre, as well as potential sources of organic matter fueling hypoxia in southeastern Corpus Christi Bay. Corpus Christi Bay receives freshwater inflow from the Nueces River via Nueces Bay as well as episodic flows of wastewater out of Oso Bay (Longley 1994; Wetz unpubl. data). However, due to relatively low precipitation in the watershed as well as dams on the Nueces River, riverine

discharge into Nueces-Corpus Christi Bay is typically minimal and thus salinities are high on average, while nutrient levels are often very low (Longley, 1994). Consequently, phytoplankton biomass is typically low and frequently nutrient-limited (Longley, 1994). Nonetheless, episodic phytoplankton blooms, including of harmful algal bloom species, are known to occur in Corpus Christi Bay (e.g., Buskey 1996; Texas Parks & Wildlife unpubl. reports). Furthermore, the upper Laguna Madre has been afflicted by persistent “brown tide” blooms since the early 1990’s, yet the sources of nutrients that trigger and maintain these blooms is largely unknown.

In addition to experiencing episodic algal blooms, the southeastern portion of Corpus Christi Bay adjacent to both Oso Bay and the upper Laguna Madre has been shown to experience episodic hypoxia from spring-fall (Ritter and Montagna 1999), causing negative effects on benthic communities (Montagna and Ritter 2006; Montagna and Froeschke 2009). To date, no studies have identified the source(s) of organic matter fueling hypoxia in Corpus Christi Bay. Wetz et al. (in review) suggest that export of wastewater-influenced organic matter out of Oso Bay is likely to be an important mechanism for hypoxic formation, but this export only occurs episodically. Thus other sources of organic matter may be important as well. In this study, we report on the spatial-temporal (seasonal) distribution of key water quality parameters relevant to phytoplankton growth as well as hypoxia formation.

Previous studies in the area (TWDB, 2003; Breier et al., 2010; Nyquist et al, 2008; USDA, 2012) as well as the hydraulic conditions indicate that groundwater flows toward the coast, eventually discharging into the bays and estuaries (Figure 1). Annual mean precipitation and evaporation rates are on average 74 cm/yr (78.1 cm for 2014) and 90 to 115 cm/yr, respectively. However, evaporation rates can be as high as 150 cm/yr during drought periods when the net annual moisture loss is around 31 cm/yr

<http://www.twdb.texas.gov/surfacewater/conditions/evaporation/>). Tropical storms and hurricanes from the Gulf of Mexico may deliver larger quantities of rainfall during late summer and early fall on an irregular basis (Armstrong, 1987). The regions semi-arid climate on these shallow waters manifests not only through reduced freshwater inflows but also increased salinity levels within the bay and estuary system caused by high evaporation rates and salt evapo-concentration (Bighash and Murgulet, 2015).

Soils

Nueces County is comprised of eight unique soil compositions, three of which come into contact with Corpus Christi Bay and the Upper Laguna Madre: Victoria Association, Orelia-Banquete Association, and Galveston-Mustang Tidal Flats Association (Figure 2) (USDA, 1992). The Victoria Association soils are dark-gray, calcareous heavy clays with slow infiltration rates. The Orelia-Banquete soils are comprised mostly of a thin sandy surface layer overlaying a large clay layer, with slow infiltration rates. In contrast, the Galveston-Mustang Tidal Flats soils form a surface layer of light-gray fine sand with small amounts of humus with subsoil composed of light-grey fine grain sand commonly saturated with water (USDA, 1992). The Galveston soils are in contact with majority of Corpus Christi bay and the Upper Laguna Madre but are generally imbedded within large Beaumont clay formations (see section on hydrogeology). The fine-grained sands of the Galveston soils could potentially act as legitimate conduits for shallow groundwater discharge to Corpus Christi Bay and the Upper Laguna Madre.

Hydrogeology

The Gulf Coast Aquifer is a leaky artesian aquifer comprised of a complex of clays, silts, sands, and gravels (Ashworth and Hopkins, 1995) that form the Chicot, Evangeline, and Jasper aquifers (Waterstone et al., 2003). Corpus Christi Bay and the surrounding systems are generally in

direct contact with the Chicot aquifer, which is the shallowest of the mentioned aquifers. The stratigraphic units of the Chicot aquifer consist of an overlying alluvial formation preceded by Beaumont and Lissie formations ([Ashworth and Hopkins, 1995](#)), which are generally composed of clays and clayey silts with intermittent sand and gravel lenses that continue out into the Gulf of Mexico ([Waterstone et al., 2003](#)). The sandy and gravel lenses and dredged channels within the investigated system provide conduits for SGD despite the potentially limiting clay/impermeable formations.

METHODS

Sampling Design

Five sampling transects were selected within Corpus Christi Bay and the Upper Laguna Madre: transect T1-Laguna Madre; Transect T2-Oso Bay Inlet; Transect T3-Laguna Madre Inlet/Mouth; Transect T4-Shamrock Island; and Transect T5-University Beach (Figure 1). Water samples from porewater and water column were collected from six sampling sites placed along each transect, spanning 2 km from near shore to offshore (Figure 1). Transects were selected within the area reported to be affected by hypoxia and areas with significant external input such as discharge from Oso Bay (discharge points) and outputs such as the Laguna Madre mouth. Samples and resistivity data were collected during three events (i.e. winter - January, summer - July and fall - November to early December) to capture groundwater discharge rates, nutrient, and biomass distribution and levels under different environmental conditions (Figure 3). Sampling techniques for water column and porewater comply with standard sampling techniques ([Brown et al., 1970](#); [Wood, 1976](#); [RCRA SOP, 2009](#)). At each location, the water depth was measured using a pre-labeled line attached to a weight. Station depth is used to determine the necessary number of samples to be collected at each location. Samples from the water column

were collected in increments of 0.5 m. Mid- and porewater samples were collected at stations with depths <1 m. Surface, bottom, and porewater samples were collected at locations with water depths between 1-1.5 m. At stations with water depths >1.5 m samples were collected from surface, mid, bottom, and porewater. Field parameters were measured before sample collection using an YSI multiparameter water quality meter. The YSI meter was placed at each sampling depth within the water column for several minutes to allow proper circulation of sample and instrument stability before parameters were recorded.

Surface and column water samples were collected using a Van Dorn water sampler. A Van Dorn water sampler is a large cartridge with sealed caps on each end centrally attached with a rubber chord. Before deployment, the caps are pulled into the open position and placed within the trigger mechanism. The Van Dorn sampler is deployed to the desired depth and given a few minutes to allow water to circulate throughout the cartridge and then a weight is sent down the line to engage the trigger mechanism, thus closing the cartridge. The sampler is then pulled on board the vessel to fill the desired sampling bottles. Sampling bottles are rinsed three times and then overfilled, capped, and placed on ice depending on the required procedure for each analyte. A porewater sampler (AMS Retract-a-Tip) was used to collect porewater samples. The porewater sampler consists of 1 m sections of hollow steel pipe attached to a retract-a-tip point that is injected about 0.2 to 1 m below the sediment-water interface. The injection depth is critical to (isolate porewater from bottom water intrusion) sampling to prevent bottom waters from contaminating porewater samples ([RCRA SOP, 2009](#)). Silicone tubing is ran inside the steel pipe and attached to the retract-a-tip on one end and a peristaltic pump on the other. The silicone tubing is purged to the extent in which little sediment resides in the sample and then sampling bottles are rinsed three times, overfilled, and placed on ice.

Resistivity Imaging

Data collection

The resistivity data collection started with a reconnaissance survey of the study area. Land and water-based resistivity profiling were collected to locate possible locations of submarine groundwater discharge in the study area. We used the Advanced Geosciences, Inc. SuperStingR8 Marine system with patented graphite electrodes and EarthImager software with induced polarization imaging system and geophysical interpretive tools to differentiate between types of lithology and water with differing resistivity/electrical conductivity in order to map out groundwater seepage faces and to quantify groundwater discharge rates and associated salinities. The system is equipped with a 112 meter cable consisting of 56 graphite electrodes spaced 2 meters apart with the ability to accurately image to a depth of approximately 20% the length of the cable. Resistivity readings of the area surveyed are collected through a dipole-dipole system that injects direct current through two current producing electrodes and measures the difference in voltage received by two potential electrode pairs ([Advanced Geosciences, Inc.](#)). The SuperSting R8/IP is an 8-channel imaging system that has the ability to take up to eight readings for each current electrode allowing for a substantial decrease in survey time and increase in error correction and accuracy. The system used offers the advantage of imaging both the water column (cable is deployed on the water surface) and the underlying sediments in a single run. Continuous resistivity profiles (CRP) were collected in the Corpus Christi Bay and the Upper Laguna Madre along each sampling transect reaching from the water banks waterward (Figure 1). These images help determine the dimensions and exact scale of discharge and were used to select sampling sites and groundwater discharge measurements. For these marine surveys the electrode cable is towed behind a boat along the desired transect (Figure 4). The beginning and end coordinates of

each surveyed transect are entered into a Lowrance GPS to ensure an accurate path along the desired transect. Based on these initial assessments three locations were selected to conduct time-lapse resistivity imaging and continuous radon measurements in July and November/December, 2014 as described below.

Current is injected every 3 seconds and 8 apparent resistivity values representing 8 depth levels are read for each current injection. Depth of penetration depends on length of the cable and array type (typically approximately 20% of the electrode spread length) ([Advanced Geosciences, Inc.](#)). The July and November/December time-lapse stationary resistivity images were acquired along the same survey line. Time-lapse images are conducted with the resistivity cable deployed along the bottom of the bay during which measurements are taken in sequence to fully capture the groundwater discharge during tidal cycles. Each individual electrical resistivity (ER) sounding was gathered into a continuous dataset or tomograph and then inverted to earth model resistivity values using the 2D AGI EarthImager with a maximally smooth least squares algorithm ([Samouëlian et al., 2005](#)). Using an initial estimate, the element resistivities are iteratively adjusted until calculated resistivities best match the measured values within a specified tolerance or until the best fit model is obtained using the root mean square error (RMS) and L-2 norm values as indicators of best fit. The prominent reason for high RMS and L-2 norm values is usually noisy raw data originating from any factors that would inhibit proper signal communication between current and potential electrodes (i.e. bent survey lines or insufficient contact with the electrodes and the medium). Each set of time-lapse surveys were collected during different environmental conditions to capture resistivity changes over time and estimate groundwater discharge during periods of transition from dry to wet (July to November, 2014) environmental conditions.

Field observations on porewater electrical conductivity are used to constrain the inversion results to decrease the error associated with the estimation of groundwater discharge rates. Given the conductive nature of the imaged sediments and porewaters, and the small percent changes on subsurface sediment types (i.e. unconsolidated clays to silty-sands), we believe that the local resistivity contrasts and resulting noise levels are negligible and will not affect the resolution of the resulting ER tomography (Friedel, 2003).

Salinity Mass Balance and Submarine Groundwater Discharge Flux Calculations

Time-difference inversion algorithms were used to calculate the percent difference in resistivity between the six consecutive images collected over an eight-hour period for the July and November/December events. Through this process the image collected at time=1 is used as the base image from which the image collected at time=2 is subtracted and normalized. Furthermore, the image collected at time=2 is used as the base image from which the image collected at time=3 is subtracted and normalized and so on. Changes in the subsurface bulk resistivity can be monitored between each time step. However, an overall resulting difference-image reveals changes in bulk resistivity over the entire monitoring period which is assumed to be caused by variations in pore fluid chemistry while the matrix properties remain constant (Nyquist et al., 2008). Groundwater plumes were identified and separated into boxed zones for each time-difference inversion image and the volume (V) of each zone was estimated using a 2-meter horizontal distance (Dimova et al., 2012; Bighash and Murgulet, 2015). The defined zones for each difference image were superimposed onto the original ER images of their corresponding collection time and location. Porewater salinities were corrected using the relationship between formation factor (F) and sediment porosity (ϕ) using equation 1 given by Archie's law (Archie, 1942). Based on sediment core description and well logs developed in the formation extending

under the Corpus Christy Bay and the Upper Laguna Madre, we assume a clay content of approximately 25%. Clay corrected Archie's constants have been derived using a least-squares fitting of log-porosity and log-resistivity values (Lee and Collett, 2006). The clay corrected constants that assume a 25% clay content yield “*m*” and “*a*” values of 1.89 and 1.03, respectively. The porewater resistivity (R_p , Ωm) is then calculated using Archie's law for fully saturated media as expressed in equation 2. Salinity values for each superimposed zone were then estimated using equation (3) which allows for the conversion of ER-derived resistivity (R_p , Ωm) to salinity (*S*, parts per thousand (ppt)) (Manheim et al., 2004):

$$F = a * \phi^{-m} \tag{1}$$

$$F = R_f/R_p \tag{2}$$

$$S = 7.042 \times R_p^{-1.0233} \tag{3}$$

Once the salinity for each zone was calculated, average porewater salinity was derived for the beginning (*S*₁) and end (*S*₂) of each time-lapse survey. With this information, the volume of groundwater discharge was calculated using a salinity mass balance approach calculated using the percent change in salinity between the initial and final time of resistivity data collection using equation 4.

$$V_{gwd} = V_{sal}[(S_1-S_2)/S_2] \tag{4}$$

In the above mass balance approach the principle of conservation of both mass and salt is applied. Assuming a steady-state condition over a specified time, the SGD rate is calculated as the difference between the salinity inputs and outputs, not accounting for saltwater dispersion (or diffusion). Mass balances for each box are determined using the following criteria: fluxes into (out of) a box are positive (negative). The mass balance is based on changes in salinity

concentrations over time within the surveyed area. For a detailed description of this method please refer to [Dimova et al. \(2011; 2012\)](#). Equation (4) is based on the assumption that the entire volume of groundwater plumes, fresh or saline, will eventually discharge into surface waters under hydrologic conditions favoring groundwater discharge to surface water (i.e. upward hydraulic gradients).

Radiogenic Isotopes

Sampling and lab measurements

Samples for radium isotope measurements were collected in four to five 20 L jugs at each location. Short-lived and long-lived radium isotopes (i.e. ^{224}Ra and ^{226}Ra , respectively) and radon-in-water were measured using a *Durridge RAD7* radon-in-air monitor and the RAD AQUA accessory. The RAD AQUA is used to bring the radon concentration in a closed air loop into equilibrium with the radon concentration in a flow-through water supply. This method was used for continuous measurements of radon in water that are used to calculate groundwater discharge rates as described in the next section. For radium isotope measurements, pre-washed MnO₂ impregnated fibers are packed into a gas-tight cartridge through which 50 to 90 liters (L) of water samples are passed at a rate <1 L/min. Radium is quantitatively absorbed and concentrated by the fibers. Radon gas produced from radium decay is pumped from the cartridge to a RAD7 detector. Radon's polonium daughters are plated on the detector where the alpha emissions are counted. Radium-224 ($t_{1/2} = 3.66$ d) is measured shortly after collection. To measure ^{226}Ra ($t_{1/2} = 1600$ y), the gas-tight cartridge with the fibers is flushed with inert gas and sealed for at least 21 days to allow for ingrowth of ^{222}Rn ($T_{1/2} = 3.82$ d).

Submarine groundwater flux calculations

Radon (^{222}Rn) is much enriched in groundwater when compared to surface waters (typically 1000-fold or greater). Because of its unreactive nature and short half-life ($T_{1/2} = 3.83 \text{ d}$) ^{222}Rn is an excellent tracer to identify areas of significant groundwater discharge (Burnett and Dulaiova, 2003). Recent studies demonstrate that continuous radon measurements could provide reasonably high-resolution data to evaluate changes of radon concentration of surface water at one location over time (Burnett et al., 2001b; Burnett and Dulaiova, 2003). Continuous measurements of ^{222}Rn were conducted at 3 selected locations where time-lapse ER profiles were also acquired. The automated radon system (RAD 7 and the RAD AQUA accessories) was placed at the end of each resistivity transect on the deck of the research vessel. The monitoring system measures ^{222}Rn from a constant stream of water (driven by a peristaltic pump) passing through an air-water exchanger. The exchanger distributes radon from a running flow of water to a closed air loop that feeds to the RAD 7 radon-in-air monitor. A detailed description of RAD 7 capabilities and measurement principles can be found in Burnett and Dulaiova (2003). Radon measurements were integrated over 45 minute intervals.

The main principle behind using continuous radon measurements to quantify groundwater discharge rates to surface waters is based on the inventory of ^{222}Rn over time accounting for losses due to mixing with waters of different radon concentrations (i.e. low concentrations offshore waters) and atmospheric evasion (Figure 5). Thus, changes over time, if any, can be converted to radon fluxes. Using the advective fluid radon concentrations ^{222}Rn fluxes are converted to water fluxes (Burnett and Dulaiova, 2003).

The atmospheric loss of Rn was estimated using the equations presented by Macintyre et al. (1995) that calculate the gas exchange across sea-air interface using the radon concentration

gradient, temperature and wind speed. Fluxes of radon could not be measured for longer than eight hours for each of the two events because of adverse weather conditions (e.g., at winds of more than 12 miles per hour bay conditions become very difficult for sampling and data collection. Consequently, the effect of tides could not be fully addressed using the presented methods. Nevertheless, changes in water levels of no more than 1 foot are recorded in this area due to tidal fluctuations (NOAA, 2014). It is assumed that the lower radon fluxes observed during the monitoring time are due to mixing with offshore waters of lower concentration. The maximum absolute values of the observed negative fluxes during each time-series event at each location are used to correct radon fluxes for losses via mixing (Dulaiova et al., 2006). These losses estimates due to atmospheric evasion and mixing with low radon offshore waters are added to the net fluxes resulting in a total radon flux used to calculate SGD rates calculated using equations presented by Burnett and Dulaiova (2003). Furthermore, sediment fluxes were calculated using laboratory equilibration experiments from sediment cores collected at each time station using the following equation (4) presented by Corbet et al. (2000). Finally, we calculate water fluxes (q , cm/d) by dividing the total estimated ^{222}Rn fluxes (T_{total} , $\text{Bq/m}^2\cdot\text{s}$) by the concentration of excess ^{222}Rn ($\text{Ex } ^{222}\text{Rn}_{\text{gw}}$, Bq/m^3) in the fluids entering the system (i.e. equation 4 presented by Burnett and Dulaiova (2003)):

$$q(\text{m/s}) = F_{\text{total}}/\text{Ex } ^{222}\text{Rn}_{\text{gw}} \quad (4)$$

Residence time of water mass

Time-series radon fluxes from bottom sediment at seven locations were calculated to determine radon contribution from sediment resuspension or diffusion from the bottom of the bay. These laboratory experiments conducted using sediment cores and the RAD7 show that fluxes from bottom sediment alone are negligible (see ‘Radioisotope-derived SGD rates’ section). Therefore,

we can assume that the major input of radium comes from groundwater rather than from sediment diffusion or resuspension. Water residence times are calculated using the ratio of the short-lived (^{224}Ra) to the long-lived (^{226}Ra or ^{228}Ra) isotopes using equation 5 from [Dulaiova et al., \(2006\)](#) based on the model developed by Moore (2000b). The activity of the short-lived (i.e. ^{224}Ra) isotope should be decreasing as the water mass is moving away from the discharge point. This could occur due to two factors: radioactive decay and mixing with more diluted offshore waters. This is only valid if all SGD occurs near the shore and no input of radionuclides occurs from offshore groundwater discharge. The short-lived isotope is normalized to the long-lived isotope (i.e. ^{226}Ra) with activities that are expected to only decrease due to dilution. Because the half-life of ^{226}Ra is much longer ($T_{1/2} = 1600$ y). For instance, the half-life of ^{226}Ra is long with respect to mixing time and its decay rate may be neglected.

$$[\text{ex } ^{224}\text{Ra}/\text{ex } ^{226}\text{Ra}]_{\text{obs}} = [\text{ex } ^{224}\text{Ra}/\text{ex } ^{226}\text{Ra}]_i * e^{-\lambda^{224}t} \quad (5)$$

The initial $\text{ex } ^{224}\text{Ra}/\text{ex } ^{226}\text{Ra}$ was estimated for the different transects based on potential sources of radionuclides associated with both groundwater and surface water discharge (i.e transport of radionuclides from groundwater discharging to Oso Bay or Nueces Bay). Three initial $\text{ex } ^{224}\text{Ra}/\text{ex } ^{226}\text{Ra}$ ratios for each of the two investigated seasons/environmental conditions were identified: Oso Bay mouth, Upper Laguna Madre Mouth, and Shamrock Island.

Major Ions and Stable Isotope Sampling

Samples for measurements of stable isotope ratios of oxygen (^{18}O), hydrogen (D), dissolved inorganic carbon (DIC), and carbon stable isotope ratio (^{13}C) were also collected using the above procedure. Abundances of oxygen, hydrogen and carbon isotopes were measured (with an uncertainty of ± 1 per mil (‰) for δD , ± 0.1 for $\delta^{18}\text{O}$, and ± 0.2 for $\delta^{13}\text{C}$) relative to accepted

international standards, which are the Vienna Standard Mean Oceanic Water (VSMOW) (for oxygen and hydrogen) and the Vienna Pee Dee Belemnite (VPDB) (for carbon).

Major ion measurements were determined using a Dionex High Performance Ion Chromatograph (Model DX600) equipped with an autosampler, an anion-exchange column (7 mm; 4 x 250 mm; Dionex AS14A), and a conductivity detector (Dionex CD25). The detection limit of the method ranged between 0.05 and 0.1 mg/L, depending on the background signal of constituents in the samples. Cation measurements were conducted using the Flame Atomic Absorption (Flame AA) spectroscopy method with detection limits that vary by element.

Nutrient and Chlorophyll- α Sampling

Water samples were collected in January, July and November 2014 from 1-6 sites on each of five transects (Figure 1). For simplicity, we computed the average and variance for each parameter of interest for all sites along a transect. We refer to sites 1-6 as transect 1, sites 7-11 as transect 2, sites 12-17 as transect 3, sites 18-23 as transect 4, and sites 24-29 as transect 5. At each site, water samples were collected from 3 depths (surface, mid-water column, near bottom) in a Van Dorn sampling device and transferred to acid-washed amber polycarbonate bottles. An additional sample was collected from sediment porewater using the technique described in the "Sampling Design" section and transferred to an acid-washed amber polycarbonate bottle. Bottles were stored on ice until return to a shore-based facility where processing of samples occurred. Analyses were conducted for chlorophyll- α in surface (January) or surface, mid-water column and bottom samples (July, November) and for nutrients and organic matter at all depths.

Sample analyses – Chlorophyll- α was determined from samples collected on, and extracted from Whatman GF/F filters (nominal pore size 0.7 μm). Chlorophyll was extracted using 90%

acetone and analyzed fluorometrically. Inorganic nutrients (nitrate + nitrite (N+N), nitrite, silicate, orthophosphate, ammonium) were determined in the filtrate of water that passed through GF/F filters using a Seal QuAAtro autoanalyzer. Dissolved organic carbon (DOC) and total dissolved nitrogen (TDN) were determined in the filtrate of water that passed through GF/F filters using a Shimadzu TOC-V analyzer with nitrogen module. Dissolved organic nitrogen (DON) was estimated as the difference between TDN and inorganic nitrogen.

Statistical Analyses

A variety of statistical tools were used to analyze the geochemical data using SAS Software version 9.3. Univariate statistical analyses (i.e. ANOVA) were used to conduct exploratory analysis of data in order to find general distribution patterns and correlations between the categorical and continuous variables. Specifically, PROC GPLOT, PROC CORR and PROC GLM were used to create outputs that were useful in identifying general hydrogeochemical signatures for each water source, and finding correlations and interactions between individual variables. Interaction effects exist where the levels of one variable affect the relationship of two other variables. An interaction plot produces regression lines for two of the three variables and significant interaction with the third variable is evident at points where the regression lines cross. The p-values produced from the ANOVA analyses signify the probability that the variation in the model is explained by the null hypothesis. A significance level of less than 0.05 was designated for this statistical model, therefore, any p-value less than 0.05 resulted in the rejection of the null hypothesis. In this case, the null hypothesis is that there is *no* interaction between groundwater and surface water; so a p-value of less than 0.05 would indicate that interaction between these sources is likely. When dealing with a data set that has multiple variables with complex interactions and chemical processes affecting the model such as in this case (Voudouris et al.,

2000), multivariate statistical tools have the ability to derive hidden information from the data set and characterize environmental patterns in a more simplified manner (Thareja et al., 2011; Khan and Kumar, 2012).

Multiple linear regression (MLR) and Factor analysis (FA) were conducted on the data using PROC REG and PROC FACTOR (using the principal components method) in order to define the major geochemical parameters responsible for variations in water quality. MLR generates a minimum data set of indicators where all variables are included simultaneously into a single model in order to test for the potential interactions between the independent variables (Pathak, 2012). The ultimate goal of the MLR is to identify the most significant dependent variable and its associated predictor variables. The adjusted R^2 value indicates the proportion of the variation in the dependent variable attributed to the independent variables and is used as the primary indicator of how closely the model fits the data.

Factor analysis using the principal components (PCA) method allows for the reduction of complex multivariate data sets into smaller, more manageable data sets that aid in data interpretation. This is done by analyzing inter-correlations among observed variables, or scores, and extracting latent factors that better explain the underlying processes responsible for variations in water quality. Factors are extracted in order of importance based on the weight of each factor on the overall model and the results are presented graphically as vector plots. A Varimax-Orthogonal rotation is then done on the extracted factors in order to ensure that each latent factor is independent of the other. This allows for the alignment of each factor with the x, y, and z axes and facilitates interpretation of the final vector plots. Therefore, each rotated factor corresponds to an axis on the plot and the scores are the vectors. The positioning (i.e. in relation to the main axis) and length of each vector score represents the relationship and weight of that

score on the defined latent factors. For instance, the closer the vectors are aligned to the vertical axis, the more the variables associated with them are correlated with the factor represented on the “y” axis.

RESULTS AND DISCUSSION

Continuous Resistivity Profiles

Continuous resistivity profiles (CRP) were collected prior to sampling along the five main transects identified in Figure 1. These CRPs were used to identify possible areas of SGD for location of monitoring stations of both water quality and stationary (i.e. resistivity) and time-series (i.e. continuous radon measurements) surveys. Transect 1 resistivity data collected from the Upper Laguna Madre show evidence of submarine groundwater discharge near the shoreline (Figure 1; Appendix 1) and at two other locations in the offshore direction. The shape of this higher resistivity plumes shown in red to yellow color on the transect attached with this report (Appendix LM) indicate that this could be sandy pockets of freshwater upwelling from aquifer formations extending below the Laguna Madre and Gulf of Mexico. Plumes of saltier water are also observed throughout the shallow part of the profile which are likely sinking. This process, which is consistent with density-driven free convection, enhances upwelling of fresher to brackish water and discharge to surface water. [Stevens et al. \(2009\)](#) and [Bighash and Murgulet \(2015\)](#) found that such processes are common in the Laguna Madre and Oso Bay.

The second transect (2) extending from the Oso Bay Mouth offshore into Corpus Christi Bay (Figure 1) shows several spots of potential groundwater upwelling in an area just a few tens of meters from the discharge point into Corpus Christi Bay (Figure 2; Appendix 1). This is revealed by the massive disruption in the continuous low resistivity layer (i.e. low conductivity clay-rich formation) present right below the sediment-water interface. This conduit is associated with the

highest change in bathymetry (i.e. increased bottom elevation) associated with this transect. Similar conduits are observed for the Laguna Madre Mouth transect (3) extending from the mouth of Laguna Madre offshore to Corpus Christi Bay (Figure 3, Appendix 1). However, interfingering of saltwater (salinities higher than the overlaying waters) with brackish water plumes is observed within the elevated bathymetric area indicating that groundwater could be a source of increased salinity at this location.

Transects 4 and 5 collected from Shamrock Island (Figure 4; Appendix 1) and University Beach (Figure 5; Appendix 1), respectively, offshore into Corpus Christy Bay show less visible interaction between groundwater and surface water. Resistivity profiles show that in both transects possible groundwater discharge likely occurs at the shoreline face where the less conductive water (i.e. low hydraulic conductivity) layer (i.e. blue color) is discontinuous. Comparatively to all other surveyed areas, this anomaly occurs in the shallowest zones. Potential for upwelling of fresher groundwater is shown in the offshore part of the Shamrock Island transect. Based on these preliminary imaging efforts, we selected three sites for continuous measurements: the Laguna Madre mouth, the Oso Bay mouth and the Shamrock Island nearshore location (Figure 1).

Time-Lapse Resistivity Profiling and Resistivity-Derived SGD rates

Time-lapse resistivity images of the underlying sedimentary formations and porewaters were acquired to a depth of approximately 26 meters below the sediment-water interface. The range of apparent resistivity values was very narrow (0.10-1.4 Ωm) for all surveys indicating the highly saline nature of porewater/groundwater salinities in this area. The first time-lapse resistivity surveys were conducted in July, 2014, during one of the driest months of the summer (Figure 3; NOAA, 2014). The same survey lines were imaged in fall 2014 (end of November to beginning

of December 2014), when precipitation rates are slightly higher than those during the winter and summer events (Figure 3). For the time-difference resistivity tomographs, the minimum and maximum plot boundaries were set equal so that zero represented no change in resistivity and is shown as green in color.

Time-lapse ER images show potential for groundwater-surface water interaction at multiple locations within the 112-m of the survey lines for both summer and fall. Although the estimated SGD rates are very similar, the location and extent of groundwater plumes generally change from one season to another (Figures 1-6; Appendix 2.). For instance, at the Oso Inlet location input of fresher water is observed for the fall event (Figure 1 and 2; Appendix 2). Furthermore, while most change in porewater chemistry in summer occurs in the top half of the 26 m imaged-depth, percent resistivity/conductivity changes in fall, although smaller, were observed throughout the entire profile depth and more prominent in the deeper portion. The SGD rates derived from the salinity mass balance show slightly more discharge during fall (i.e. 9.2 cm/d) when compared to summer (7.4 cm/d) and they agree with the radon-derived fluxes (Figure 6).

Time-laps resistivity data for the Laguna Madre Mouth show large changes in resistivity between summer and fall and also the highest percent difference/change in porewater chemistry when compared to the other locations (Figures 3 and 4; Appendix 2). During the summer event percent change in resistivity was as high as 40% corresponding to a SGD rate of 66.6 cm/d while for the fall the change decreased to 12% but with more discharge faces resulting in a discharge rate of 74.1 cm/d (Figure 6). The change in seasonal porewater chemistry is largely caused by a shift from fresher (red-orange color; Figure 3; Appendix 2) to saltier (green color; Figure 4; Appendix 2) groundwater. For the fall event, the time steps 1 and 6 ER images (Figure 4; Appendix 2) show intrusion of fresher plumes of groundwater from the left side (i.e. from the 0 origin of the

profile) (i.e. between 5 to 22 m in horizontal direction and between 3 to 20 m in vertical direction). On the opposite side of the profile (i.e. towards the 108 m mark) a plume of saltier water (i.e. between 80 to 96 m in horizontal direction and between 6.5 to 15 m in vertical direction) is migrating laterally towards the origin.

Consequently, near-surface changes are slightly fresher given the upwelling of the fresher groundwater layer (i.e. red horizontal layer; between 3 to 8 m in vertical direction) into the salty shallow sediment. This movement of groundwater with different densities is consistent with the effects of density-driven free convection which affects the direction and magnitude of groundwater flow, thus altering the location of SGD faces (Bighash and Murgulet, 2015). Stevens et al. (2009) found that such processes are common in the Laguna Madre and Bighash and Murgulet (2015) found that the location and magnitude of groundwater discharge faces change dependent of the migration of highly saline, high density groundwater plumes.

At the Shamrock Island location, in both sampling events a fresher and sandy layer is observed between 3 to 9 m in vertical direction extending along the entire horizontal distance. Upwelling of saltier groundwater from the bottom of the profile is observed in both instances with the summer one (between 72 and 84 m in the horizontal direction) being more pronounced (Figures 5 and 6; Appendix 2). The range of resistivity values is narrower compared to the other two locations (0.14 to 0.72 Ωm). Other changes are observed to occur near the sediment-water interface (between 0 and 4 m below 0). Visible groundwater seepage faces indicating movement of slightly less saline water across the transition zone are located near the end of the transect for the summer survey and between the 38 and 54 m mark for the fall survey (Figures 5 and 6; Appendix 2). Although total percent changes in porewater chemistry within the underlying sedimentary formations are slightly larger in fall (i.e. 15%) compared to summer (i.e 10%)

within the same time frame, the resulting estimated SGD rates are greater during the former (Figure 6). Mass-balance calculations based on changes in salinity within the monitoring time period yielded SGD rates of 13.5 cm/day during the summer and 10.3 cm/day during the fall event.

Time-lapse stationary ER results imaging the first 26 m of the subsurface sediment formation and groundwater salinities show that subsurface water salinities were consistently higher in the upper 26 m than in the lower depth range (20 to 40 m) of the CRP profiles. These stationary resistivity images also show the existence of a low hydraulic conductivity layer extending from approximately 1 to 2.5 m below the sediment-water interface at most locations. While this impedes exchange between groundwater and surface water in most cases, changes in porewater chemistry from season to season and during the time-series analyses (time-lapse surveys) are evidence that areas facilitating exchange likely exists. The saturated zone, referred to as the water table, is evident below this lower hydraulic conductivity layer, starting around 2.5 m below the sediment-water interface (i.e. red band). Exchange between the saturated zone and the suspended sediment underneath the water column are more prominent where upwelling of groundwater plumes from deeper parts occur (i.e. Figure 6; Appendix 2). The consistent change in resistivity within the lower hydraulic conductivity layer is an indication that transport between the water table and the suspended bottom sediment exists. Furthermore, in most cases this seems to be the result of recirculation of surface water that mixes with the upwelling groundwater and eventually discharging into the bay waters. A different mechanism of groundwater-surface water exchange seems likely for fall in the Oso Bay inlet time-lapse ER measurements and for the Laguna Madre mouth in fall (Figures 2 and 3; Appendix 2).

Radiogenic Isotope Concentrations

Radium (^{224}Ra and ^{226}Ra) and radon (^{222}Rn) isotope concentrations have fluctuated by sampling event and transect (Table 1; Figures 7, 8). Radon concentrations were the highest in porewater with the highest concentrations in summer followed by fall while surface water concentrations are higher in fall. Porewater concentrations in general exceed concentrations supported by sediment equilibration, thus, any fluctuations in concentrations are indications of changes in groundwater fluxes that bring in higher radon concentrations. Groundwater ^{222}Rn concentrations for the shallower aquifers surrounding Corpus Christy Bay system range between 174 to 21,547 Bq/m³.

Overall the highest concentrations of ^{222}Rn were measured along transect T2 during winter and summer and along transect T5 during fall (Figure 7). For transect T2, except for porewater, the high radon concentration could result from discharge from Oso Bay. Elevated radon concentrations were previously found to be correlated with terrestrial groundwater discharge to Oso Bay (Bighash and Murgulet, 2015). On the other hand, sources of radon to all other sampling transects are likely the result of benthic fluxes from both groundwater discharge and bottom sediment. Furthermore, higher concentrations than those supported by sediment are associated with SGD which seem more visible at stations T1 (winter and summer), T2 (winter and fall), T3 (all seasons), T4 (summer and fall), and T5 (summer and fall) (Figure 7).

Radium-226 measurements were available for all three sampling events while radium-224 data were measured only for summer and fall. The long-lived ^{226}Ra was found in highest concentrations during all three seasons in samples from transect T1 and during winter and fall in samples from T2 (Figure 8 a). This should hint a close groundwater discharge source because concentrations are not altered significantly by dilution with radium depleted waters. Similar to

radon, analogous ^{226}Ra ranges are measured for Laguna Mouth transect, T3. On the other hand, the short-lived ^{224}Ra isotope concentrations are more homogeneous among transects but are larger in fall (Figure 8 b) indicating an increase in benthic fluxes which in turn facilitates the transport of dissolved chemical species between the water column and the underlying sediment.

Initial ratios representing the characteristics of the radium source (i.e. SGD at the shoreline or river discharge) were selected from locations that are consistent with the resistivity measurements: the Oso Bay inlet, Laguna Madre mouth and Shamrock Island stations. These ages equate to a water mass age of “0”. Using these initial ratios and the measured radium ratios at all other stations (along transects), water mass residence times/ages ranged from 4.4 to -8.1 days in summer and from 2.3 to 1 days in fall (Figure 9). A negative age is an indication of a recent addition of radium to the system in concentrations high enough that overcome the mixing and dilution effect during transport from the initial source. The negative age for the summer sampling event is associated with the offshore location on transect T4 (outward from the University Beach) that translates to a very rapid discharge rate of groundwater. Unfortunately, due to time and weather condition constraints, no SGD rates are available at this station to confirm this “hot spot”. The fall age however at this location, is among the oldest (3.9 days). Water mass ages are also slightly negative in the Laguna Madre with likely more groundwater discharge away from the shoreline. Water mass ages are expected to increase further from the shore or a source area such as a river. Our data do not show a steady increase but rather sudden decreases such as in the Laguna Madre, the Laguna Madre mouth (station 11) or offshore in Corpus Christi Bay. This is a considerable indication that additional inputs of radium, such as groundwater discharge, exists away from the shore.

Radon-derived SGD rates

Every time-lapse resistivity survey was accompanied by radon monitoring on the station. The radon monitor and field parameter YSI troll were installed on the boat platform and deployed during the same time period. Monitoring efforts were done over a 8-hour period and for as long as the ER time-lapse data collection was conducted. It should be noted that while the radon monitoring is integrated over one square meter (m^2), the resistivity monitoring is done over a 112 m^2 . Therefore, the resulting SGD rates using the ^{222}Rn fluxes do not incorporate the Hydrologic and hydrogeologic "heterogeneity". Using the two techniques for calculating SGD rates it allowed us to differentiate between fresh groundwater and recirculated seawater, delineate seepage faces as depended of sediment heterogeneity and convective flow caused by density differences.

Although short when compared to other studies in different areas outside Texas, we produced a continuous record of ^{222}Rn inventory as well as concentration over time. After normalizing for tidal height (i.e. almost negligible in south Texas estuaries) and correcting for atmospheric loss, mixing loss, and supported radon (i.e. sediment equilibration radon concentrations), we estimated net ^{222}Rn fluxes ranging between -3.5×10^{-3} and 3×10^{-2} $\text{Bq}/m^2 \cdot s$ for summer and -6×10^{-4} to 5×10^{-2} $\text{Bq}/m^2 \cdot s$ for fall. Although no correlations are evident between these fluxes and the change in tide, these fluxes seem to fluctuate within the 8-hour period indicating the existence of other players influencing rates of groundwater discharge.

The total estimated radon fluxes ($\text{Bq}/m^2 \cdot s$) were divided by the apparent ^{222}Rn activity of the advective fluids determined from multiple wells surrounding our study area ($7106 \text{ Bq}/m^3$) for each time interval (1 h in this experiment). This results in integrated average water fluxes (over the 8-hour period) ranging from 0–40.3 cm/day (average = $11.8 \pm 5 \text{ cm}/\text{d}$; $n = 14$) in summer and

from 0–60.8 cm/d (average = 20 ± 8 cm/d; $n = 12$) for fall (Figure 6). Using the radon-derived integrated estimated seepage rates and the resistivity time-lapse spatial distribution of seepage faces we converted these fluxes to groundwater discharge rates characteristic for a 112-m band. These values were normalized for per unit length of bottom sediment (m³/m.d). This yielded groundwater discharge rates ranging from 1.6 to 10.7 m³/m.d in summer and from 1.1 to 18.5 m³/m.d for fall (Figure 6).

We find some major differences when comparing the radon-derived groundwater fluxes to those calculated from the ER time-lapses. For the Laguna Madre inlet for instance, radon-derived fluxes are lower by an order of magnitude than the resistivity ones for both summer and fall monitoring efforts. Furthermore, the estimated groundwater flux for the Oso Bay inlet in fall is larger by an order of magnitude and for Shamrock Island in summer is higher by an order of magnitude using the groundwater fluxes derived using radon concentrations. We learned from the ER time-lapse data that not only the intensity of the groundwater discharge rates varies temporally and spatially, but the extent of these seepage faces are also variable, thus resulting in large uncertainties when using spot measurements. Furthermore, we also found that the range of groundwater ²²²Rn concentrations vary significantly within the area surrounding Corpus Christi Bay system (174 to 21,547 Bq/m³). Since changes in hydrologic conditions are expected and can dictate the direction of groundwater flow as well as the source of groundwater discharge, it is likely that the geochemical signature of groundwater discharging at any location within the bay will vary spatially and temporally.

Groundwater fluxes determined using radon concentrations are extremely sensitive to the concentration of radon in the upwelling fluid (i.e. radon fluxes are divided by the advective pore fluid ²²²Rn concentration. A change of one order of magnitude in radon concentration will result

in an increase or decrease of the groundwater flux by one order of magnitude as well. For instance, groundwater fluxes calculated using the ER data for Laguna Madre inlet are higher by an order of magnitude than those estimated using ^{222}Rn concentrations (Figure 6). On the other hand, the opposite is observed for Oso Bay inlet. Groundwater ^{222}Rn concentrations in shallow wells adjacent to Corpus Christi Bay are in average $11,457 \text{ Bq/m}^3$. Dividing the radon flux values at Oso mouth by this the new apparent ^{222}Rn activity of the advective fluids lowers the SGD rates to almost half (i.e. summer SGD drops from 24 to 15 cm/d). At this location it is likely that the discharge of Oso Bay waters is expected to contribute high concentrations of ^{222}Rn as indicated by a previous study which shows significant groundwater contribution (Bighash and Murgulet 2015). Furthermore, surficial recirculation of water could increase the radon flux that is not related to lateral groundwater discharge. To limit the uncertainty associated with these calculations for nutrient flux estimates we use an average groundwater discharge rate integrating both types of measurements used in this study (Figure 6).

Major Ion and Stable Isotopes

Major Ions

In an effort to further constrain the groundwater flux estimations, porewater and surface water samples were analyzed for major ions such as sulfate (SO_4), chloride (Cl), sodium (Na), potassium (K), manganese (Mn), magnesium (Mg), calcium (Ca), and iron (Fe). Most of these major ions are conservative elements. The solubility of the minerals that supply these elements is high in seawater (i.e. NaCl, KCl, MgSO_4 , and CaSO_4). The concentration of these elements normalized to salinity or Cl is generally constant and the ratio of one conservative element to another should be constant also. Until recently, Mg was assumed to be conservative but studies show local anomalies of Mg in deep waters and it can be completely removed in high temperature hydrothermal vent solutions. Furthermore, SO_4 is conservative in oxic waters but not in anoxic sediments and waters. Sulfate reducing bacteria use SO_4 and forms HS^- or H_2S . The concept of residence time is informative in several ways (http://www.ocean.washington.edu/courses/oc400/Lecture_Notes/CHPT4.pdf). Residence time of these elements offers insight related to their fate in seawater. For instance, elements such as Na and Cl have long residence times in the ocean and tend to be very soluble in sea water as well as evenly mixed throughout the ocean. Therefore, they occur in the same ratio to one another throughout the ocean regardless of the total salinity. Elements with short residence times such as iron are relatively reactive, or insoluble in sea water (i.e. pH dependent) and therefore, they are easily removed and are unevenly distributed throughout the ocean.

Ratios of the major elements to chlorinity have been used in this study to analyze sources of water to the investigated embayments. Ratios of SO_4/Cl varied by season with the largest ratios measured during the summer event followed by winter (Figure 10). The highest ratios are

associated with lower Cl concentrations as displayed in the SO_4/Cl versus Cl graph (Figure 10). This indicates that at some locations there is an additional source of sulfate other than the seawater. Mass ratios of Mg/Cl and K/Cl show very similar trends for all three seasons. Although an inverse relationship between the ratios and Cl are still observed, it can be noted that winter samples have lower concentrations of Mg and K when compared to summer and fall (Figure 11 and 12). This relationship could be the result of mineral dissolution enhanced by increased temperature and likely decrease in pH due to biological activities. Also, sediment fluxes will enhance transport of these elements to surface waters. Mass ratios of Ca/Cl and Na/Cl show similar trends for winter and summer but are slightly different for the winter event when Na/Cl ratios are more elevated than the summer ones (Figure 13 and 14). These ratios show that chemical characteristics of water are significantly different from season to season and especially between winter and summer and fall.

In most cases the sample ratios exceed the typical seawater ratio (at 35,000 mg/L salinity) extending towards higher ratios that are characteristic of freshwater or fresher water environments such as groundwater or river discharge. Since, sampling events were conducted during the lowest precipitation events (Figure 2), the contribution from runoff can be assumed negligible although, the higher concentrations of Mg, Ca, and Na in relation to Cl hint at riverine source of fresher water. Furthermore, assuming that during summer and fall as the SGD rates and inflows of fresher waters to the system are likely to occur through bottom sediment, dissolution of some elements such as K will increase the concentration of this element compared to winter. Studies show that dilution of interstitial water in the sediments could enhance dissolution of some elements from the sediment and increase the total abundance in elements ([Parashiva and Ferrell, 1973](#)).

Given the high content of clay minerals in the bottom sediments it is likely that K will be released during the summer and fall seasons. Sulfate concentrations increase over the summer with similar concentrations in surface water and porewaters, relative to the conservative seawater ratio with Cl (0.0517 (M)). These enrichments occur during some of the driest, warmest, and increased anoxic conditions over the study period. Some of the greatest enrichments were found along the Laguna Madre transect with no riverine inflows and with the lowest interstitial DO concentrations (0.15 to 4.6 mg/L). By fall most excess SO_4 has been removed from the water column (Figure 10) presumably due to dilution with runoff or due to SO_4 reduction in anoxic interstitial and surface/bottom waters. The highest SO_4/Cl ratios are the highest in the Laguna Madre and along Laguna Madre inlet, Shamrock Island, and University Beach transects. Lower ratios are recorded in close proximity of Oso Bay inlet indicating that water chemistry is likely influenced by different sources and chemical processes. A similar trend has been observed in other estuaries such as the Pamlico and Neuse River estuaries in North Carolina (Matson and Brinson, 1985). Although during summer the anoxic conditions are more prevalent (porewater average: 1.12 mg/L DO; water column average: 5.18 mg/L DO) compared to fall (porewater average 1.51 mg/L DO; water column average: 8.77 mg/L DO), it appears that bacterial uptake of SO_4 is not significant or the input from a source other than marine waters may be overcoming the uptake. Input of O_2 could be a major stimulant for oxidation of sedimentary S (Matson and Brinson, 1984) therefore, increasing the flux of SO_4 from sediments. Furthermore, radon data show the existence of benthic and groundwater fluxes which can increase SO_4 concentration if supply exceeds consumption by bacteria.

Iron is an important metal for living organisms. Like other nutrients, iron availability can limit primary production and therefore, the food availability for heterotrophic organisms. Iron

limitation of phytoplankton has received attention especially in oceanic regions with low biomass, despite high nutrient levels (Gran, 1931; De Baar et al., 1999; Martin et al., 1994). Studies show that although phytoplankton is not iron-starved per se, but the low ambient iron concentrations may inhibit biomass accumulation (Martin et al. 1994, Coale et al. 1996, Boyd et al. 2000). The sources of iron for the pelagic community are several: aeolian input with terrigenous matter; riverine input especially in coastal areas; re-mineralization of organic matter can release iron in deeper waters and after upwelling this can be a source of iron (Bowie et al. 2002). Finally, sediments can be a source of iron if sedimentary iron oxides are reduced (directly or indirectly) during anaerobic mineralization processes and then escape to the overlying water. This last process couples the iron cycle to the carbon cycle.

Iron concentrations are the highest in winter followed by some occurrences in fall (Figure 15). Summer concentrations seem to be nearly constant within all five transects except for a few instances located along the Shamrock Island and University Beach transects. Winter concentrations in the Laguna Madre drop below the average summer and fall abundances for the Laguna Madre, Osos Bay inlet, and Shamrock Island (Appendix 3). Similar to sulfate, iron concentrations may be increasing due to fluxes from the sediment caused by the reduction of oxides during anoxic conditions. However, a strong possibility exists that iron is being consumed for primary production of phytoplankton. Since the lowest production is expected during winter, iron concentrations are expected to be the highest. It can be inferred from our data that iron is preferentially consumed starting with summer and, by late fall, iron has been consumed leaving behind a much more depleted pool compared to winter and summer.

Because the reduced form of manganese is more soluble, it occurs as solute mostly in porewater. Our samples are more enriched in manganese in porewater compared to surface water. Although

concentrations vary by season in both porewater and water column (Figure 16), concentrations are always 2-3 fold higher in the interstitial water. Most surface water samples are below the detection limit (<0.05 mg/L) for the winter season although porewater concentrations are among the most elevated for the three seasons. Reduced manganese can also adsorb onto particles or Mn-oxides therefore disappearing from solution (Slomp et al., 1997). Reduction of Manganese oxide was found to occur coupled to the oxidation of organic carbon and at low reduction rates it could be a controlling factor of microbial reduction (Burdige et al., 1992). Manganese oxide reduction can also occur coupled to the re-oxidation of Fe (II), or pyrite and iron sulphide oxidation (Schippers and Jorgensen, 2001). A speciation analysis of different cations is necessary to understand processes driving variation in manganese concentrations in this estuary.

Stable Isotopes

Carbon Stable Isotopes and Dissolved Inorganic Carbon

A summary of all geochemical data collected over the course of the project can be found in Appendix 3. Observed $\delta^{13}\text{C}$ and Dissolved Inorganic Carbon (DIC) signatures vary for the three sampling events (Figure 17). In January the $\delta^{13}\text{C}$ and DIC concentrations ranged between -10.3 to 3.25 ‰ PDB (average -0.97 ± 0.2 ‰) and from 198 to 6,828 micromolar (μmol) (average 2,249 μmol), respectively. In summer the $\delta^{13}\text{C}$ ratios were slightly more depleted ranging from -11.3 to -1.0 ‰ (average -3.4 ± 0.2 ‰) while DIC concentrations increased spanning from 1,585 to 7,005 μmol (average 2,386 μmol).

Isotopic $\delta^{13}\text{C}$ ratios are furthermore depleted during the fall event ranging from -22.1 to -2.1 ‰ PDB (average -4.6 ± 0.2 ‰) while DIC concentrations increased as well going from 1,728 to 12,507 μmol (average 2,543 μmol). A detail worth noting is that there were several instances of porewater with concentrations of CO_2 much greater than the measurement capabilities of the

mass spectrometer and that most of the depleted isotope ratios and enriched DIC concentrations are recorded in porewater during the summer and fall events.

The more depleted $\delta^{13}\text{C}$ ratios observed in summer and fall could reflect signatures indicative of input of groundwater bicarbonate (HCO_3) and freshwater carbonate (Figures 17 and 18). On the other hand, microbial sulfate reduction coupled with anaerobic oxidation of methane in oxygen depleted environments such as those observed in summer and fall is also likely (Figure 18) (Michaelis et al., 2002; Yoshinaga et al., 2014). Although considerable depleted $\delta^{13}\text{C}$ ratios are associated with the bacterial production of methane (-60 to -80 ‰), the water signature could be altered during mixing processes resulting in more enriched abundance. However, an increase of SO_4 concentrations in summer is observed in relation to chlorinity (i.e. all samples but one have SO_4/Cl ratios greater than that of seawater) (Figure 10) likely ruling out the microbial reduction of SO_4 and production of methane that would cause depletion of $\delta^{13}\text{C}$ ratios and DIC enrichment. On the other hand, resources originating from marine environments (i.e. oceanic DIC and marine limestone) have $\delta^{13}\text{C}$ signatures averaging around 0‰ \pm 10‰ (Mook, 2000; Grossman et al., 2002) which is closer to the winter signature. Groundwater $\delta^{13}\text{C}$ ratio abundances in shallow groundwater in close proximity to our study area ranged from -18.5 (summer-fall 2012) to -6.04‰ (spring 2013) (Bighash and Murgulet, 2015). Therefore, groundwater discharge is likely having an impact on the geochemical characteristics of water during summer and fall but it is less visible during winter.

Oxygen and Hydrogen Isotopes

The stable isotopes of oxygen and hydrogen in water are important tracers of the global, regional, and local hydrologic cycle. The importance of these isotopes as tracers in water management has been long recognized by the International Atomic Energy Agency (IAEA)

which maintains a Global Network of Isotopes in Precipitation (GNIP) providing the isotopic signatures of precipitation worldwide since 1961. δD and $\delta^{18}\text{O}$ ratio abundances ranged from 3.26 ‰ to 11.9 ‰ (average $5.0\text{‰} \pm 1\text{‰}$) and 0.5‰ to 2.0‰ (average $0.8 \pm 0.1\text{‰}$), respectively in spring with the most enriched ratios measured in porewater and bottom waters in the Laguna Madre and Oso Bay inlet (Appendix 3). Minimum and maximum δD ratio abundances for summer are 4.6 ‰ and 25.3‰ (average $10.6 \pm 1\text{‰}$) and -2.4‰ and 2.1 (average $1.4 \pm 0.1\text{‰}$) for $\delta^{18}\text{O}$. Porewaters samples are among the most depleted on both δD and $\delta^{18}\text{O}$ ratio abundances especially in the Laguna Madre and in close proximity to the Oso Bay Inlet. By late fall, porewaters are again more enriched in both stable isotope ratio abundances especially in the Laguna Madre. Minimum and maximum ratios of δD and $\delta^{18}\text{O}$ of 4.8 ‰ to 13.1 ‰ (average $7.5 \pm 1\text{‰}$) and 0.7‰ to 2.0‰ (average $1.0 \pm 1\text{‰}$), respectively are comparable to winter signatures.

Enriched δD and $\delta^{18}\text{O}$ ratios are generally correlated with lower amounts of rainfall and higher evaporation rates (Katz et al., 1997) which are the result of both high winds and temperatures, conditions. The magnitude of enrichment in heavy isotope composition due to evaporation was attributed in the past to the Rayleigh Equilibrium Isotope fractionation process which predicts that δD and $\delta^{18}\text{O}$ ratios of residual brines become more enriched during evaporation as more of the isotopically depleted H_2^{16}O enters the vapor phase (Craig et al., 1963; Lloyd, 1966). Groundwater δD and $\delta^{18}\text{O}$ abundances are much more depleted in groundwater around this area as reported by Bighash and Murgulet (2015). The average δD and $\delta^{18}\text{O}$ for groundwater samples collected as part of their study in summer 2012 ($-16.8 \pm 1\text{‰}$ and $-0.9 \pm 0.1\text{‰}$, respectively) and spring 2013 ($-9.5 \pm 1\text{‰}$ and $-1.8 \pm 0.1\text{‰}$, respectively) show a change towards more enriched δD ratios and slightly depleted $\delta^{18}\text{O}$ for the 2013 dry spring season. This clearly shows that groundwater isotope signature could be variable as dependent on recharge conditions.

We attribute the observed depletion of porewaters in the Corpus Christi Bay and Upper Laguna Madre during the summer to the upwelling of groundwater into the top sediment layers and discharge to surface waters. This flux of depleted groundwater may be enough to overcome significant isotope enrichment of surface water due to evaporative effects. Given that groundwater fluxes are shown to be in the same order of magnitude in summer and fall, we believe that the source of groundwater discharge is likely changing between the 2 seasons going from a more distant and deeper source to a shallow source recharged on the evaporation tidal salt flats surrounding the embayment (i.e. evaporation of rising groundwater or a temporary stagnant water). The evaporative effects on surface water and percolating water to aquifers during summer are clearly indicated by this study as shown in Figure 19. The greater evaporation effect is more visible for the Laguna Madre which exhibits some of the most enriched ratios of both isotopes in porewater during winter.

Spatial-temporal Distribution of Phytoplankton and Nutrients

A significant observation of this study, consistent across all three seasons in which sampling occurred (winter, summer, fall), was that inorganic nutrient and chlorophyll *a* concentrations were consistently low throughout the water column. Others have noted that estuaries of the south-central Texas coast are subjected to riverine nutrient pulses only during significant rain events, and function on recycled nutrients in between these events (e.g., Longley 1994). Our results are consistent with these previous findings, yet as will be discussed later, data collected in this study also points to groundwater as a potential source of nutrients that has not been previously quantified in these systems.

Chlorophyll *a* concentrations were consistently low in January (<6 µg/l) (Figures 20-22), likely a result of low light levels and low water temperature (Appendix 3; Longley 1994), coupled with

low nutrient levels. In regards to the latter, ammonium was the dominant inorganic N form in the water column, although concentrations were $<2\text{-}3\ \mu\text{mol}$ (Figure 23). Ammonium concentrations were nearly uniform throughout the water column (Figure 21). Nitrate was virtually absent from the water column (Figure 23). In contrast to the low inorganic N concentrations, DON was high on all transects, ranging from 18.2 to $24.9\ \mu\text{mol}$ (Figure 24). Phosphate concentrations were also low, consistently $<0.4\ \mu\text{mol}$ (Figure 25). The inorganic N:P ratio in surface waters ranged from 6.9 to 77.6 (Figure 26), with localized presence of N-limitation (i.e., $\text{N:P} < 6$) on transects 2 and 4, and P-limitation (i.e., $\text{N:P} > 16$) on transects 1, 3 and 5. Most estuarine studies have focused on N as limiting to phytoplankton growth, but these findings argue that N or P may limit phytoplankton growth in these systems during winter. It is important to note that silicate concentrations were also very low ($<10\ \mu\text{mol}$) (Figure 26), which could act to prevent diatom growth if conditions were otherwise conducive for growth.

During July, chlorophyll *a* concentrations were mostly homogenous in the water column and higher than January, ranging from 5.4 to $13.6\ \mu\text{g/l}$ (Figures 27-29). We attribute this to a combination of warmer water temperatures and higher light levels (Appendix 3). In terms of nutrients however, there was no obvious difference between January and July. For example, ammonium was the dominant inorganic N form in July, but concentrations were $<3\ \mu\text{mol}$ (Figure 28), similar to January. Likewise, nitrate concentrations were $<0.1\ \mu\text{mol}$ and orthophosphate concentrations were $<0.2\ \mu\text{mol}$ (Figures 30, 31, respectively). Inorganic N:P ratios were less than or near 16, indicative of either N-limiting conditions or N and P as both limiting (Figure 28). Silicate concentrations were much higher than in January, ranging from 14.4 to $49.9\ \mu\text{mol}$ (Figure 32). With the low inorganic N and P concentrations observed, it is not entirely clear as to the source(s) of nutrients supporting the higher phytoplankton biomass during summer. One

possibility would be organic nutrients, with DON concentrations ranging from 29.2 μmol to 85.2 μmol (Figure 33), and presumably the dissolved organic phosphorus pool, which was not measured here but is known to support phytoplankton growth in coastal systems (Glibert et al. 2004; Huang et al. 2007). Another potential source that must be considered is groundwater. Porewaters were enriched in ammonium by 1-3 orders of magnitude over water column concentrations (Figure 28), by 2-4 fold over water column silicate concentrations (Figure 32), and to a lesser degree in orthophosphate during July (Figure 31).

Estimated discharge rates show that groundwater could be a significant source of nutrients (see sections on *Radon – derived SGD rates* and *Nutrient Fluxes*). A groundwater sample collected from a well approximately 8-m deep located in close proximity to Oso Bay shows very high levels of nutrients: 594.3 $\mu\text{mol/L}$ DOC; 1,814.8 $\mu\text{mol/L}$ TDN; 1,606 $\mu\text{mol/L}$ NO_3 ; and 196.8 $\mu\text{mol/L}$ silicate. These concentrations are much greater than those measured in surface water and could explain the higher silicate and DON levels in surface waters as well as porewaters. Recirculation of bay waters as well as benthic fluxes will likely enhance transport of these constituents to surface waters. In the following section we present an estimate of nutrient discharge rates based on the estimated average SGD rates.

During November, chlorophyll *a* concentrations were lower than summer, presumably due to decreasing light levels and water temperatures (Figures 34- 36). Ammonium was generally the dominant inorganic N form as in previous months, but once again averaged <2 μmol (Figure 35). However, a few instances of nitrate concentrations reaching 1-4 μmol were observed, particularly on transect 2 (Figure 37). DON was once again prevalent, ranging from 19.3 to 42.9 μmol (Figure 38). Orthophosphate concentrations were low, averaging <0.4 μmol (Figure 39). Finally, silicate concentrations had dropped precipitously from July (Figure 40), suggesting that

the July peak was due in large part to remineralization of biogenic silica in the sediments, a phenomenon observed in adjacent Oso Bay (Wetz et al. in review) and other estuarine systems (e.g., [Aller and Benninger 1981](#); [Yamada and D'Elia 1984](#)). Groundwater discharge rates are higher for Oso Bay Inlet and Shamrock Island and can be a continuous source of nutrients to the estuaries in the study area. The highest SGD rate measured at Oso Bay Inlet could be the cause of the increase in nitrate concentrations. Nitrogen in the nitrate form is rarely found in surface water unless a supplying source is extremely close. Given the land use in the close proximity, nitrate is likely originating from groundwater that is discharging at a nearby location to Oso Bay inlet. The presence of nitrate is also suggesting that the rate of discharge is fast enough that nitrate is not being transformed to other forms of nitrogen via denitrifications under anoxic conditions.

Organic Matter Distributions

Dissolved organic carbon concentrations were lowest in January, ranging from 247 to 326 μmol (Figure 41). These concentrations were still enriched above typical seawater concentrations observed at Port Aransas however, which are $<100 \mu\text{mol}$ ([Wetz, unpubl. data](#)). Much higher DOC concentrations were observed in July, ranging from 359 to 955 μmol (Figure 42). These higher concentrations are believed to be due, in part, to production by seagrasses and phytoplankton ([Wetz, unpubl. data](#)). By November, DOC concentrations had decreased, ranging from 265 to 633 μmol (Figure 43). With a few exceptions, DOC concentrations were uniform throughout the water column (Figure 41-43). In contrast to several of the nutrient analytes, DOC concentrations were not enriched in porewater in most cases (Figure 41-43). Only in a few instances were porewater DOC concentrations higher than in the overlying water column, with 3-10 fold enrichment observed (Figures 42, 43). Thus it is likely that the influence of porewaters

on water column DOC concentrations and microbial respiration is likely to be patchy at best in these systems, at least under the environmental conditions during our sampling regime.

Nutrient Fluxes

Groundwater-derived nutrient fluxes were calculated using the average SGD rate integrating both sediment and groundwater fluxes presented in Figure 6. Groundwater discharge rates vary by season and location. Furthermore, nutrient concentrations measured in the interstitial porewater also vary spatially and temporally (Figure 44). As a result, the SGD-derived nutrient fluxes are also dynamic as a function of hydrologic conditions and nutrient availability. Nutrient fluxes for Oso Bay Inlet are the highest during summer, followed by the Laguna Madre inlet and lastly, by the Shamrock Island (Figure 45). These flux estimates are in agreement with the groundwater fluxes which show the greatest SGD rates at the Oso Bay mouth/inlet while the highest nutrient concentrations were measured at the Laguna Madre mouth.

In fall, most nutrient fluxes increase by an order of magnitude at all locations (Figures 45, 46) and except for ammonia, all nutrient fluxes are slightly higher at the Shamrock Island than at the Laguna Madre inlet. Nutrient fluxes at Oso Bay inlet are much larger than in summer and compared to the other two locations. This is not only explained by the larger groundwater fluxes, but also by the increased nutrient fluxes measured in porewaters at this location. The highest *chlorophyll- a* concentrations are also at the Oso Bay mouth during the fall event (Figure 38). Additionally, it is apparent that groundwater may be supplying nutrients along the shoreline just west of the University Beach. Groundwater discharge measurements were not conducted at this location but from our independent radium and radon measurements it is obvious that groundwater could have a high contribution to the nutrient budget at this location. On the other hand, *chlorophyll-a* levels are highest at the Laguna Madre inlet in summer although the highest

nutrient fluxes show higher discharges at the Oso Bay inlet. The difference in fluxes however, is not that high among stations during the summer when compared to fall (Figure 47). The lower *chlorophyll-a* at the Oso Bay inlet during the summer could be explained by dilution with waters discharging from Oso Bay.

Overall, groundwater seems to supply a large amount of DOC, TDN, Ammonia, and silicate to the system during both summer and fall, with larger fluxes in fall (Figure 47). Phytoplankton productivity is lower in fall in the Corpus Christi Bay except at the Oso Bay inlet and with some spotty higher occurrences at the Laguna Madre Inlet and along the Laguna Madre transect. Although nutrient fluxes are higher in fall, phytoplankton growth is likely reduced due to reduced light exposure and lower temperature. Nevertheless, the much higher productivity than expected for late fall is explained by the large nutrient supply by groundwater which is also expected to be warmer than surface water during late fall and winter.

Spatial and Temporal Extent of Hypoxia

Winter DO levels show an almost homogeneous distribution within Corpus Christi Bay (Figure 48) with the lowest concentrations associated with the locations where submarine groundwater discharge was found to occur as part of this study: Shamrock Island, Laguna Madre inlet, and to a lesser extent at the Oso Bay inlet transects. Dissolved oxygen levels were relatively high during winter and fall (Figures 49, 50) in surface waters with concentrations ranging from 8.0 to 10.1 mg/L DO and from 7.12 to 11.0 mg/L DO, respectively. Porewater DO concentrations and other filed parameters are not available for winter but based on all other chemical parameters we expected that levels are similar to those from fall ranging from 0.4 to 5.2 mg/L DO (Figure 49). Summer surface water DO levels ranged between 1.4 and 8.3 mg/L DO (average 5.2 mg/L DO) for porewater and between 0.1 and 4.5 mg/L DO (average 2.1 mg/L DO) for surface water. DO

levels below the 2 mg/L threshold are only recorded during the summer event when temperatures and light exposure are longest enhancing phytoplankton growth leading to hypoxia. During summer the lowest DO concentrations (drack blue color on Figure 51) are associated with areas with high SGD nutrient fluxes, low porewater DO levels, along transect T2 away from the groundwater monitoring station, and at the nearshore location of the Laguna Madre transect (Figure 51).

Seasonal Trend Analyses Using SAS

Chlorophyll- α

Chlorophyll- α concentrations are highest in summer and lowest in winter in surface waters. In both summer and fall, when samples were collected at multiple depths in the surface waters, the bottom samples, collected at approximately 0.2m above the sediment/water interface, have greater chlorophyll- α concentrations than samples collected at middle and surface depths (Appendix 4, Figure 1).

Nitrogen Nutrients

Ammonium, NH_4 , concentrations are consistently one to two orders of magnitude greater in the porewater than in the surface waters, with the greatest concentrations in fall, 254.5 $\mu\text{mol/L}$, and the lowest concentrations in winter, 57.1 $\mu\text{mol/L}$ (Appendix 4, Figure 2). Additionally, in the surface water, the bottom samples show higher concentrations of NH_4 than middle samples in all seasons and surface samples in winter and fall. In summer surface samples show greater concentrations than bottom samples. Average surface sample concentrations are also generally greater than middle depth concentrations (Appendix 4, Figure 3). Summer shows the lowest concentrations of nitrate+nitrite in all sample depths, which corresponds with the elevated summer chlorophyll- α concentrations. Porewater NO_3+NO_2 concentrations in winter are almost

an order of magnitude higher than in surface waters. Surface, bottom, and pore depths have much greater concentrations than middle depths in fall (Appendix 4, Figure 4).

Nitrite (NO_2) concentrations are consistently elevated in porewater compared to surface samples, with the greatest concentrations in winter, $0.51 \mu\text{mol/L}$. The NO_2 concentrations in surface waters do not show large variations by season (Appendix 4, Figure 5). Total Dissolved Nitrogen (TDN) concentrations are consistently an order of magnitude greater in porewater than in surface waters, with the greatest concentrations in fall and the lowest concentrations in winter (Appendix 4, Figure 6). TDN is elevated in the surface waters in summer relative to fall and winter (Appendix 4, Figure 7).

Phosphate

Phosphate concentrations in porewater are consistently an order of magnitude greater than in surface waters, with the highest concentrations in fall, $7.05 \mu\text{mol/L}$, and the lowest concentrations in winter, $2.11 \mu\text{mol/L}$ (Appendix 4, Figure 8). In surface waters, phosphate concentrations are elevated in fall relative to summer and winter (Appendix 4, Figure 9) which could be related to the higher groundwater input as indicated by both resistivity and radon SGD fluxes.

Silicate

Average silicate, SiO_4 , concentrations in porewater are consistently an order of magnitude greater in porewater than in surface water, with the highest concentrations in fall, $192.35 \mu\text{mol/L}$, and the lowest concentrations in winter, $67.78 \mu\text{mol/L}$ (Appendix 4, Figure 10). Surface water concentrations are greatest in summer, almost twice fall concentration and three times winter concentrations (Appendix 4, Figure 11).

Radio-isotopes

Porewater concentrations of radon-222 were consistently an order of magnitude greater than concentrations in surface waters, with average summer porewater concentrations being 138 Bq/m³ and 185 Bq/m³ greater than the average concentrations in fall and winter, respectively (Appendix 4, Figure 12). In surface waters, the winter average Rn-222 concentrations are almost twice those in fall and summer. (Appendix 4, Figure 13). The elevated Rn-222 concentrations in the surface waters in winter are an indication of greater groundwater discharge in winter than in fall or summer, which corresponds with the SGD fluxes determined from continuous radon measurements at Oso Inlet and Shamrock Island for the colder season (fall).

Radium-224 does not show a significant difference by event (Appendix 4, Figure 14); however, radium-226 does show a significant difference by event with January samples being elevated relative to July and November/December samples. November/December Ra-226 samples have the smallest variation in concentrations (Appendix 4, Figure 15). Thus, as with radon measurements, a higher groundwater discharge may occur during the colder season.

Stable Isotopes

Average $\delta^{18}\text{O}$ and δD concentrations are elevated in summer relative to fall and winter. Additionally, $\delta^{18}\text{O}$ and δD concentrations in porewater are elevated relative to surface waters in fall and winter, but not in summer (Appendix 4, Figures 16 & 17).

Average $\delta^{13}\text{C}$ concentrations in porewater are consistently more negative than surface waters, with the most negative values in fall and the least negative values in winter. This same trend is seen when looking solely at the surface waters, with the fall and summer values being 2-3 times more negative than the winter values (Appendix 4, Figure 18). Given that groundwater is characterized by more depleted (i.e. negative) signatures, this further shows that groundwater is

likely to have a higher contribution to surface waters during the colder late fall and winter seasons.

Principal Component Factor Analysis

A Principal Component Factor Analysis of all variables with less than 10% of the data missing reveals 5 principal components (eigen values > 1) account for approximately 71% of the variation in the dataset. Only the first two factors are discussed below as they seem to show the most significant correlations among variables. Factors 1 and 2 account for the greatest proportion of the variation in the dataset at 32% and 18%, respectively (Appendix 4, Table 1 and Figure 19). Factor 1 shows an inverse relationship between temperature, conductivity, Mg, K, SO₄, Cl, DOC, DIC, δ¹⁸O, δD and δ¹³C. Based on groundwater characteristics for the shallow aquifer in this area and other analyses presented in this report, these variables are likely correlated with a groundwater component. Factor 2 indicates an inverse relationship between TDN, NH₄, and PO₄ and pH likely showing the biological impacts on water characteristics.

SUMMARY

A significant observation of this study, consistent across all three seasons in which sampling occurred (winter, summer, fall), was that inorganic nutrient and chlorophyll-*a* concentrations were consistently low throughout the water column. Others have noted that estuaries of the south-central Texas coast are subjected to riverine nutrient pulses only during significant rain events, and function on recycled nutrients in between these events. Our results are consistent with these previous findings, yet data collected in this study also points to groundwater as a potential source of nutrients that has not been previously quantified in these systems.

Statistical analyses show that *chlorophyll-a* concentrations are highest in summer and lowest in winter in surface waters. Ammonia concentrations are consistently one to two orders of magnitude greater in the porewater than in the surface waters, with the greatest concentrations in fall, 254.5 $\mu\text{mol/L}$, and the lowest concentrations in winter, 57.1 $\mu\text{mol/L}$. Additionally, in the surface water, the bottom samples show higher concentrations of NH_4 than middle samples in all seasons and surface samples in winter and fall. This hints at the groundwater as source of nutrients to surface water during the colder seasons. Summer shows the lowest concentrations of nitrate + nitrite in all sample depths, which is consistent with the more elevated summer chlorophyll- α concentrations and therefore uptake during biomass production. Porewater nitrate + nitrite concentrations in winter are almost an order of magnitude higher than in surface waters. Nitrite concentrations are consistently elevated in porewater compared to surface samples, with the greatest concentrations in winter, 0.51 $\mu\text{mol/L}$ and do not show large variations in surface water by season. Total Dissolved Nitrogen concentrations are consistently an order of magnitude greater in porewater than in surface waters, with the greatest concentrations in fall and the lowest

concentrations in winter and are more elevated in the surface waters in summer relative to fall and winter.

Similar to NH_4 , nitrite, and TDN, phosphate concentrations in porewater are consistently an order of magnitude greater than in surface waters, with the highest concentrations in fall, $7.05\ \mu\text{mol/L}$, and the lowest concentrations in winter, $2.11\ \mu\text{mol/L}$. In surface waters, phosphate concentrations are elevated in fall relative to summer and winter which could be related to the higher groundwater input as indicated by both resistivity and radon SGD fluxes. Furthermore, average SiO_4 concentrations in porewater are also consistently an order of magnitude greater in porewater than in surface water, with the highest concentrations in fall, $192.35\ \mu\text{mol/L}$, and the lowest concentrations in winter, $67.78\ \mu\text{mol/L}$. Surface water concentrations are greatest in summer, almost twice fall concentration and three times winter concentrations.

In addition, radon-222 concentrations in porewater were also consistently an order of magnitude greater than concentrations in surface waters, with average summer porewater concentrations being $138\ \text{Bq/m}^3$ and $185\ \text{Bq/m}^3$ greater than the average concentrations in fall and winter, respectively. In surface waters, the winter average Rn-222 concentrations are almost twice those in fall and summer which could be indication that SGD rates are higher in winter than in fall or summer. Given that SGD fluxes determined from continuous radon measurements at Oso Inlet and Shamrock Island are greater during late fall, it is likely that groundwater discharge rates are greater during the colder season (late fall and winter). Furthermore, while radium-224 does not show a significant difference by event, radium-226 is also more elevated in winter compared to late fall. Thus, both radon and radium measurements indicate that a higher groundwater discharge may occur during the colder season.

Average $\delta^{18}\text{O}$ and δD ratio abundances are elevated/enriched in summer relative to fall and winter which reflect the effect of evaporation due to exposure to high temperature and winds. Additionally, $\delta^{18}\text{O}$ and δD ratios in porewater are more enriched relative to surface waters in fall and winter, but more depleted (mostly negative) in summer. Average $\delta^{13}\text{C}$ abundances in porewater are consistently more negative (i.e. depleted) than surface waters, with the most depleted ratios in fall and the least depleted ratios in winter. This same trend is evident when looking solely at the surface waters, with the fall and summer ratios being 2-3 times more depleted than the winter ones. Given that groundwater is characterized by more depleted (i.e. negative) signatures, this further shows that groundwater is likely to have a higher contribution to surface waters during the colder- late fall and winter- seasons.

Furthermore, the Principal Component Factor Analysis indicate the likely occurrence of two main factors influencing the chemistry of the waters. Factor 1 shows an inverse relationship between temperature, conductivity, Mg, K, SO_4 , Cl, DOC, DIC, $\delta^{18}\text{O}$, δD and $\delta^{13}\text{C}$ which are likely correlated with a groundwater source. Factor 2 indicates an inverse relationship between TDN, NH_4 , and PO_4 and pH likely showing the biological impacts on water characteristics.

Similar to the above-mentioned results, groundwater fluxes determined as part of this study are also indicative of a strong groundwater component that needs to be considered on estimating nutrient budgets for the Corpus Christi Bay system. Average groundwater fluxes, measured using time-lapse ER measurements and continuous ^{222}Rn , ranged from 1.1 to 5.7 $\text{m}^3/\text{m.d}$ in summer and from 1.5 to 9.7 $\text{m}^3/\text{m.d}$ in fall. Measured SGD rates and nutrient concentrations were used to calculate nutrient loads discharged into the study area. The estimates suggest that SGD delivers a dissolved inorganic nitrogen (DIN) load of 1.326 mol/day, 5.5 mol/day of DOC, 1.329 mol/day TDN, 1.4 mol/day silicate, and a 0.09 mol/day load of $\text{PO}(4)$ per meter of bottom sediment into

the Bay of Corpus Christi during summer. By late fall the estimated nutrient loads increase by an order of magnitude and are as follows: (DIN) load of 16.22 mol/day, 32.48 mol/day of DOC, 22.02 mol/day TDN, 5.03 mol/day silicate, and a 0.3 mol/day load of PO(4) per meter of bottom sediment.

The identified potential SGD sites correlate well with the location of the hypoxia occurrence in the Corpus Christi Bay. Thus, it is likely that the influence of porewaters on water column nutrient concentrations and microbial respiration, although patchy, is significant in these systems, at least under the environmental conditions in which our sampling regime took place. Because the ER and stable and radiogenic isotopes show the high hydrogeologic and hydrologic “heterogeneity” of the investigated systems, further investigations are necessary to better characterize the system to project input loads to the entire Corpus Christi Bay system. Furthermore, more research is necessary to clarify what is the nutrient contribution of Oso Bay to the Corpus Christi Bay. It is likely that groundwater can have an indirect contribution to nutrient loading to Corpus Christi Bay through discharge upstream into Oso Bay. This research also shows that the Upper Laguna Madre is significantly influenced by groundwater discharge which could potentially trigger the brown tide outbreaks. This study indicates that SGD may have a large impact on the biogeochemical cycles of the Corpus Christi Bay system, including Upper Laguna Madre.

REFERENCES

- AGI (2013). Advanced Geosciences Inc. Marine System. 2015, from <http://www.agiusa.com/marinesystem.shtml>
- Alexander, H. D., & Dunton, K. H. (2006). Treated wastewater effluent as an alternative freshwater source in a hypersaline salt marsh: Impacts on salinity, inorganic nitrogen, and emergent vegetation. *Journal of Coastal Research*, 22(2), 377-392. doi: 10.2112/04-0234.1
- Aller, R. C., & Benninger, L. K. (1981). Spatial and Temporal Patterns of Dissolved Ammonium, Manganese, and Silica Fluxes from Bottom Sediments of Long-Island-Sound, USA. *Journal of Marine Research*, 39(2), 295-314.
- Armstrong, N. E., Brody, M. S., Funicelli, N., & National Wetlands Research Center (U.S.). (1987). *The ecology of open-bay bottoms of Texas : a community profile*. Washington, DC: U.S. Dept. of the Interior, Fish and Wildlife Service, Research and Development, National Wetlands Research Center.
- Ashworth, J. B. & Hopkins, J. (1995). *Major and minor aquifers of Texas*. (Report 345).
- Behrens, E. W., & Watson, R. L. (1973). *Corpus Christi Water Exchange Pass: a Case History of Sedimentation and Hydraulics During its First Year*. (DACW 72-72-C-0026). USDA 1992.
- Bighash, P., & Murgulet, D. (2015). Application of factor analysis and electrical resistivity to understand groundwater contributions to coastal embayments in semi-arid and hypersaline coastal settings. *Science of the Total Environment*, 532, 688-701.
- Board, T. W. D. (2015). Precipitation & Lake Evaporation Data. 2015, from <http://www.twdb.texas.gov/surfacewater/conditions/evaporation/>
- Bowie, A. R., Achterberg, E. P., Sedwick, P. N., Ussher, S., & Worsfold, P. J. (2002). Real-time monitoring of picomolar concentrations of iron(II) in marine waters using automated flow injection-chemiluminescence instrumentation. *Environmental Science & Technology*, 36(21), 4600-4607. doi: 10.1021/es020045v
- Boyd, P. W., Watson, A. J., Law, C. S., Abraham, E. R., Trull, T., Murdoch, R., . . . Zeldis, J. (2000). A mesoscale phytoplankton bloom in the polar Southern Ocean stimulated by iron fertilization. *Nature*, 407(6805), 695-702. doi: Doi 10.1038/35037500
- Breier, J. A., Breier, C. F., & Edmonds, H. N. (2010). Seasonal dynamics of dissolved Ra isotopes in the semi-arid bays of south Texas. *Marine Chemistry*, 122(1-4), 39-50. doi: 10.1016/j.marchem.2010.08.008
- Brown, R., McClelland, N., Deininger, R., & Tozer, R. (1970). A water quality index—do we dare? *Proceedings, National Symposium on Data and Instrumentation for Water Quality Management, Volume 117*, 339-343.
- Burdige, D. J., Dhakar, S. P., & Nealson, K. H. (1992). Effects of Manganese Oxide Mineralogy on Microbial and Chemical Manganese Reduction. *Geomicrobiology Journal*, 10(1), 27-48.

- Burnett, W. C., & Dulaiova, H. (2003). Estimating the dynamics of groundwater input into the coastal zone via continuous radon-222 measurements. *Journal of Environmental Radioactivity*, 69(1-2), 21-35. doi: 10.1016/S0265-931x(03)00084-5
- Burnett, W. C., Lambert, M., & Dulaiova, H. (2001). Tracing groundwater discharge into the ocean via continuous radon-222 measurements. *Oceans 2001 Mts/Ieee: An Ocean Odyssey, Vols 1-4, Conference Proceedings*, 251-255.
- Buskey, E. J., Stewart, J., Peterson, J., & Collumb, C. (1996). *Current status and historical trends of brown tide and red tide phytoplankton blooms in the Corpus Christi Bay National Estuary Program study area*. (CCBNEP-07 174). Austin, TX.
- Cable, J. E., Martin, J. B., Swarzenski, P. W., Lindenberg, M. K., & Steward, J. (2004). Advection Within Shallow Pore Waters of a Coastal Lagoon, Florida. *Ground Water*, 42(7), 1011-1020. doi: 10.1111/j.1745-6584.2004.tb02640.x
- Cardenas, M. B., Zamora, P. B., Siringan, F. P., Lapus, M. R., Rodolfo, R. S., Jacinto, G. S., . . . Senal, M. I. (2010). Linking regional sources and pathways for submarine groundwater discharge at a reef by electrical resistivity tomography, Rn-222, and salinity measurements. *Geophysical Research Letters*, 37. doi: 10.1029/2010gl044066
- Church, T. M. (1996). An underground route for the water cycle. *Nature*, 380(6575), 579-580. doi: 10.1038/380579a0
- Coale, K. H., Johnson, K. S., Fitzwater, S. E., Gordon, R. M., Tanner, S., Chavez, F. P., . . . Kudela, R. (1996). A massive phytoplankton bloom induced by an ecosystem-scale iron fertilization experiment in the equatorial Pacific Ocean. *Nature*, 383(6600), 495-501. doi: 10.1038/383495a0
- Corbett, D. R., Dillon, K., Burnett, W., & Chanton, J. (2000). Estimating the groundwater contribution into Florida Bay via natural tracers, Rn-222 and CH₄. *Limnology and Oceanography*, 45(7), 1546-1557.
- Craig, H., 1961, Isotopic variations in meteoric waters: *Science*, v. 133, p. 1,702–1,703
- Craig, H., Gordon, L.I., and Horie, Y. (1963). Isotopic exchange effects in the evaporation of water: 1. Low temperature results. *J. Geophys. Res.* 68: 5079-5087.
- de Baar, H. J. W., de Jong, J. T. M., Nolting, R. F., Timmermans, K. R., van Leeuwe, M. A., Bathmann, U., . . . Sildam, J. (1999). Low dissolved Fe and the absence of diatom blooms in remote Pacific waters of the Southern Ocean. *Marine Chemistry*, 66(1-2), 1-34. doi: Doi 10.1016/S0304-4203(99)00022-5
- Dimova, N. T., Burnett, W. C., Chanton, J. P., & Corbett, J. E. (2013). Application of radon-222 to investigate groundwater discharge into small shallow lakes. *Journal of Hydrology*, 486, 112-122. doi: 10.1016/j.jhydrol.2013.01.043
- Dimova, N. T., Burnett, W. C., & Speer, K. (2011). A natural tracer investigation of the hydrological regime of Spring Creek Springs, the largest submarine spring system in Florida. *Continental Shelf Research*, 31(6), 731-738. doi: 10.1016/j.csr.2011.01.010
- Dimova, N. T., Swarzenski, P. W., Dulaiova, H., & Glenn, C. R. (2012). Utilizing multichannel electrical resistivity methods to examine the dynamics of the fresh water-seawater

- Dulaiova, H., Burnett, W.C., Chanton, J.P., Moore, W.S., Bokuniewicz, H.J., Charette, M.A., Sholkovitz, E., 2006. Assessment of groundwater discharge into West Neck Bay, New York, via natural tracers. *Continental Shelf Research* 26 (16), 1971–1983
- interface in two Hawaiian groundwater systems. *Journal of Geophysical Research-Oceans*, 117. doi: 10.1029/2011jc007509
- EPA, U. (1999). *Ecological condition of estuaries in the Gulf of Mexico*. (EPA 620-R-98-004). National Health and Environmental Effects Research Laboratory, Gulf Ecology Division, Gulf Breeze, Florida.
- Friedel, S. (2003). Resolution, stability and efficiency of resistivity tomography estimated from a generalized inverse approach. *Geophysical Journal International*, 153(2), 305-316. doi: DOI 10.1046/j.1365-246X.2003.01890.x
- Geophysics, U. O. o. G. B. o. (2013). Continuous Resistivity Profiling. Retrieved 9/1/2015, 2015, from <http://water.usgs.gov/ogw/bgas/crp/>
- Gran, H. H. (1931). On the conditions for the production of plankton in the sea. *Rapports et Procès-Verbaux des Réunions du Conseil International Permanent pour l'Exploration de la Mer*, 75, 37-46.
- Greenwood, W. J., Kruse, S., & Swarzenski, P. (2006). Extending electromagnetic methods to map coastal pore water salinities. *Ground Water*, 44(2), 292-299. doi: 10.1111/j.1745-6584.2005.00137.x
- Grossman, E. L. (2002). Stable Carbon isotopes as indicators of microbial activity in aquifers. *American Society for Microbiology Press*, 565-575.
- Guo, W., Langevin, C. D., & Geological Survey (U.S.). (2002). *User's guide to SEAWAT : a computer program for simulation of three-dimensional variable-density ground-water flow*. Tallahassee, Fla.
- Johnson, T. C., Versteeg, R. J., Rockhold, M., Slater, L. D., Ntarlagiannis, D., Greenwood, W. J., & Zachara, J. (2012). Characterization of a contaminated wellfield using 3D electrical resistivity tomography implemented with geostatistical, discontinuous boundary, and known conductivity constraints. *Geophysics*, 77(6), En85-En96. doi: 10.1190/Geo2012-0121.1
- Kennish, M. J. (1997). *Practical handbook of estuarine and marine pollution*. Boca Raton: CRC Press.
- Khan, M. N., & Kumar, R. A. (2012). Interpretation of groundwater quality using correlation and linear regression analysis from Tiruchengode taluk, Namakkal district, Tamilnadu, India. *Journal of Chemical and Pharmaceutical Research*, 4(10), 4214-4521.
- Kim, H. C., & Montagna, P. A. (2012). Effects of climate-driven freshwater inflow variability on macrobenthic secondary production in Texas lagoonal estuaries: A modeling study. *Ecological Modelling*, 235, 67-80. doi: 10.1016/j.ecolmodel.2012.03.022

- Lee, M. W., & Collett, T. S. (2006). Gas hydrate and free gas saturations estimated from velocity logs on Hydrate Ridge, offshore Oregon, USA. *Proc. Ocean Drill. Program Sci. Results*, 204, 1-25. doi: 10.2973
- Longley, W. L., Powell, G. L., Green, A. W., & Texas Water Development Board. (1994). *Freshwater inflows to Texas bays and estuaries : ecological relationships and methods for determination of needs*. Austin, TX: Texas Water Development Board.
- MacIntyre, S., Wanninkhoe, R., & Chanton, J. P. (1995). Trace gas exchange across the air-water interface in freshwaters and coastal marine environments. 52-57.
- Martin, J. H., Coale, K. H., Johnson, K. S., Fitzwater, S. E., Gordon, R. M., Tanner, S. J., . . . Tindale, N. W. (1994). Testing the Iron Hypothesis in Ecosystems of the Equatorial Pacific-Ocean. *Nature*, 371(6493), 123-129. doi: 10.1038/371123a0
- Matson, E. A., & Brinson, M. M. (1985). Sulfate Enrichments in Estuarine Waters of North-Carolina. *Estuaries*, 8(3), 279-289. doi: Doi 10.2307/1351488
- Michaelis, W., Seifert, R., Nauhaus, K., Treude, T., Thiel, V., Blumenberg, M., . . . Gulin, M. B. (2002). Microbial reefs in the Black Sea fueled by anaerobic oxidation of methane. *Science*, 297(5583), 1013-1015. doi: DOI 10.1126/science.1072502
- Montagna, P. A., & Froeschke, J. (2009). Long-term biological effects of coastal hypoxia in Corpus Christi Bay, Texas, USA. *Journal of Experimental Marine Biology and Ecology*, 381, S21-S30. doi: 10.1016/j.jembe.2009.07.006
- Montagna, P. A., & Ritter, C. (2006). Direct and indirect effects of hypoxia on benthos in Corpus Christi Bay, Texas, USA. *Journal of Experimental Marine Biology and Ecology*, 330(1), 119-131. doi: 10.1016/j.jembe.2005.12.021
- Mook, W. G. (2000). *Environmental Isotopes in the Hydrological Cycle: Principles and Applications*. Vienna (2000).
- Moore, W. S. (1996). Large groundwater inputs to coastal waters revealed by Ra-226 enrichments. *Nature*, 380(6575), 612-614. doi: Doi 10.1038/380612a0
- Moore, W. S. (2000). Determining coastal mixing rates using radium isotopes. *Continental Shelf Research*, 20(15), 1993-2007. doi: Doi 10.1016/S0278-4343(00)00054-6
- Morehead, S., Montagna, P., & Kennicutt, M. C. (2008). Comparing fixed-point and probabilistic sampling designs for monitoring the marine ecosystem near McMurdo Station, Ross Sea, Antarctica. *Antarctic Science*, 20(5), 471-484. doi: 10.1017/S0954102008001326
- Morell, I., Gimenez, E., & Esteller, M. V. (1996). Application of principal components analysis to the study of salinization on the Castellon Plain (Spain). *Science of the Total Environment*, 177, 161-171. doi: 10.1016/0048-9697(95)04893-6
- Murgulet, D., & Tick, G. R. (2015). Nitrate Flux to Coastal Waters in Response to Variable-Density Groundwater Flow. . *Journal of Hydrological Processes [In Press]*
- Murray, J. (2004). Major Ions of Seawater. 2015, from http://www.ocean.washington.edu/courses/oc400/Lecture_Notes/CHPT4.pdf

- Nelson, K. M., P. A. (2009). Causes and Monitoring of Hypoxia in Corpus Christi Bay. Coastal Bend Bays & Estuaries Program.
- Ni, S. B., W. C., Eller, K. T., Macintyre, H. L., Mortazavi, B., Liefer, J. D., & Novoveska, L. (2011). Radon and Radium isotopes, groundwater discharge and harmful algal blooms in Little Lagoon, Alabama. *Interdisciplinary Studies on Environmental Chemistry- Environmental Pollution and Ecotoxicology*, 329-337.
- NOAA. (2014). National Oceanic and Atmospheric Administration's, National Weather Service. 2015, from <http://www.ncdc.noaa.gov>
- Nyquist, J. E., Freyer, P. A., & Toran, L. (2008). Stream bottom resistivity tomography to map ground water discharge. *Ground Water*, 46(4), 561-569. doi: 10.1111/j.1745-6584.2008.00432.x
- Palmer, T. A., Montagna, P. A., Pollack, J. B., Kalke, R. D., & DeYoe, H. R. (2011). The role of freshwater inflow in lagoons, rivers, and bays. *Hydrobiologia*, 667(1), 49-67. doi: 10.1007/s10750-011-0637-0
- Parashiva Murthy, A. S., & Ferrell, R. E., Jr. (1972). Distribution of major cations in estuarine sediments. *Clays and Clay Minerals*, 21, 161-165.
- Pathak, H. (2012). Valuation of ground water quality using multiple linear regression and mathematical equation modeling. *Annals of the University of Oradea—Geography Series*, 2, 304-307.
- Procedures, R. S. O. (2009). *Protocol for Groundwater/Surface Water Interface Sampling Using a Pore Water Sampler*.
- Ritter, C., & Montagna, P. A. (1999). Seasonal hypoxia and models of benthic response in a Texas bay. *Estuaries*, 22(1), 7-20. doi: Doi 10.2307/1352922
- Samouelian, A., Cousin, I., Tabbagh, A., Bruand, A., & Richard, G. (2005). Electrical resistivity survey in soil science: a review. *Soil & Tillage Research*, 83(2), 173-193. doi: 10.1016/j.still.2004.10.004
- Schippers, A., & Jorgensen, B. B. (2001). Oxidation of pyrite and iron sulfide by manganese dioxide in marine sediments. *Geochimica Et Cosmochimica Acta*, 65(6), 915-922. doi: Doi 10.1016/S0016-7037(00)00589-5
- Slopp, C. P., Malschaert, J. F. P., Lohse, L., & VanRaaphorst, W. (1997). Iron and manganese cycling in different sedimentary environments on the North Sea continental margin. *Continental Shelf Research*, 17(9), 1083-1117. doi: 10.1016/S0278-4343(97)00005-8
- Stanford. Major Ions, Conservative Elements and Dissolved Gases in Seawater Retrieved 9/1/2015, 2015, from http://ocean.stanford.edu/courses/bomc/chem/lecture_04.pdf
- Stevens, J. D., Sharp, J. M., Simmons, C. T., & Fenstermaker, T. R. (2009). Evidence of free convection in groundwater: Field-based measurements beneath wind-tidal flats. *Journal of Hydrology*, 375(3-4), 394-409. doi: 10.1016/j.jhydrol.2009.06.035
- Thareja, S., Choudhury, S., & Trivedi, P. (2011). Assessment of water quality of Ganga River in Kanpur by using principal components analysis. *Advances in Applied Science Research*, 2(5), 84-911.

- Voudouris, K., Panagopoulos, A., & Koumantakis, J. (2000). Multivariate statistical analysis in the assessment of hydrochemistry of the northern korinthia prefecture alluvial aquifer system (Peloponnese, Greece). *Natural Resources Research*, 9(2), 135-146.
- Waterstone. (2003). *Groundwater availability of the central Gulf Coast aquifer—Numerical simulations to 2050, Central Gulf Coast, Texas*. Texas Water Development Board, Austin, Texas, variously paginated.
- Wetz, M. S., Hayes, K. C., Fisher, K. V. B., Price, L., & Sterba-Boatwright, B. Water quality dynamics in an urbanizing subtropical estuary (Oso Bay, Texas) [In Review]. *Marine Pollution Bulletin*.
- White, P. A. (1988). Measurement of Groundwater Parameters Using Salt-Water Injection and Surface Resistivity. *Ground Water*, 26(2), 179-186. doi: 10.1111/j.1745-6584.1988.tb00381.x
- Wood, W. W. (1976). *Guidelines for collection and field analysis of ground-water samples for selected unstable constituents*. Techniques of Water Resources Investigation, Book 1, Ch D2: Retrieved from <http://pubs.usgs.gov/twri/twri1-d2/>.
- Yamada, S. S., & Delia, C. F. (1984). Silicic-Acid Regeneration from Estuarine Sediment Cores. *Marine Ecology Progress Series*, 18(1-2), 113-118. doi: Doi 10.3354/Meps018113
- Yoshinaga, M. Y., Holler, T., Goldhammer, T., Wegener, G., Pohlman, J. W., Brunner, B., . . . Elvert, M. (2014). Carbon isotope equilibration during sulphate-limited anaerobic oxidation of methane. *Nature Geoscience*, 7(3), 190.

TABLE LEGEND

Table 1. Average Radium and radon concentrations and water mass ages by sampling transect.

Table 2. Ratio of inorganic nitrogen (ammonium, N+N) to orthophosphate at the surface in January, July and November 2014

Sampled transects	Rn (Bq/cm ³)	²²⁶ Ra (dpm/m ³)	²²⁴ Ra (dpm/m ³)	²²⁴ Ra/ ²²⁶ Ra	Water Mass Age (days)
Winter 2014					
T1	138	--	--	--	--
T2	274	1098.9	--	--	--
T3	111	1386.9	--	--	--
T4	31	460.8	--	--	--
T5	57	--	--	--	--
Total average	122	982.2	--	--	--
Summer 2014					
T1	206	762.2	275.6	3.6	4.4
T2	358	1004.2	267.2	8.9	2.1
T3	137	483.5	190.3	3.5	4.4
T4	99	612.0	200.1	7.4	-8.1
T5	104	--	--	--	--
Total average	181	715.5	233.3	5.9	0.7
Fall 2014					
T1	37	831.9	367.2	2.3	2.3
T2	51	420.3	419.6	1.7	1.0
T3	113	372.8	320.6	1.3	1.2
T4	91	369.6	354.1	1.5	1.0
T5	296	--	--	--	--
Total average	118	498.6	365.4	1.7	1.4

Table 1.

Date	Transect #	DIN:DIP
January/Winter	1	45
	2	15
	3	28
	4	9
	5	16
July/Summer	1	10
	2	18
	3	19
	4	9
	5	19
November/December (Fall)	1	22
	2	20
	3	8
	4	5
	5	8

Table 2.

FIGURE LEGEND

Figure 1. Study area and sampling sites and transects location.

Figure 2. Study area soil types.

Figure 3. Monthly mean precipitation depths for 2014. Arrows indicate sampling and resistivity data collection months.

Figure 4. Image showing the continuous recording and storing of data from a GPS receiver using the SuperSting Marine. Figure 4. The SuperSting Marine continuously records and stores data from a GPS receiver. Current is injected every 3 seconds and 8 apparent resistivity values representing 8 depth levels are read for each current injection. Depth of penetration depends on length of the cable and array type (typically approximately 20% of the electrode spread length) (Advanced Geosciences, Inc.).

Figure 5. Conceptual model showing the radon inventory per unit area for estimating groundwater discharge (Burnett and Dulaiova, 2003).

Figure 6. Average radon and ER discharge fluxes (cm/d) and SGD rates ($\text{m}^3/\text{m.d}$) for all three flux monitoring stations.

Figure 7. Average ^{222}Rn concentrations by sampling transect sampling event.

Figure 8. Average ^{224}Ra (a) and ^{226}Ra (b) by sampling transect sampling event.

Figure 9. Water mass ages displayed by sampling transect and event. Note that ages are not available for the winter event.

Figure 10. Relationship between mass ratios of sulfate to chlorinity (SO_4/Cl) and chloride (mg/L).

Figure 11. Relationship between mass ratios of magnesium to chlorinity (Mg/Cl) and chloride (mg/L). The horizontal line represents the typical seawater Mg/Cl ratio at 35 parts per million salinity.

Figure 12. Relationship between mass ratios of potassium to chlorinity (K/Cl) and chloride (mg/L). The horizontal line represents the typical seawater K/Cl ratio at 35 parts per million salinity.

Figure 13. Relationship between mass ratios of calcium to chlorinity (Ca/Cl) and chloride (mg/L). The horizontal line represents the typical seawater Ca/Cl ratio at 35 parts per million salinity.

Figure 14. Relationship between mass ratios of sodium to chlorinity (Na/Cl) and chloride (mg/L). The horizontal line represents the typical seawater Na/Cl ratio at 35 parts per million salinity.

Figure 15. Distribution of Iron concentrations (mg/L) by season. Number of samples start with transect one and end with transect five in chronological order.

Figure 16. Distribution of manganese concentrations (mg/L) by season. Number of samples start with transect one and end with transect five in chronological order.

Figure 17. Cross-correlation of $\delta^{13}\text{C}$ (‰ PDB) with DIC ($\mu\text{mol/L}$) for winter, summer, and fall 2014. Blue lines represent intervals associated with the $\delta^{13}\text{C}$ signatures of different water types.

Figure 18. Typical $\delta^{13}\text{C}$ signatures in nature. Note the enclosed areas representing potential sources of dissolved CO_2 in the investigated system.

Figure 19. Cross-correlation between $\delta^{18}\text{O}$ (‰ V-SMOW) and δD (‰ V-SMOW) showing the large variation of water signatures between each season and the more depleted $\delta^{18}\text{O}$ of porewaters. The meteoric waterlines from Waco (WMWL) and that of global precipitation from Craig (1961) (GMWL) are included.

Figure 20. Chlorophyll *a* concentration ($\mu\text{g/l}$) in surface (“S”) waters of Corpus Christi Bay and Laguna Madre, January 2014.

Figure 21. Ammonium concentration (μmol) in surface (“S”), mid water column (“M”), near bottom (“B”) and porewater (“P”) of Corpus Christi Bay and Laguna Madre, January 2014.

Figure 22. Spatial distribution of chlorophyll-*a* ($\mu\text{g/l}$) for winter 2014.

Figure 23. Nitrate + nitrite concentration (μmol) in surface (“S”), mid water column (“M”), near bottom (“B”) and porewater (“P”) of Corpus Christi Bay and Laguna Madre, January 2014.

Figure 24. Dissolved organic nitrogen concentration (μmol) in surface (“S”), mid water column (“M”), near bottom (“B”) and porewater (“P”) of Corpus Christi Bay and Laguna Madre, January 2014.

Figure 25. Orthophosphate concentration (μmol) in surface (“S”), mid water column (“M”), near bottom (“B”) and porewater (“P”) of Corpus Christi Bay and Laguna Madre, January 2014.

Figure 26. Silicate concentration (μmol) in surface (“S”), mid water column (“M”), near bottom (“B”) and porewater (“P”) of Corpus Christi Bay and Laguna Madre, January 2014.

Figure 27. Chlorophyll *a* concentration ($\mu\text{g/l}$) in surface (“S”), mid water column (“M”), near bottom (“B”) and porewater (“P”) of Corpus Christi Bay and Laguna Madre, July 2014.

Figure 28. Ammonium concentration (μmol) in surface (“S”), mid water column (“M”), near bottom (“B”) and porewater (“P”) of Corpus Christi Bay and Laguna Madre, July 2014.

Figure 29. Spatial distribution of chlorophyll-a ($\mu\text{g/l}$) for summer 2014.

Figure 30. Nitrate + nitrite concentration (μmol) in surface (“S”), mid water column (“M”), near bottom (“B”) and porewater (“P”) of Corpus Christi Bay and Laguna Madre, July 2014.

Figure 31. Orthophosphate concentration (μmol) in surface (“S”), mid water column (“M”), near bottom (“B”) and porewater (“P”) of Corpus Christi Bay and Laguna Madre, July 2014.

Figure 32. Silicate concentration (μmol) in surface (“S”), mid water column (“M”), near bottom (“B”) and porewater (“P”) of Corpus Christi Bay and Laguna Madre, July 2014.

Figure 33. Dissolved organic nitrogen concentration (μmol) in surface (“S”), mid water column (“M”), near bottom (“B”) and porewater (“P”) of Corpus Christi Bay and Laguna Madre, July 2014.

Figure 34. Chlorophyll *a* concentration ($\mu\text{g/l}$) in surface (“S”), mid water column (“M”), near bottom (“B”) and porewater (“P”) of Corpus Christi Bay and Laguna Madre, November 2014.

Figure 35. Ammonium concentration (μmol) in surface (“S”), mid water column (“M”), near bottom (“B”) and porewater (“P”) of Corpus Christi Bay and Laguna Madre, November 2014.

Figure 36. Spatial distribution of chlorophyll-a ($\mu\text{g/l}$) for fall 2014.

Figure 37. Nitrate + nitrite concentration (μmol) in surface (“S”), mid water column (“M”), near bottom (“B”) and porewater (“P”) of Corpus Christi Bay and Laguna Madre, November 2014.

Figure 38. Dissolved organic nitrogen concentration (μmol) in surface (“S”), mid water column (“M”), near bottom (“B”) and porewater (“P”) of Corpus Christi Bay and Laguna Madre, November 2014.

Figure 39. Orthophosphate concentration (μmol) in surface (“S”), mid water column (“M”), near bottom (“B”) and porewater (“P”) of Corpus Christi Bay and Laguna Madre, November 2014.

Figure 40. Silicate concentration (μmol) in surface (“S”), mid water column (“M”), near bottom (“B”) and porewater (“P”) of Corpus Christi Bay and Laguna Madre, November 2014.

Figure 41. Dissolved organic carbon concentration (μmol) in surface (“S”), mid water column (“M”), near bottom (“B”) and porewater (“P”) of Corpus Christi Bay and Laguna Madre, January 2014.

Figure 42. Dissolved organic carbon concentration (μmol) in surface (“S”), mid water column (“M”), near bottom (“B”) and porewater (“P”) of Corpus Christi Bay and Laguna Madre, July 2014.

Figure 43. Dissolved organic carbon concentration (μmol) in surface (“S”), mid water column (“M”), near bottom (“B”) and porewater (“P”) of Corpus Christi Bay and Laguna Madre, November 2014.

Figure 44. Nutrient Concentrations measured in porewater in summer (a) and fall (b) at groundwater monitoring stations. Summer ammonia concentration for the Laguna Madre was above the limit of detection and is assumed to be the same with the highest recorded concentration in porewater for the season. Fall ammonia concentrations were above the limit of detection and are assumed to be the same as in summer.

Figure 45. Groundwater nutrient fluxes by monitoring station for summer 2014.

Figure 46. Groundwater nutrient fluxes by monitoring station for fall 2014.

Figure 47. Total groundwater nutrient fluxes for summer and fall 2014.

Figure 48. Spatial distribution of average water column DO concentrations (mg/L) during winter 2014.

Figure 49. Minimum, maximum, and average DO concentrations for porewater and water column.

Figure 50. Spatial distribution of average water column DO concentrations (mg/L) during fall 2014.

Figure 51. Spatial distribution of average water column DO concentrations (mg/L) during summer 2014.

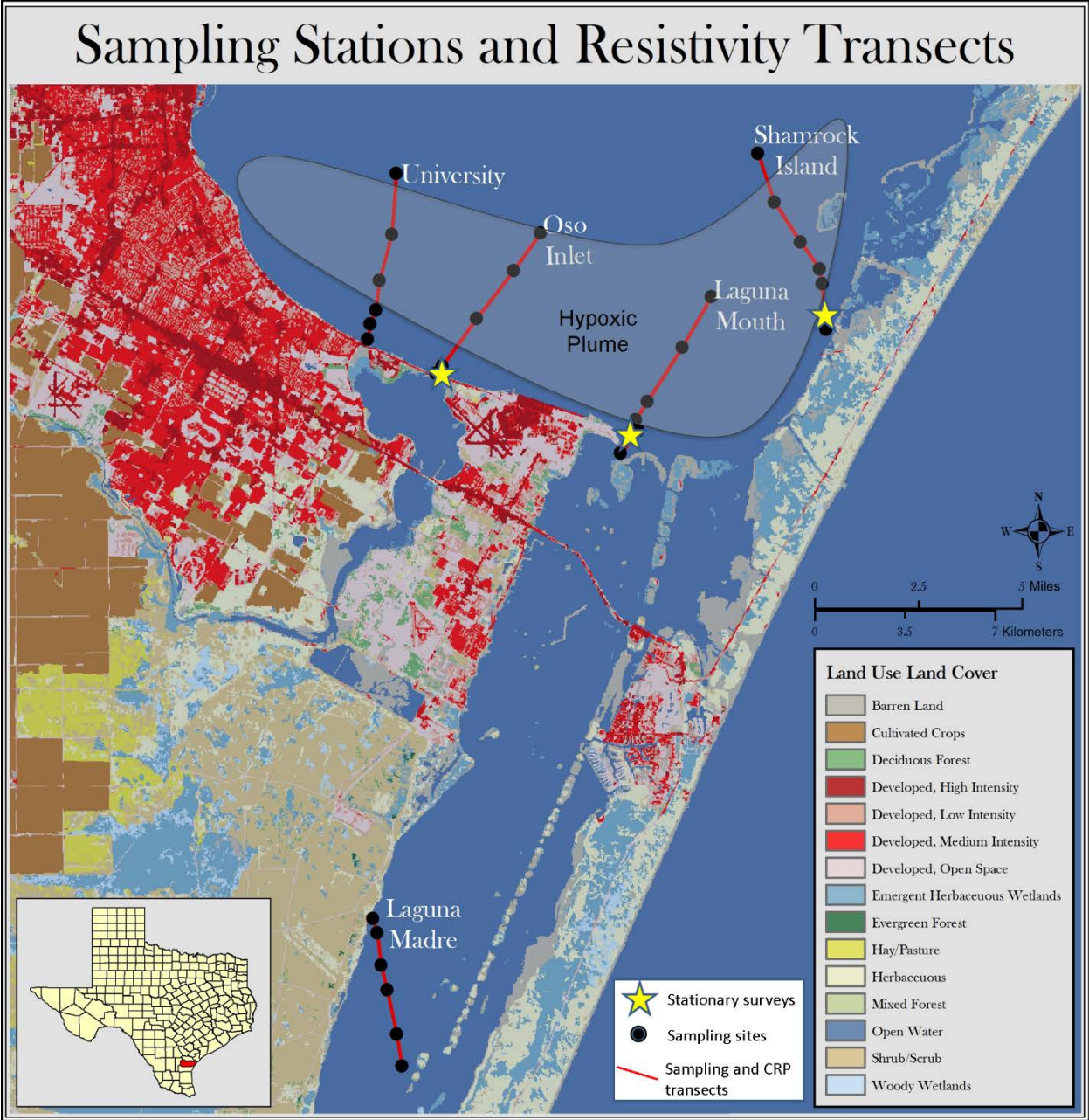


Figure 1.

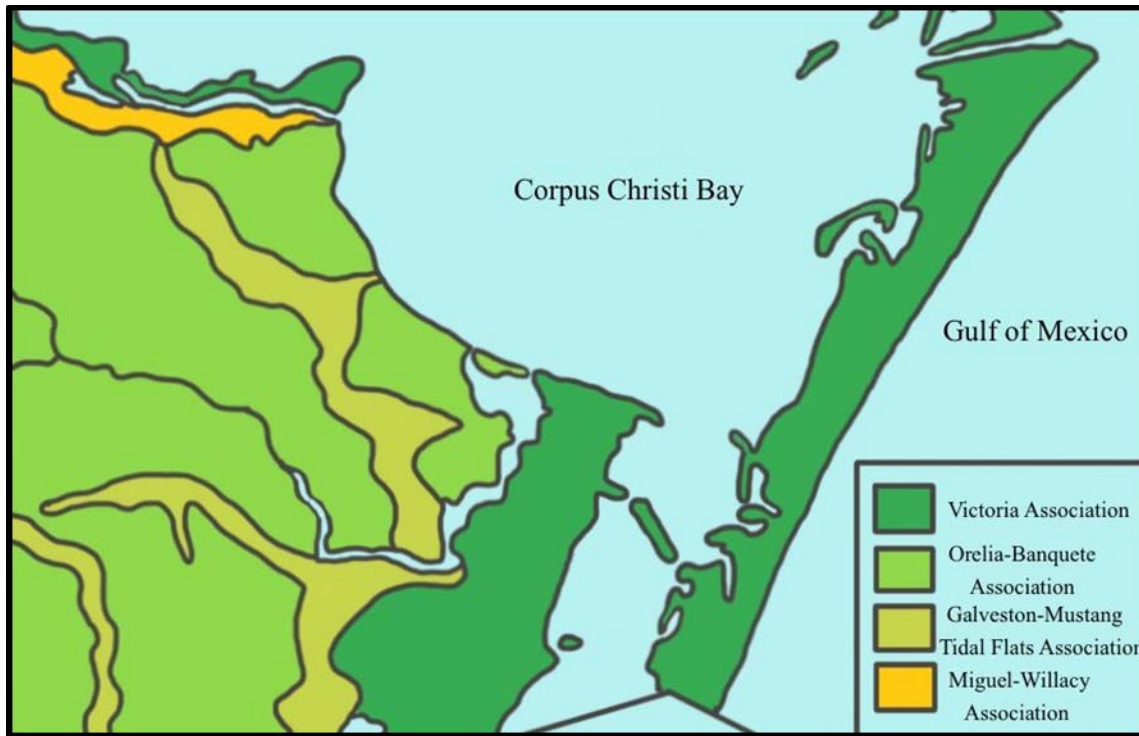


Figure 2.

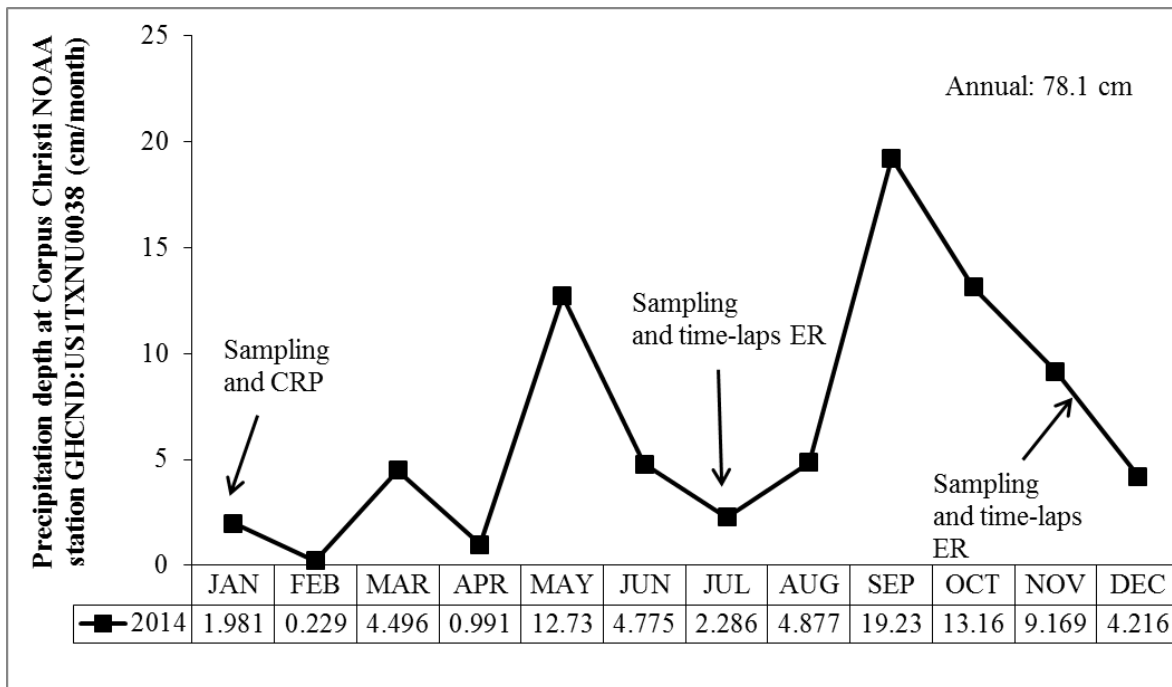


Figure 3.

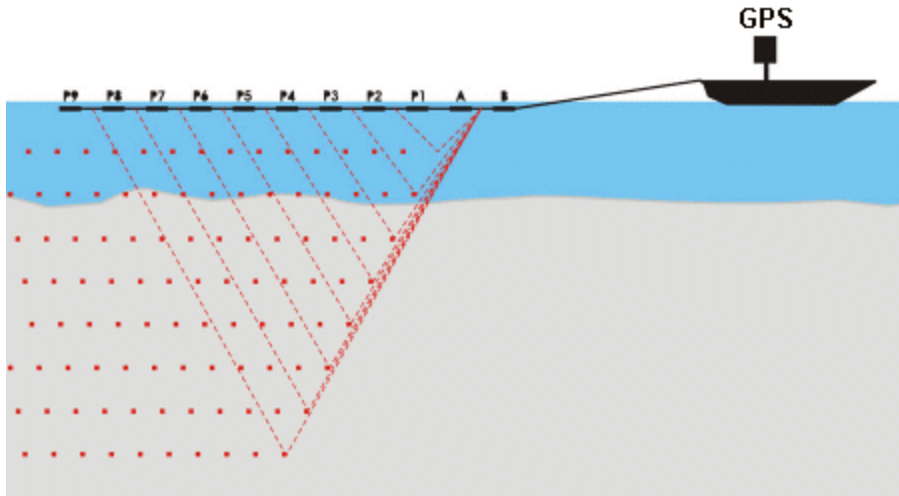


Figure 4.

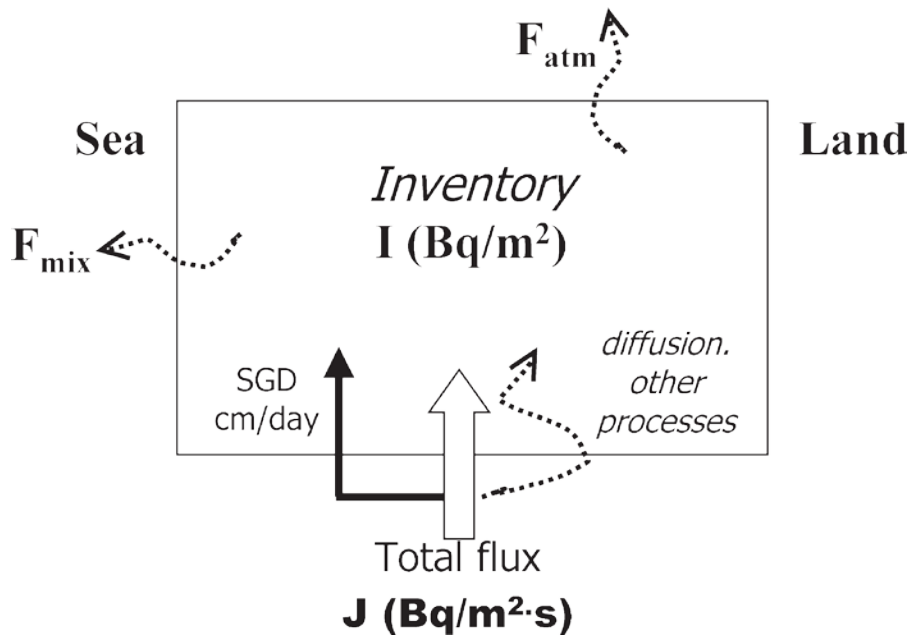


Figure 5.

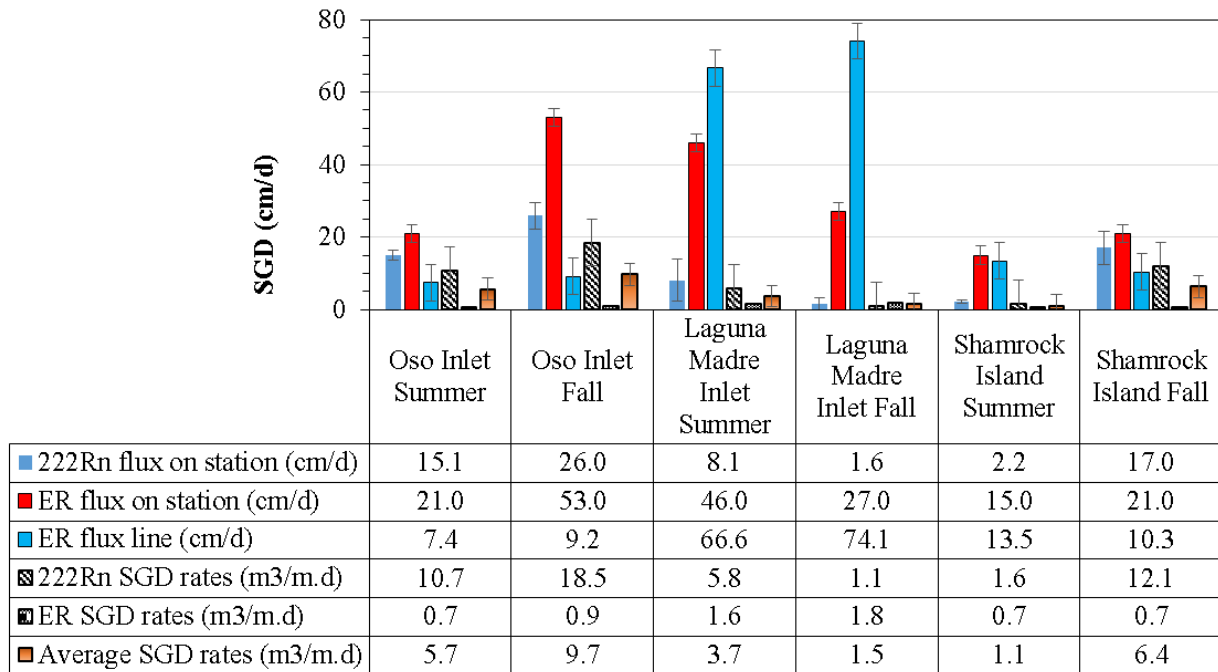


Figure 6.

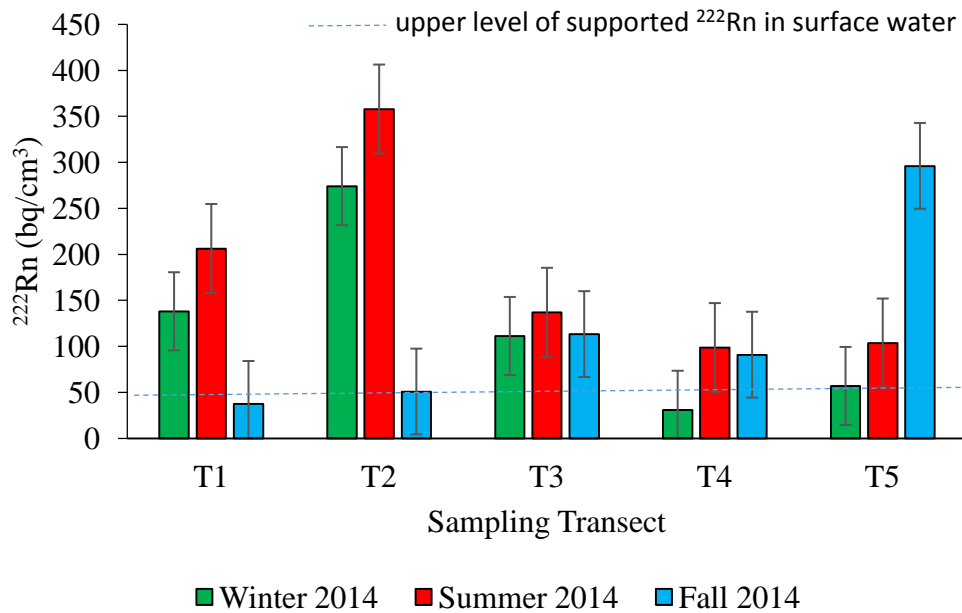


Figure 7.

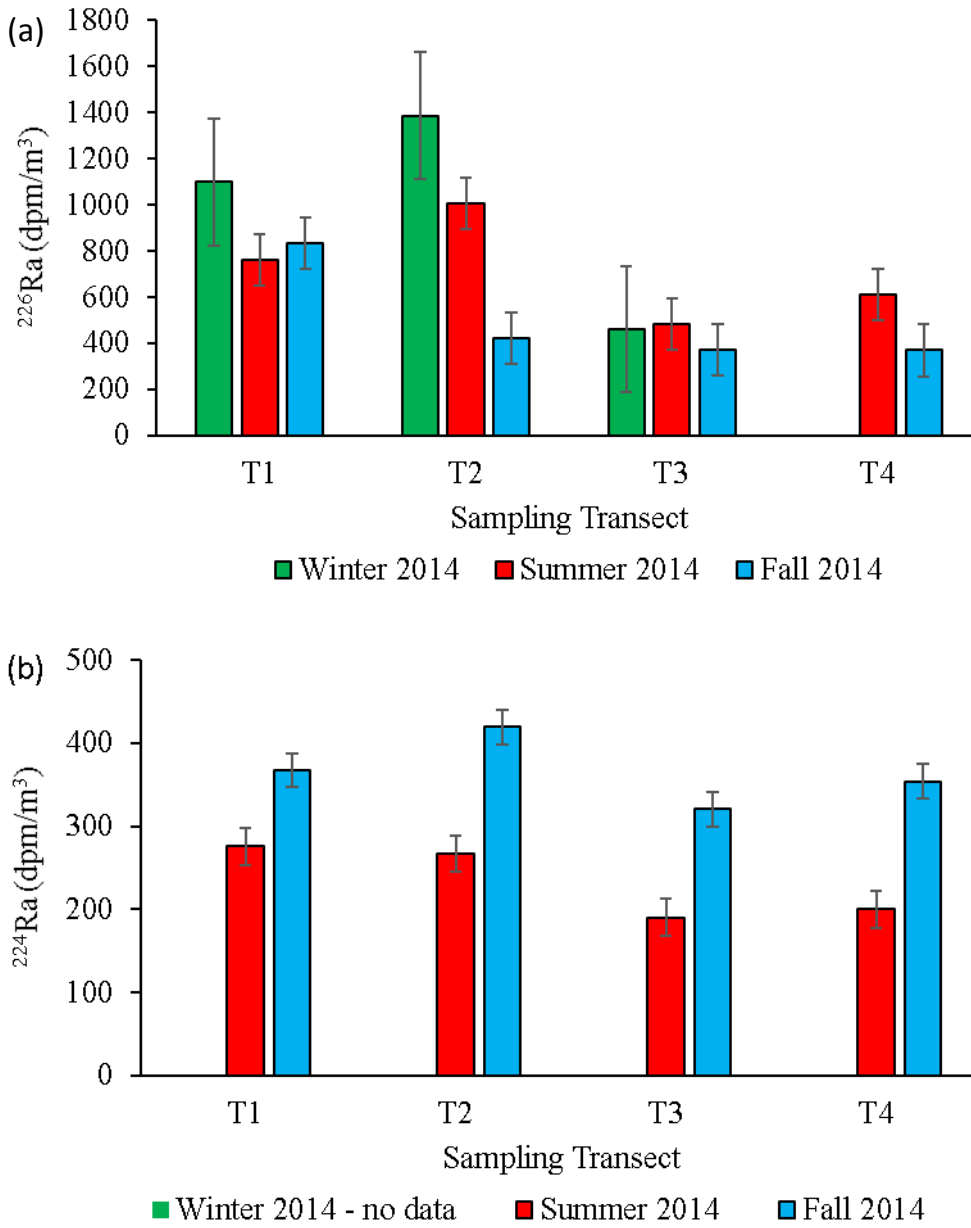


Figure 8.

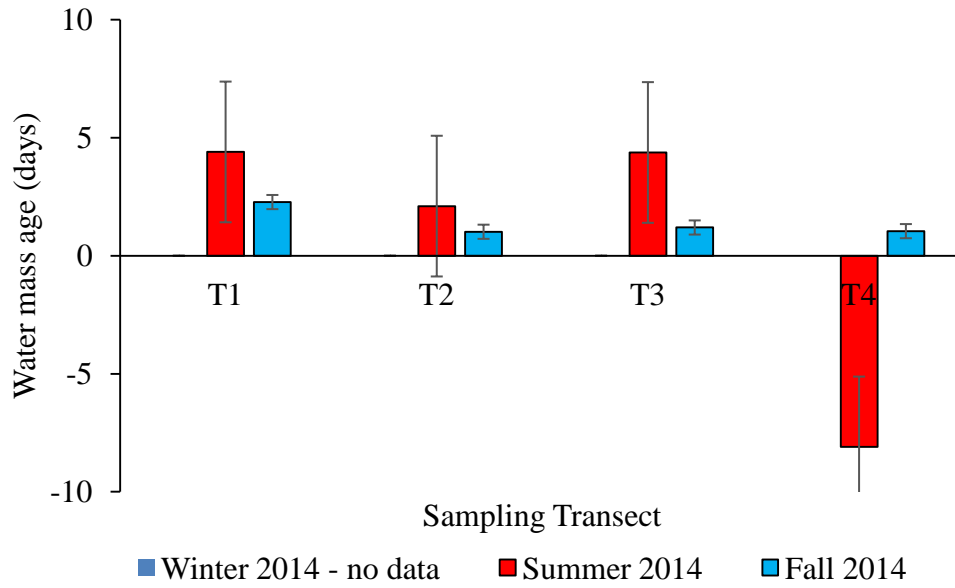


Figure 9.

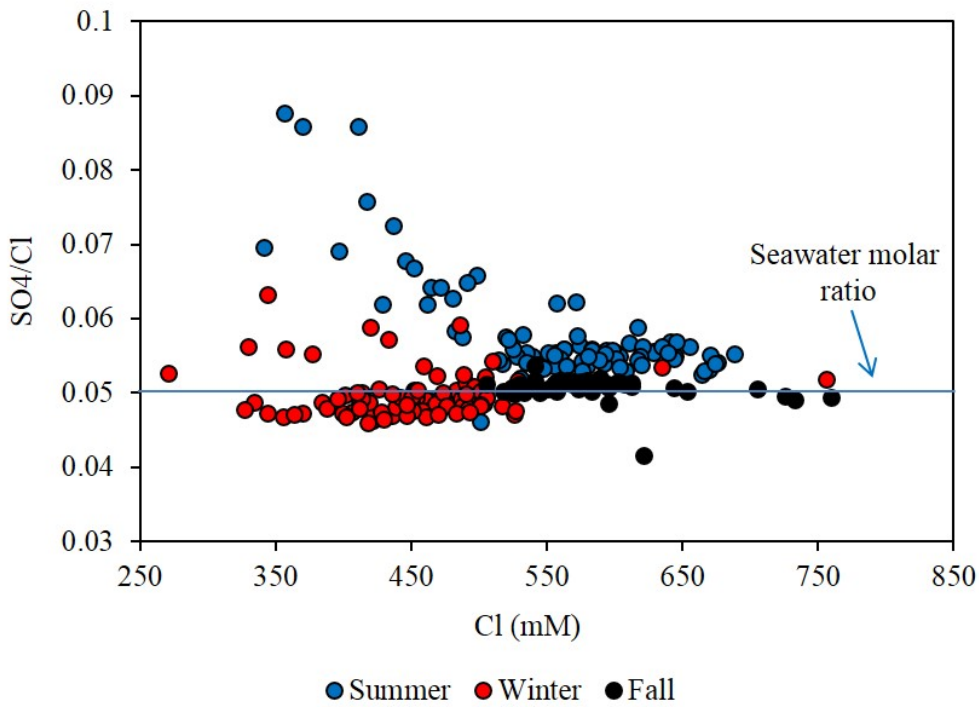


Figure 10.

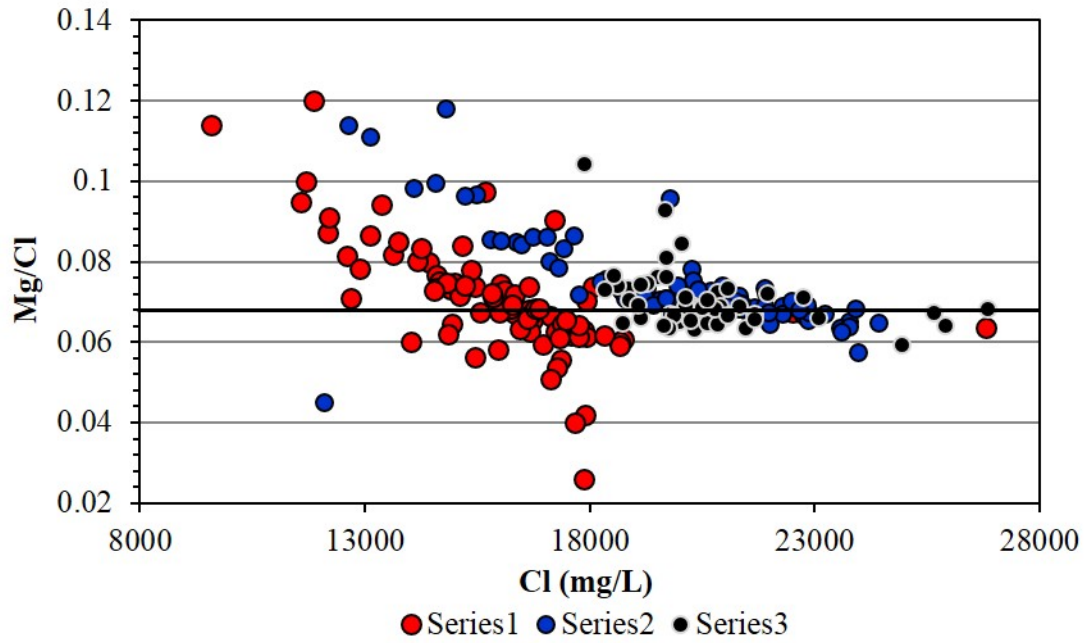


Figure 11.

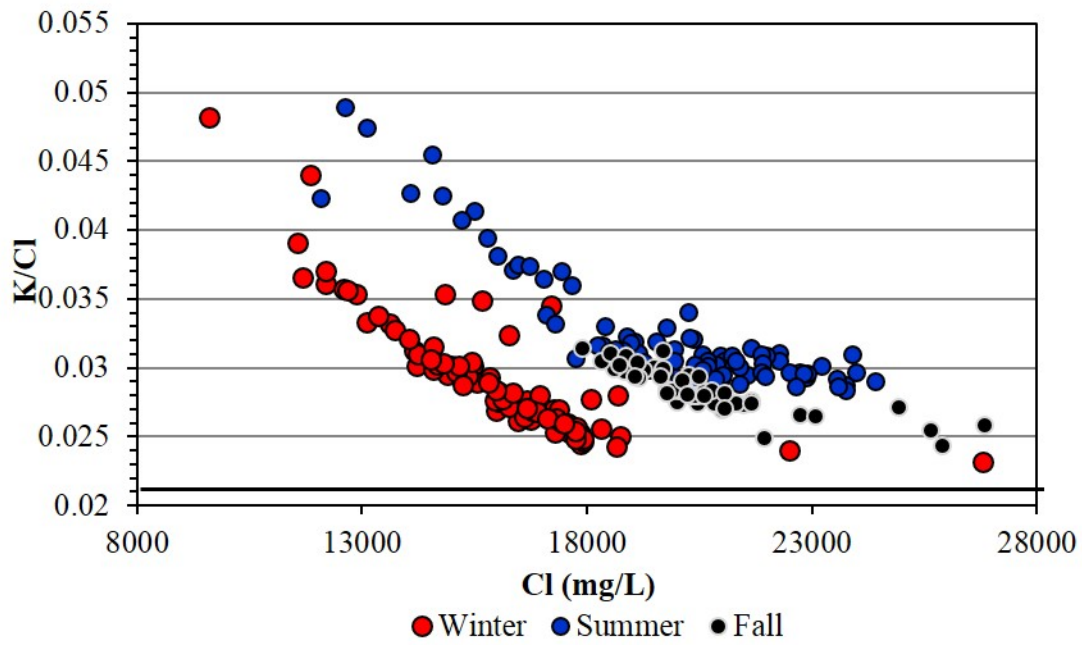


Figure 12.

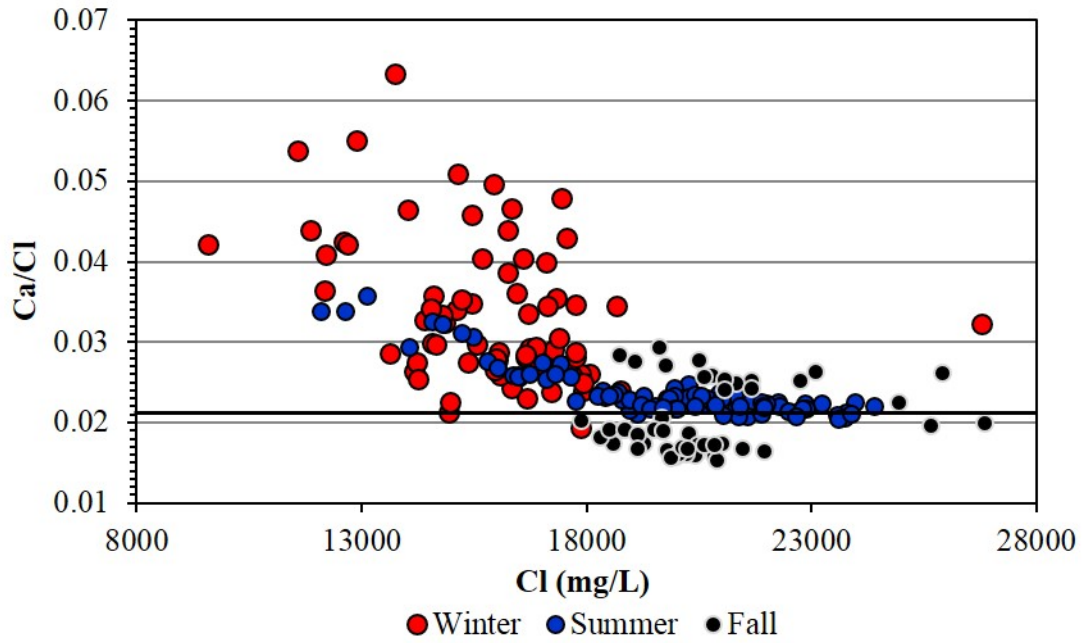


Figure 13.

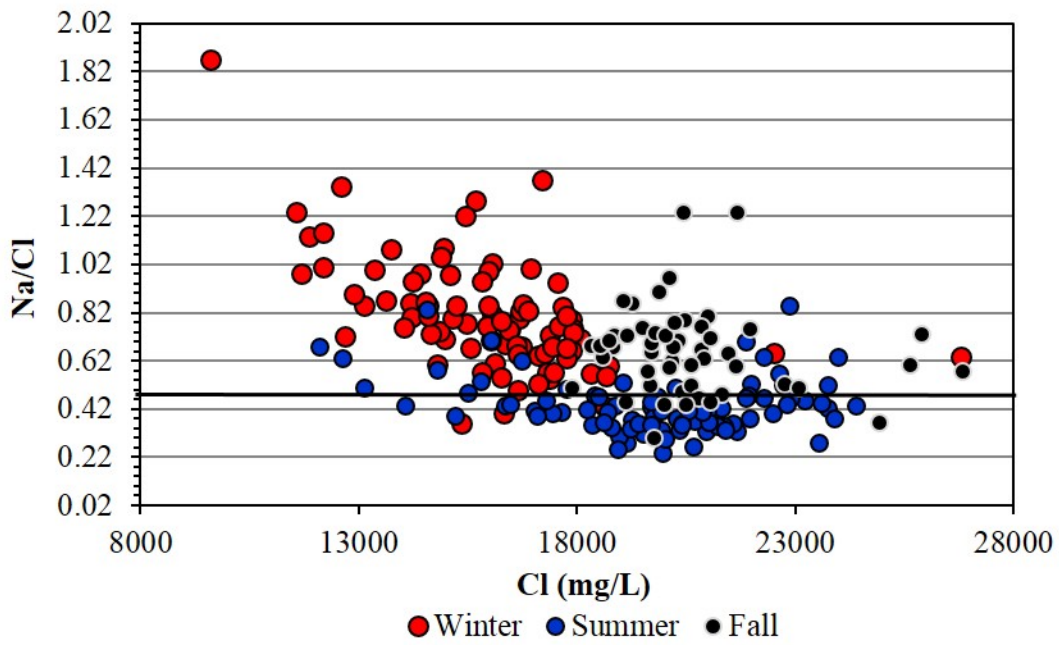


Figure 14.

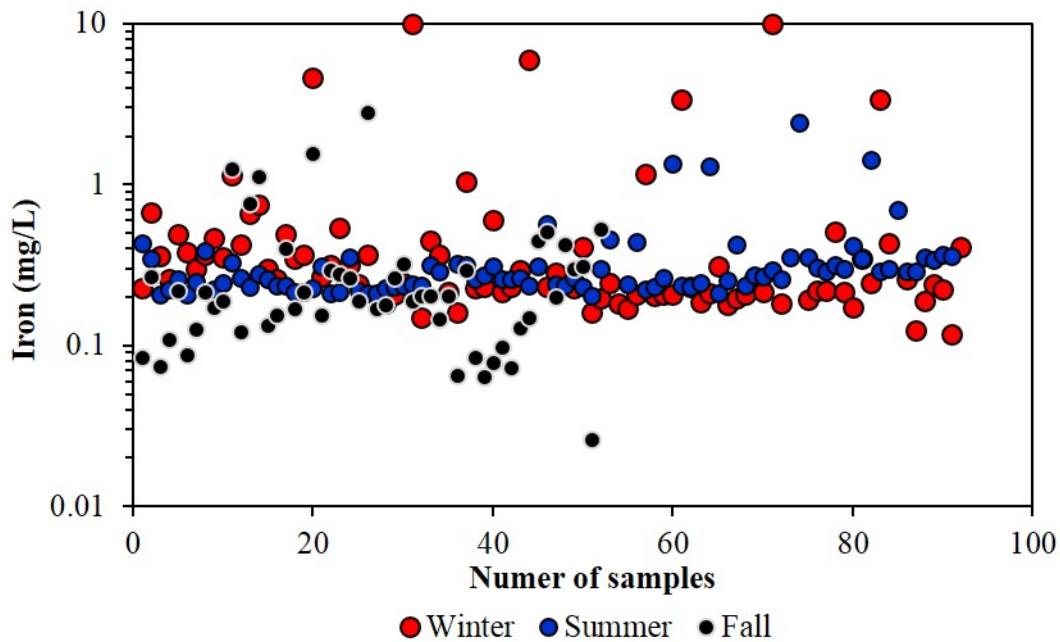


Figure 15.

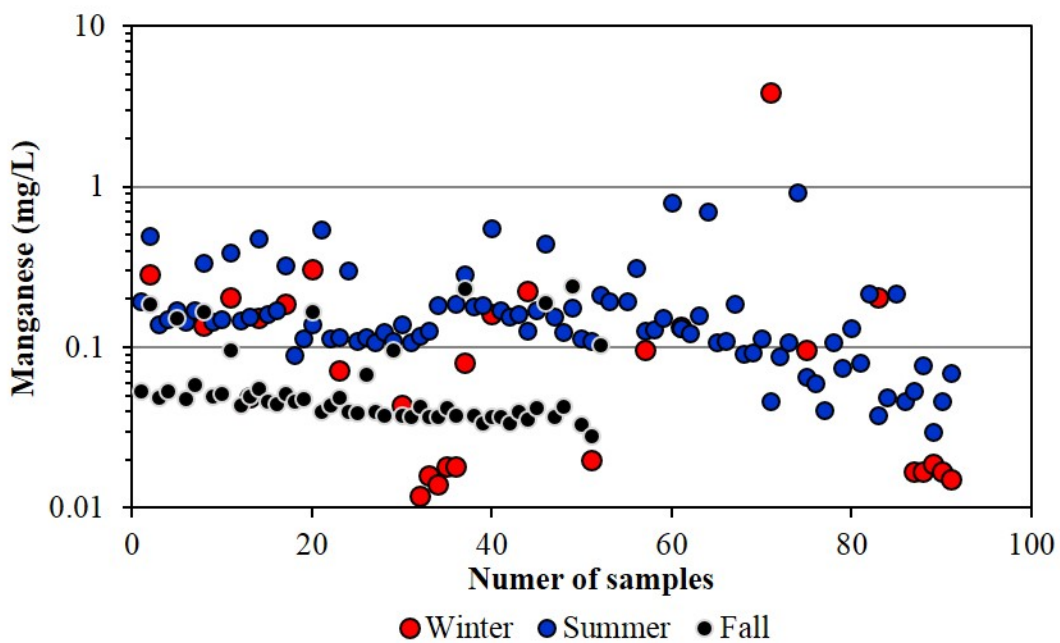


Figure 16.

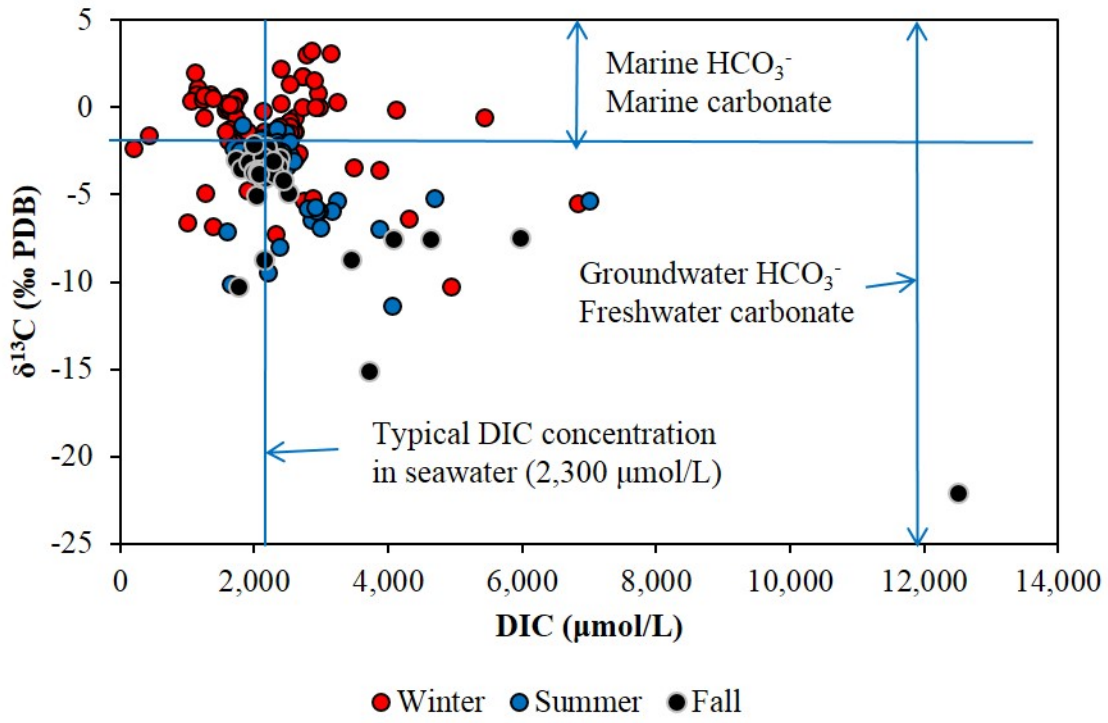


Figure 17.

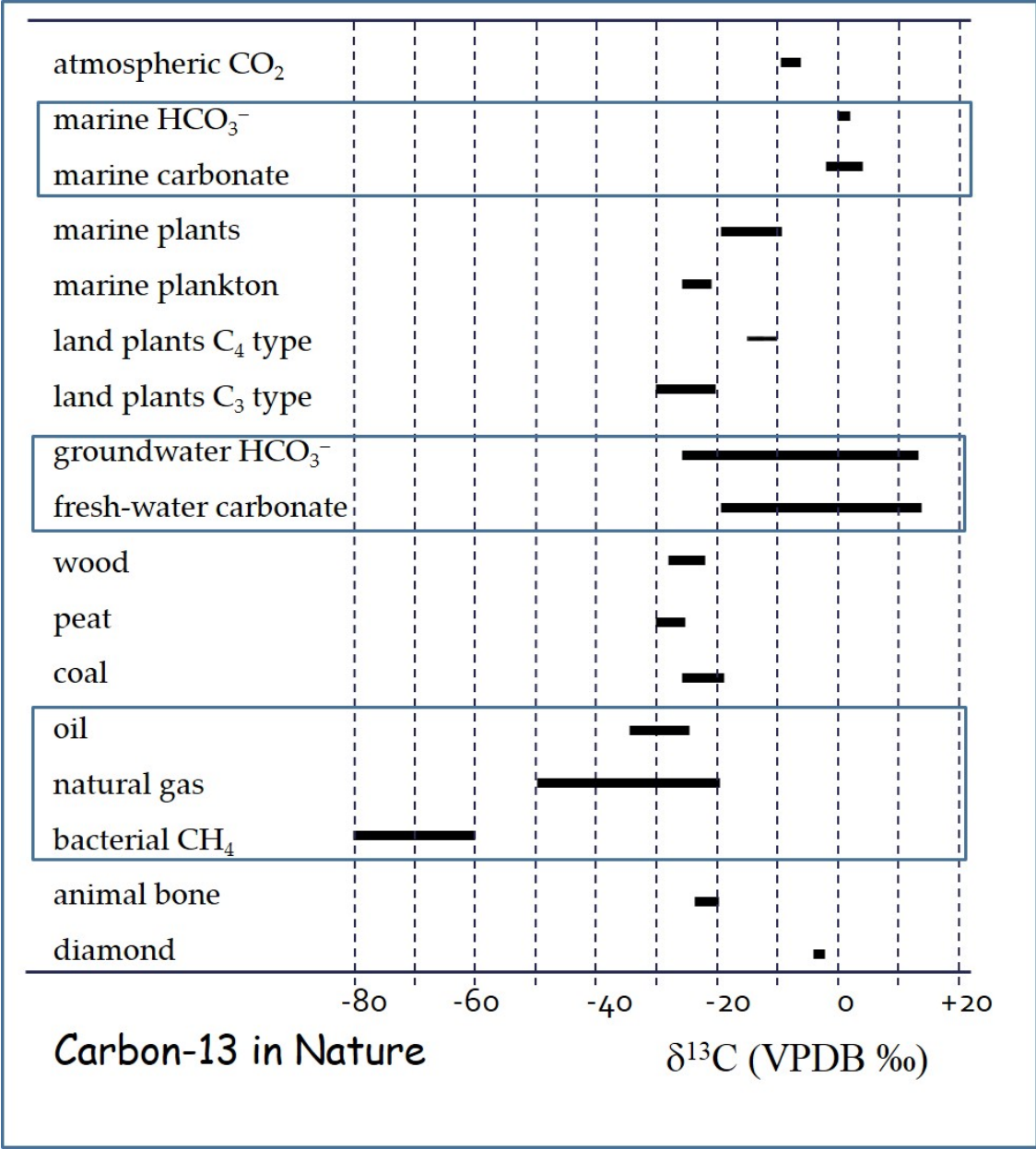


Figure 18.

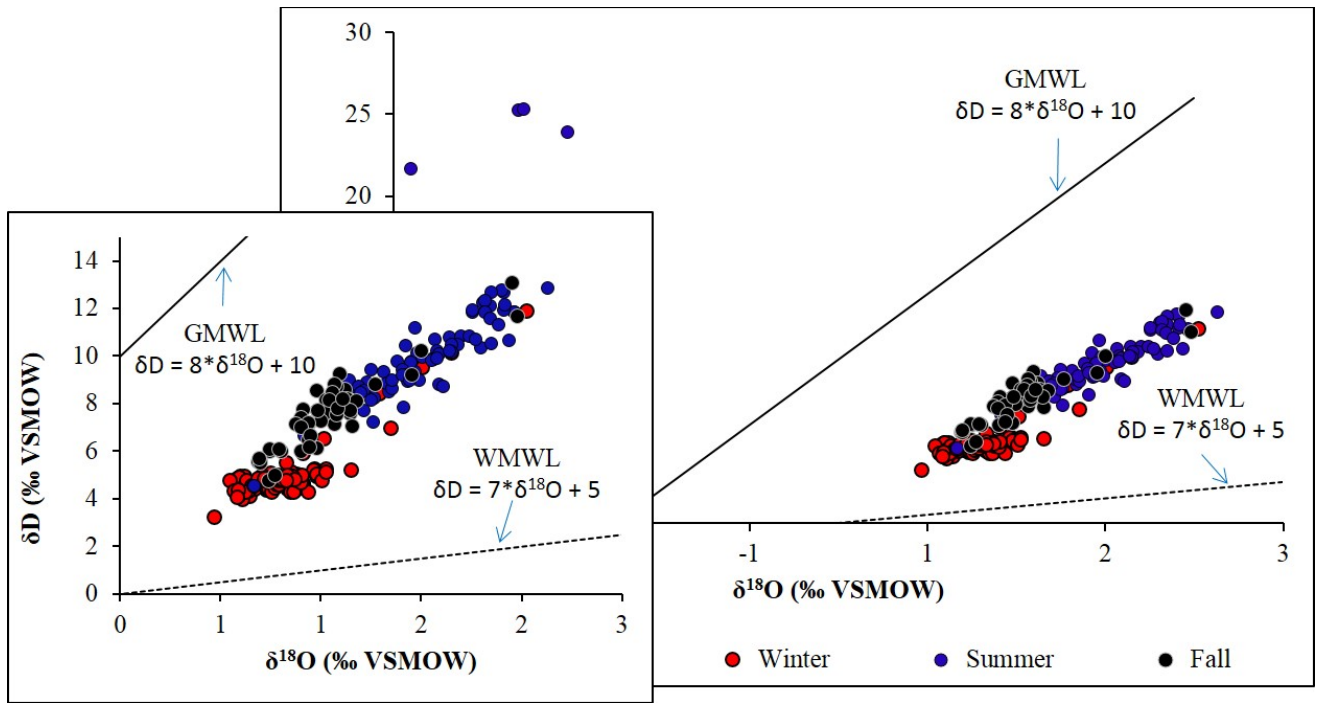


Figure 19.

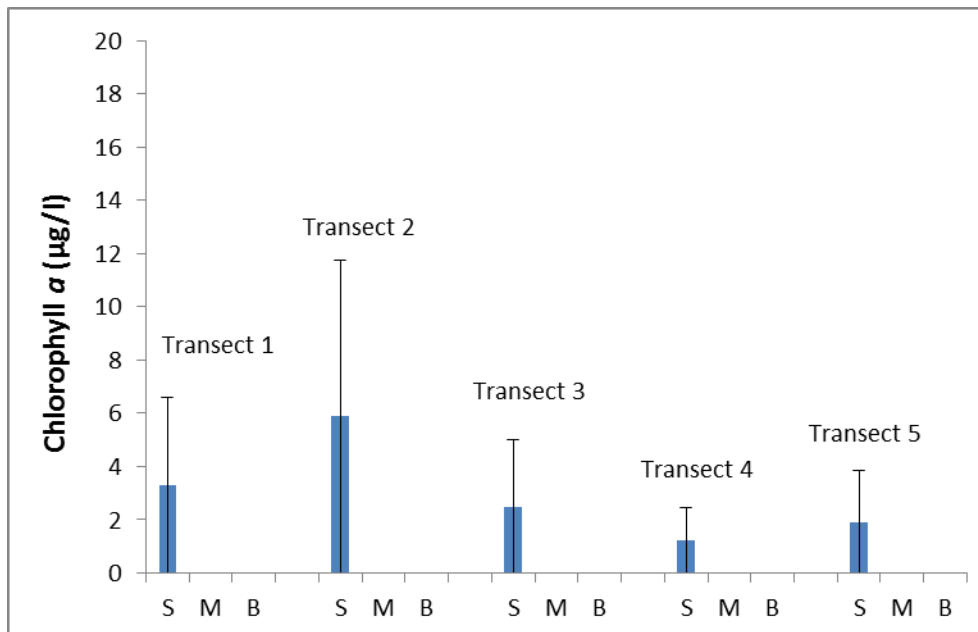


Figure 20.

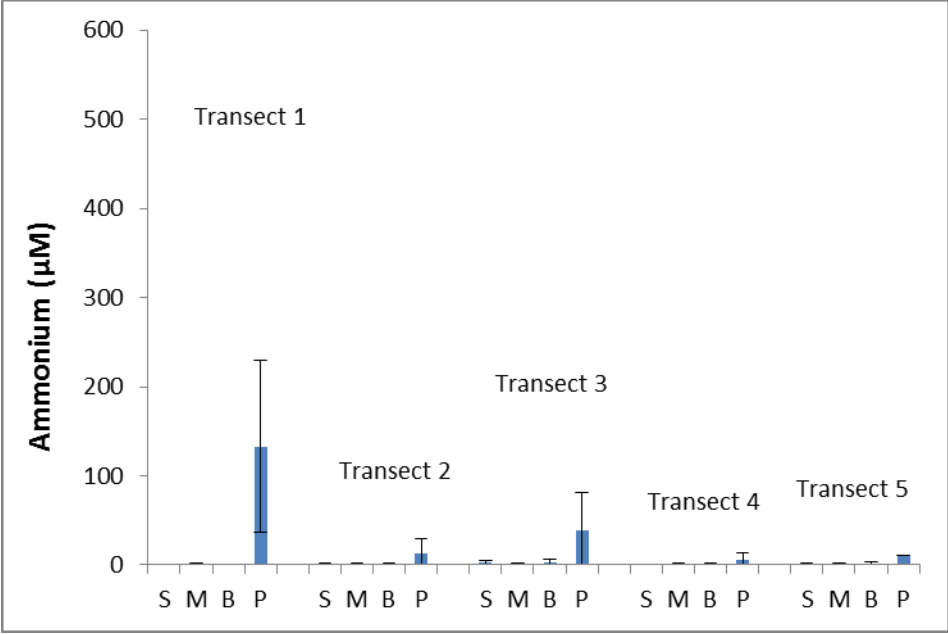


Figure 21.

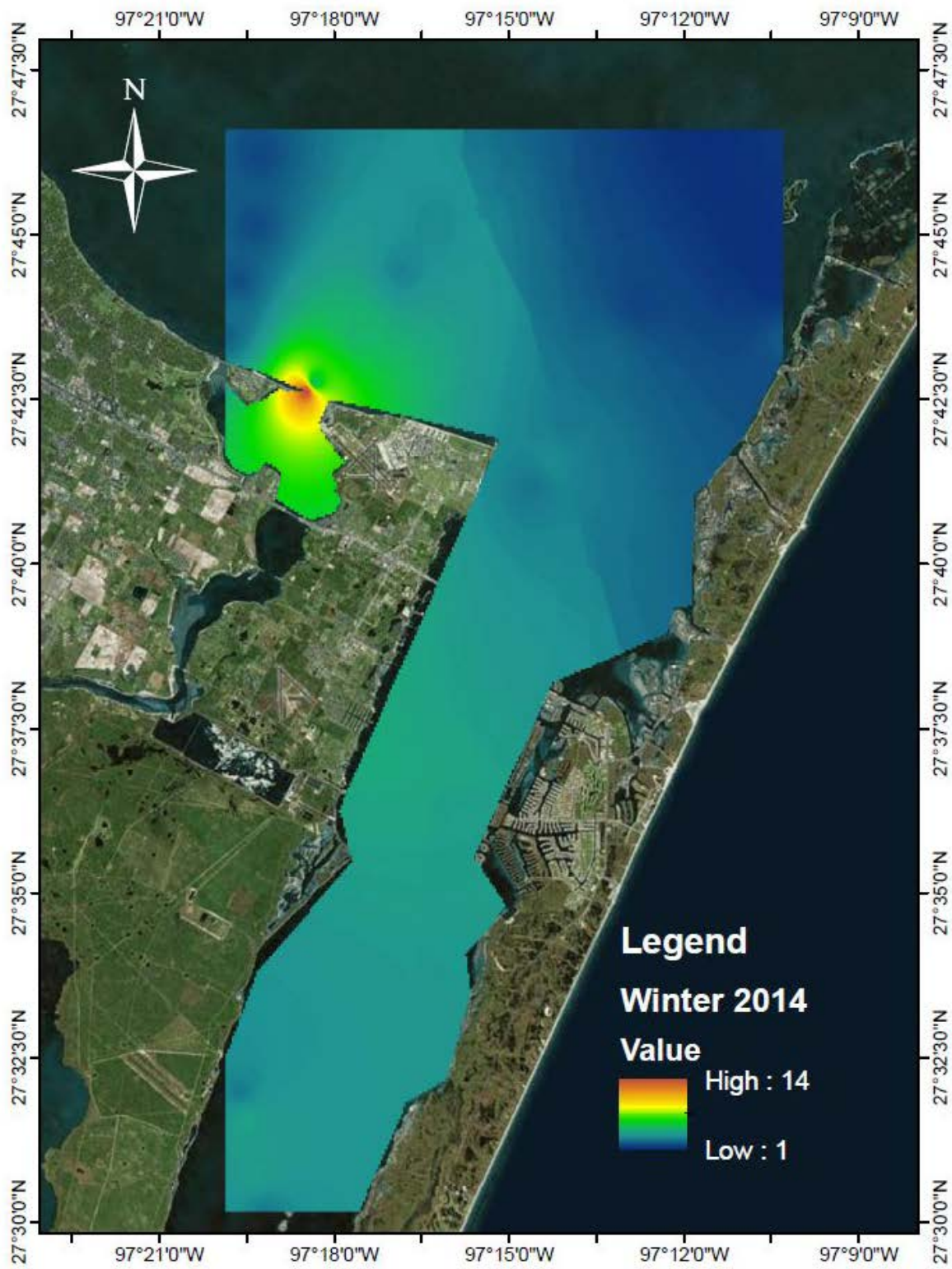


Figure 22.

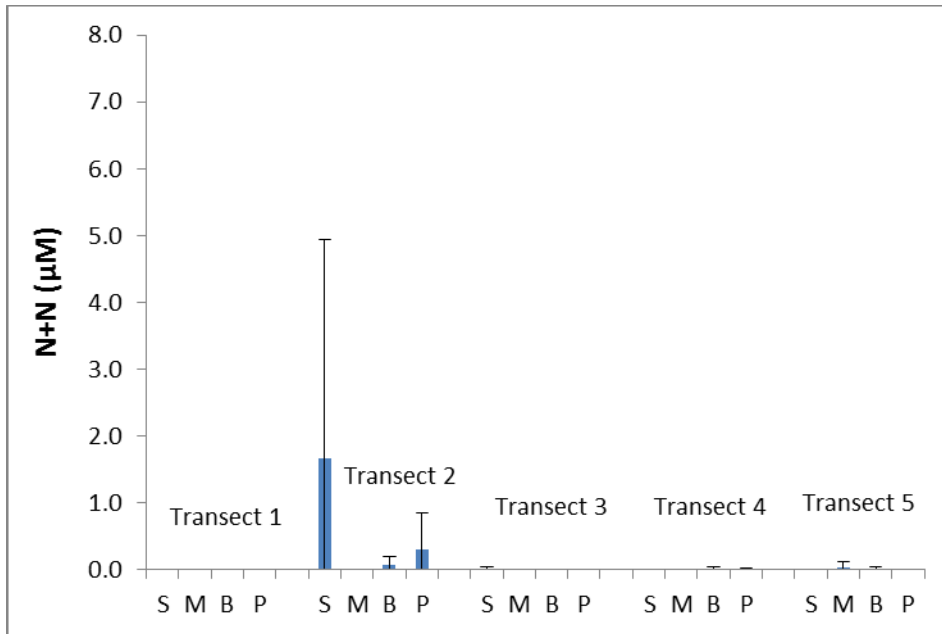


Figure 23.

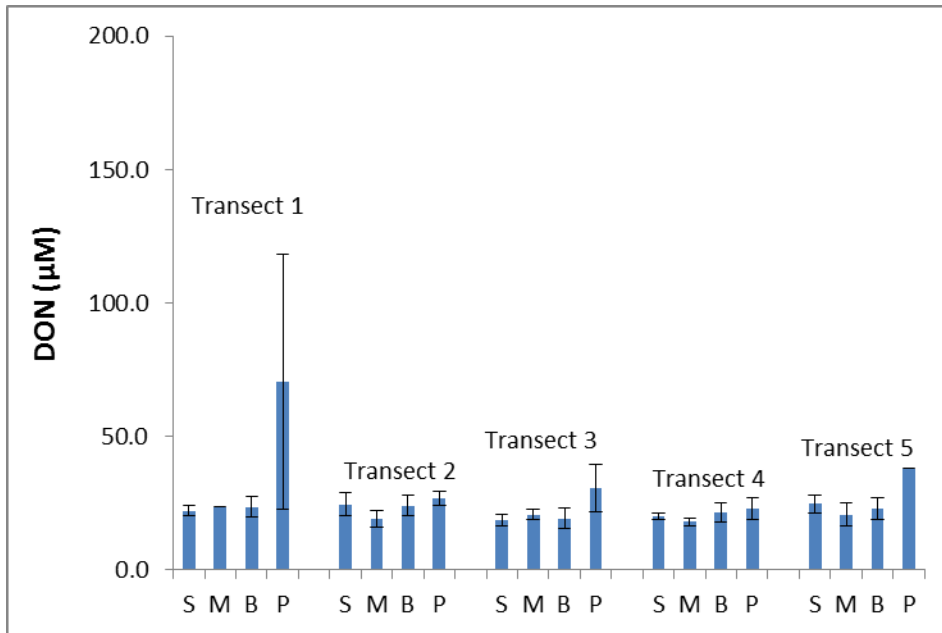


Figure 24.

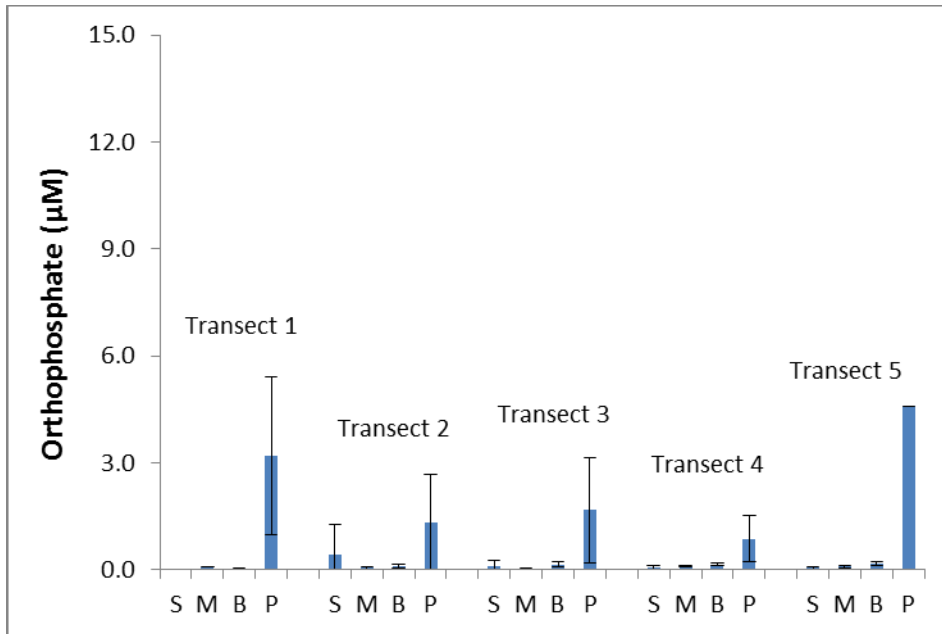


Figure 25.

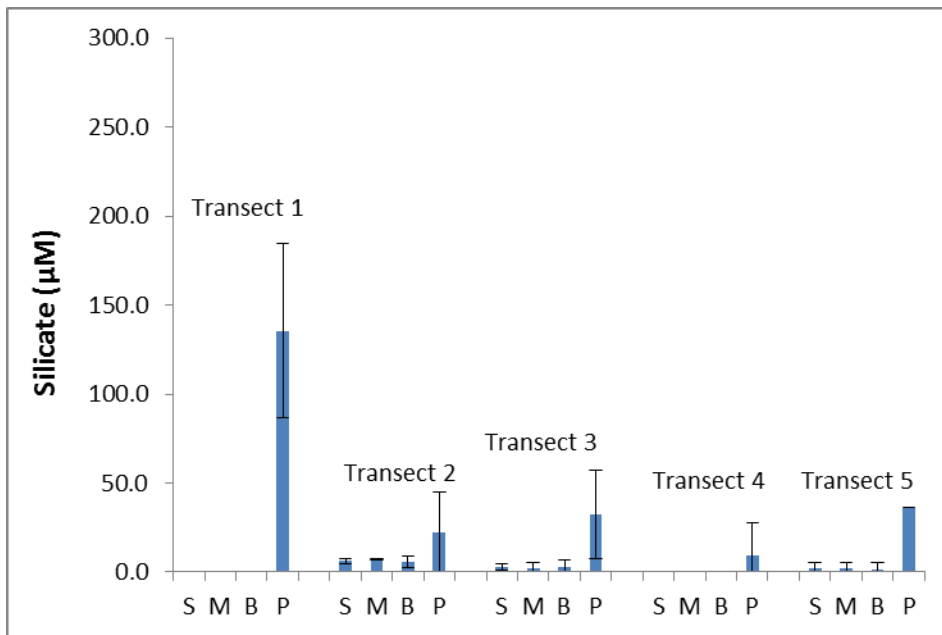


Figure 26.

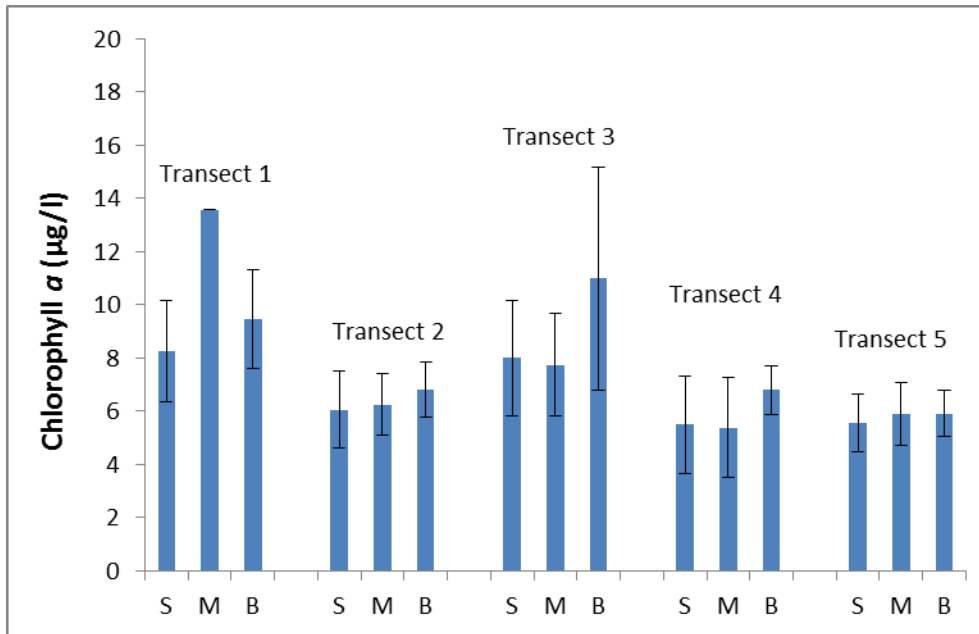


Figure 27.

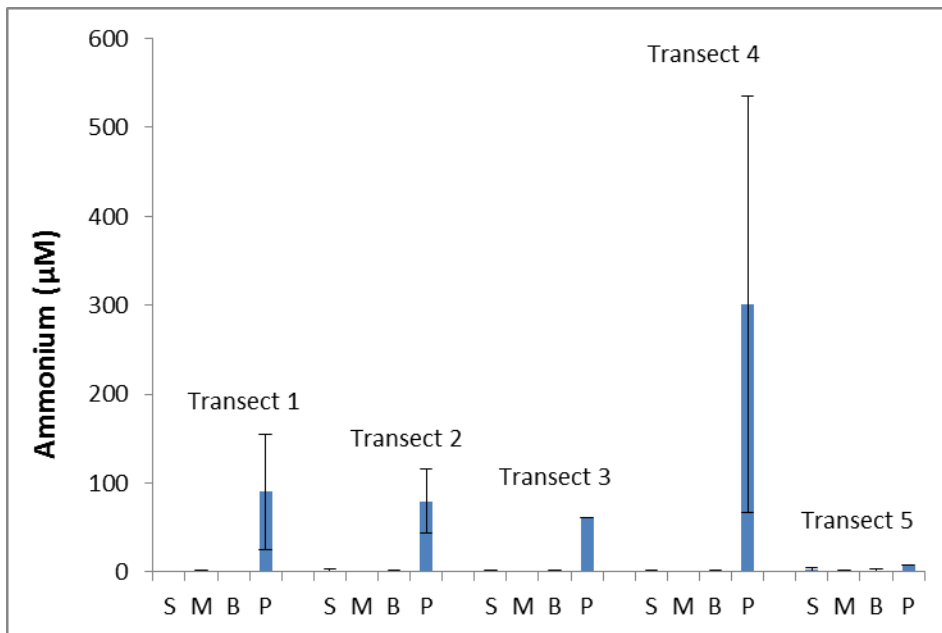


Figure 28.

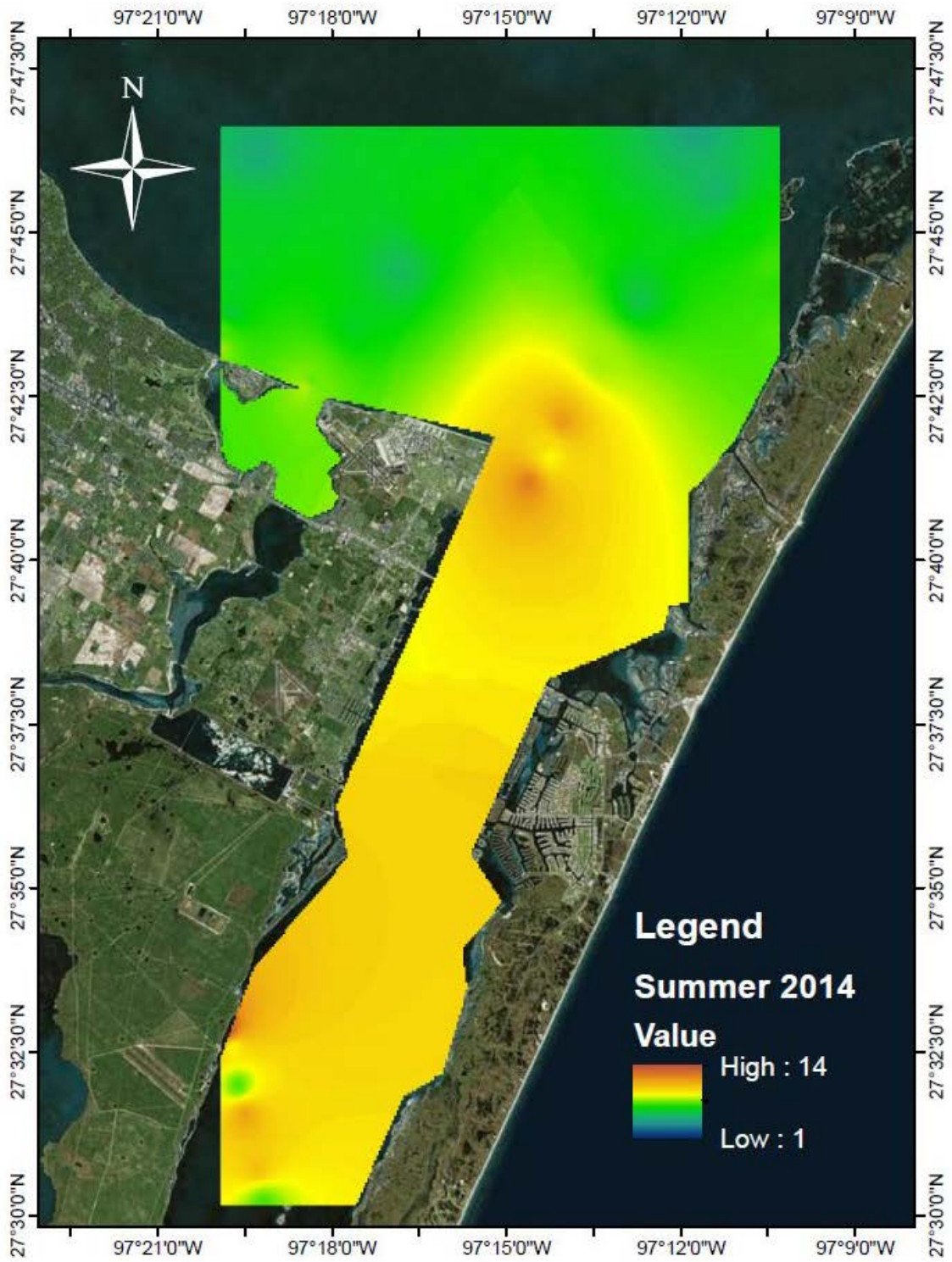


Figure 29.

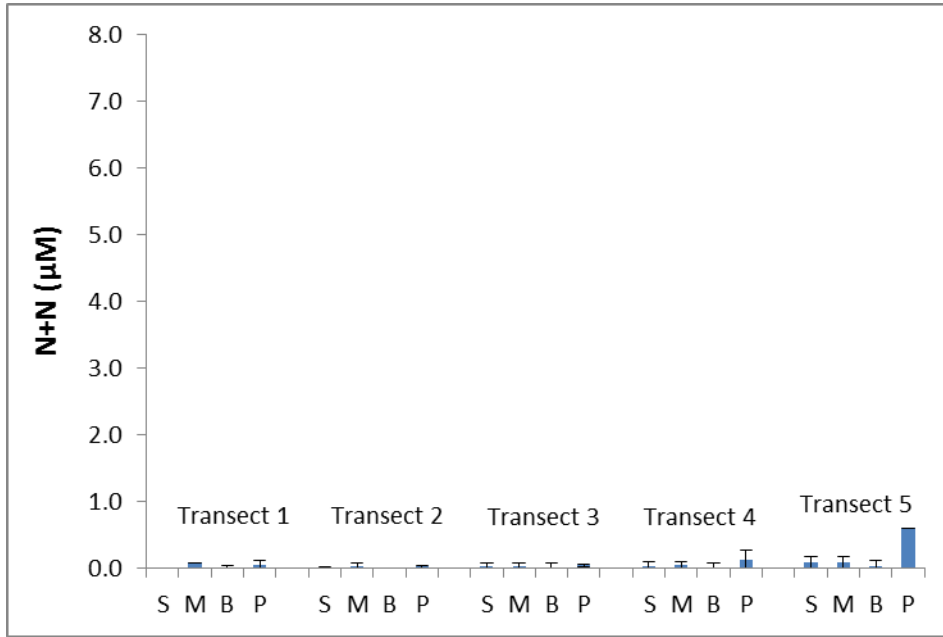


Figure 30.

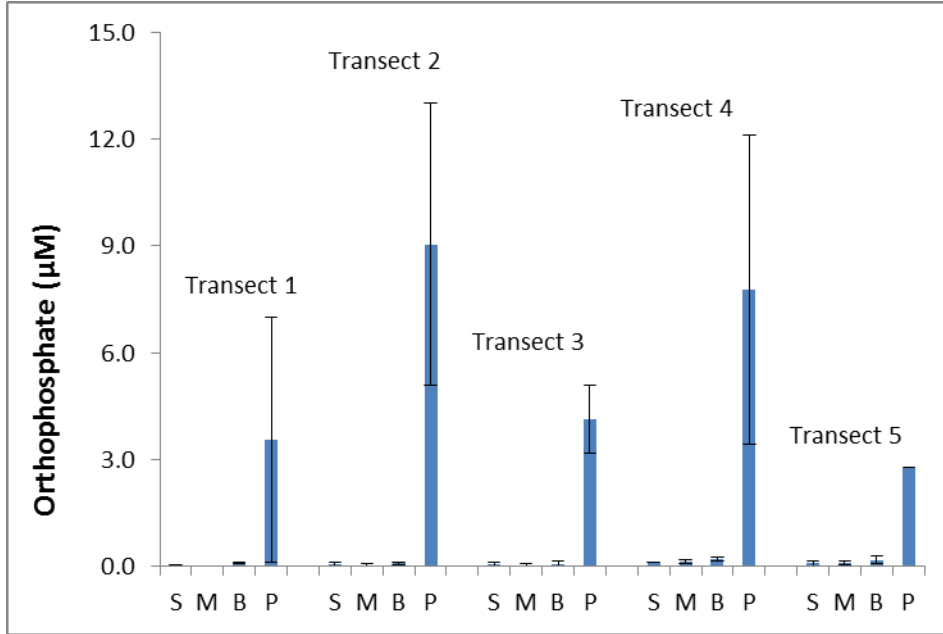


Figure 31.

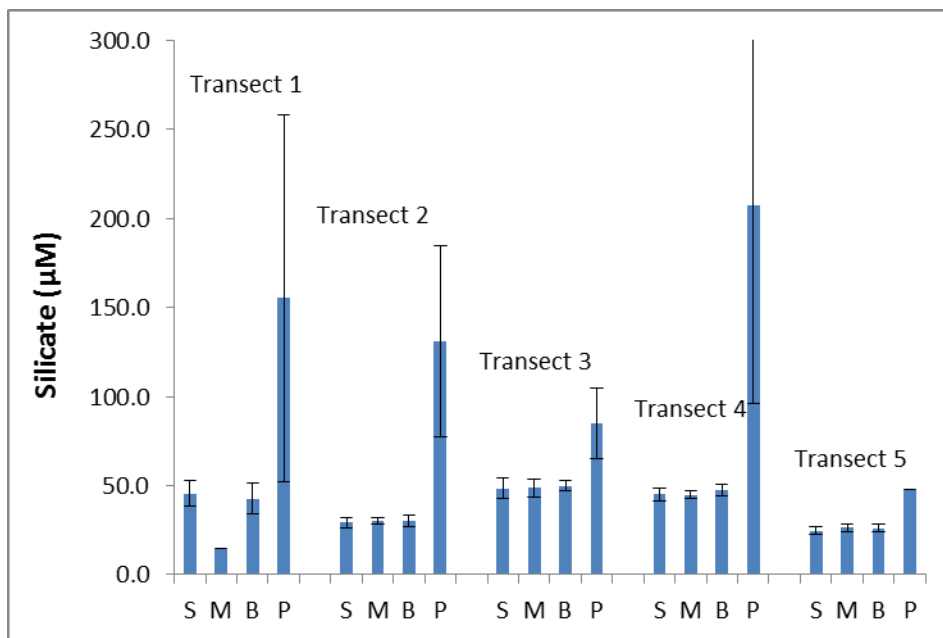


Figure 32.

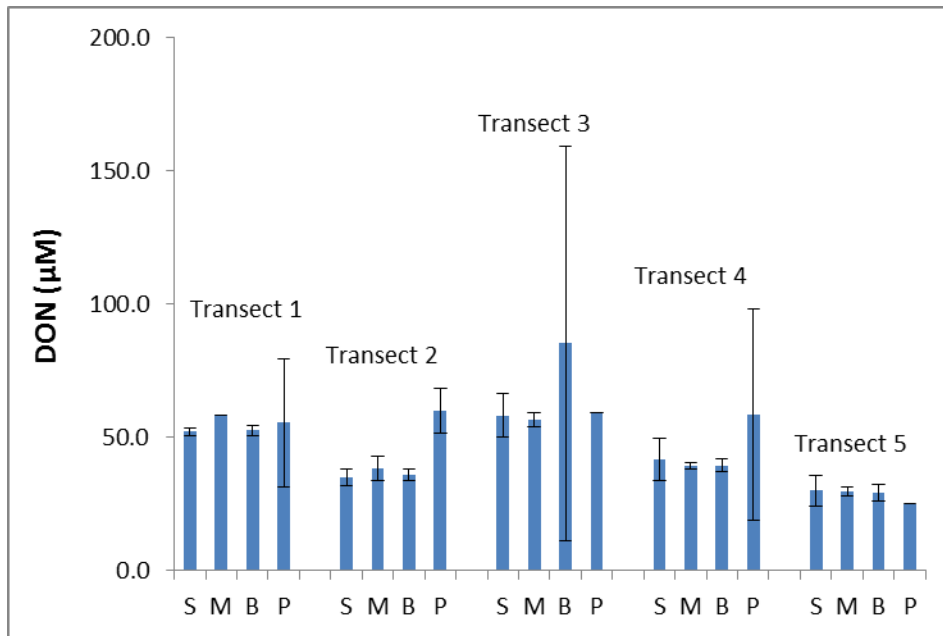


Figure 33.

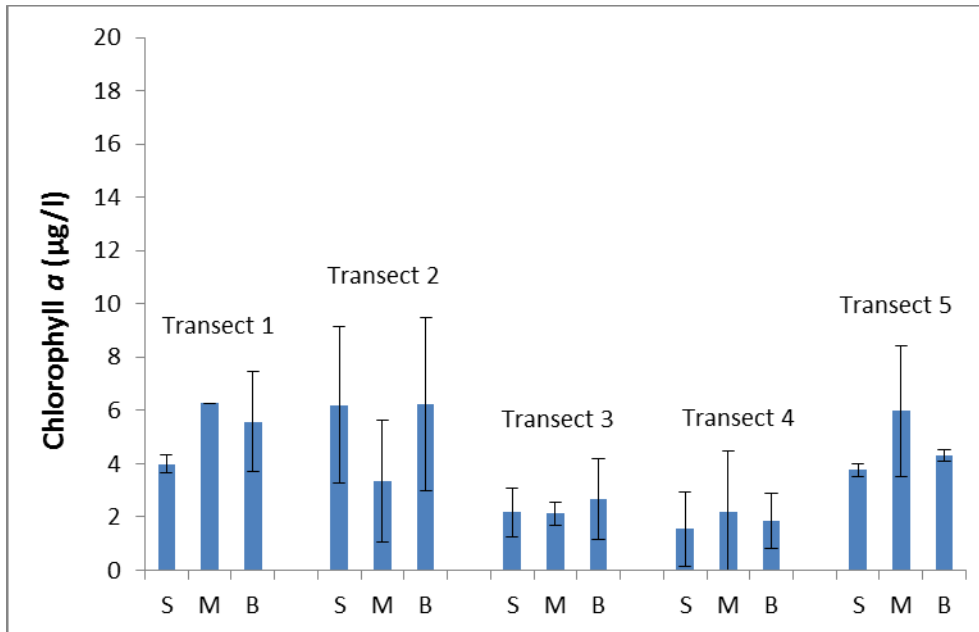


Figure 34.

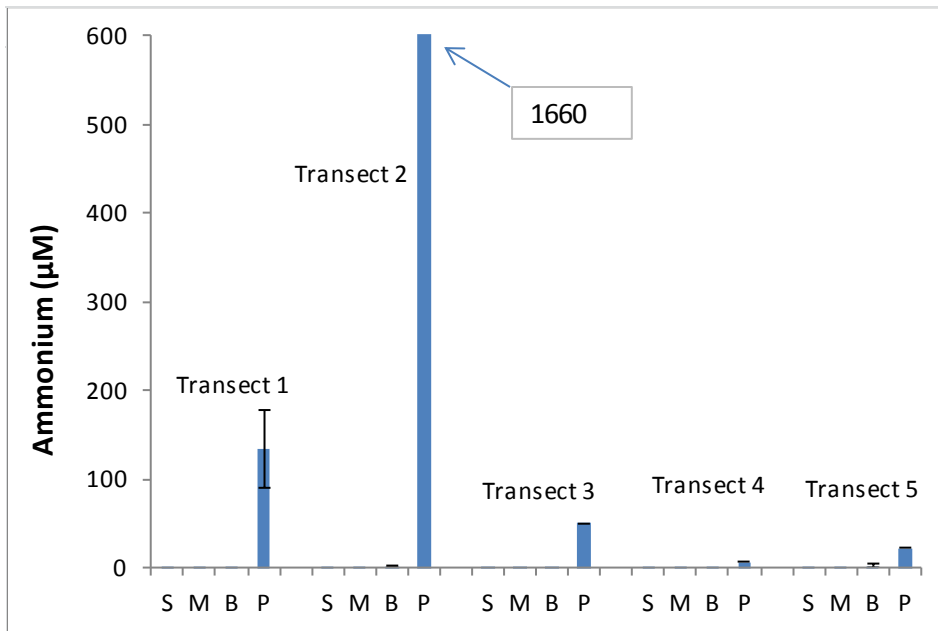


Figure 35.

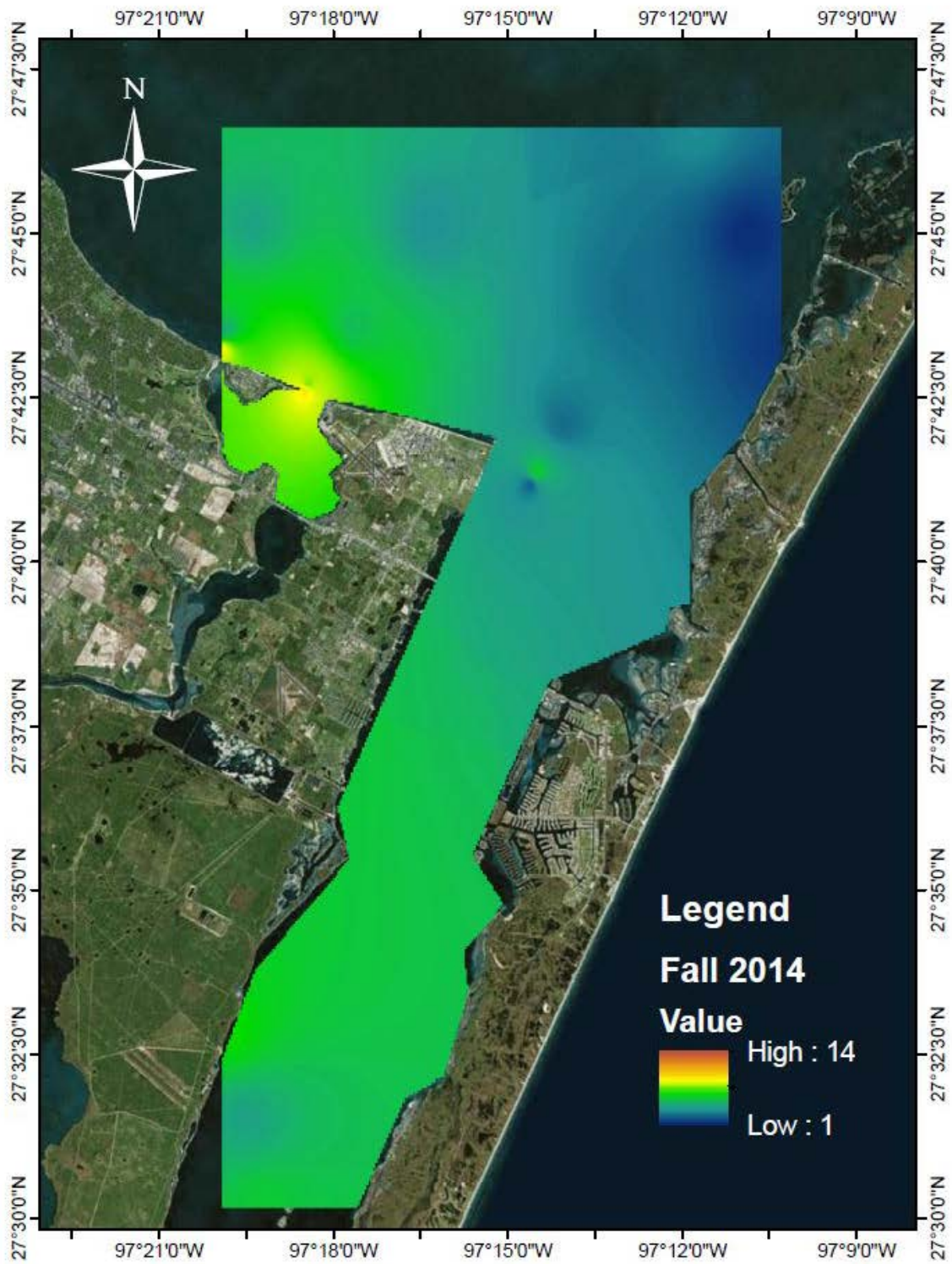


Figure 36.

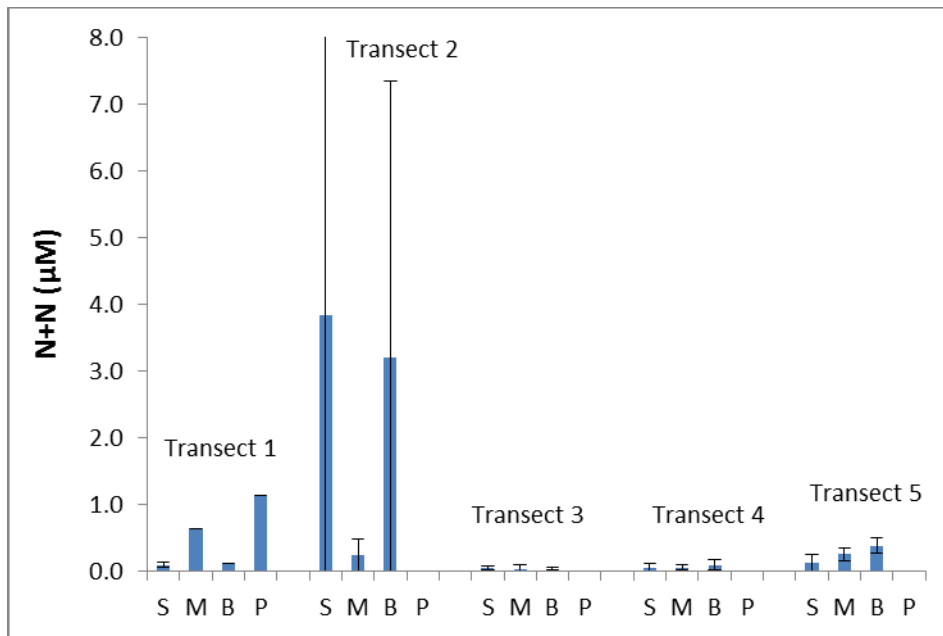


Figure 37.

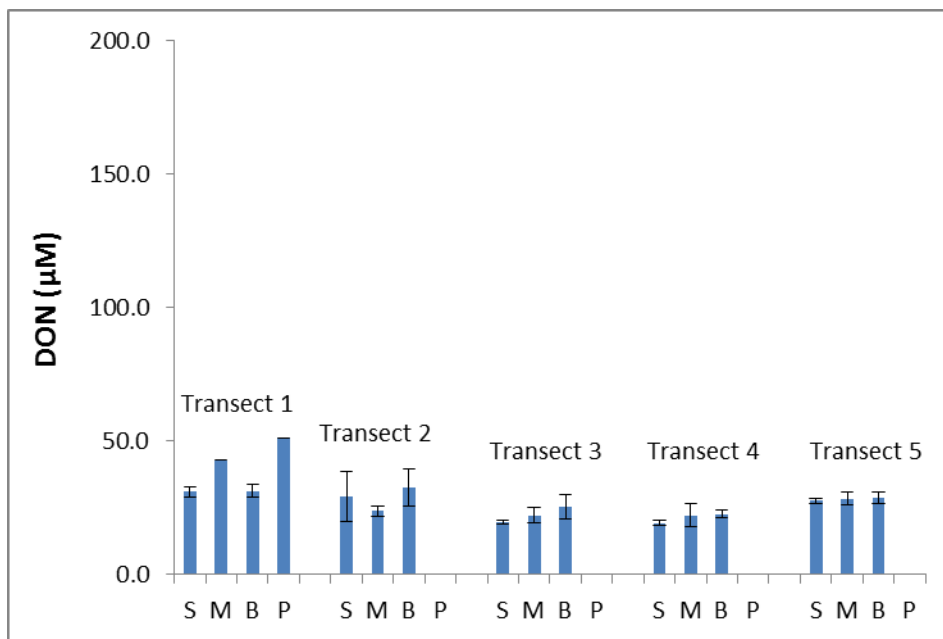


Figure 38.

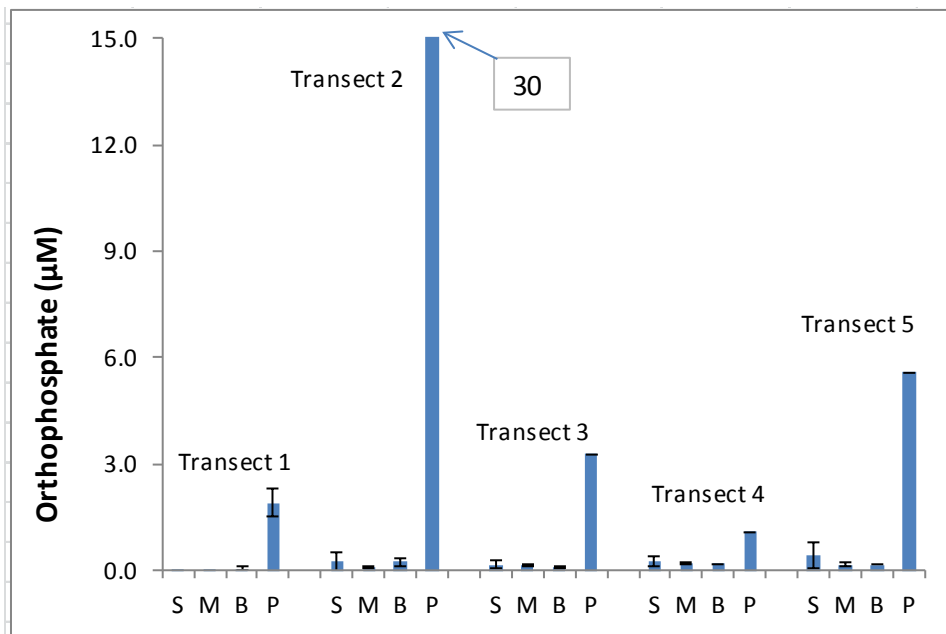


Figure 39.

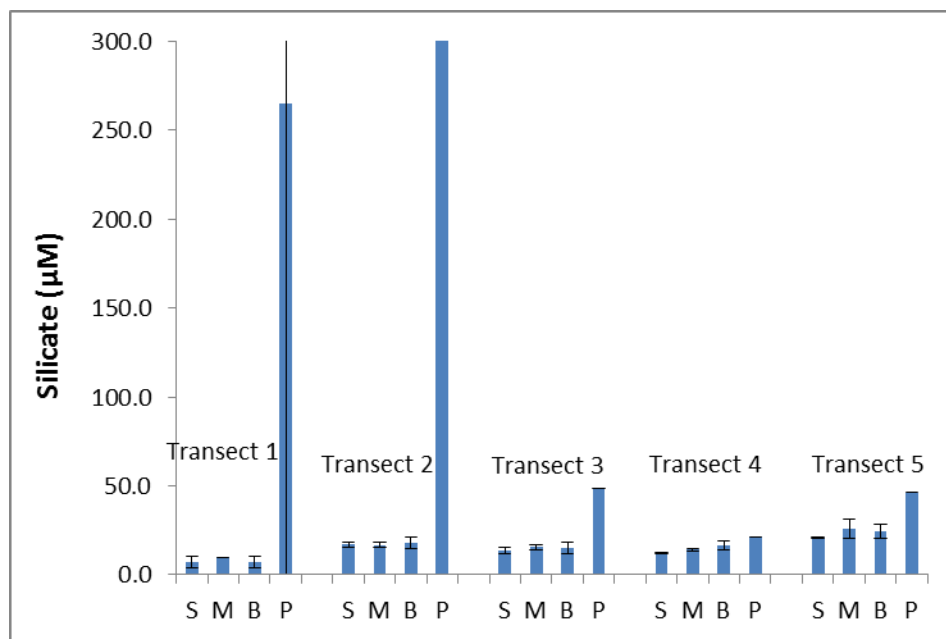


Figure 40.

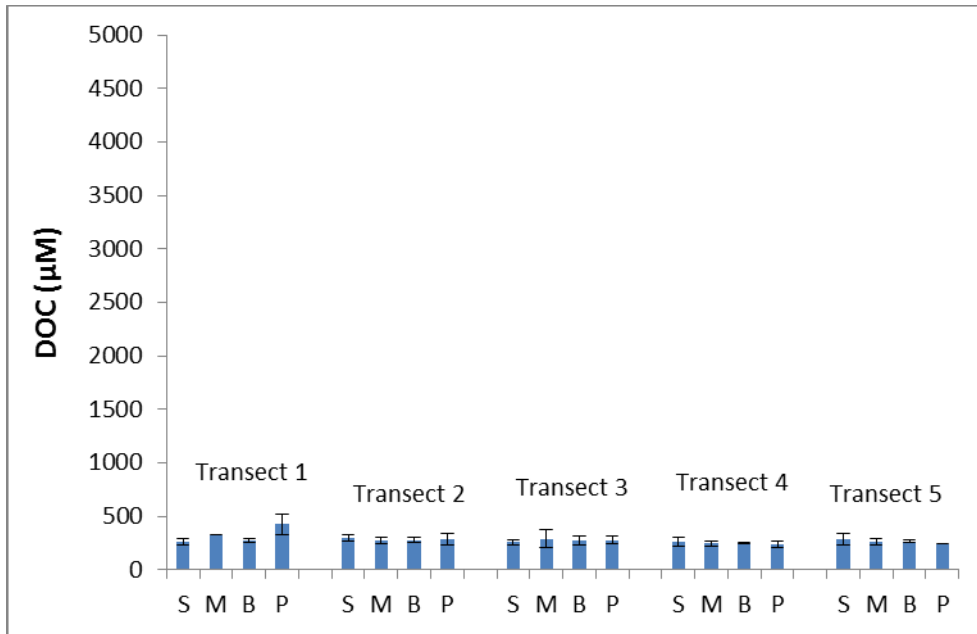


Figure 41.

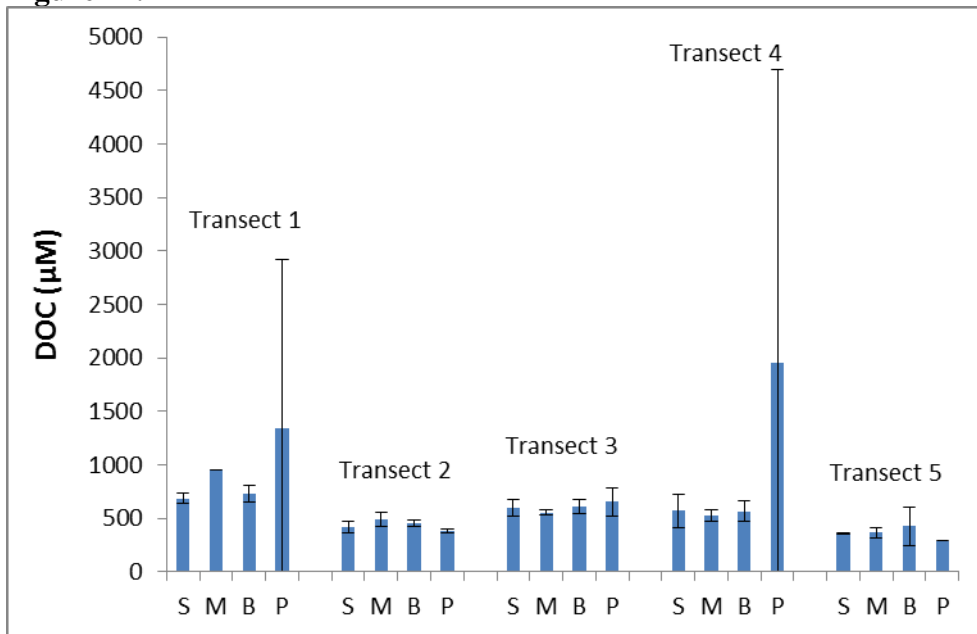


Figure 42.

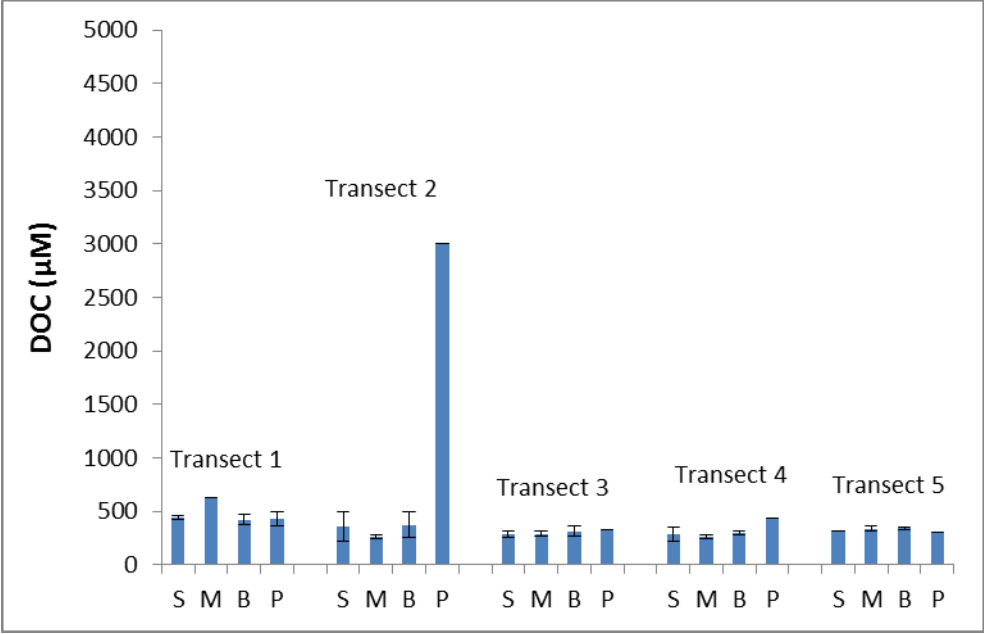


Figure 43.

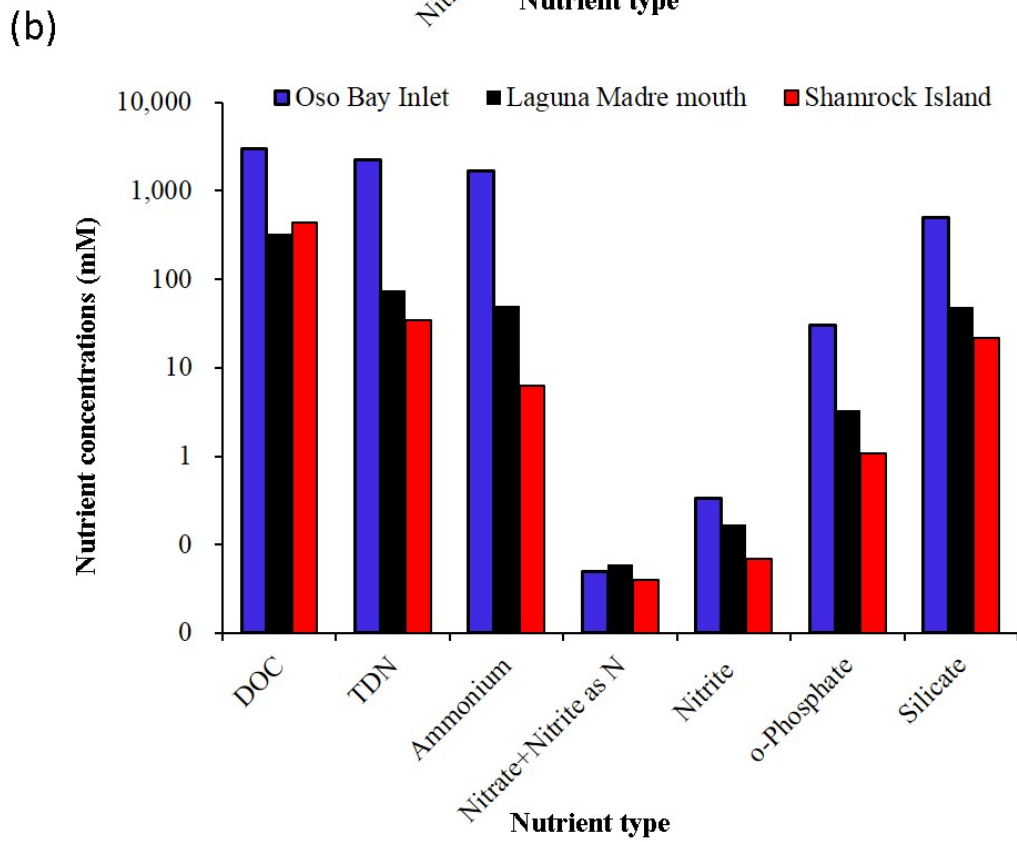
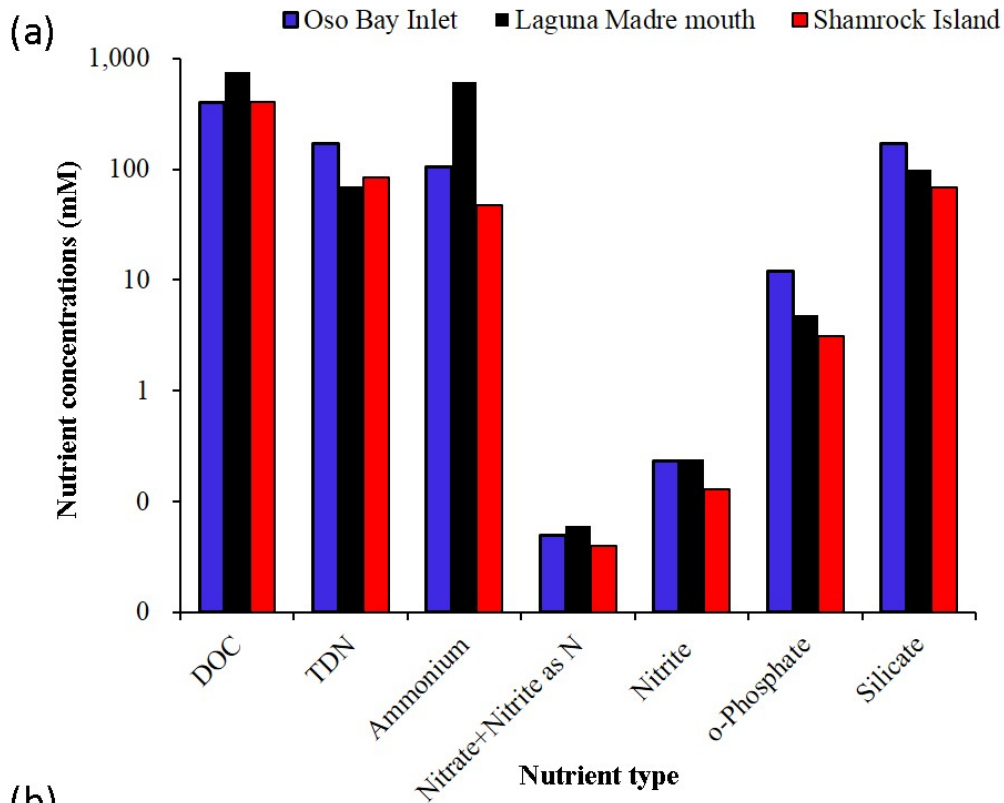


Figure 44.

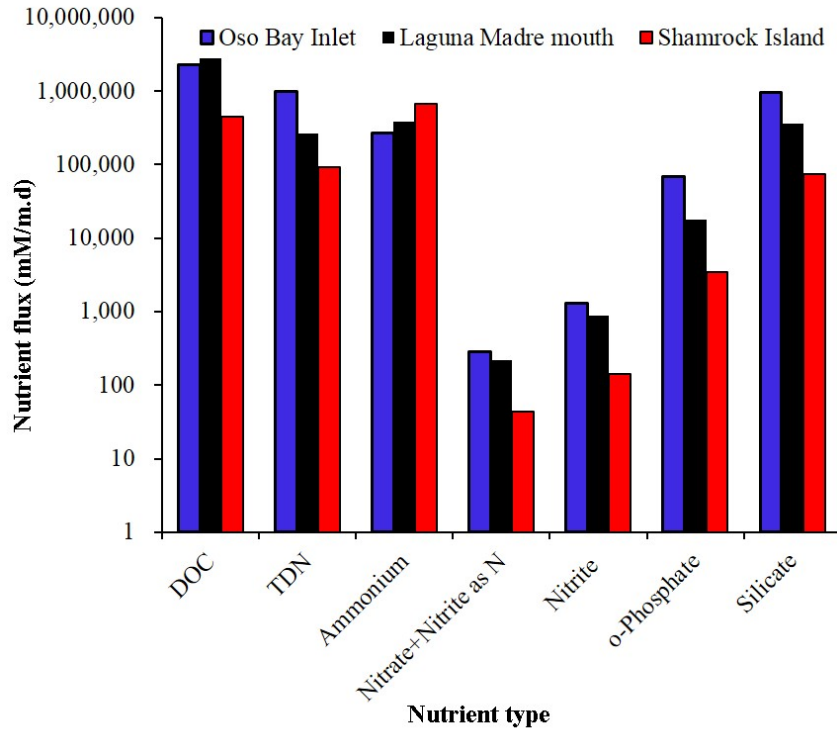


Figure 45.

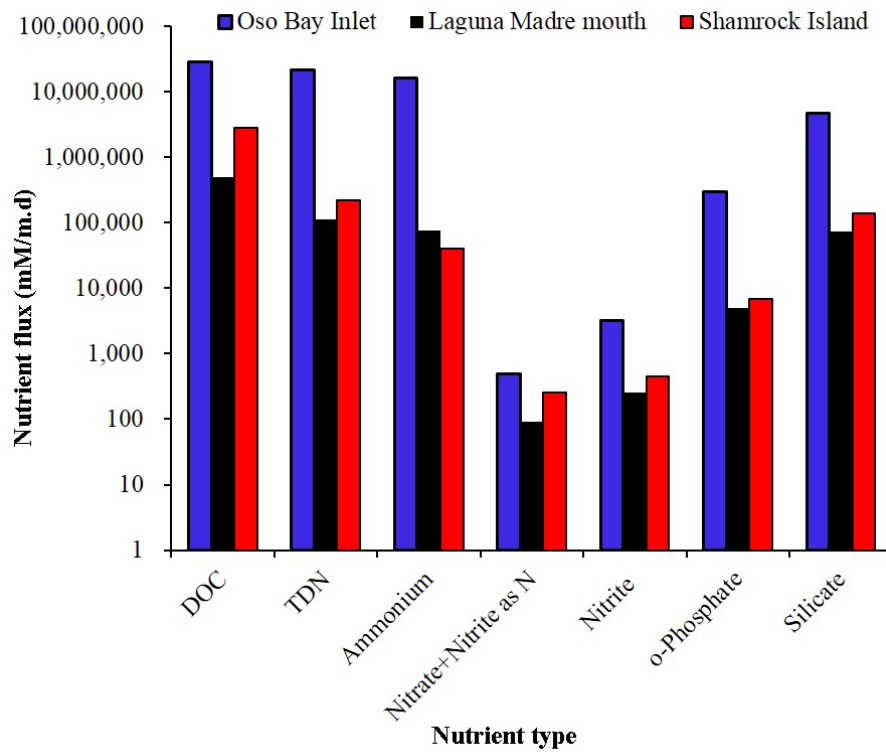
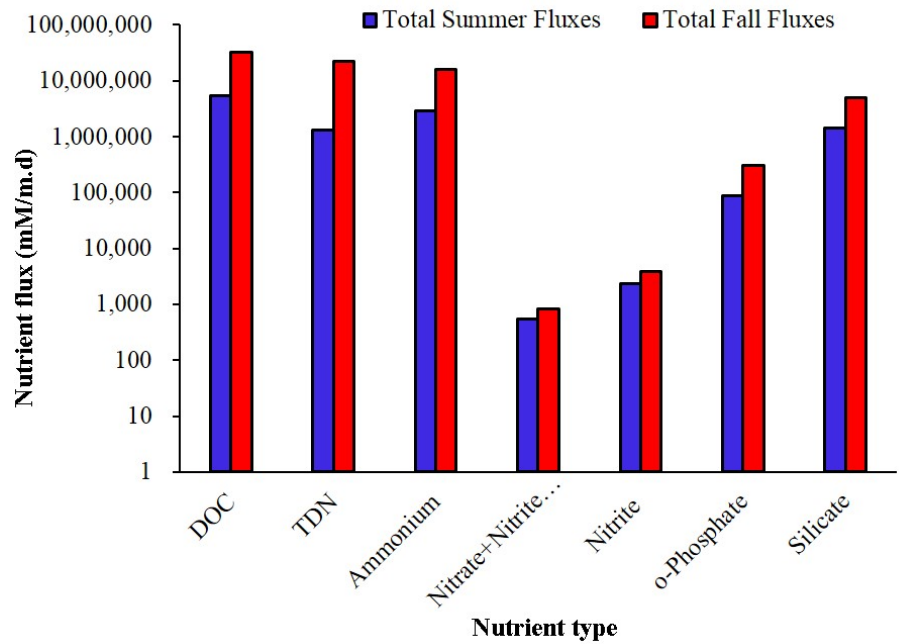


Figure 46.



Figure

47.

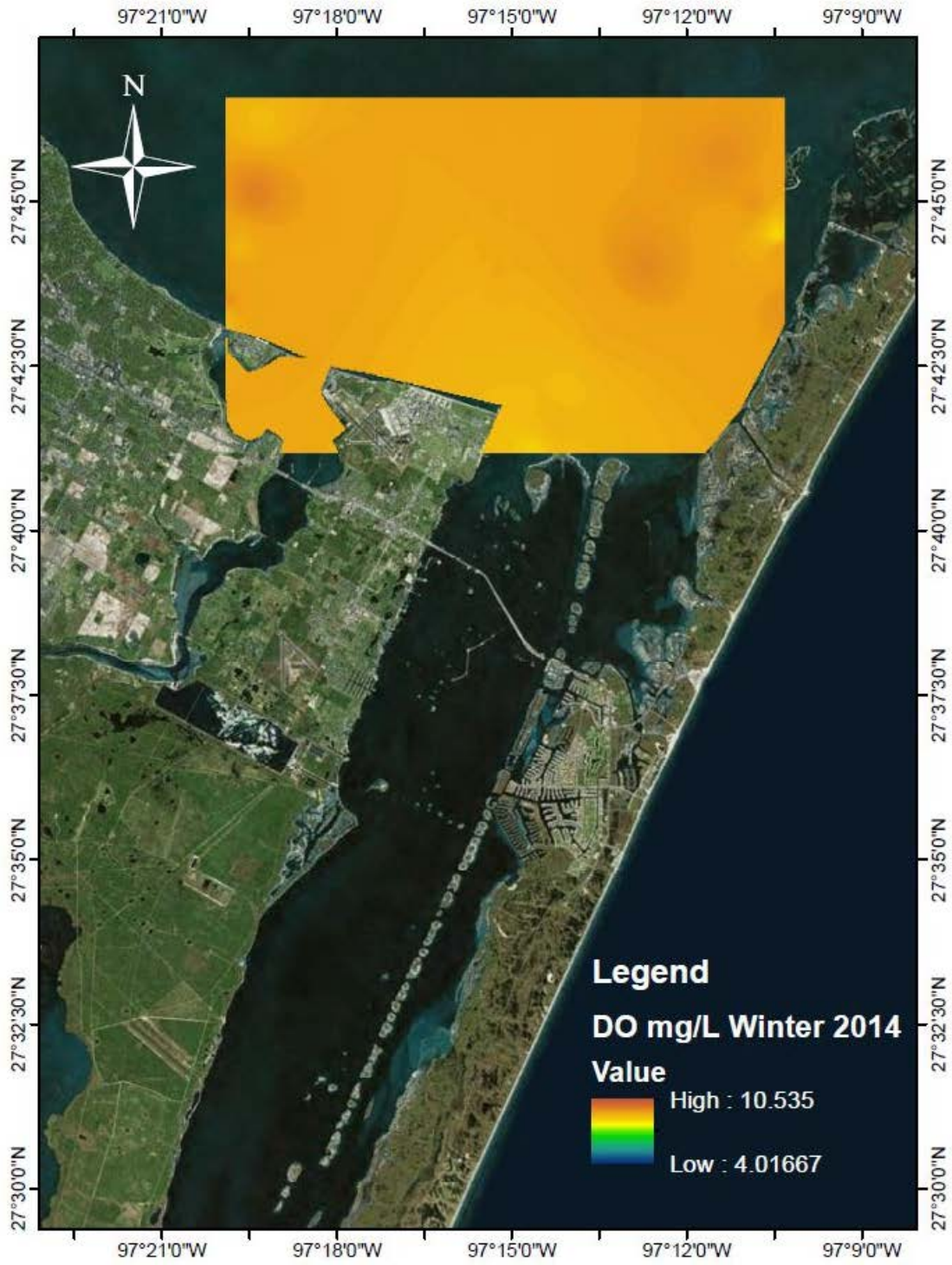


Figure 48.

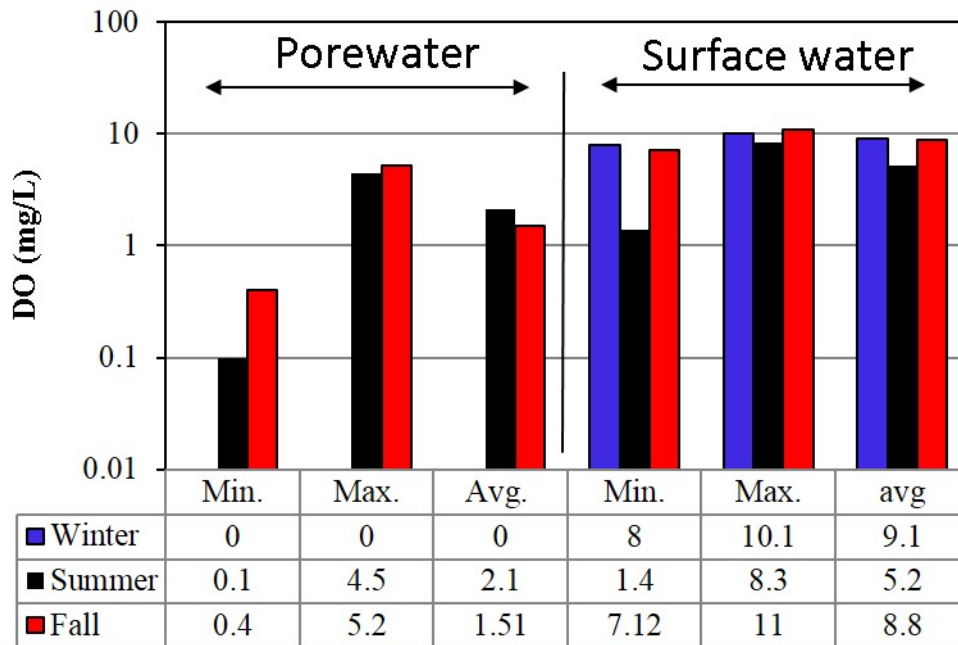


Figure 49.

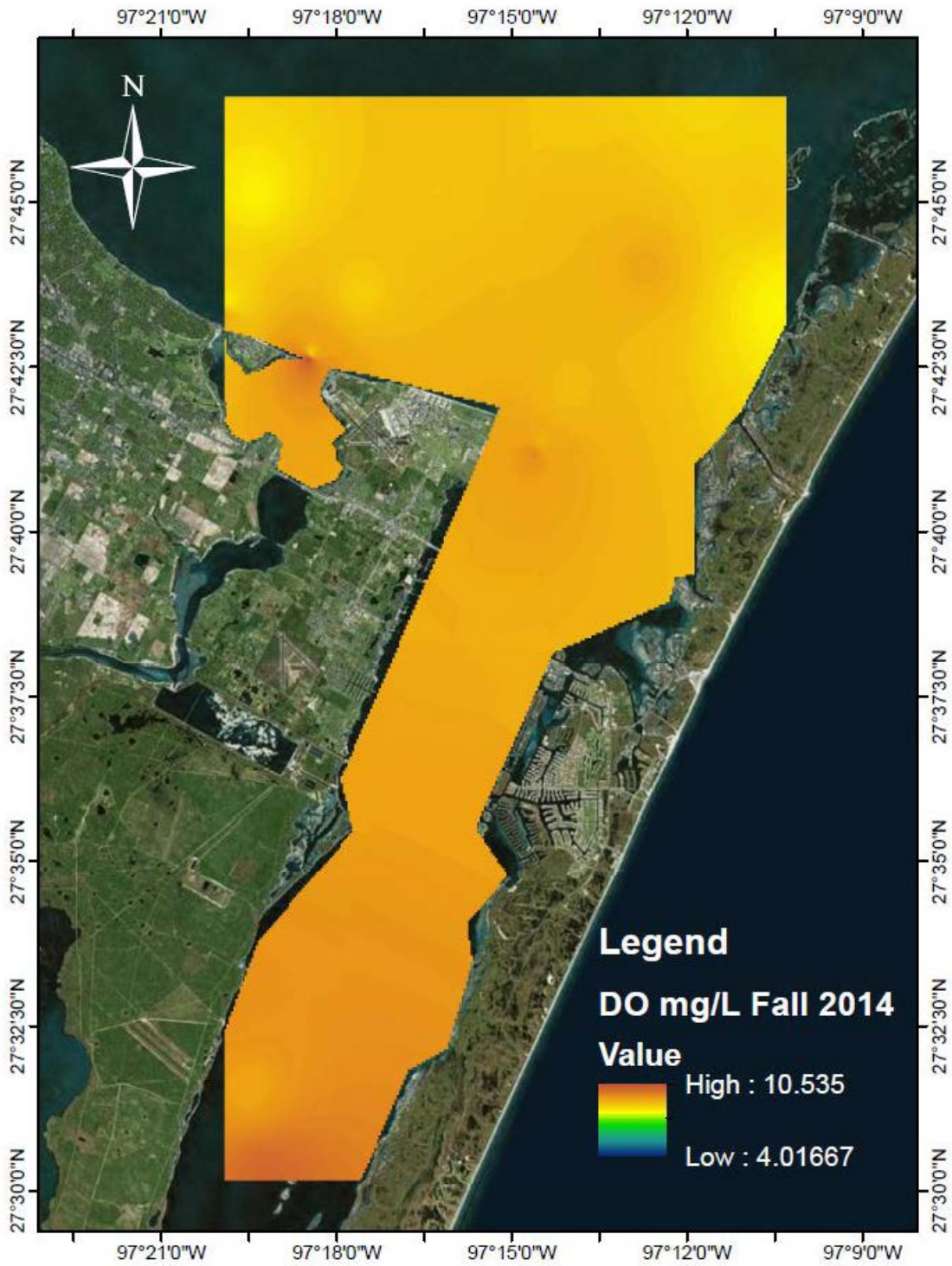


Figure 50.

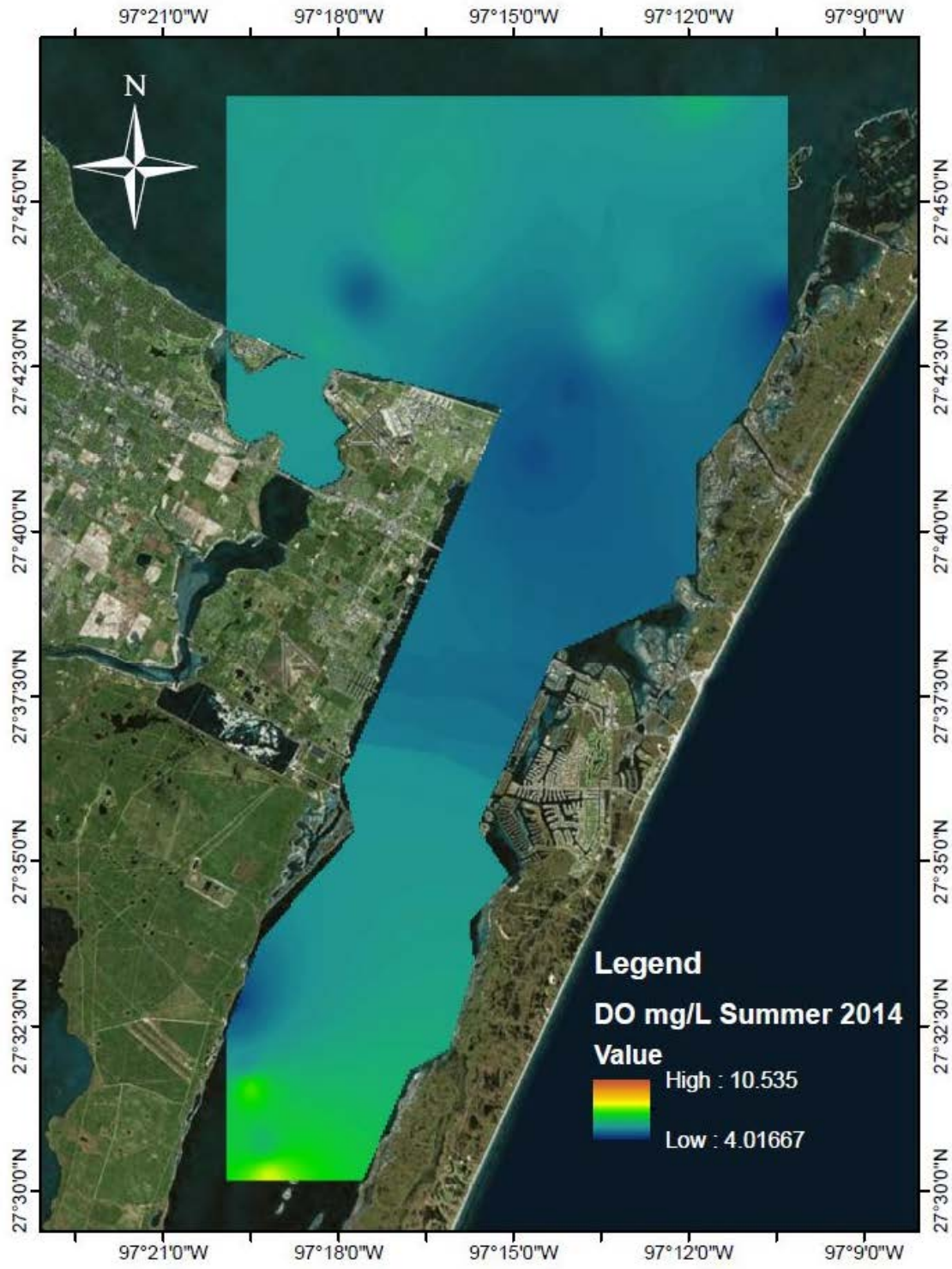


Figure 51.

APPENDIX LEGEND

Appendix 1. Continuous Resistivity Profiles (CRP) for transects 1 through 5 collected during winter 2013-2014.

Appendix 2. Time-lapse electrical resistivity (ER) inversions for first and last monitoring time and the final percent change in resistivity images for groundwater monitoring stations: Oso Bay Inlet, Laguna Madre mouth, and Shamrock Island (see Figure 1 in the main report for locations).

Appendix 3. Summary of all geochemical and isotope data collected in winter, summer and fall, 2014.

Appendix 4. SAS statistical analyses graphs and tables.

Appendix 5. Statistical analyses SAS output.

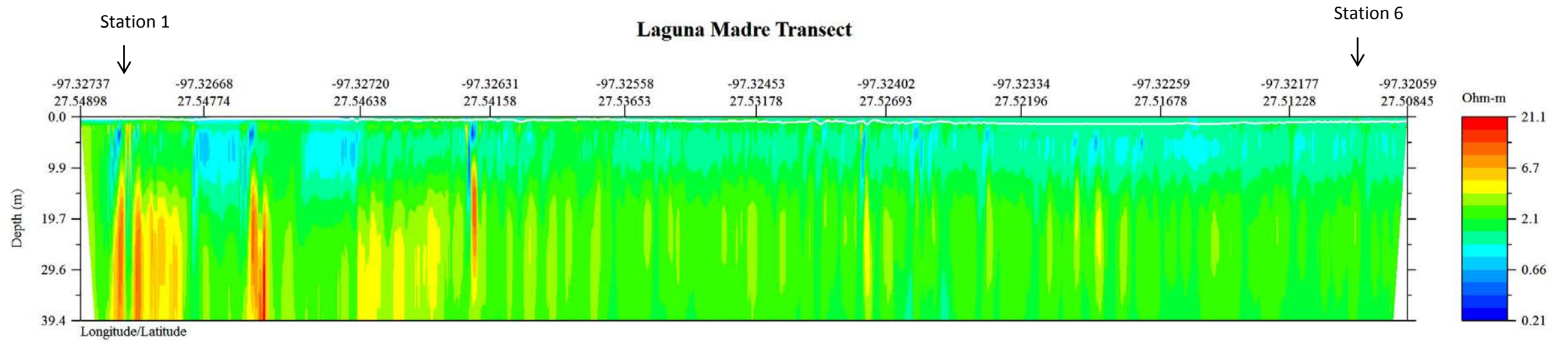


Figure 1. Continuous Resistivity Profile of the Laguna Madre transect (T1).

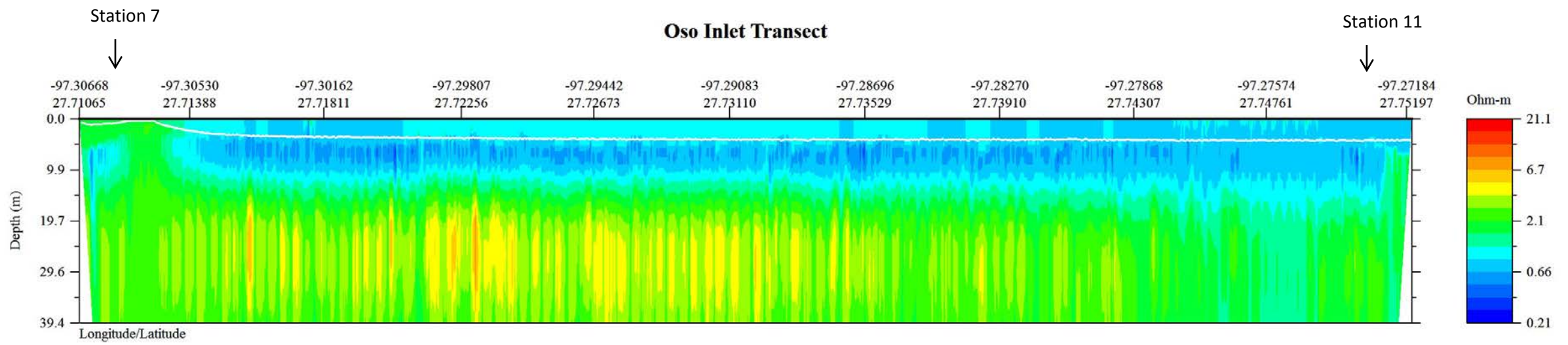


Figure 2. Continuous Resistivity Profile of the Oso Bay mouth transect (T2).

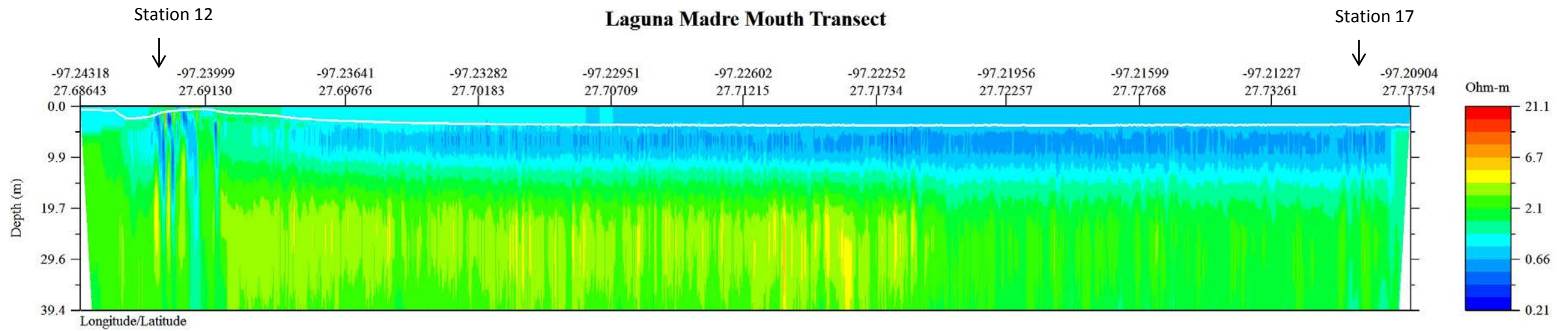


Figure 3. Continuous Resistivity Profile of the Laguna Madre mouth transect (T3).

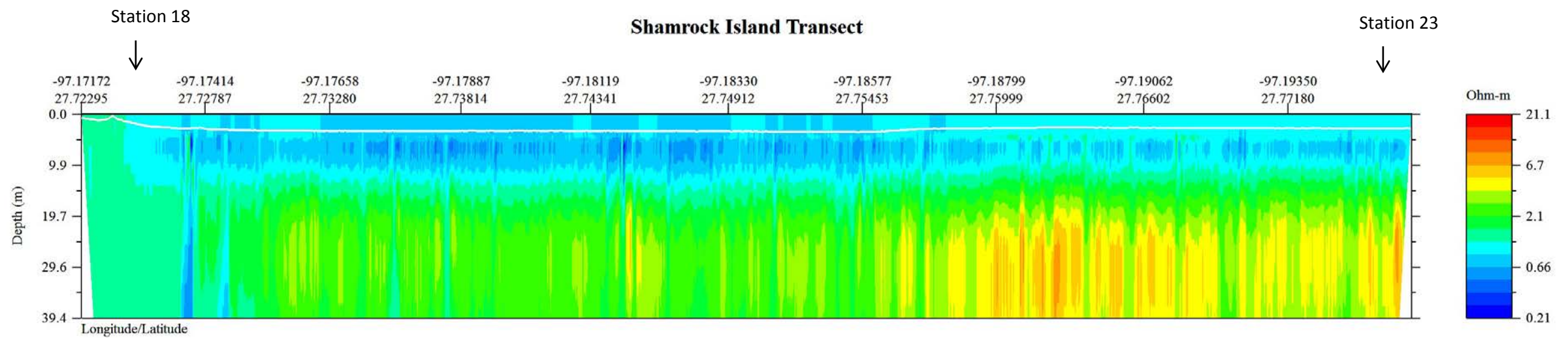


Figure 4. Continuous Resistivity Profile of the Shamrock Island transect (T4).

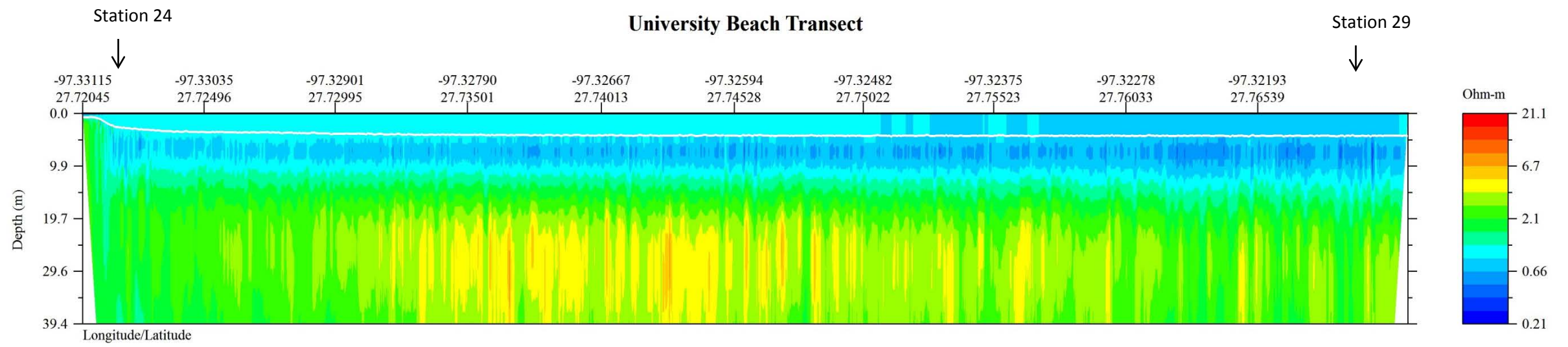


Figure 5. Continuous Resistivity Profile of the University Beach transect (T5).

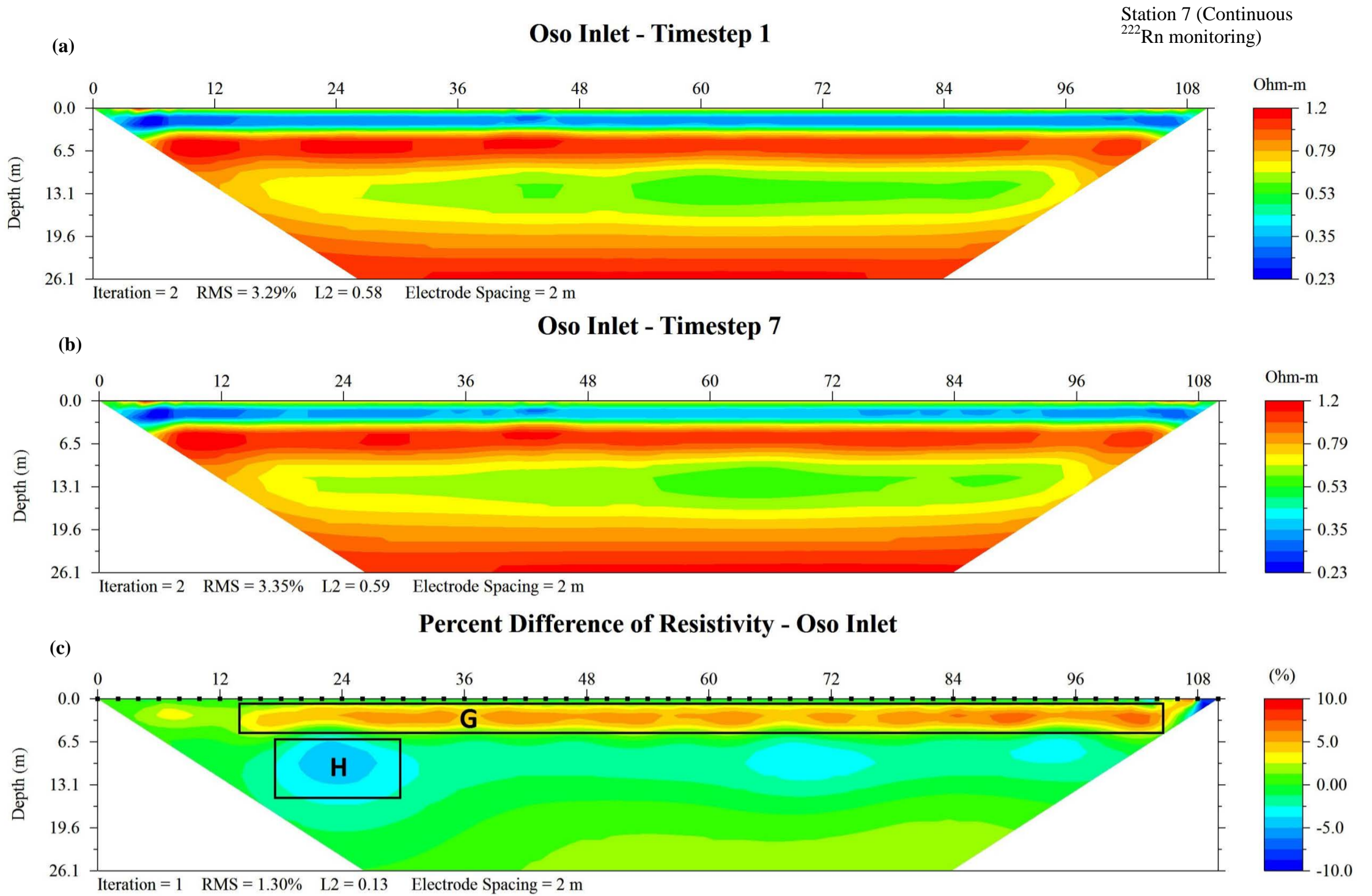


Figure TL 1. Summer time-lapse resistivity profiles (first (a) and last (b) time steps) for station 7 on Oso Bay inlet (see Figure 1 for geographic reference). The computed percent difference in resistivity (c) shows the change in porewater resistivity over a seven-hour period.

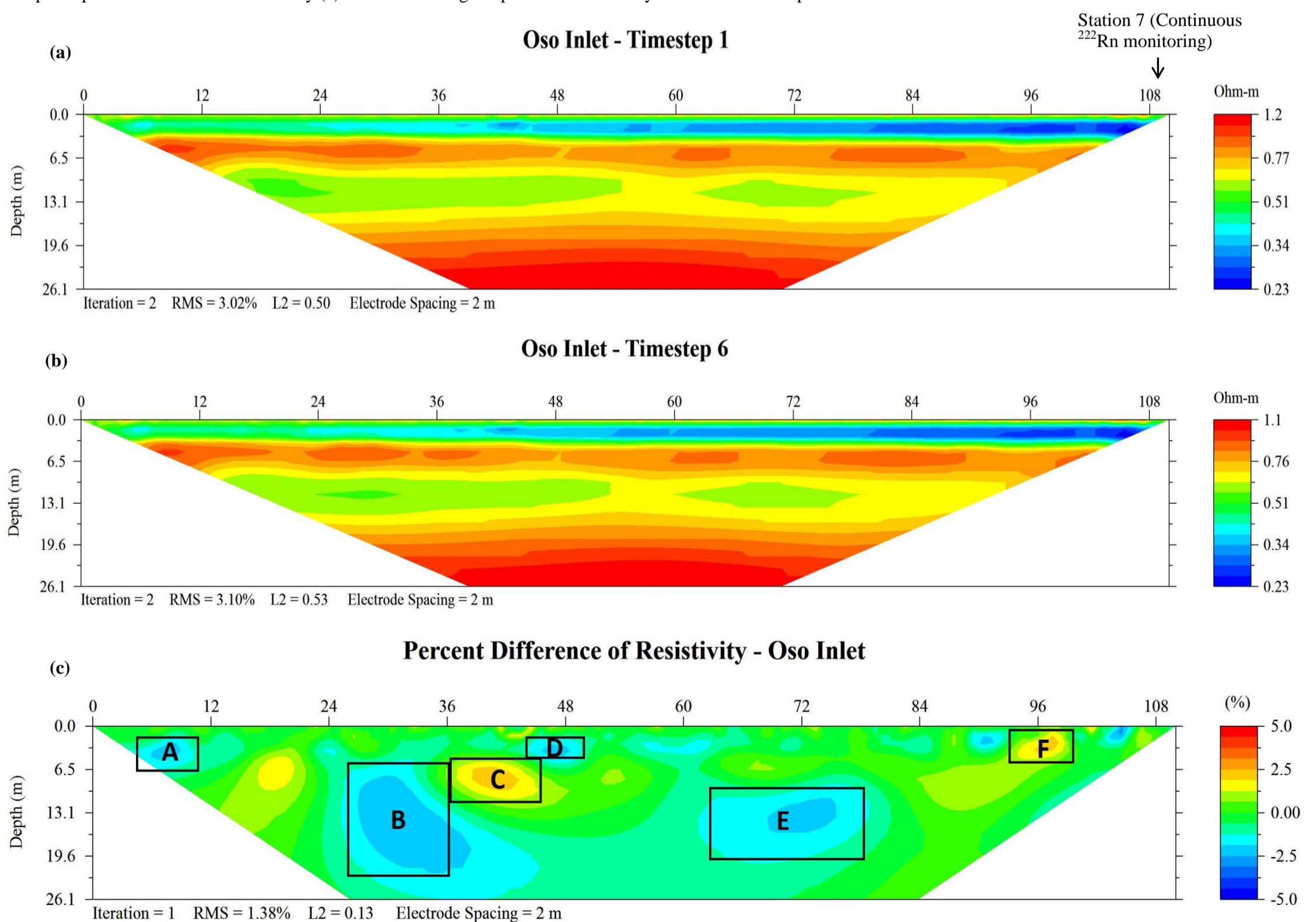


Figure TL 2. Fall time-lapse resistivity profiles (first (a) and last (b) time steps) for station 7 on Oso Bay inlet (see Figure 1 for geographic reference). The computed percent difference in resistivity (c) shows the change in porewater resistivity over a seven-hour period.

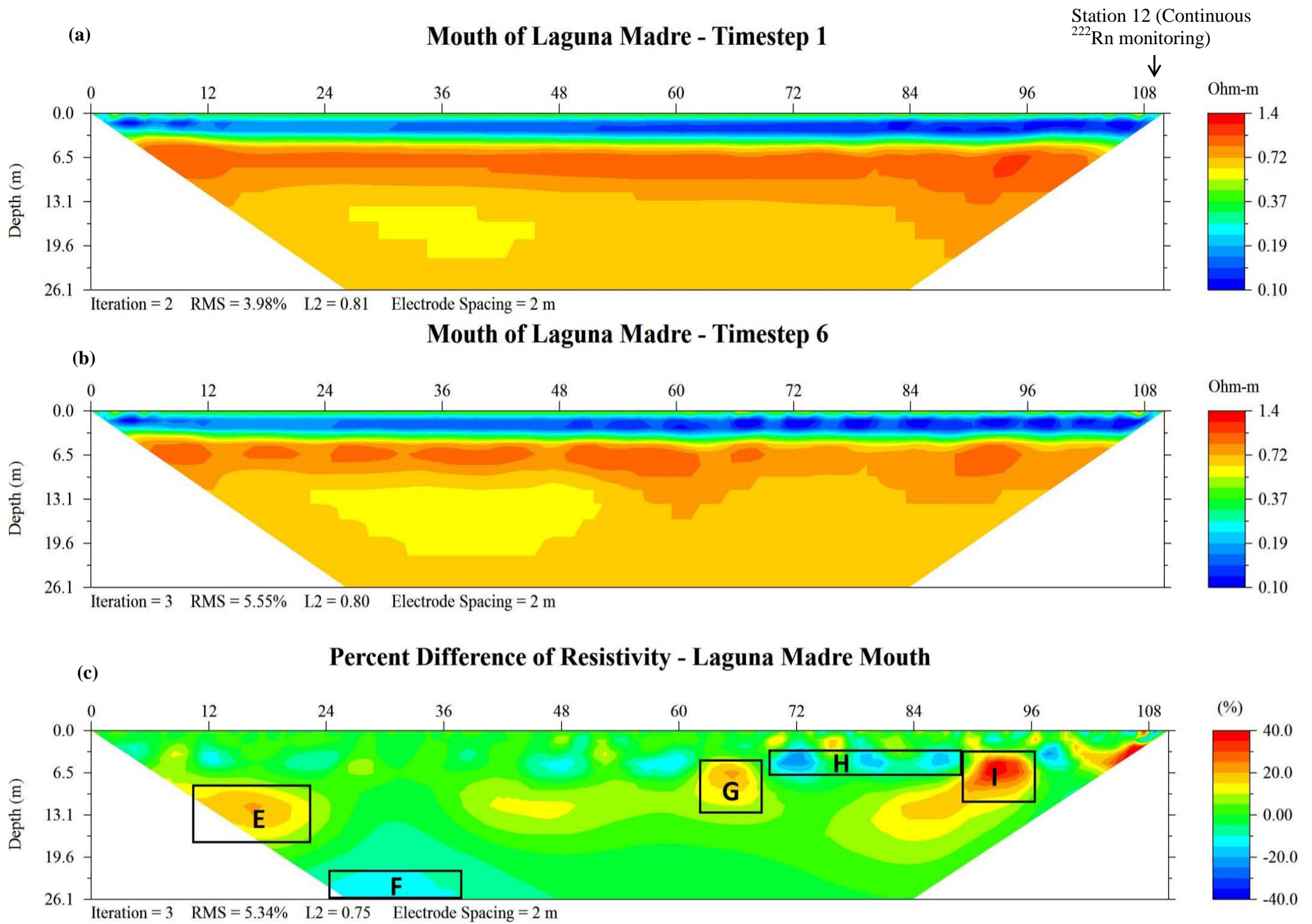


Figure TL 3. Summer time-lapse resistivity profiles (first (a) and last (b) time steps) for station 12 on Laguna Madre inlet/mouth (see Figure 1 for geographic reference). The computed percent difference in resistivity (c) shows the change in porewater resistivity over a seven-hour period.

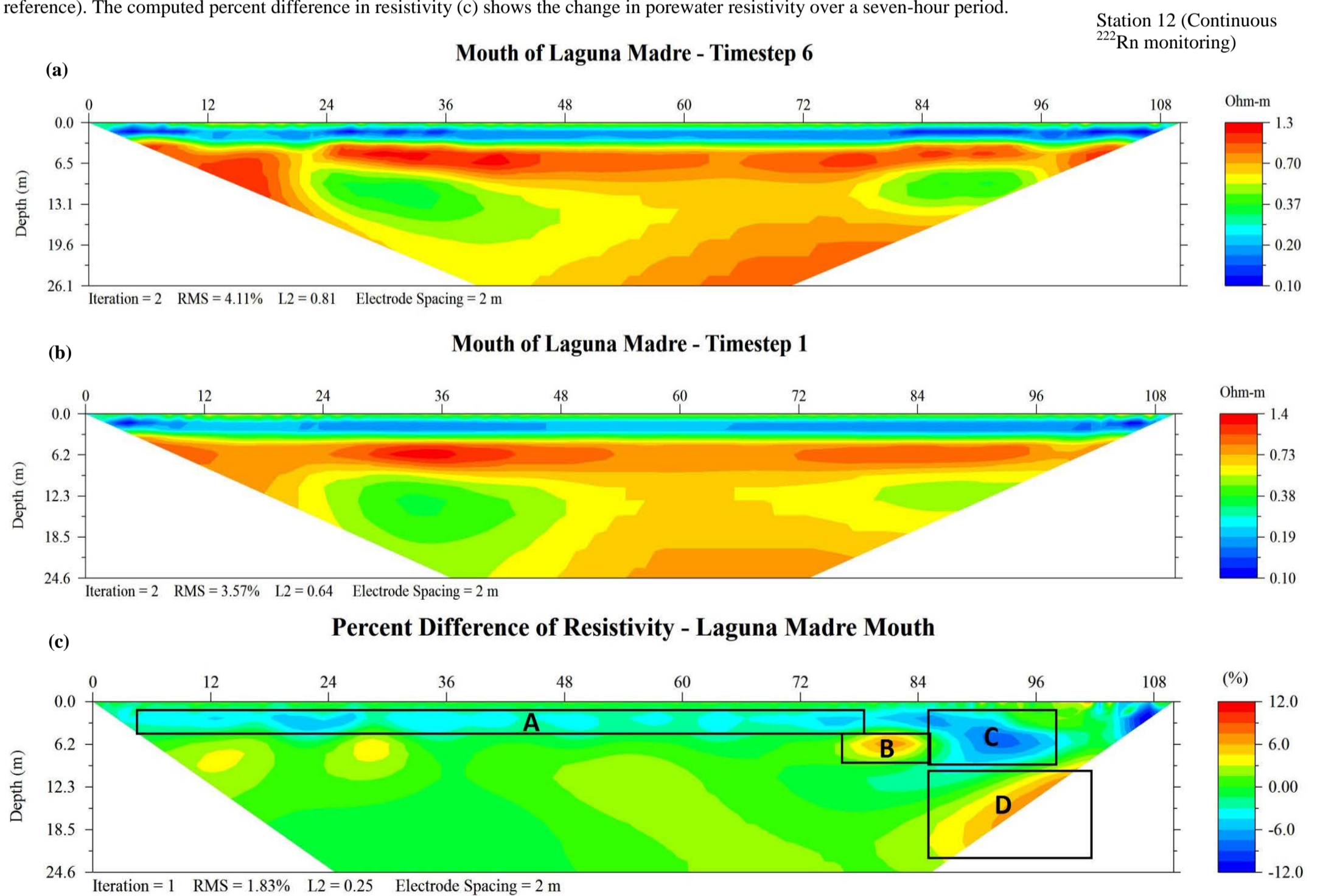


Figure TL 4. Fall time-lapse resistivity profiles (first (a) and last (b) time steps) for station 12 on Laguna Madre inlet/mouth (see Figure 1 for geographic reference). The computed percent difference in resistivity (c) shows the change in porewater resistivity over a seven-hour period.

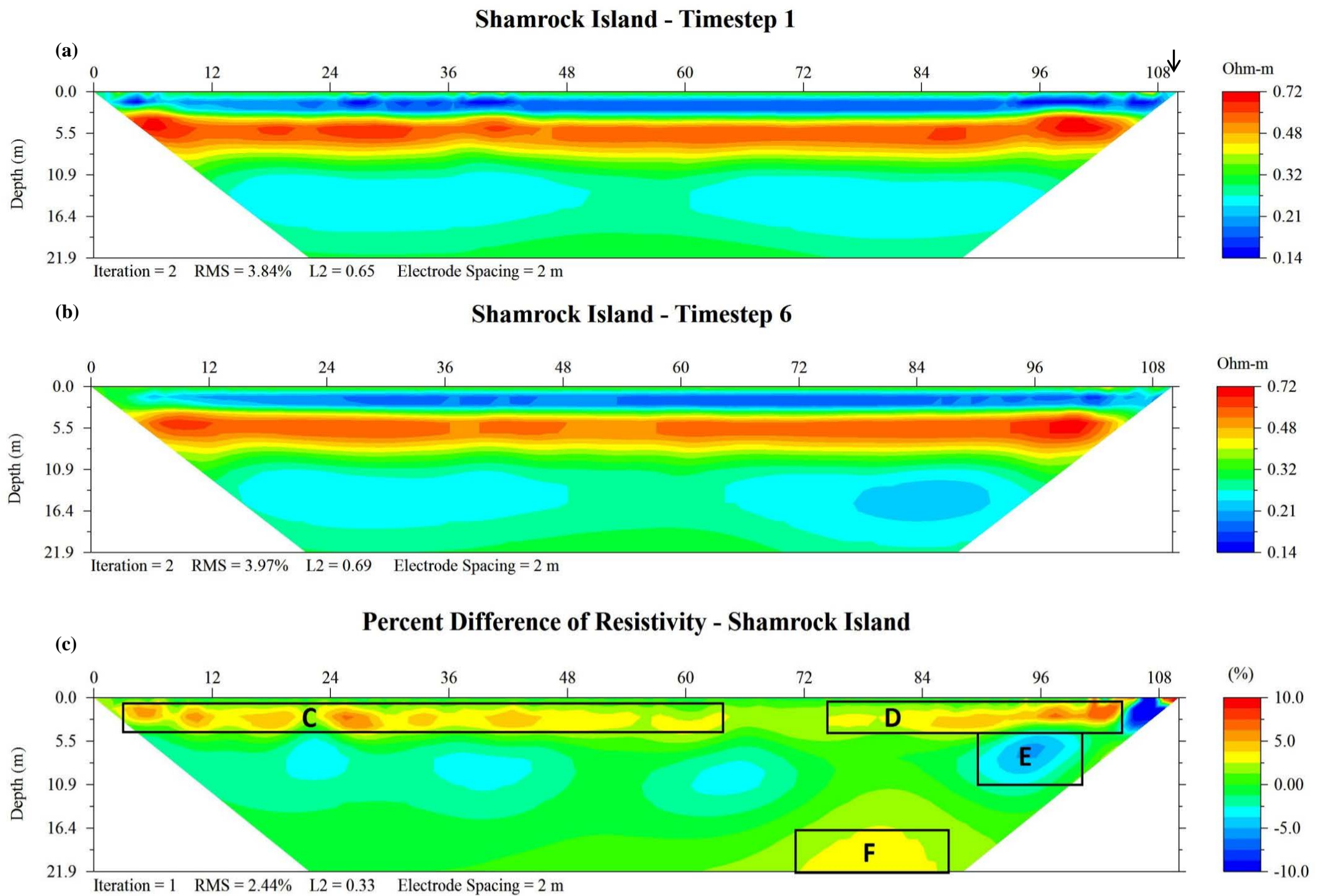


Figure TL 5. Summer time-lapse resistivity profiles (first (a) and last (b) time steps) for station 18 on Shamrock Island (see Figure 1 for geographic reference). The computed percent difference in resistivity (c) shows the change in porewater resistivity over a seven-hour period

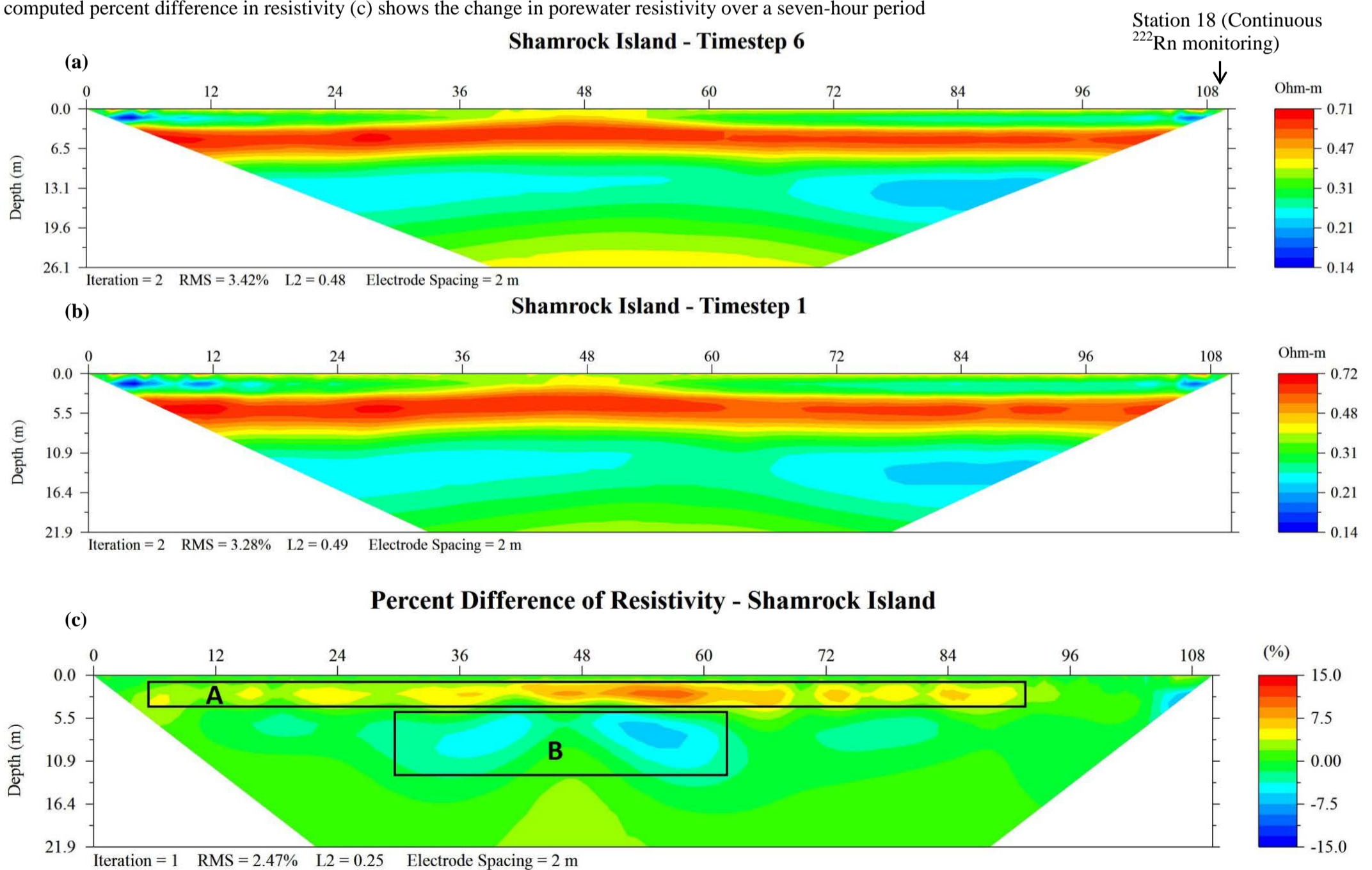


Figure TL 6. Fall time-lapse resistivity profiles (first (a) and last (b) time steps) for station 18 on Shamrock Island (see Figure 1 for geographic reference). The computed percent difference in resistivity (c) shows the change in porewater resistivity over a seven-hour period

APPENDIX 4: SAS Analysis Output

In the following Appendix, the seasons are defined as: Winter includes samples collected in January 2014; Summer includes samples collected July and August 2014; and Fall includes samples collected in November and December 2014. All surface water sample depths are defined as: S is surface depths of 0.2m below the water/air interface; M is middle depths of half the station depth, half the depth between the sediment/water interface and the water/air interface (varies by station depth); and B is bottom depths of 0.2m above the sediment/water interface. The P samples are pore water samples collected by push-point piezometer from within the sediment. Depth within the sediment for successful pore water extraction ranged from 0.5m to 2.5m below the sediment/water interface.

Figure 1: Average Chlorophyll- α (mg/L) concentrations in surface waters by season.

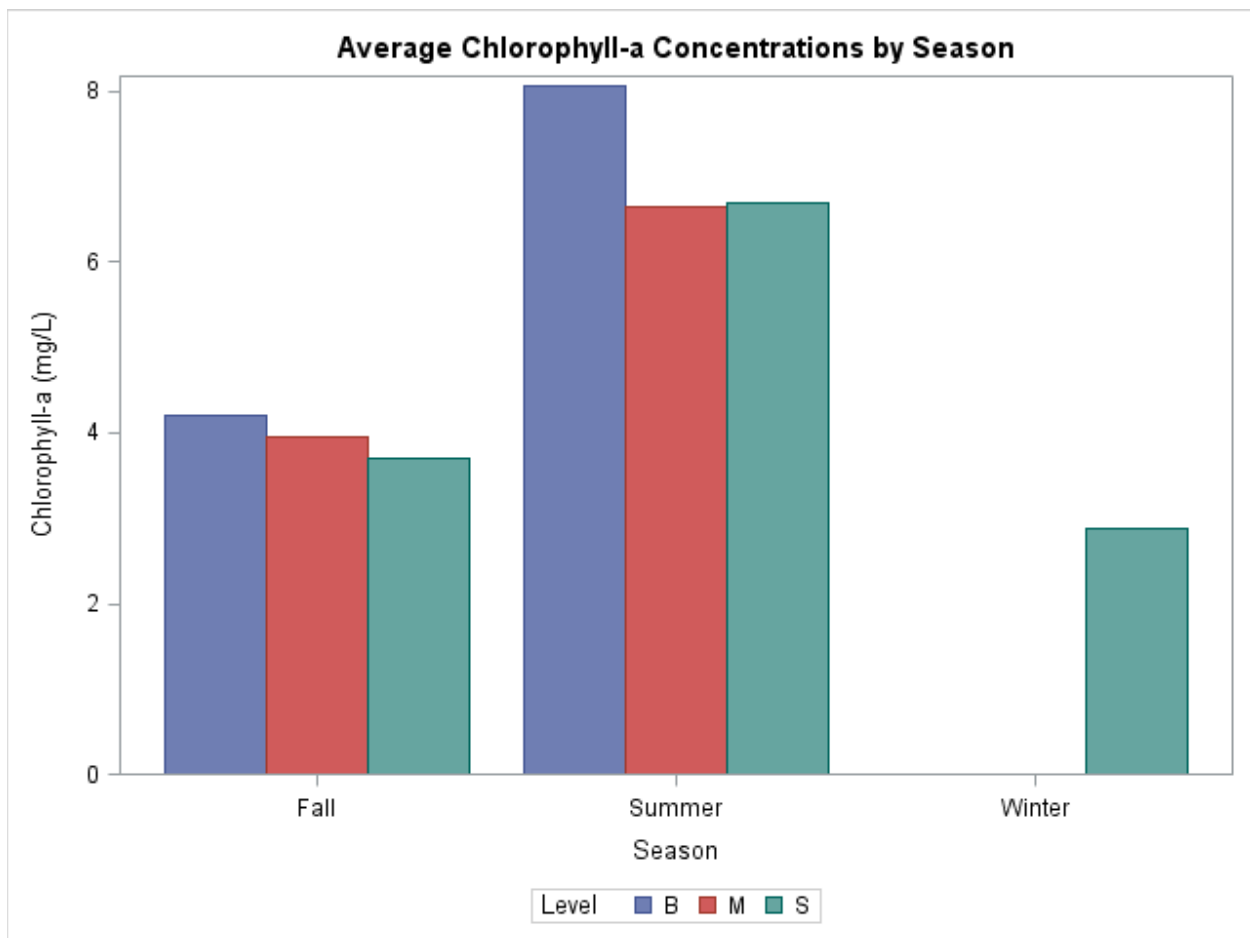


Figure 2: Average Ammonia (umol/L) concentrations by season.

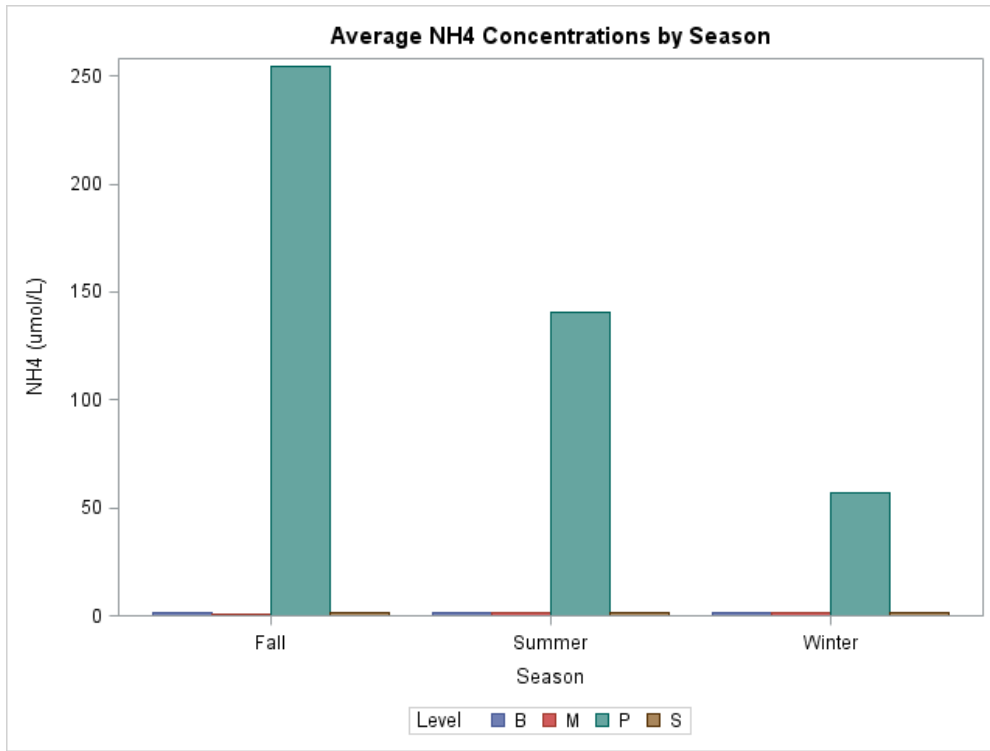


Figure 3: Average Ammonia (umol/L) concentrations in surface waters by season.

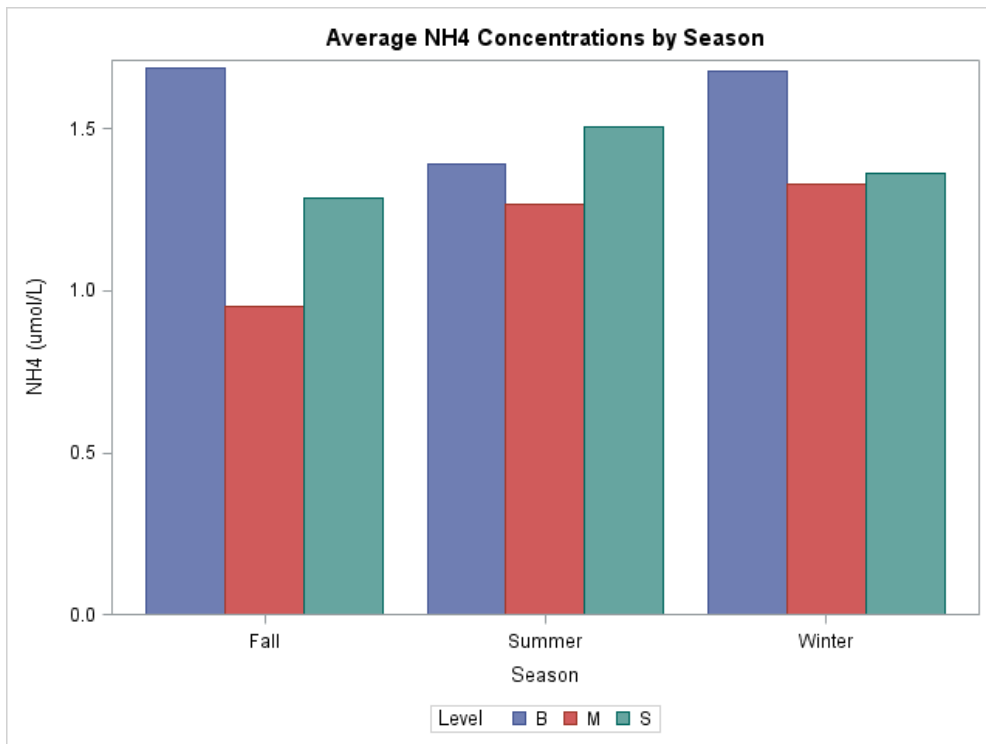


Figure 4: Average Nitrate+Nitrite ($\mu\text{mol/L}$) concentrations by season.

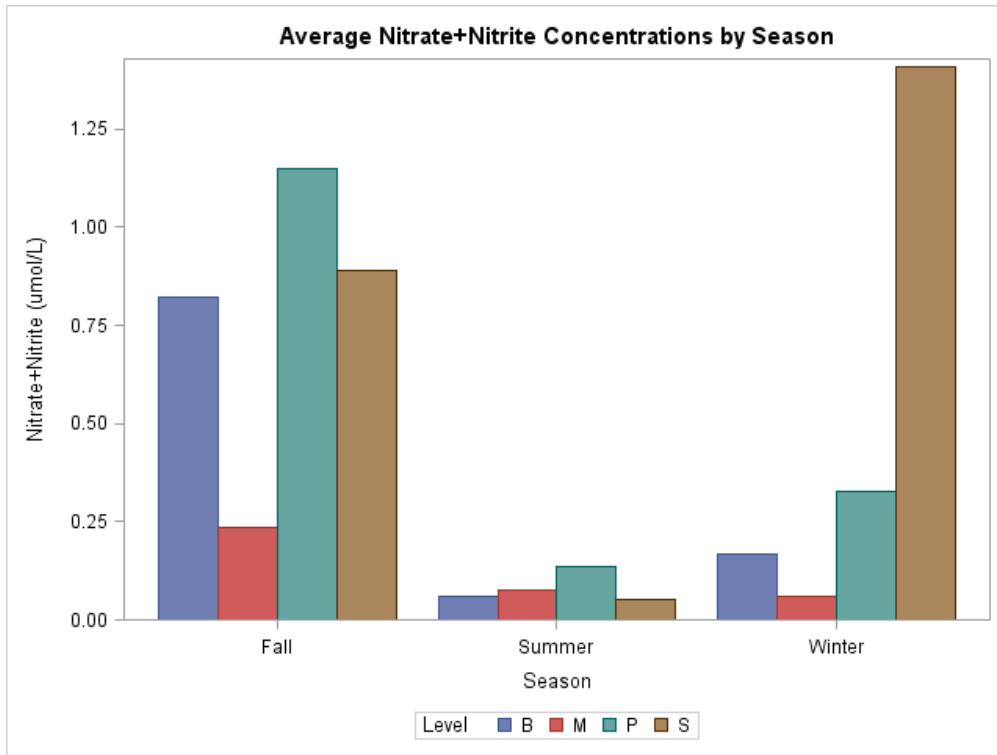


Figure 5: Average Nitrite ($\mu\text{mol/L}$) concentrations by season.

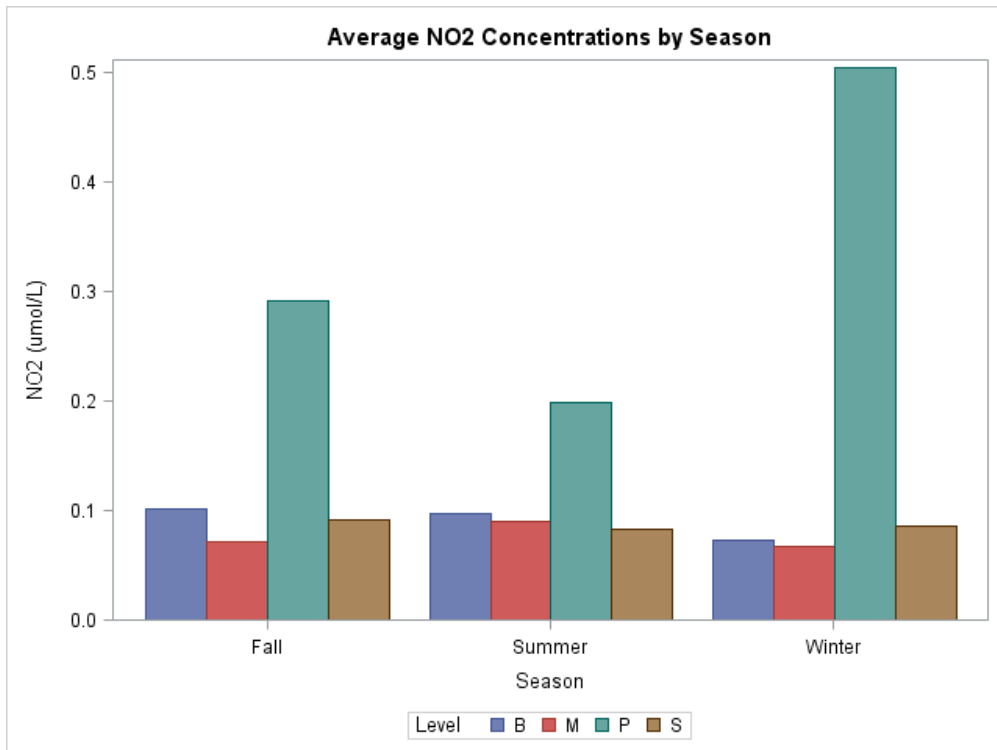


Figure 6: Average Total Dissolved Nitrogen (umol/L) concentrations by season.

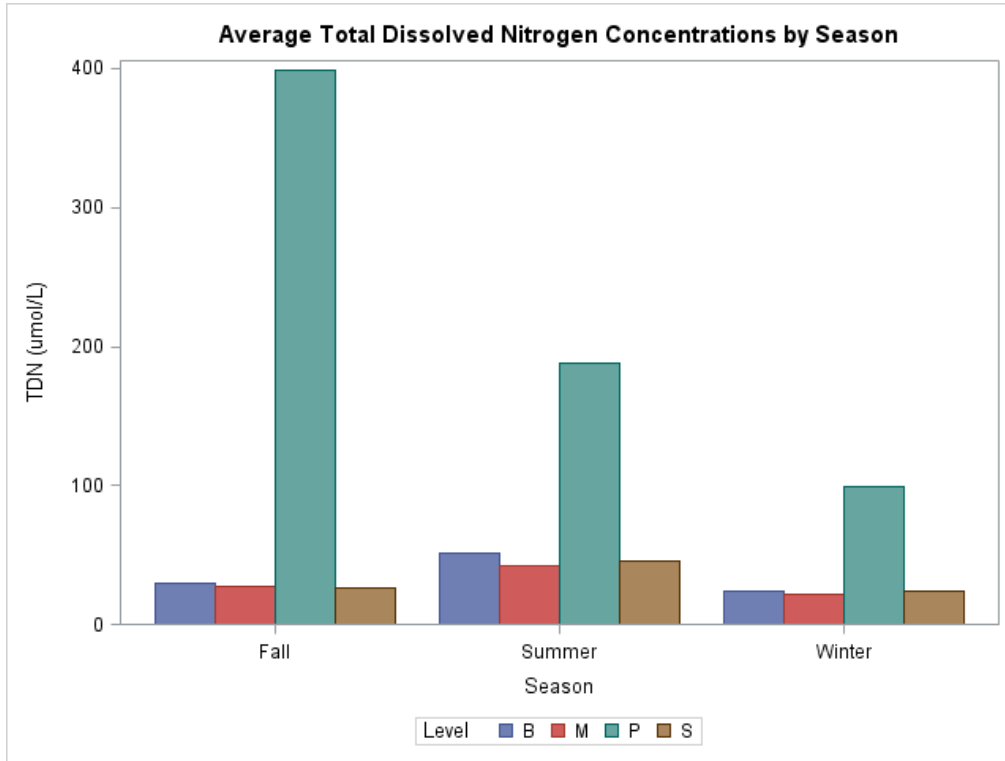


Figure 7: Average Total Dissolved Nitrogen (umol/L) concentrations in surface waters by season.

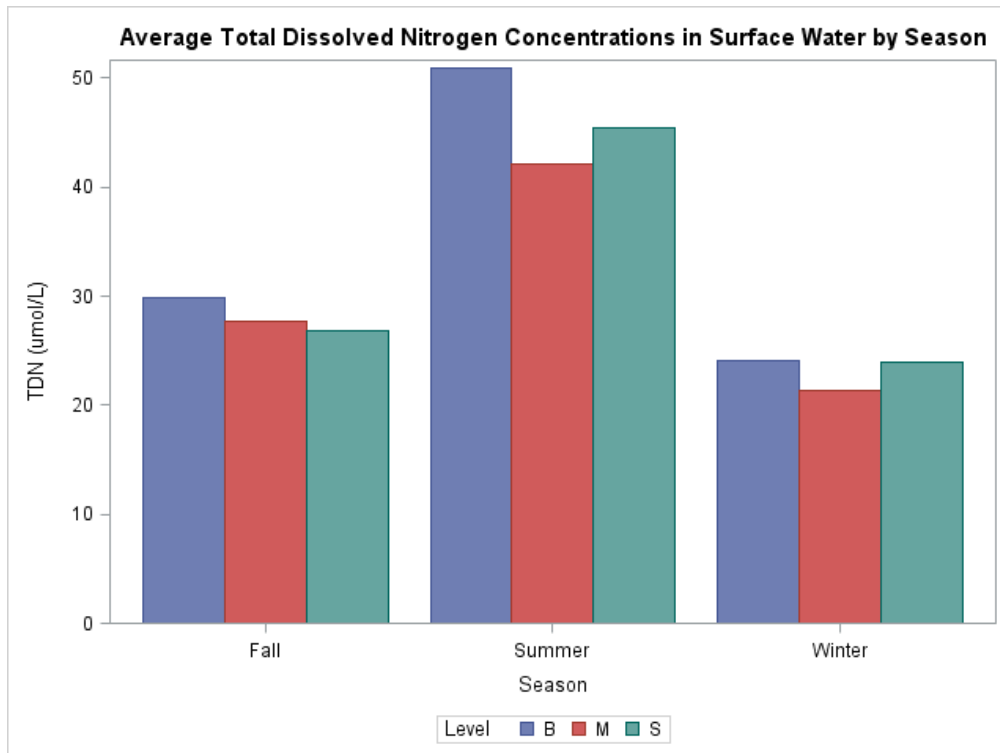


Figure 8: Average Phosphate (umol/L) concentrations by season.

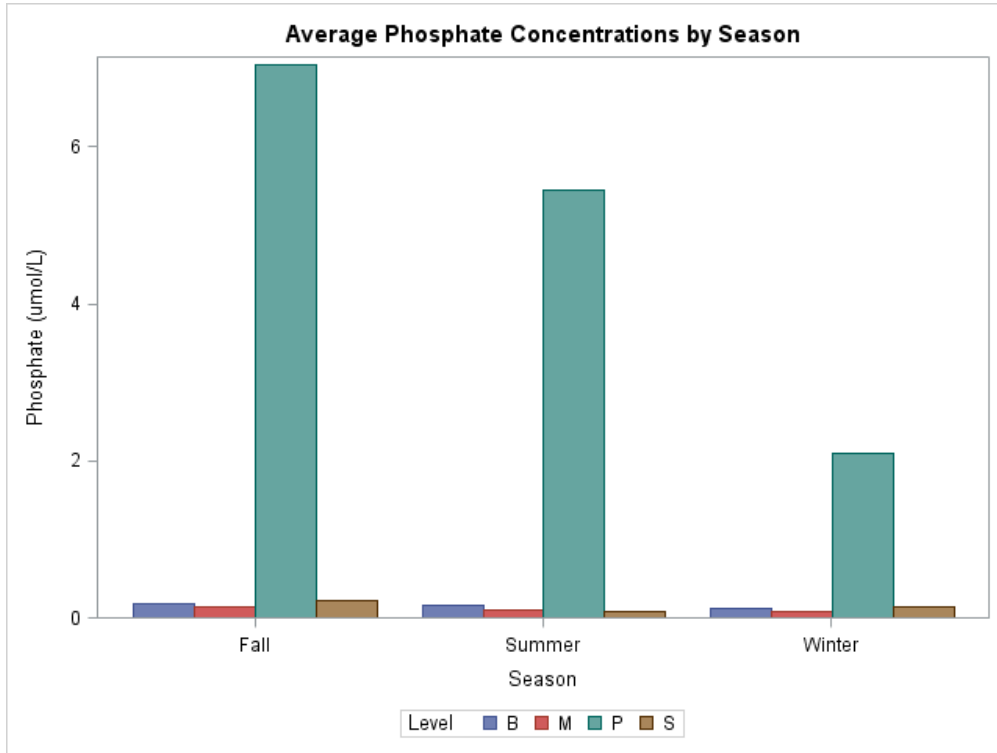


Figure 9: Average Phosphate (umol/L) concentrations in surface waters by season.

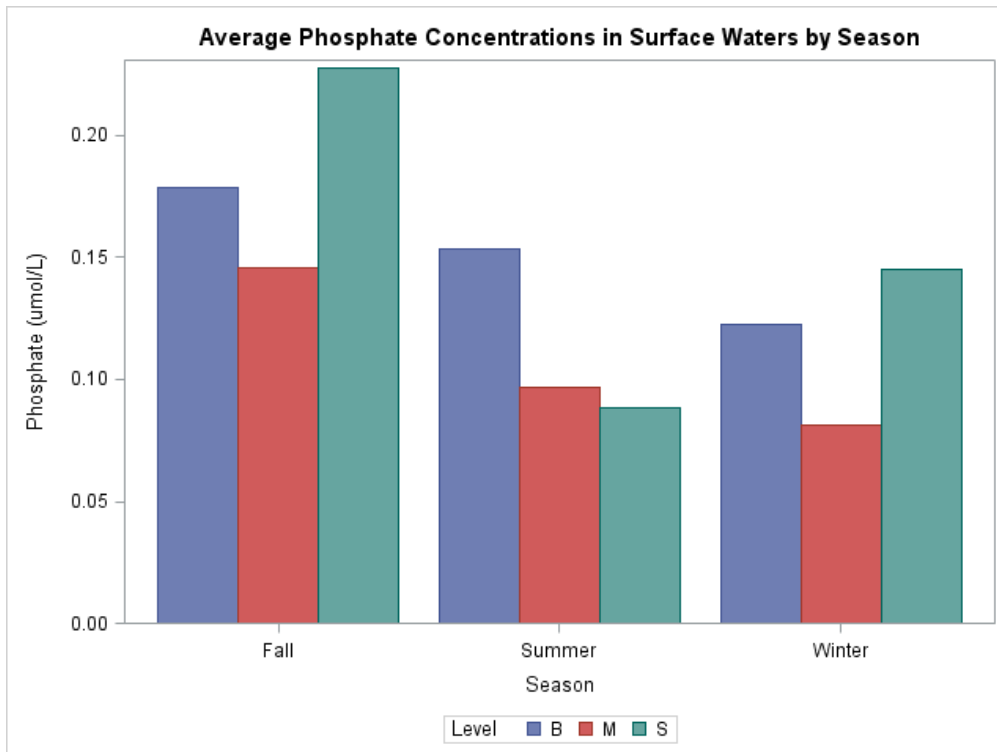


Figure 10: Average Silicate ($\mu\text{mol/L}$) concentrations by season.

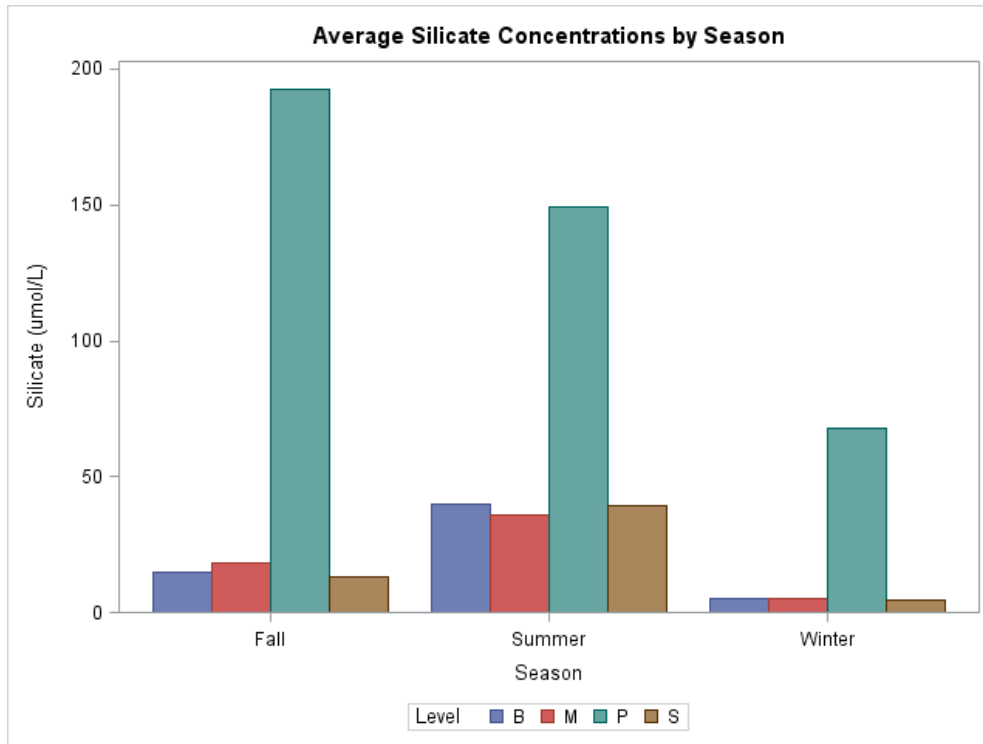


Figure 11: Average Silicate ($\mu\text{mol/L}$) concentrations in surface waters by season.

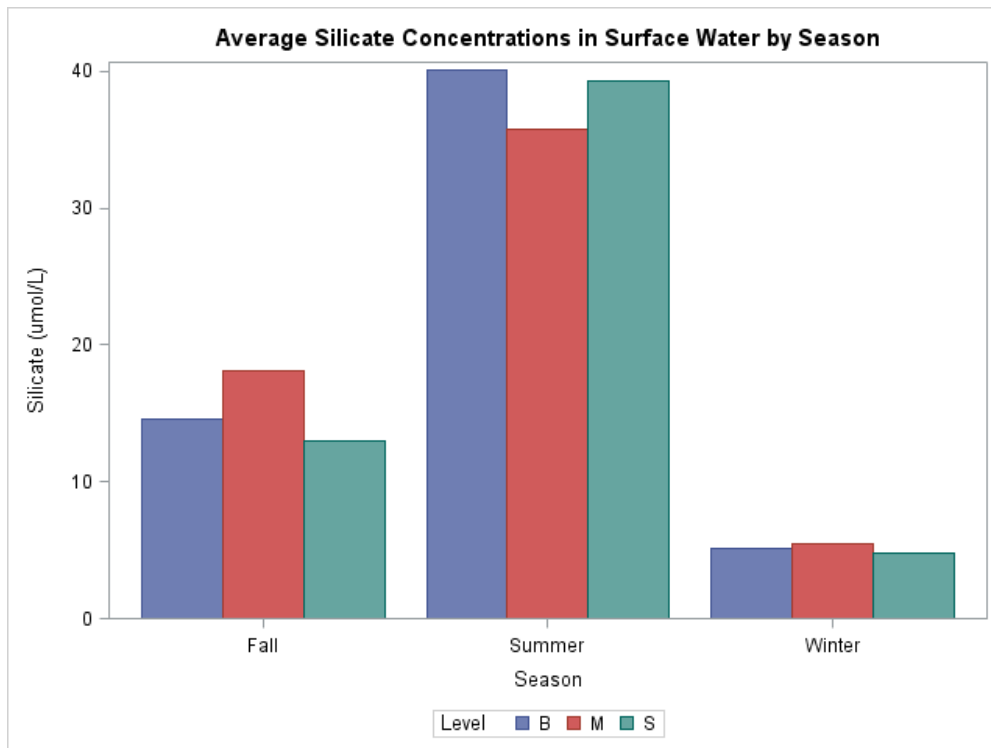


Figure 12: Average Radon-222 (Bq/m^3) concentrations by season.

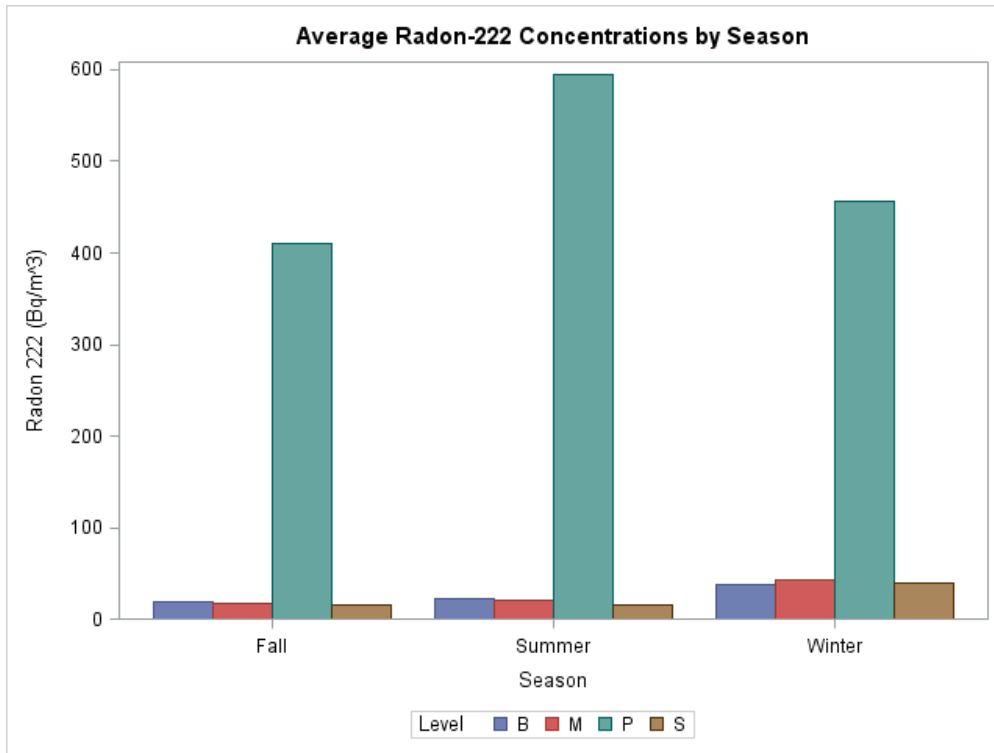


Figure 13: Average Radon-222 (Bq/m^3) concentrations in surface waters by season.

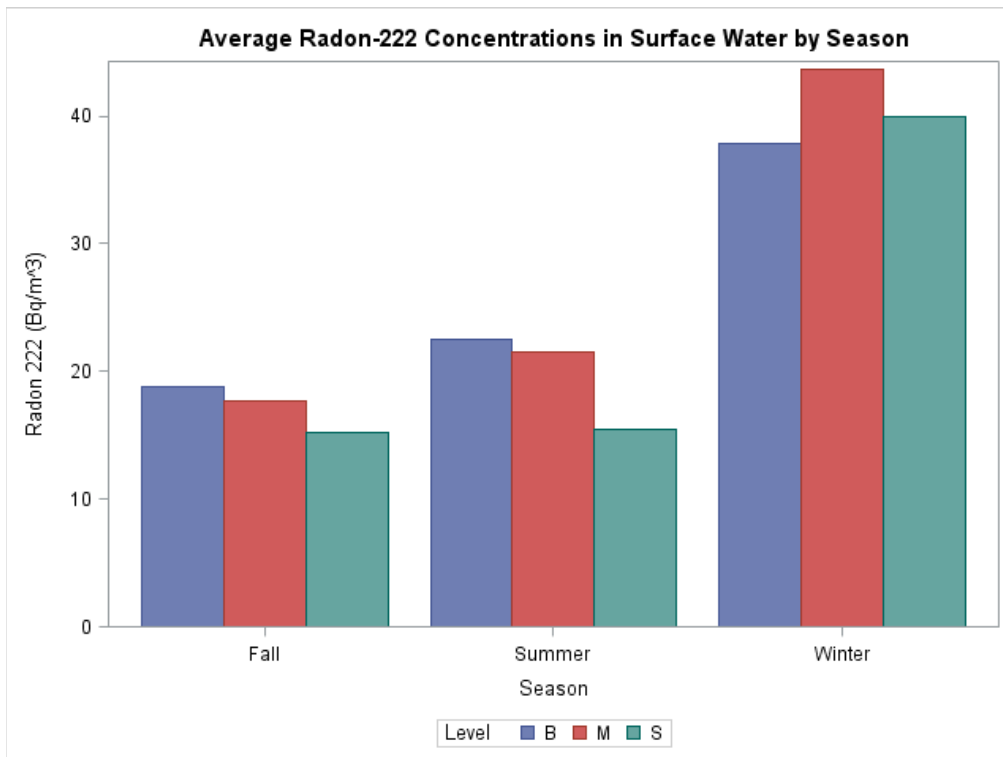


Figure 14: Distribution of Radium-224 (dpm/m³) by event. (Note: Radium-224 samples were not measured for the January 2014 samples.)

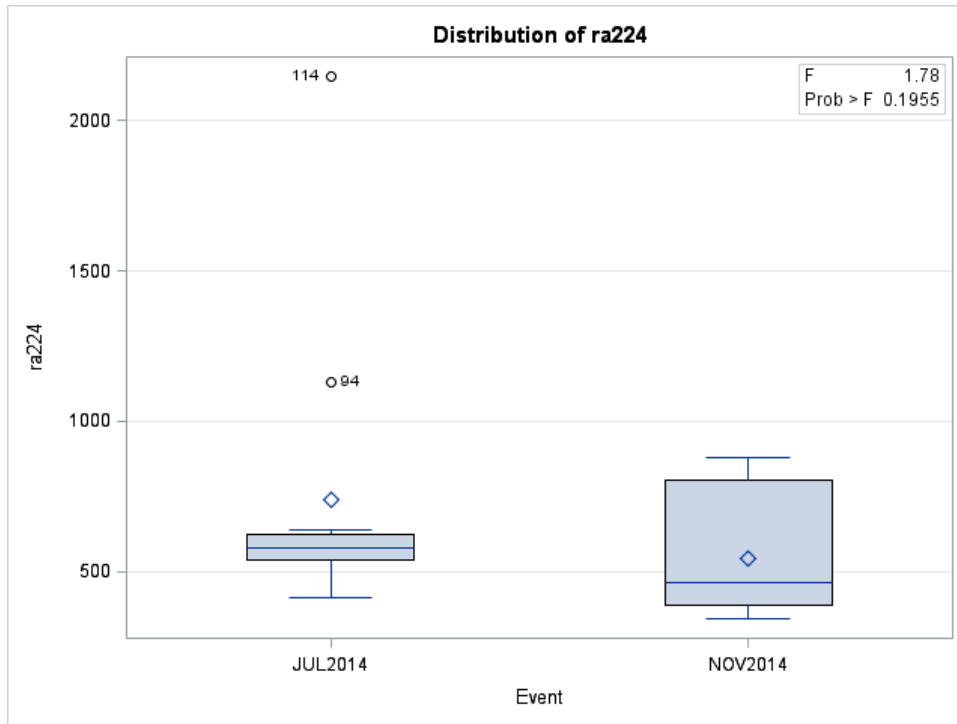


Figure 15: Distribution of Radium-226 (dpm/m³) by event.

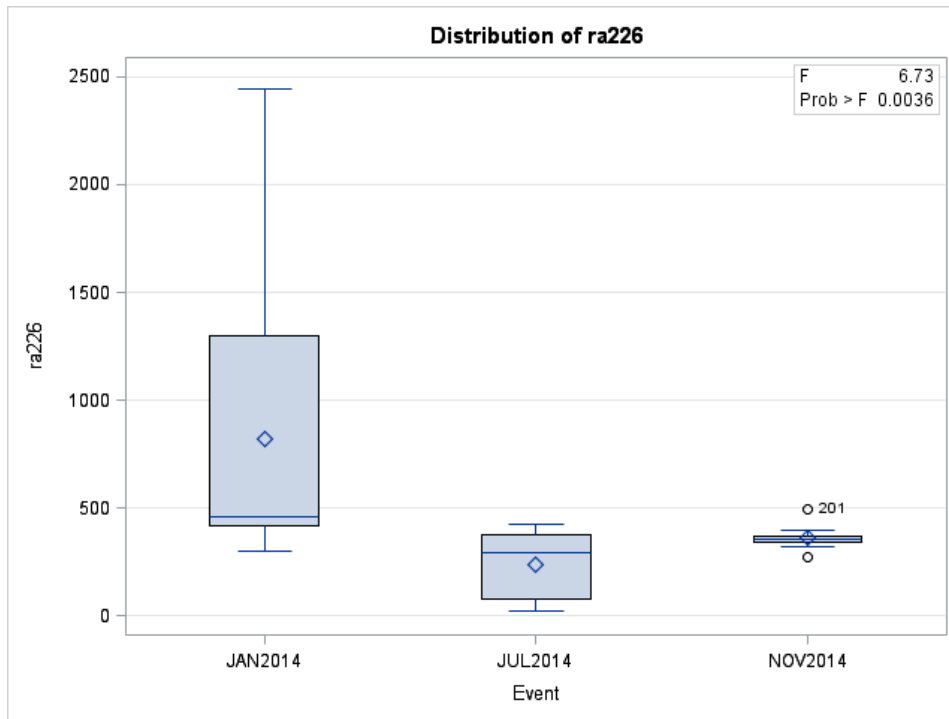


Figure 16: Average δ Oxygen-18 (% VSMOW) concentrations by season.

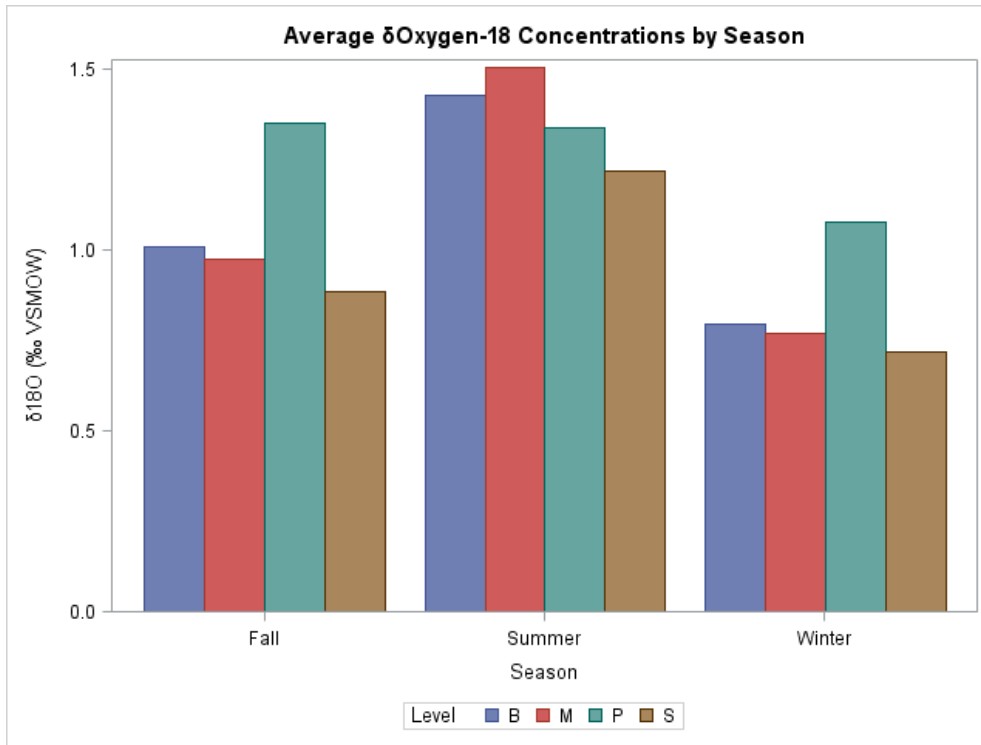


Figure 17: Average δ Deuterium (% VSMOW) concentrations by season.

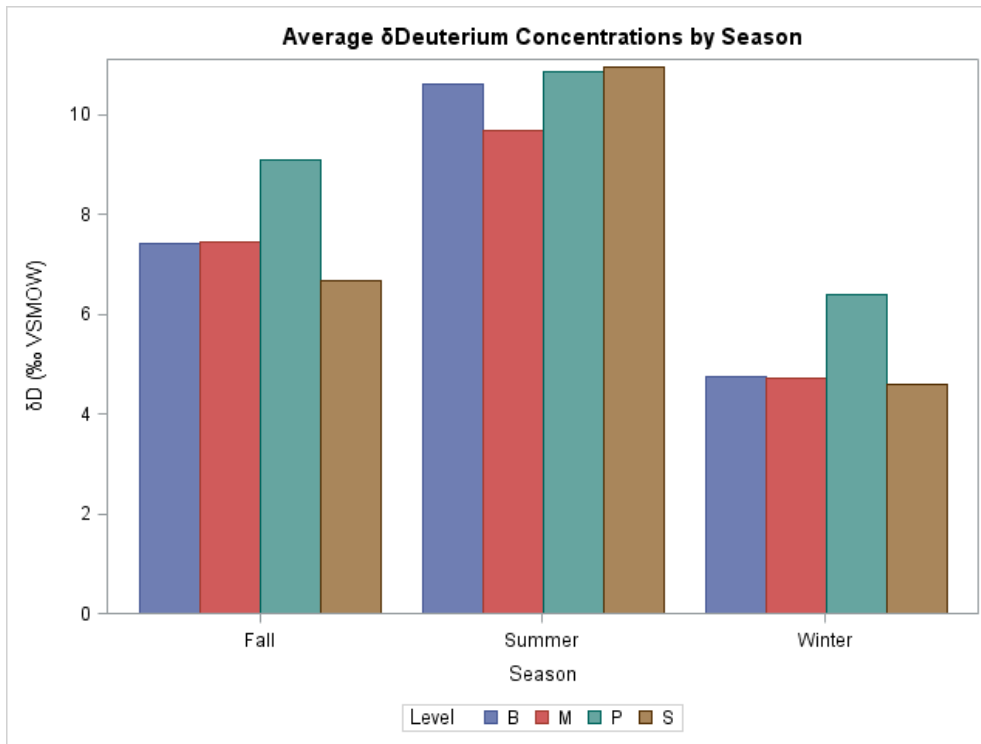


Figure 18: Average δ Carbon-13 (‰ VPDB) concentrations by season.

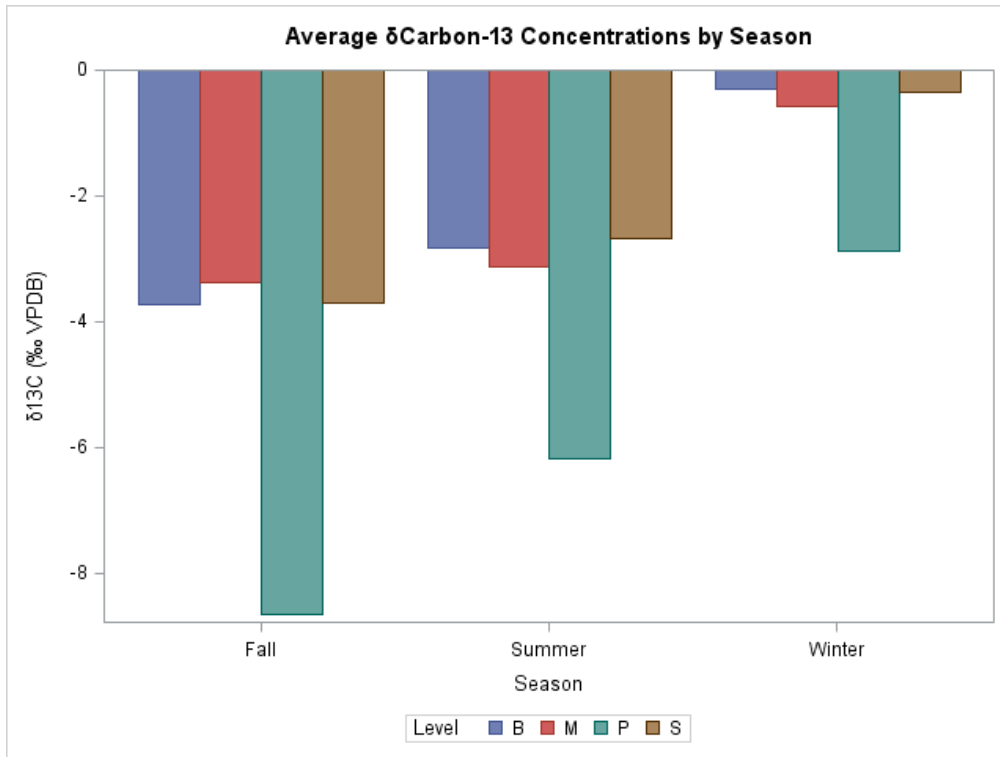


Figure 19: Scree plot for Principal Component Analysis of full dataset (excluding variables missing more than 10% of data).

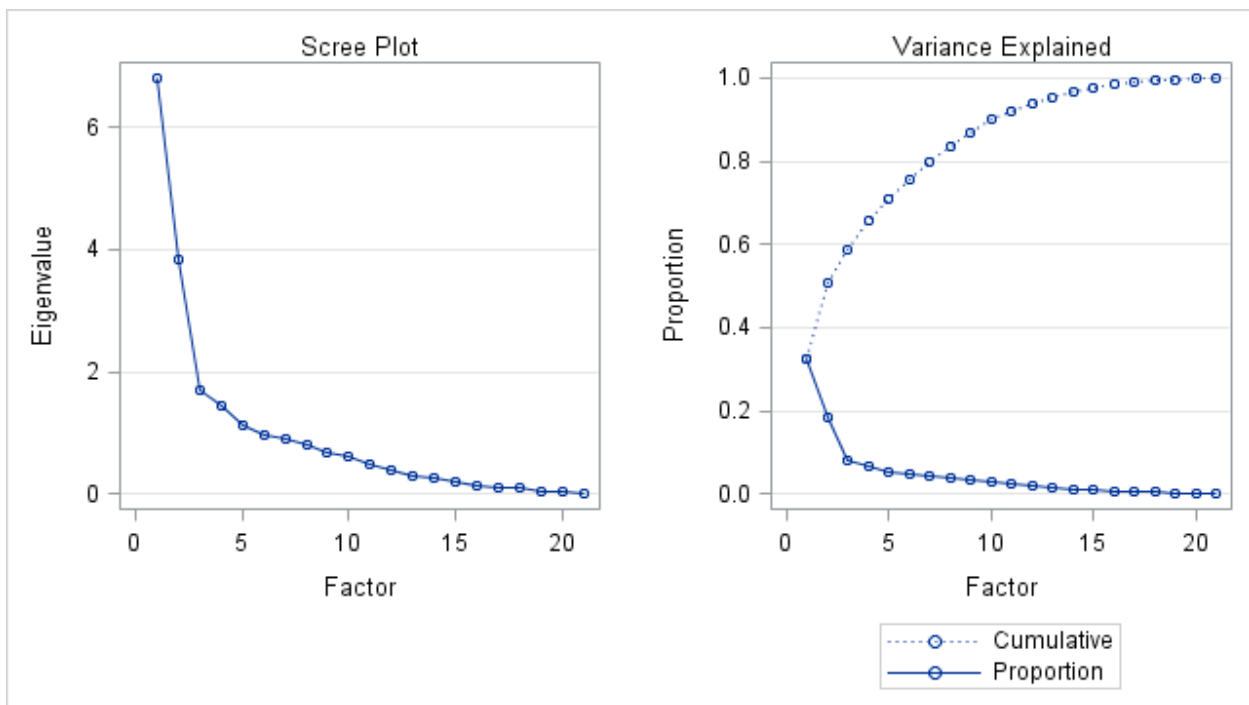


Table 1: Principal Component Analysis output of eigenvalues, proportion of variance explained by each factor, and cumulative variation explained by factors. Factors with eigenvalues >1 are considered significant.

Eigenvalues of the Correlation Matrix: Total = 21 Average = 1				
	Eigenvalue	Difference	Proportion	Cumulative
1	6.79900631	2.97380066	0.3238	0.3238
2	3.82520566	2.12580310	0.1822	0.5059
3	1.69940256	0.25015915	0.0809	0.5868
4	1.44924341	0.33784725	0.0690	0.6559
5	1.11139616	0.13821774	0.0529	0.7088
6	0.97317841	0.05946943	0.0463	0.7551
7	0.91370898	0.12276746	0.0435	0.7986
8	0.79094152	0.09608320	0.0377	0.8363
9	0.69485832	0.06774738	0.0331	0.8694
10	0.62711094	0.14549361	0.0299	0.8992
11	0.48161733	0.09009578	0.0229	0.9222
12	0.39152155	0.09746197	0.0186	0.9408
13	0.29405958	0.02820400	0.0140	0.9548
14	0.26585558	0.05562579	0.0127	0.9675
15	0.21022979	0.07376666	0.0100	0.9775
16	0.13646313	0.01552054	0.0065	0.9840
17	0.12094258	0.01614773	0.0058	0.9897
18	0.10479486	0.04754142	0.0050	0.9947
19	0.05725343	0.00856401	0.0027	0.9975
20	0.04868943	0.04416898	0.0023	0.9998
21	0.00452044		0.0002	1.0000

Average Ratio Sulfate to Chloride Concentrations by Season

The CONTENTS Procedure

Data Set Name	CCB.RAW_SORT	Observations	475
Member Type	DATA	Variables	47
Engine	V9	Indexes	0
Created	08/30/2015 22:10:52	Observation Length	464
Last Modified	08/30/2015 22:10:52	Deleted Observations	0
Protection		Compressed	NO
Data Set Type		Sorted	YES
Label			
Data Representation	WINDOWS_64		
Encoding	utf-8 Unicode (UTF-8)		

Engine/Host Dependent Information	
Data Set Page Size	65536
Number of Data Set Pages	4
First Data Page	1
Max Obs per Page	141
Obs in First Data Page	128
Number of Data Set Repairs	0
ExtendObsCounter	YES
Filename	C:\Users\adouglas\Desktop\SAS\CCB\raw_sort.sas7bdat
Release Created	9.0401M2
Host Created	X64_8HOME

Alphabetic List of Variables and Attributes						
#	Variable	Type	Len	Format	Informat	Label
20	Ammonia	Num	8			Ammonia
28	Ca	Num	8			Ca
36	Ca_Cl	Num	8			Ca/Cl
17	Chla	Num	8			Chla
32	Cl	Num	8			Cl
14	Cond25	Num	8			Cond25
41	DIC	Num	8			DIC
18	DOC	Num	8			DOC
13	DOconc	Char	15	\$15.	\$15.	DOconc
12	DOPrcnt	Char	18	\$18.	\$18.	DOPrcnt
8	Depth	Num	8			Depth
47	Event	Num	8	MONYY7.		
25	Fe	Num	8			Fe
29	K	Num	8			K

Average Ratio Sulfate to Chloride Concentrations by Season

The CONTENTS Procedure

Alphabetic List of Variables and Attributes						
#	Variable	Type	Len	Format	Informat	Label
37	K_Cl	Num	8			K/Cl
3	Level	Char	3	\$3.	\$3.	Level
27	Mg	Num	8			Mg
34	Mg_Ca	Num	8			Mg/Ca
35	Mg_Cl	Num	8			Mg/Cl
26	Mn	Char	12	\$12.	\$12.	Mn
33	Mn_Mg	Num	8			Mn/Mg
21	N_N	Char	18	\$18.	\$18.	N+N
30	Na	Num	8			Na
38	Na_Cl	Num	8			Na/Cl
22	Nitrite	Num	8			Nitrite
4	Rep	Num	8			Rep
44	Rn	Num	8			Rn
31	SO4	Num	8			SO4
39	SO4_Cl	Num	8			SO4/Cl
15	Salinity	Char	15	\$15.	\$15.	Salinity
9	Sample_Depth	Num	8			Sample Depth
24	Silicate	Char	21	\$21.	\$21.	Silicate
2	Station	Num	8			Station
19	TDN	Num	8			TDN
10	Temp	Num	8			Temp
7	TimeOff	Num	8	TIME8.	TIME8.	TimeOff
6	TimeOn	Num	8	TIME8.	TIME8.	TimeOn
1	Transect	Num	8			Transect
5	TransectDesc	Char	36	\$36.	\$36.	TransectDesc
45	_24Ra	Num	8			224Ra
46	_26Ra	Num	8			226Ra
40	d13C	Num	8			d13C
42	d18O	Num	8			d18O
43	dD	Num	8			dD
11	mmHg	Char	15	\$15.	\$15.	mmHg
23	o_Phosphate	Num	8			o-Phosphate
16	pH	Num	8			pH

Sort Information	
Sortedby	Event Transect Station Level Rep
Validated	YES
Character Set	ANSI

Average Ratio Sulfate to Chloride Concentrations by Season

The CONTENTS Procedure

Data Set Name	CCB.RAWFORM	Observations	475
Member Type	DATA	Variables	46
Engine	V9	Indexes	0
Created	08/30/2015 22:10:53	Observation Length	392
Last Modified	08/30/2015 22:10:53	Deleted Observations	0
Protection		Compressed	NO
Data Set Type		Sorted	NO
Label			
Data Representation	WINDOWS_64		
Encoding	utf-8 Unicode (UTF-8)		

Engine/Host Dependent Information	
Data Set Page Size	65536
Number of Data Set Pages	3
First Data Page	1
Max Obs per Page	167
Obs in First Data Page	153
Number of Data Set Repairs	0
ExtendObsCounter	YES
Filename	C:\Users\adouglas\Desktop\SAS\CCB\rawform.sas7bdat
Release Created	9.0401M2
Host Created	X64_8HOME

Alphabetic List of Variables and Attributes						
#	Variable	Type	Len	Format	Informat	Label
18	Ca	Num	8			Ca
26	Ca_Cl	Num	8			Ca/Cl
13	Chla	Num	8			Chla
22	Cl	Num	8			Cl
11	Cond25	Num	8			Cond25
31	DIC	Num	8			DIC
35	DO	Num	8			
14	DOC	Num	8			DOC
8	Depth	Num	8			Depth
34	Event	Num	8	MONYY7.		
16	Fe	Num	8			Fe
19	K	Num	8			K
27	K_Cl	Num	8			K/Cl
3	Level	Char	3	\$3.	\$3.	Level

Average Ratio Sulfate to Chloride Concentrations by Season

The CONTENTS Procedure

Alphabetic List of Variables and Attributes						
#	Variable	Type	Len	Format	Informat	Label
17	Mg	Num	8			Mg
24	Mg_Ca	Num	8			Mg/Ca
25	Mg_Cl	Num	8			Mg/Cl
36	Mn_	Num	8			
23	Mn_Mg	Num	8			Mn/Mg
37	NN	Num	8			
20	Na	Num	8			Na
28	Na_Cl	Num	8			Na/Cl
46	PO4	Num	8			
42	Ra224	Num	8			
43	Ra226	Num	8			
4	Rep	Num	8			Rep
41	Rn222	Num	8			
21	SO4	Num	8			SO4
29	SO4_Cl	Num	8			SO4/Cl
38	Sal	Num	8			
9	Sample_Depth	Num	8			Sample Depth
39	SiO4	Num	8			
2	Station	Num	8			Station
15	TDN	Num	8			TDN
10	Temp	Num	8			Temp
7	TimeOff	Num	8	TIME8.	TIME8.	TimeOff
6	TimeOn	Num	8	TIME8.	TIME8.	TimeOn
1	Transect	Num	8			Transect
5	TransectDesc	Char	36	\$36.	\$36.	TransectDesc
30	d13C	Num	8			d13C
32	d18O	Num	8			d18O
33	dD	Num	8			dD
40	mmHg_	Num	8			
44	nh4	Num	8			
45	no2	Num	8			
12	pH	Num	8			pH

Average Ratio Sulfate to Chloride Concentrations by Season

The CORR Procedure

29 Variables:	temp mn_	cond25 NN	ph sal	chla sio4	doc mmhg_	tdn rn222	fe ra224	mg ra226	ca nh4	k no2	na po4	so4 po4	cl	d13c	dic	d18o	dd	do_conc
--------------------------------	-------------	--------------	-----------	--------------	--------------	--------------	-------------	-------------	-----------	----------	-----------	------------	----	------	-----	------	----	---------

Simple Statistics							
Variable	N	Mean	Std Dev	Sum	Minimum	Maximum	Label
temp	210	19.88905	8.41322	4177	6.90000	31.60000	Temp
cond25	210	56832	6680	11934768	27794	83055	Cond25
ph	210	8.25552	0.26827	1734	7.04000	8.72000	pH
chla	142	5.41169	3.07862	768.46000	0.26000	18.03000	Chla
doc	222	453.36999	525.83218	100648	197.84419	6022	DOC
tdn	222	62.61709	163.76613	13901	18.09239	2236	TDN
fe	225	0.40533	0.63373	91.19956	0.02600	5.96380	Fe
mg	230	1325	206.55319	304733	545.66667	1896	Mg
ca	230	451.11563	92.95229	103757	312.46875	1314	Ca
k	230	555.61979	82.65485	127793	426.55313	740.25938	K
na	230	11260	3582	2589725	4712	26085	Na
so4	228	27.54629	5.57011	6281	0.26736	39.12289	SO4
cl	228	519.32169	94.41824	118405	1.06264	759.37289	Cl
d13c	221	-2.73061	2.88896	-603.46522	-22.07191	3.24557	d13C
dic	223	1514	1477	337638	0.19880	12507	DIC
d18o	223	1.07037	0.56590	238.69155	-2.40328	2.12764	d18O
dd	223	7.64726	3.39489	1705	3.26143	25.33762	dD
do_conc	192	6.47969	2.80888	1244	0.13000	10.91000	
mn_	170	0.15600	0.31524	26.52000	0.01000	3.85000	
NN	114	0.36936	1.45138	42.10750	0	11.26100	
sal	179	36.47034	4.45792	6528	0.21000	48.95000	
sio4	186	47.70747	73.98355	8874	0.08300	576.02500	
mmhg_	191	763.58377	3.00829	145845	751.40000	770.70000	
rn222	222	113.19502	318.02309	25129	0	3272	
ra224	25	638.25124	368.29939	15956	343.43000	2146	
ra226	35	449.64343	444.08410	15738	22.73000	2441	
nh4	228	25.47794	124.41588	5809	0.19450	1660	
no2	228	0.13484	0.16985	30.74300	0.02650	1.41500	
po4	223	0.95995	2.90402	214.06850	0.00300	30.34250	

Average Ratio Sulfate to Chloride Concentrations by Season

The CORR Procedure

Pearson Correlation Coefficients											
Prob > r under H0: Rho=0											
Number of Observations											
	temp	cond25	ph	chla	doc	tdn	fe	mg	ca	k	na
temp Temp	1.00000 210	0.69668 <.0001 192	-0.03484 0.6156 210	0.57348 <.0001 142	0.29795 <.0001 199	0.09532 0.1805 199	0.08708 0.2156 204	0.51895 <.0001 208	0.35605 <.0001 208	0.74977 <.0001 208	-0.57577 <.0001 208
cond25 Cond25	0.69668 <.0001 192	1.00000 210	-0.00671 0.9264 192	0.72700 <.0001 132	0.23916 0.0007 198	0.20478 0.0038 198	0.02510 0.7242 200	0.72051 <.0001 205	0.26268 0.0001 205	0.74273 <.0001 205	-0.07851 0.2632 205
ph pH	-0.03484 0.6156 210	-0.00671 0.9264 192	1.00000 210	0.49860 <.0001 142	-0.46456 <.0001 199	-0.53854 <.0001 199	-0.28589 <.0001 204	-0.06101 0.3813 208	-0.15340 0.0270 208	-0.10246 0.1408 208	-0.10038 0.1491 208
chla Chla	0.57348 <.0001 142	0.72700 <.0001 132	0.49860 <.0001 142	1.00000 142	0.71139 <.0001 136	0.61084 <.0001 136	0.05323 0.5307 141	0.50178 <.0001 142	0.33088 <.0001 142	0.62189 <.0001 142	-0.29026 0.0005 142
doc DOC	0.29795 <.0001 199	0.23916 0.0007 198	-0.46456 <.0001 199	0.71139 <.0001 136	1.00000 222	0.58220 <.0001 222	0.05615 0.4116 216	0.25791 0.0001 220	0.03792 0.5759 220	0.28797 <.0001 220	-0.10524 0.1196 220
tdn TDN	0.09532 0.1805 199	0.20478 0.0038 198	-0.53854 <.0001 199	0.61084 <.0001 136	0.58220 <.0001 222	1.00000 222	0.14793 0.0297 216	0.18046 0.0073 220	0.01576 0.8162 220	0.11417 0.0912 220	0.03933 0.5617 220
fe Fe	0.08708 0.2156 204	0.02510 0.7242 200	-0.28589 <.0001 204	0.05323 0.5307 141	0.05615 0.4116 216	0.14793 0.0297 216	1.00000 225	-0.15163 0.0232 224	-0.04720 0.4822 224	-0.14465 0.0304 224	-0.02094 0.7552 224
mg Mg	0.51895 <.0001 208	0.72051 <.0001 205	-0.06101 0.3813 208	0.50178 <.0001 142	0.25791 0.0001 220	0.18046 0.0073 220	-0.15163 0.0232 224	1.00000 230	0.14963 0.0232 230	0.84043 <.0001 230	-0.12774 0.0530 230
ca Ca	0.35605 <.0001 208	0.26268 0.0001 205	-0.15340 0.0270 208	0.33088 <.0001 142	0.03792 0.5759 220	0.01576 0.8162 220	-0.04720 0.4822 224	0.14963 0.0232 230	1.00000 230	0.22310 0.0007 230	-0.00557 0.9330 230
k K	0.74977 <.0001 208	0.74273 <.0001 205	-0.10246 0.1408 208	0.62189 <.0001 142	0.28797 <.0001 220	0.11417 0.0912 220	-0.14465 0.0304 224	0.84043 <.0001 230	0.22310 0.0007 230	1.00000 230	-0.27198 <.0001 230
na Na	-0.57577 <.0001 208	-0.07851 0.2632 205	-0.10038 0.1491 208	-0.29026 0.0005 142	-0.10524 0.1196 220	0.03933 0.5617 220	-0.02094 0.7552 224	-0.12774 0.0530 230	-0.00557 0.9330 230	-0.27198 <.0001 230	1.00000 230
so4 SO4	0.62065 <.0001 208	0.61061 <.0001 204	-0.11351 0.1026 208	0.50068 <.0001 142	0.19716 0.0035 218	0.06611 0.3313 218	-0.08611 0.2002 223	0.71834 <.0001 227	0.28307 <.0001 227	0.81796 <.0001 227	-0.21661 0.0010 227
cl Cl	0.30451 <.0001 208	0.44293 <.0001 204	-0.21300 0.0020 208	0.32099 <.0001 142	0.16883 0.0125 218	0.15374 0.0232 218	-0.06129 0.3623 223	0.60594 <.0001 227	0.25267 0.0001 227	0.62774 <.0001 227	-0.04060 0.5428 227
d13c d13C	-0.28324 <.0001 199	-0.40508 <.0001 198	0.56403 <.0001 199	-0.06109 0.4750 139	-0.56865 <.0001 210	-0.62133 <.0001 210	-0.06177 0.3686 214	-0.50435 <.0001 219	-0.13692 0.0430 219	-0.46982 <.0001 219	-0.03019 0.6568 219
dic DIC	0.48459 <.0001 200	0.41597 <.0001 199	-0.51058 <.0001 200	0.37840 <.0001 139	0.68791 <.0001 213	0.57577 <.0001 213	-0.04421 0.5181 216	0.61951 <.0001 222	-0.02860 0.6717 222	0.70989 <.0001 222	-0.20533 0.0021 222
d18o d18O	0.41324 <.0001 200	0.43655 <.0001 198	-0.09493 0.1812 200	0.30134 0.0004 135	0.12084 0.0777 214	0.08782 0.2007 214	-0.01526 0.8236 216	0.43784 <.0001 222	0.15484 0.0210 222	0.46167 <.0001 222	-0.15810 0.0184 222
dd dD	0.68323 <.0001 200	0.68900 <.0001 198	-0.02632 0.7114 200	0.59796 <.0001 135	0.23448 0.0005 214	0.07279 0.2891 214	-0.12306 0.0711 216	0.69470 <.0001 222	0.14529 0.0305 222	0.80824 <.0001 222	-0.24248 0.0003 222
do_conc	-0.71028 <.0001 192	-0.68970 <.0001 192	0.43292 <.0001 192	-0.59747 <.0001 132	-0.40851 <.0001 181	-0.35939 <.0001 181	-0.28274 <.0001 186	-0.48477 <.0001 190	-0.34414 <.0001 190	-0.64501 <.0001 190	0.34728 <.0001 190

Average Ratio Sulfate to Chloride Concentrations by Season

The CORR Procedure

Pearson Correlation Coefficients											
Prob > r under H0: Rho=0											
Number of Observations											
	so4	cl	d13c	dic	d18o	dd	do_conc	mn_	NN	sal	sio4
temp Temp	0.62065 <.0001 208	0.30451 <.0001 208	-0.28324 <.0001 199	0.48459 <.0001 200	0.41324 <.0001 200	0.68323 <.0001 200	-0.71028 <.0001 192	0.45638 <.0001 153	-0.23580 0.0131 110	0.50458 <.0001 179	0.22218 0.0037 169
cond25 Cond25	0.61061 <.0001 204	0.44293 <.0001 204	-0.40508 <.0001 198	0.41597 <.0001 199	0.43655 <.0001 198	0.68900 <.0001 198	-0.68970 <.0001 192	0.07322 0.3515 164	-0.06185 0.5249 108	0.90257 <.0001 166	0.37947 <.0001 170
ph pH	-0.11351 0.1026 208	-0.21300 0.0020 208	0.56403 <.0001 199	-0.51058 <.0001 200	-0.09493 0.1812 200	-0.02632 0.7114 200	0.43292 <.0001 192	-0.49652 <.0001 153	0.11939 0.2141 110	-0.03080 0.6823 179	-0.79760 <.0001 169
chla Chla	0.50068 <.0001 142	0.32099 <.0001 142	-0.06109 0.4750 139	0.37840 <.0001 139	0.30134 0.0004 135	0.59796 <.0001 135	-0.59747 <.0001 132	0.74772 <.0001 119	0.37116 0.0003 89	0.54972 <.0001 120	0.54439 <.0001 126
doc DOC	0.19716 0.0035 218	0.16883 0.0125 218	-0.56865 <.0001 210	0.68791 <.0001 213	0.12084 0.0777 214	0.23448 0.0005 214	-0.40851 <.0001 181	0.14224 0.0701 163	-0.01077 0.9098 113	0.14974 0.0520 169	0.60131 <.0001 179
tdn TDN	0.06611 0.3313 218	0.15374 0.0232 218	-0.62133 <.0001 210	0.57577 <.0001 213	0.08782 0.2007 214	0.07279 0.2891 214	-0.35939 <.0001 181	0.10039 0.2023 163	-0.00362 0.9696 113	0.12843 0.0961 169	0.69096 <.0001 179
fe Fe	-0.08611 0.2002 223	-0.06129 0.3623 223	-0.06177 0.3686 214	-0.04421 0.5181 216	-0.01526 0.8236 216	-0.12306 0.0711 216	-0.28274 <.0001 186	0.30589 <.0001 169	-0.00019 0.9984 114	-0.09891 0.1941 174	0.11361 0.1246 184
mg Mg	0.71834 <.0001 227	0.60594 <.0001 227	-0.50435 <.0001 219	0.61951 <.0001 222	0.43784 <.0001 222	0.69470 <.0001 222	-0.48477 <.0001 190	-0.08138 0.2929 169	0.08168 0.3897 113	0.57291 <.0001 178	0.24198 0.0009 184
ca Ca	0.28307 <.0001 227	0.25267 0.0001 227	-0.13692 0.0430 219	-0.02860 0.6717 222	0.15484 0.0210 222	0.14529 0.0305 222	-0.34414 <.0001 190	0.69021 <.0001 169	-0.12815 0.1761 113	0.15505 0.0388 178	0.28666 <.0001 184
k K	0.81796 <.0001 227	0.62774 <.0001 227	-0.46982 <.0001 219	0.70989 <.0001 222	0.46167 <.0001 222	0.80824 <.0001 222	-0.64501 <.0001 190	0.08194 0.2895 169	-0.14120 0.1358 113	0.62352 <.0001 178	0.28194 0.0001 184
na Na	-0.21661 0.0010 227	-0.04060 0.5428 227	-0.03019 0.6568 219	-0.20533 0.0021 222	-0.15810 0.0184 222	-0.24248 0.0003 222	0.34728 <.0001 190	-0.02955 0.7029 169	0.11932 0.2081 113	-0.23791 0.0014 178	0.06429 0.3859 184
so4 SO4	1.00000 228	0.87343 <.0001 228	-0.44773 <.0001 218	0.60016 <.0001 219	0.36576 <.0001 219	0.68376 <.0001 219	-0.55135 <.0001 190	0.20928 0.0066 167	-0.14921 0.1164 112	0.61848 <.0001 178	0.22457 0.0023 182
cl Cl	0.87343 <.0001 228	1.00000 228	-0.47804 <.0001 218	0.53312 <.0001 219	0.25234 0.0002 219	0.51288 <.0001 219	-0.39575 <.0001 190	0.11197 0.1497 167	-0.06760 0.4788 112	0.44023 <.0001 178	0.26111 0.0004 182
d13c d13C	-0.44773 <.0001 218	-0.47804 <.0001 218	1.00000 221	-0.68791 <.0001 220	-0.26974 <.0001 212	-0.31900 <.0001 212	0.52670 <.0001 182	-0.05184 0.5071 166	0.09698 0.3091 112	-0.34675 <.0001 172	-0.64893 <.0001 180
dic DIC	0.60016 <.0001 219	0.53312 <.0001 219	-0.68791 <.0001 220	1.00000 223	0.30386 <.0001 215	0.51637 <.0001 215	-0.66359 <.0001 183	0.01274 0.8705 166	-0.05740 0.5477 112	0.52311 <.0001 173	0.59397 <.0001 182
d18o d18O	0.36576 <.0001 219	0.25234 0.0002 219	-0.26974 <.0001 212	0.30386 <.0001 215	1.00000 223	0.04596 0.4947 223	-0.39945 <.0001 182	0.05767 0.4674 161	-0.09396 0.3357 107	0.48844 <.0001 172	0.22710 0.0024 177
dd dD	0.68376 <.0001 219	0.51288 <.0001 219	-0.31900 <.0001 212	0.51637 <.0001 215	0.04596 0.4947 223	1.00000 223	-0.53014 <.0001 182	-0.01042 0.8956 161	-0.06180 0.5272 107	0.63556 <.0001 172	0.20415 0.0064 177
do_conc	-0.55135 <.0001 190	-0.39575 <.0001 190	0.52670 <.0001 182	-0.66359 <.0001 183	-0.39945 <.0001 182	-0.53014 <.0001 182	1.00000 192	-0.68590 <.0001 149	0.22127 0.0233 105	-0.63917 <.0001 166	-0.61541 <.0001 155

Average Ratio Sulfate to Chloride Concentrations by Season

The CORR Procedure

Pearson Correlation Coefficients Prob > r under H0: Rho=0 Number of Observations							
	mmhg_	rn222	ra224	ra226	nh4	no2	po4
temp Temp	-0.11898 0.1012 191	0.09470 0.1834 199	0.18305 0.3811 25	-0.35859 0.0344 35	0.04990 0.4785 204	0.13872 0.0479 204	0.11624 0.1021 199
cond25 Cond25	0.03520 0.6288 191	0.13392 0.0606 197	0.22742 0.2743 25	-0.54656 0.0015 31	0.15998 0.0226 203	0.44317 <.0001 203	0.18374 0.0096 198
ph pH	-0.07190 0.3230 191	-0.29786 <.0001 199	0.05202 0.8050 25	-0.06176 0.7245 35	-0.58602 <.0001 204	-0.39241 <.0001 204	-0.67425 <.0001 199
chla Chla	-0.13346 0.1271 132	0.12896 0.1289 140	0.58486 0.0034 23	-0.11642 0.5475 29	-0.01061 0.9010 140	0.42936 <.0001 139	0.27211 0.0015 134
doc DOC	0.07652 0.3072 180	0.05757 0.4054 211	0.28689 0.1844 23	-0.27291 0.1244 33	0.58825 <.0001 221	0.11307 0.0936 221	0.50693 <.0001 216
tdn TDN	0.12176 0.1035 180	0.08886 0.1986 211	0.26179 0.2276 23	-0.33556 0.0563 33	0.99176 <.0001 221	0.27466 <.0001 221	0.87482 <.0001 216
fe Fe	0.17864 0.0150 185	0.23078 0.0006 215	-0.16529 0.4510 23	-0.08183 0.6562 32	0.16706 0.0127 222	0.32591 <.0001 222	0.21260 0.0016 217
mg Mg	0.10737 0.1414 189	-0.00731 0.9143 219	0.18918 0.3873 23	-0.41954 0.0151 33	0.13102 0.0492 226	0.14466 0.0297 226	0.13805 0.0403 221
ca Ca	-0.36403 <.0001 189	0.09413 0.1651 219	0.21095 0.3340 23	-0.13827 0.4429 33	0.01310 0.8448 226	0.31371 <.0001 226	0.07200 0.2866 221
k K	0.08227 0.2604 189	0.04663 0.4924 219	0.23567 0.2790 23	-0.50552 0.0027 33	0.05729 0.3913 226	0.04884 0.4651 226	0.11861 0.0785 221
na Na	0.13960 0.0554 189	0.00461 0.9459 219	-0.24154 0.2668 23	0.22650 0.2050 33	0.06934 0.2993 226	0.19337 0.0035 226	0.04636 0.4930 221
so4 SO4	0.06176 0.3985 189	0.01857 0.7851 218	0.05211 0.8133 23	-0.47588 0.0051 33	0.02597 0.6997 223	0.07189 0.2851 223	0.09427 0.1655 218
cl Cl	0.09141 0.2109 189	0.03184 0.6401 218	0.05186 0.8142 23	-0.39597 0.0225 33	0.13087 0.0510 223	0.10031 0.1354 223	0.19195 0.0045 218
d13c d13C	-0.00766 0.9185 181	-0.13655 0.0471 212	0.20851 0.3397 23	0.42763 0.0164 31	-0.61803 <.0001 216	-0.30361 <.0001 216	-0.64747 <.0001 211
dic DIC	0.18466 0.0126 182	0.10053 0.1437 213	0.38306 0.0712 23	-0.51372 0.0031 31	0.55631 <.0001 219	-0.03391 0.6177 219	0.55233 <.0001 214
d18o d18O	-0.02221 0.7666 181	0.08377 0.2245 212	0.21887 0.3278 22	-0.43805 0.0122 32	0.05046 0.4575 219	0.12965 0.0554 219	0.10161 0.1375 215
dd dD	0.06358 0.3951 181	0.01535 0.8242 212	0.27908 0.2085 22	-0.44717 0.0103 32	0.02107 0.7566 219	0.06136 0.3661 219	0.04190 0.5412 215
do_conc	0.05587 0.4427 191	-0.42441 <.0001 181	-0.20674 0.3214 25	0.41979 0.0187 31	-0.35238 <.0001 186	-0.51030 <.0001 186	-0.50414 <.0001 181

Average Ratio Sulfate to Chloride Concentrations by Season

The CORR Procedure

Pearson Correlation Coefficients											
Prob > r under H0: Rho=0											
Number of Observations											
	temp	cond25	ph	chla	doc	tdn	fe	mg	ca	k	na
mn_	0.45638 <.0001 153	0.07322 0.3515 164	-0.49652 <.0001 153	0.74772 <.0001 119	0.14224 0.0701 163	0.10039 0.2023 163	0.30589 <.0001 169	-0.08138 0.2929 169	0.69021 <.0001 169	0.08194 0.2895 169	-0.02955 0.7029 169
NN	-0.23580 0.0131 110	-0.06185 0.5249 108	0.11939 0.2141 110	0.37116 0.0003 89	-0.01077 0.9098 113	-0.00362 0.9696 113	-0.00019 0.9984 114	0.08168 0.3897 113	-0.12815 0.1761 113	-0.14120 0.1358 113	0.11932 0.2081 113
sal	0.50458 <.0001 179	0.90257 <.0001 166	-0.03080 0.6823 179	0.54972 <.0001 120	0.14974 0.0520 169	0.12843 0.0961 169	-0.09891 0.1941 174	0.57291 <.0001 178	0.15505 0.0388 178	0.62352 <.0001 178	-0.23791 0.0014 178
sio4	0.22218 0.0037 169	0.37947 <.0001 170	-0.79760 <.0001 169	0.54439 <.0001 126	0.60131 <.0001 179	0.69096 <.0001 179	0.11361 0.1246 184	0.24198 0.0009 184	0.28666 <.0001 184	0.28194 0.0001 184	0.06429 0.3859 184
mmhg_	-0.11898 0.1012 191	0.03520 0.6288 191	-0.07190 0.3230 191	-0.13346 0.1271 132	0.07652 0.3072 180	0.12176 0.1035 180	0.17864 0.0150 185	0.10737 0.1414 189	-0.36403 <.0001 189	0.08227 0.2604 189	0.13960 0.0554 189
rn222	0.09470 0.1834 199	0.13392 0.0606 197	-0.29786 <.0001 199	0.12896 0.1289 140	0.05757 0.4054 211	0.08886 0.1986 211	0.23078 0.0006 215	-0.00731 0.9143 219	0.09413 0.1651 219	0.04663 0.4924 219	0.00461 0.9459 219
ra224	0.18305 0.3811 25	0.22742 0.2743 25	0.05202 0.8050 25	0.58486 0.0034 23	0.28689 0.1844 23	0.26179 0.2276 23	-0.16529 0.4510 23	0.18918 0.3873 23	0.21095 0.3340 23	0.23567 0.2790 23	-0.24154 0.2668 23
ra226	-0.35859 0.0344 35	-0.54656 0.0015 31	-0.06176 0.7245 35	-0.11642 0.5475 29	-0.27291 0.1244 33	-0.33556 0.0563 33	-0.08183 0.6562 32	-0.41954 0.0151 33	-0.13827 0.4429 33	-0.50552 0.0027 33	0.22650 0.2050 33
nh4	0.04990 0.4785 204	0.15998 0.0226 203	-0.58602 <.0001 204	-0.01061 0.9010 140	0.58825 <.0001 221	0.99176 <.0001 221	0.16706 0.0127 222	0.13102 0.0492 226	0.01310 0.8448 226	0.05729 0.3913 226	0.06934 0.2993 226
no2	0.13872 0.0479 204	0.44317 <.0001 203	-0.39241 <.0001 204	0.42936 <.0001 139	0.11307 0.0936 221	0.27466 <.0001 221	0.32591 <.0001 222	0.14466 0.0297 226	0.31371 <.0001 226	0.04884 0.4651 226	0.19337 0.0035 226
po4	0.11624 0.1021 199	0.18374 0.0096 198	-0.67425 <.0001 199	0.27211 0.0015 134	0.50693 <.0001 216	0.87482 <.0001 216	0.21260 0.0016 217	0.13805 0.0403 221	0.07200 0.2866 221	0.11861 0.0785 221	0.04636 0.4930 221

Average Ratio Sulfate to Chloride Concentrations by Season

The CORR Procedure

Pearson Correlation Coefficients											
Prob > r under H0: Rho=0											
Number of Observations											
	so4	cl	d13c	dic	d18o	dd	do_conc	mn_	NN	sal	sio4
mn_	0.20928 0.0066 167	0.11197 0.1497 167	-0.05184 0.5071 166	0.01274 0.8705 166	0.05767 0.4674 161	-0.01042 0.8956 161	-0.68590 <.0001 149	1.00000 170	-0.07221 0.4708 102	0.12804 0.1498 128	0.53671 <.0001 165
NN	-0.14921 0.1164 112	-0.06760 0.4788 112	0.09698 0.3091 112	-0.05740 0.5477 112	-0.09396 0.3357 107	-0.06180 0.5272 107	0.22127 0.0233 105	-0.07221 0.4708 102	1.00000 114	-0.10632 0.2974 98	-0.02785 0.7738 109
sal	0.61848 <.0001 178	0.44023 <.0001 178	-0.34675 <.0001 172	0.52311 <.0001 173	0.48844 <.0001 172	0.63556 <.0001 172	-0.63917 <.0001 166	0.12804 0.1498 128	-0.10632 0.2974 98	1.00000 179	0.26113 0.0016 143
sio4	0.22457 0.0023 182	0.26111 0.0004 182	-0.64893 <.0001 180	0.59397 <.0001 182	0.22710 0.0024 177	0.20415 0.0064 177	-0.61541 <.0001 155	0.53671 <.0001 165	-0.02785 0.7738 109	0.26113 0.0016 143	1.00000 186
mmhg_	0.06176 0.3985 189	0.09141 0.2109 189	-0.00766 0.9185 181	0.18466 0.0126 182	-0.02221 0.7666 181	0.06358 0.3951 181	0.05587 0.4427 191	-0.03416 0.6802 148	0.27954 0.0039 105	0.01194 0.8790 165	0.06373 0.4323 154
rn222	0.01857 0.7851 218	0.03184 0.6401 218	-0.13655 0.0471 212	0.10053 0.1437 213	0.08377 0.2245 212	0.01535 0.8242 212	-0.42441 <.0001 181	0.43478 <.0001 166	-0.01644 0.8622 114	0.05816 0.4526 169	0.19737 0.0076 182
ra224	0.05211 0.8133 23	0.05186 0.8142 23	0.20851 0.3397 23	0.38306 0.0712 23	0.21887 0.3278 22	0.27908 0.2085 22	-0.20674 0.3214 25	0.17435 0.4262 23	0.11237 0.6277 21	0.19016 0.4090 21	0.00033 0.9988 23
ra226	-0.47588 0.0051 33	-0.39597 0.0225 33	0.42763 0.0164 31	-0.51372 0.0031 31	-0.43805 0.0122 32	-0.44717 0.0103 32	0.41979 0.0187 31	-0.34631 0.0831 26	-0.01890 0.9286 25	-0.14133 0.4563 30	-0.32273 0.1006 27
nh4	0.02597 0.6997 223	0.13087 0.0510 223	-0.61803 <.0001 216	0.55631 <.0001 219	0.05046 0.4575 219	0.02107 0.7566 219	-0.35238 <.0001 186	0.11628 0.1322 169	-0.02757 0.7719 113	0.11139 0.1422 175	0.69547 <.0001 185
no2	0.07189 0.2851 223	0.10031 0.1354 223	-0.30361 <.0001 216	-0.03391 0.6177 219	0.12965 0.0554 219	0.06136 0.3661 219	-0.51030 <.0001 186	0.08386 0.2783 169	0.33573 0.0003 114	0.21921 0.0036 175	0.34988 <.0001 185
po4	0.09427 0.1655 218	0.19195 0.0045 218	-0.64747 <.0001 211	0.55233 <.0001 214	0.10161 0.1375 215	0.04190 0.5412 215	-0.50414 <.0001 181	0.19737 0.0111 165	0.00144 0.9881 111	0.12280 0.1085 172	0.71676 <.0001 181

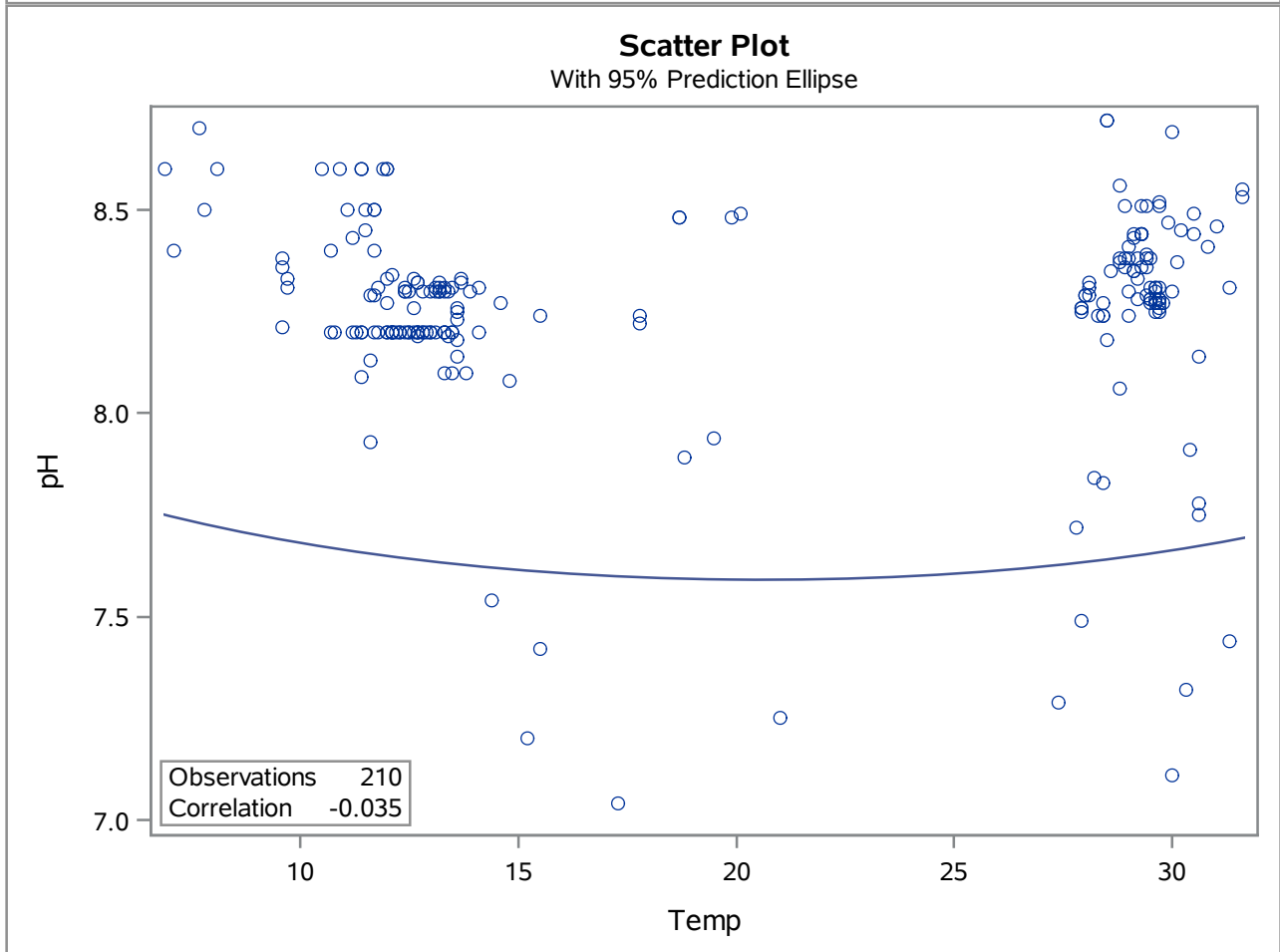
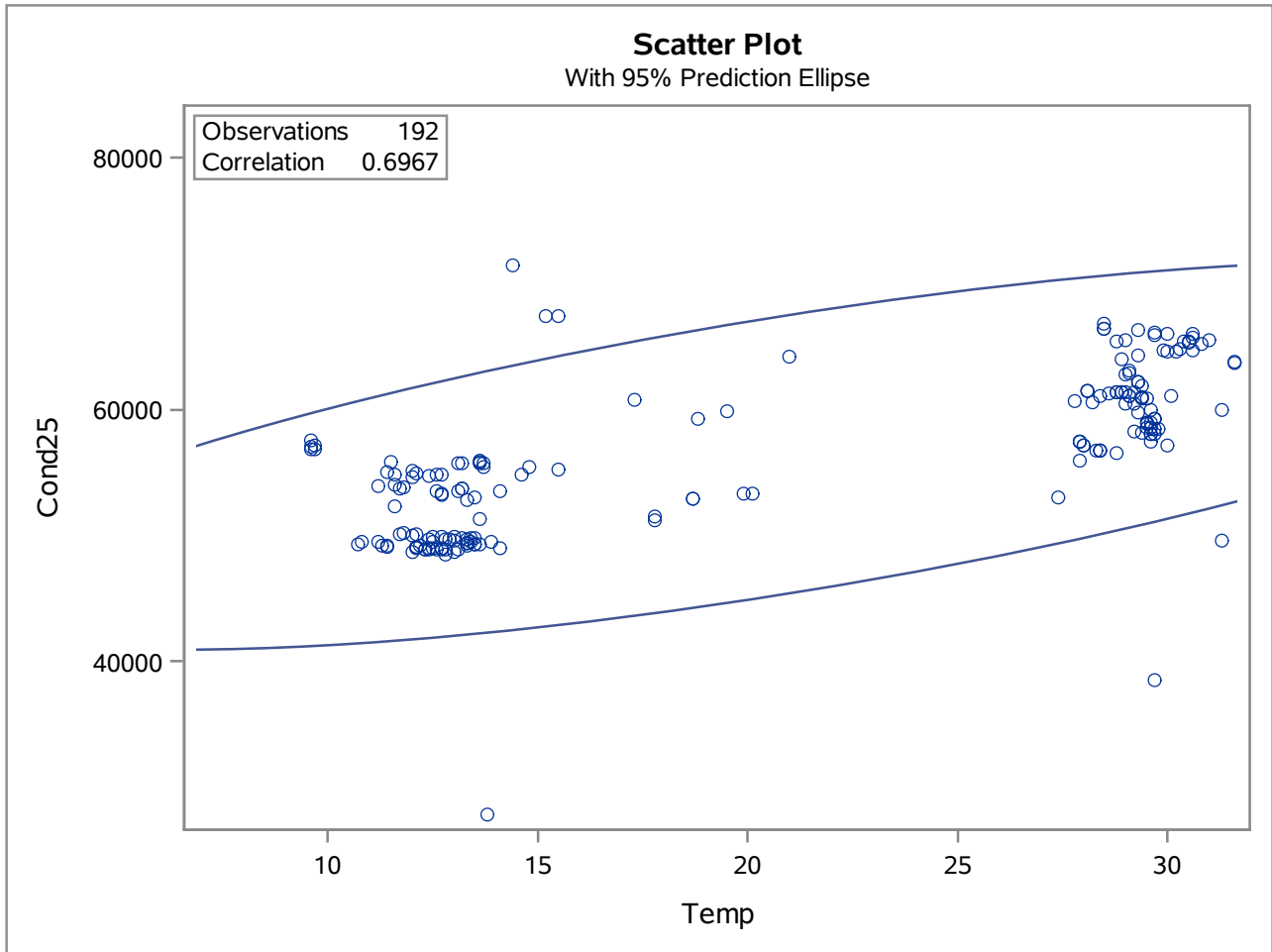
Average Ratio Sulfate to Chloride Concentrations by Season

The CORR Procedure

Pearson Correlation Coefficients Prob > r under H0: Rho=0 Number of Observations							
	mmhg_	rn222	ra224	ra226	nh4	no2	po4
mn_	-0.03416 0.6802 148	0.43478 <.0001 166	0.17435 0.4262 23	-0.34631 0.0831 26	0.11628 0.1322 169	0.08386 0.2783 169	0.19737 0.0111 165
NN	0.27954 0.0039 105	-0.01644 0.8622 114	0.11237 0.6277 21	-0.01890 0.9286 25	-0.02757 0.7719 113	0.33573 0.0003 114	0.00144 0.9881 111
sal	0.01194 0.8790 165	0.05816 0.4526 169	0.19016 0.4090 21	-0.14133 0.4563 30	0.11139 0.1422 175	0.21921 0.0036 175	0.12280 0.1085 172
sio4	0.06373 0.4323 154	0.19737 0.0076 182	0.00033 0.9988 23	-0.32273 0.1006 27	0.69547 <.0001 185	0.34988 <.0001 185	0.71676 <.0001 181
mmhg_	1.00000 191	-0.09121 0.2220 181	-0.09200 0.6618 25	-0.35253 0.0518 31	0.11637 0.1147 185	0.02306 0.7554 185	0.07253 0.3333 180
rn222	-0.09121 0.2220 181	1.00000 222	0.20577 0.3462 23	0.27348 0.1366 31	0.10261 0.1319 217	0.28273 <.0001 217	0.37229 <.0001 212
ra224	-0.09200 0.6618 25	0.20577 0.3462 23	1.00000 25	0.14369 0.4932 25	0.34508 0.1068 23	0.22380 0.3046 23	-0.07539 0.7388 22
ra226	-0.35253 0.0518 31	0.27348 0.1366 31	0.14369 0.4932 25	1.00000 35	-0.20923 0.2426 33	-0.09616 0.5945 33	-0.04552 0.8046 32
nh4	0.11637 0.1147 185	0.10261 0.1319 217	0.34508 0.1068 23	-0.20923 0.2426 33	1.00000 228	0.29046 <.0001 227	0.86656 <.0001 222
no2	0.02306 0.7554 185	0.28273 <.0001 217	0.22380 0.3046 23	-0.09616 0.5945 33	0.29046 <.0001 227	1.00000 228	0.38785 <.0001 222
po4	0.07253 0.3333 180	0.37229 <.0001 212	-0.07539 0.7388 22	-0.04552 0.8046 32	0.86656 <.0001 222	0.38785 <.0001 222	1.00000 223

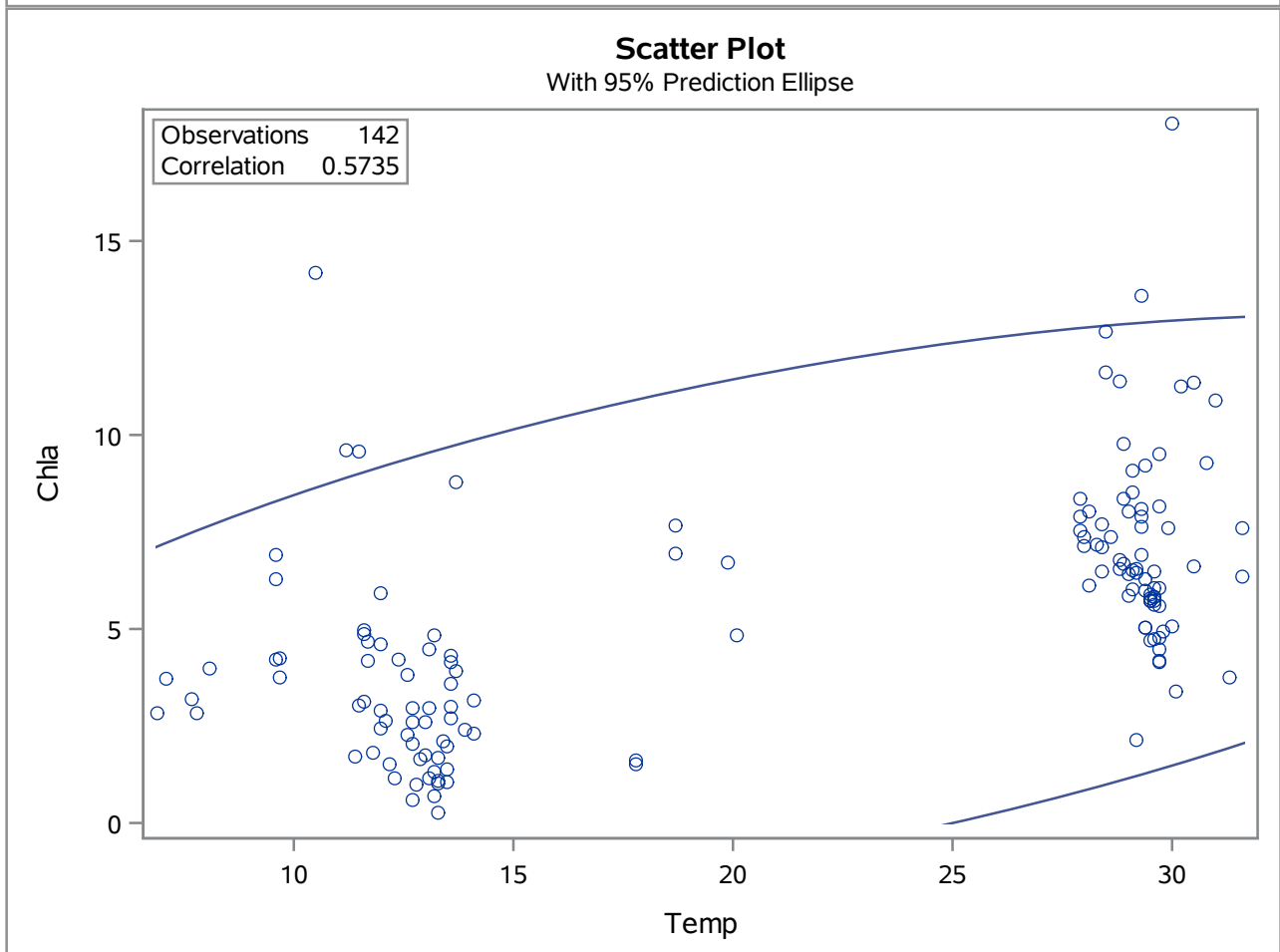
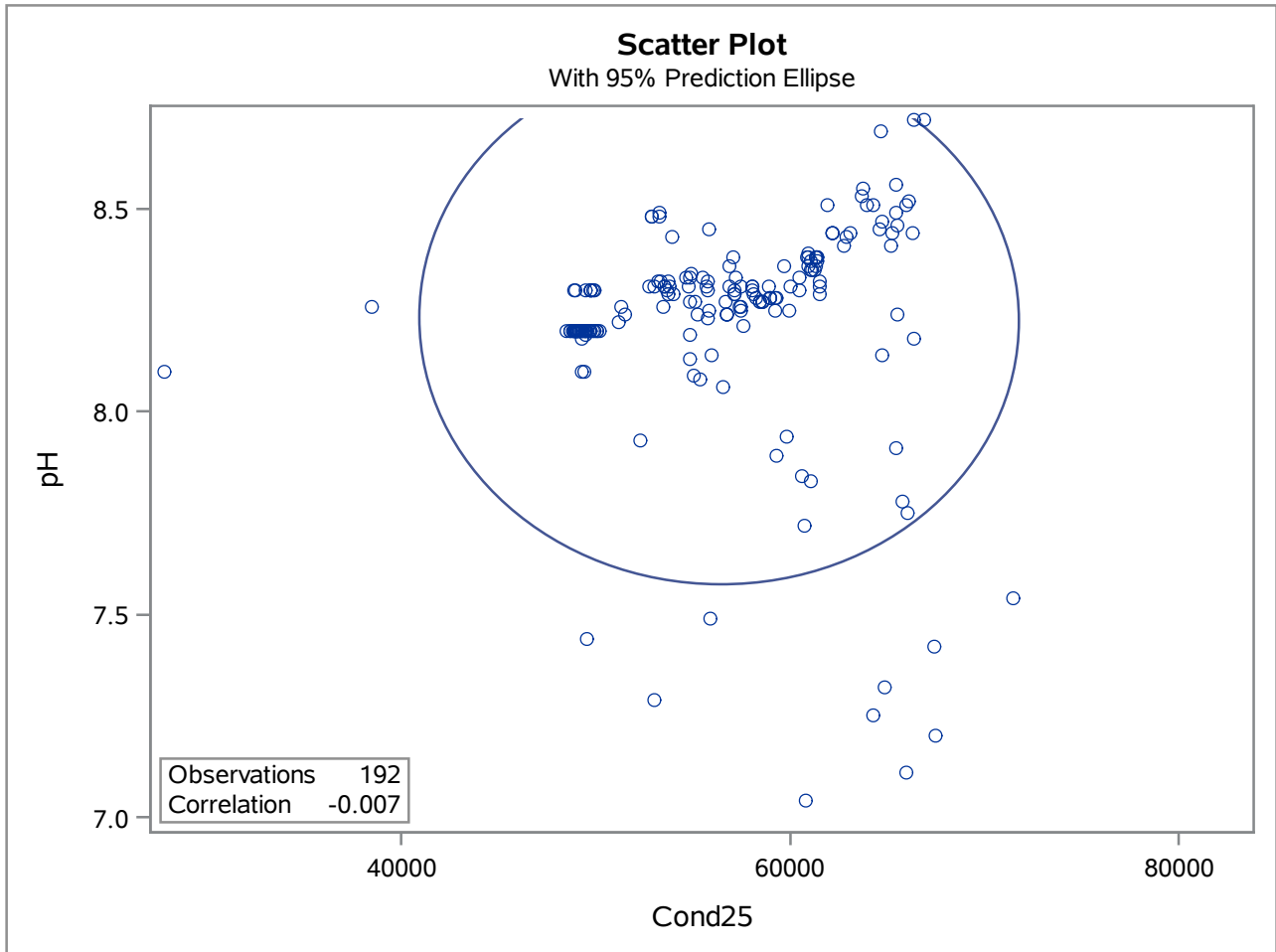
Average Ratio Sulfate to Chloride Concentrations by Season

The CORR Procedure



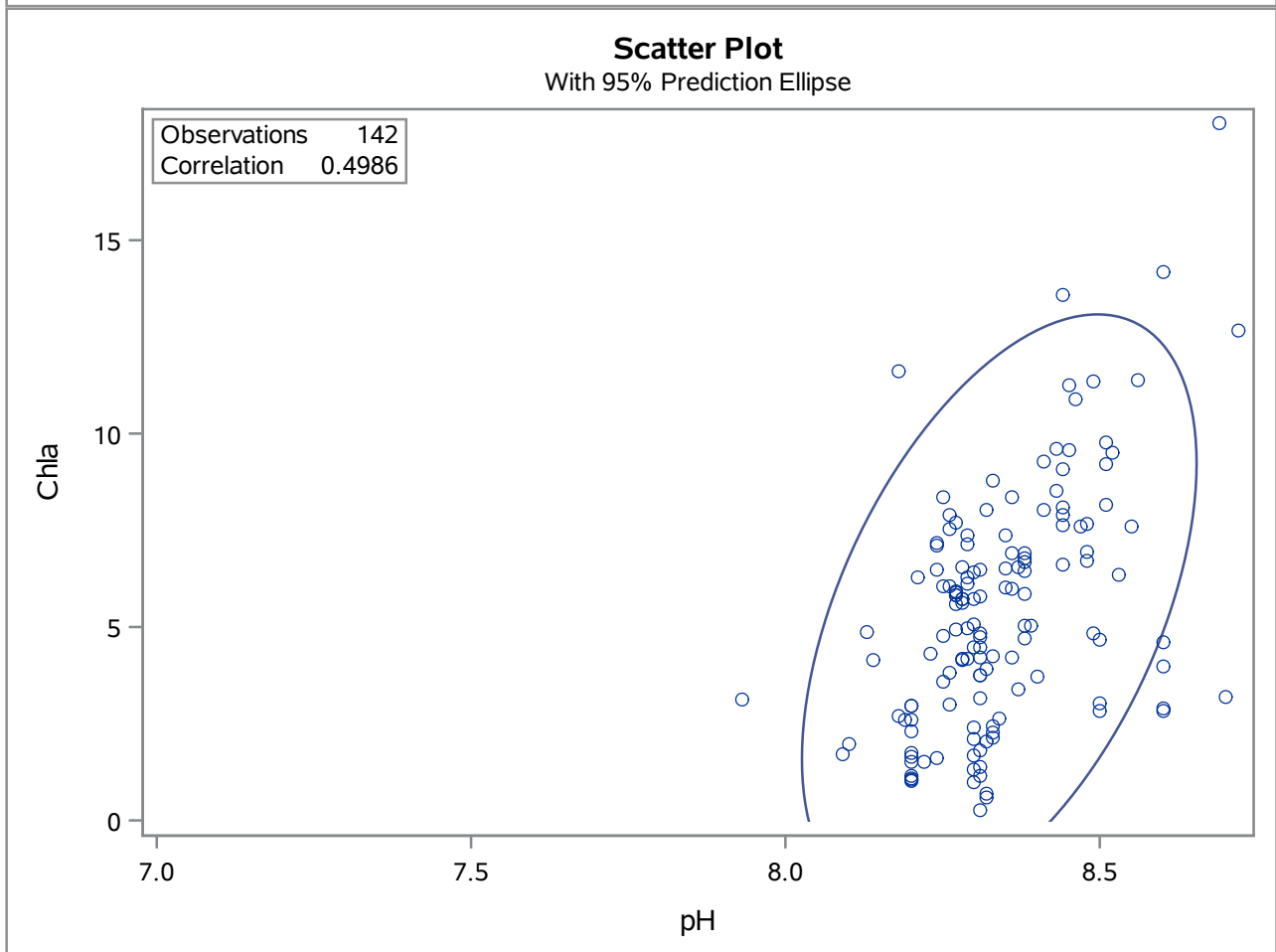
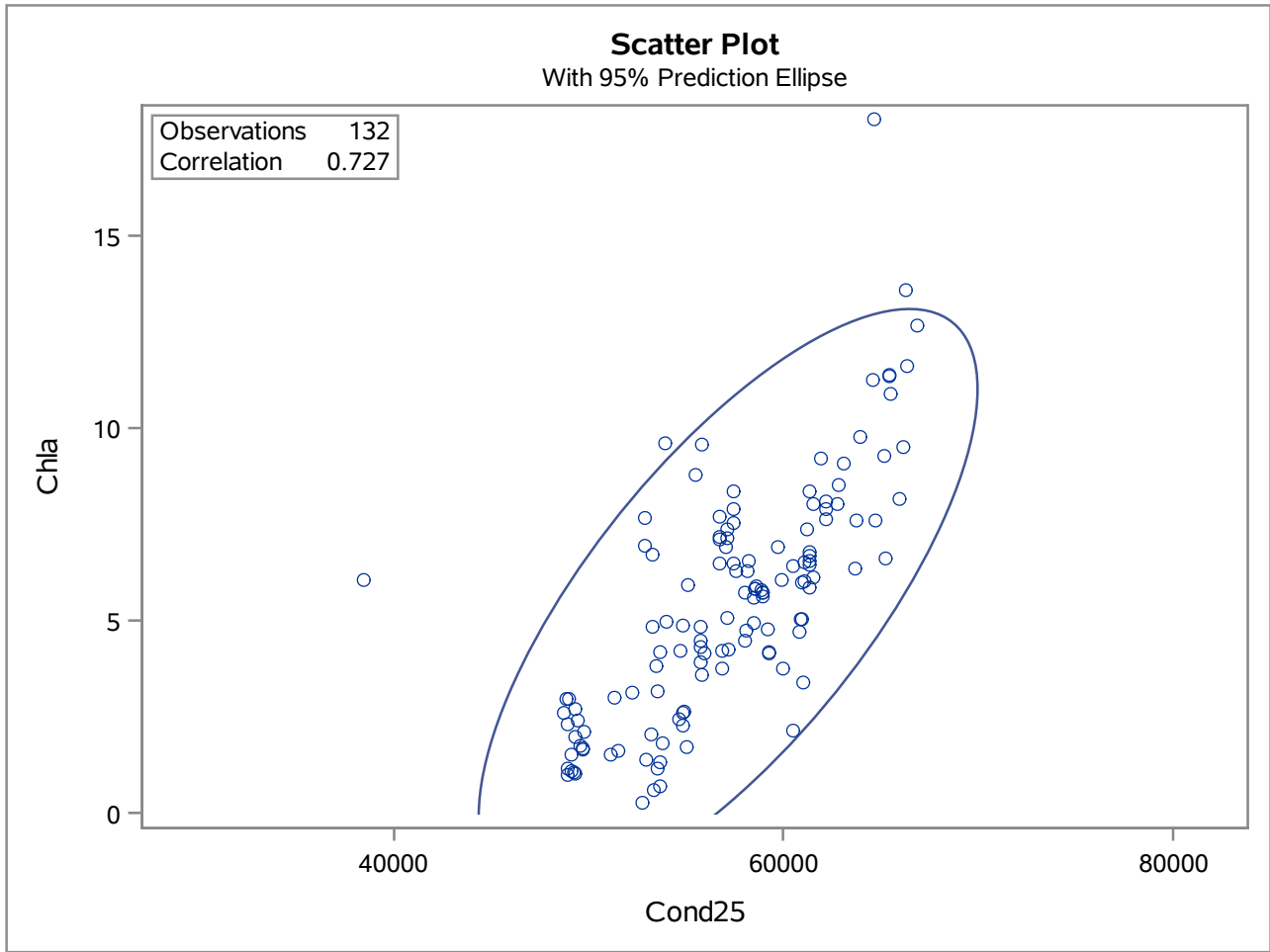
Average Ratio Sulfate to Chloride Concentrations by Season

The CORR Procedure



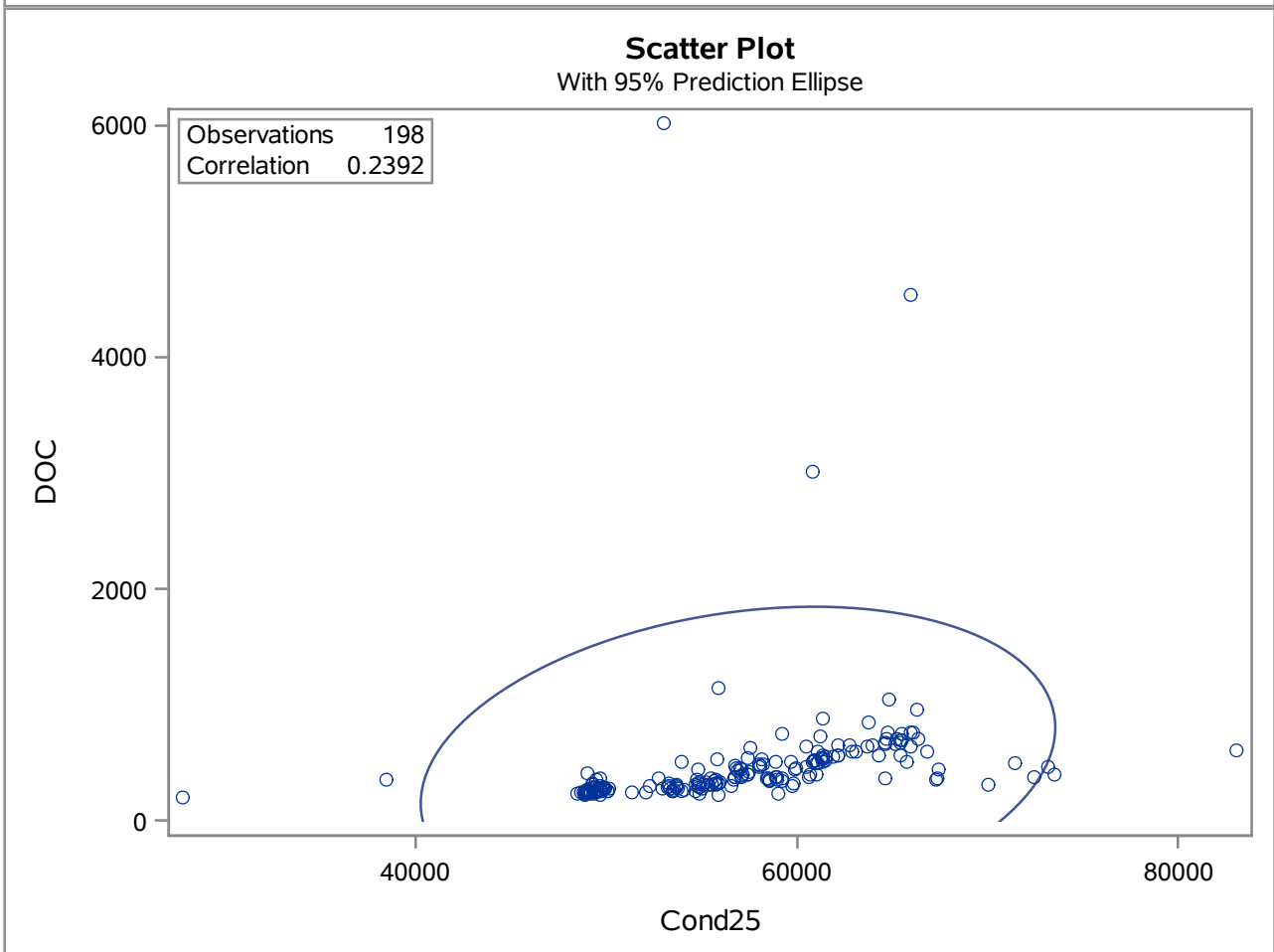
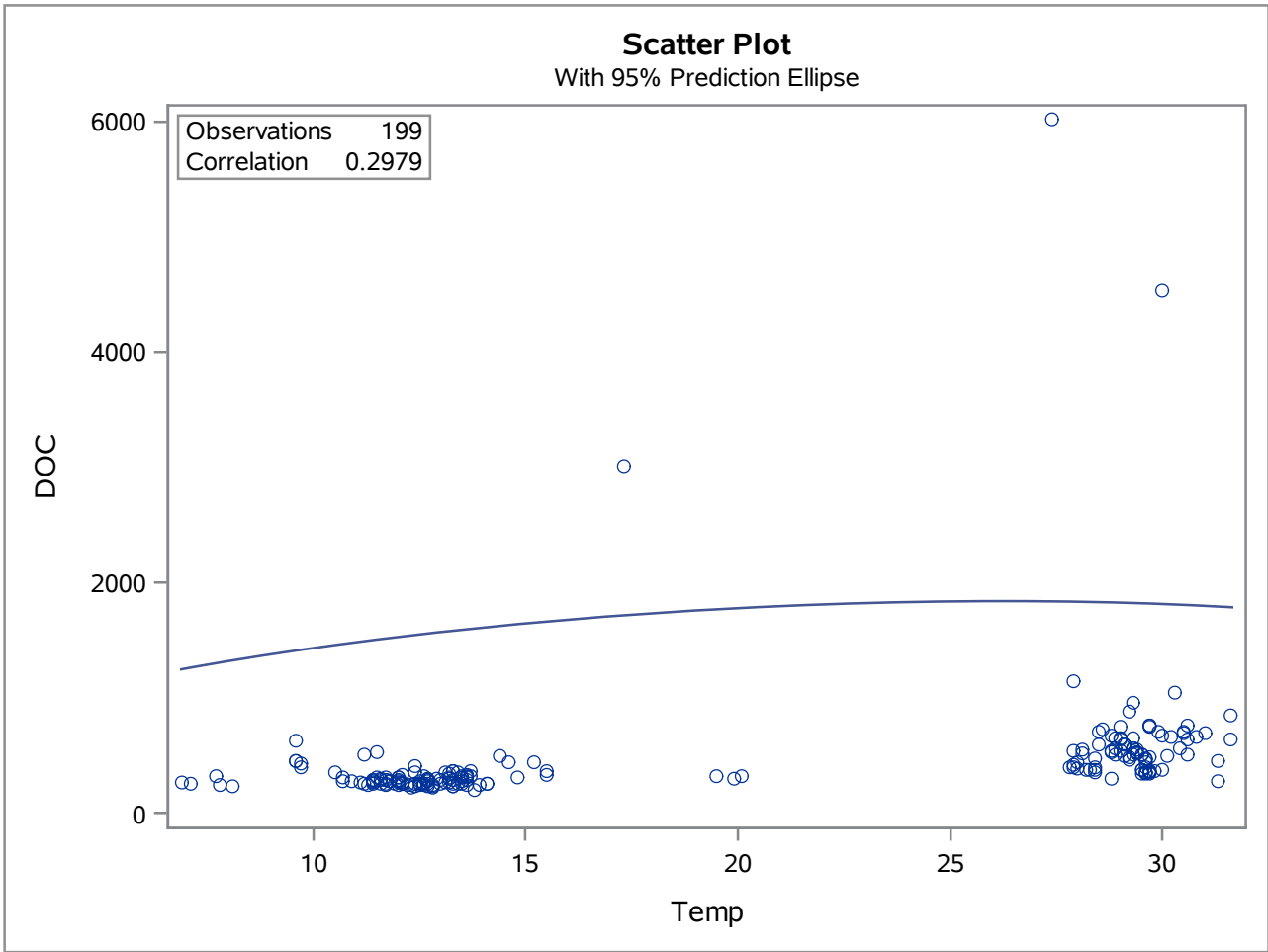
Average Ratio Sulfate to Chloride Concentrations by Season

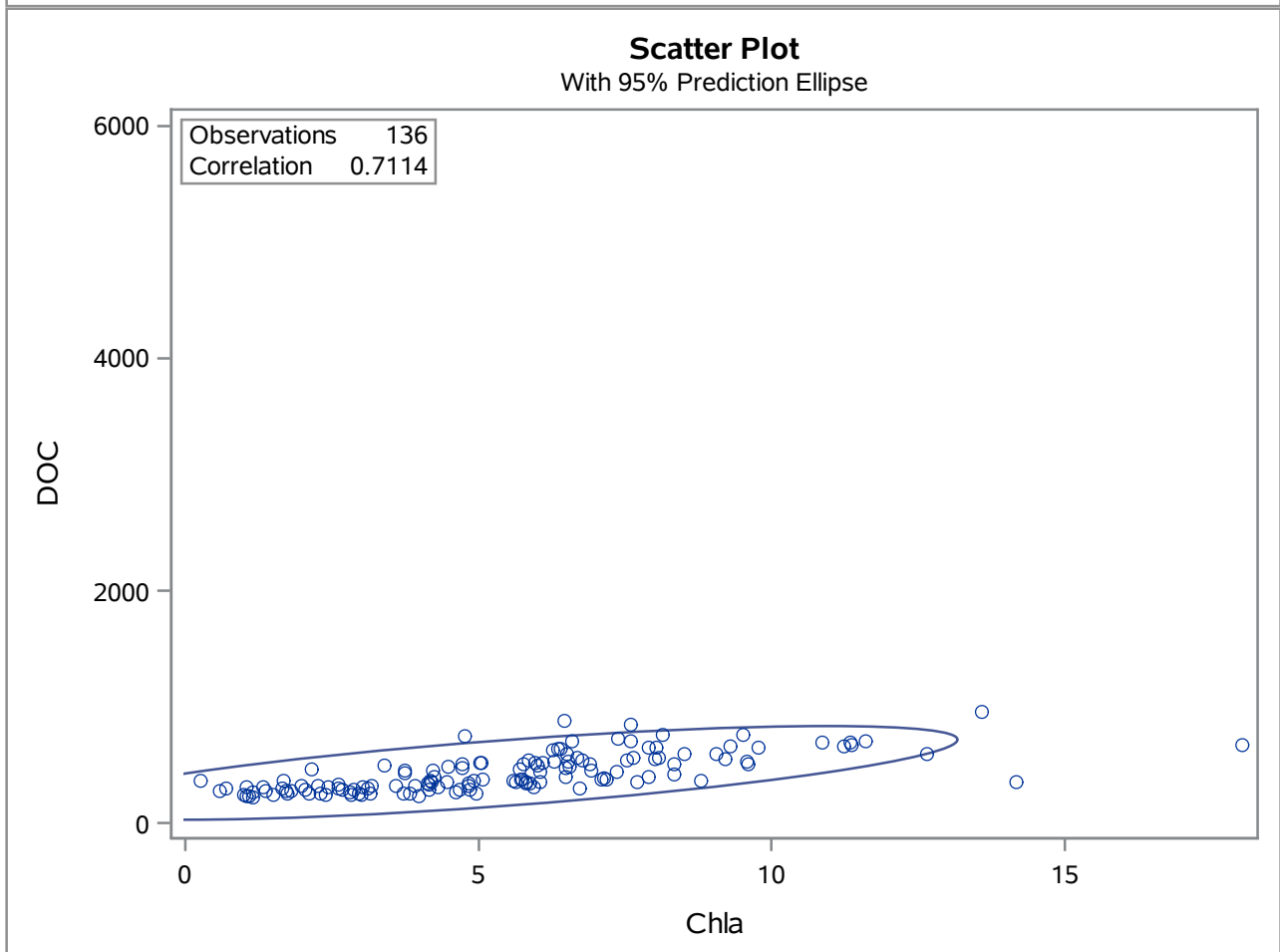
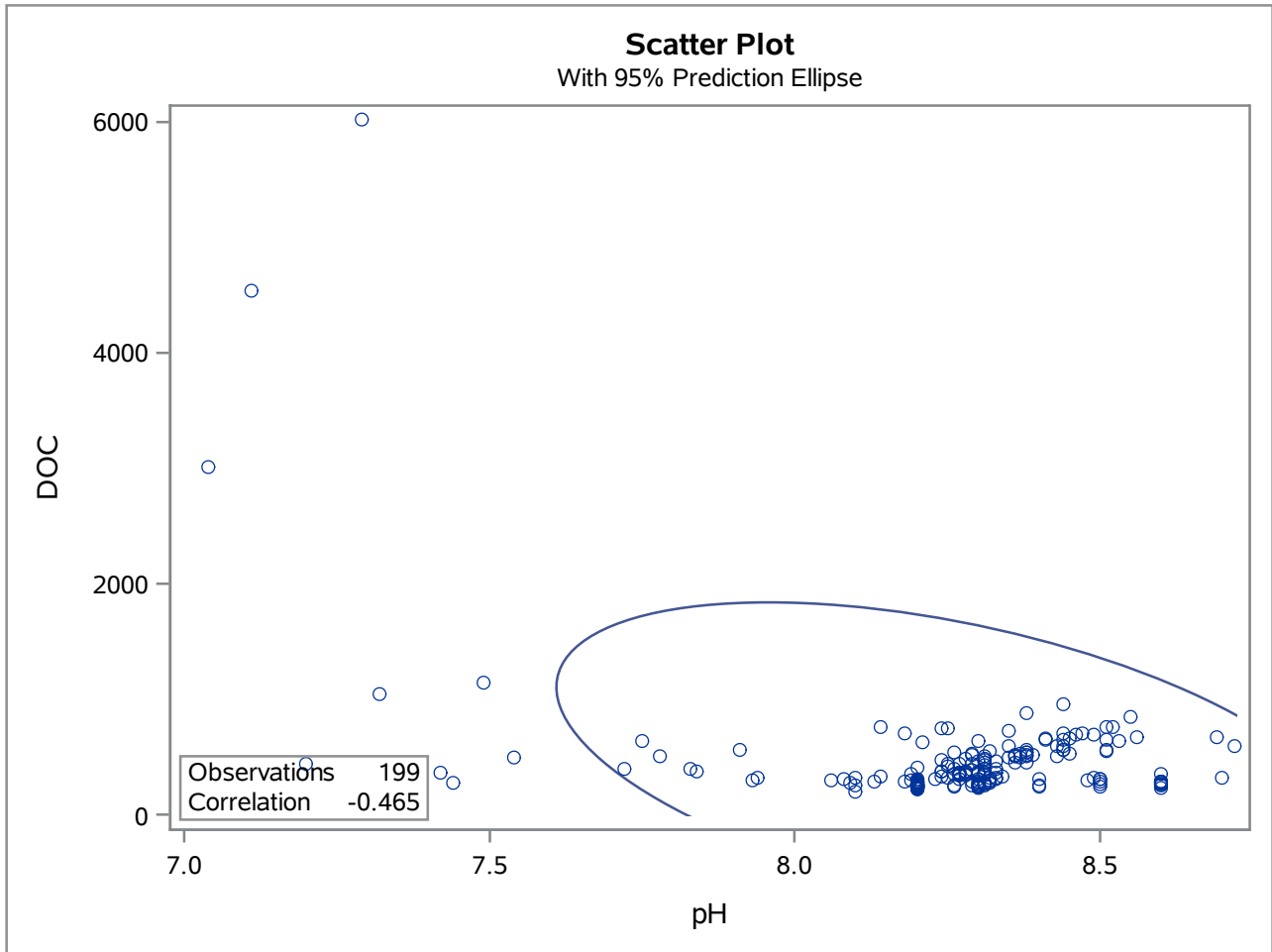
The CORR Procedure



Average Ratio Sulfate to Chloride Concentrations by Season

The CORR Procedure



Average Ratio Sulfate to Chloride Concentrations by Season**The CORR Procedure**

Average Ratio Sulfate to Chloride Concentrations by Season**The FACTOR Procedure**

Input Data Type	Raw Data
Number of Records Read	236
Number of Records Used	236
N for Significance Tests	236

Average Ratio Sulfate to Chloride Concentrations by Season

The FACTOR Procedure Initial Factor Method: Principal Components

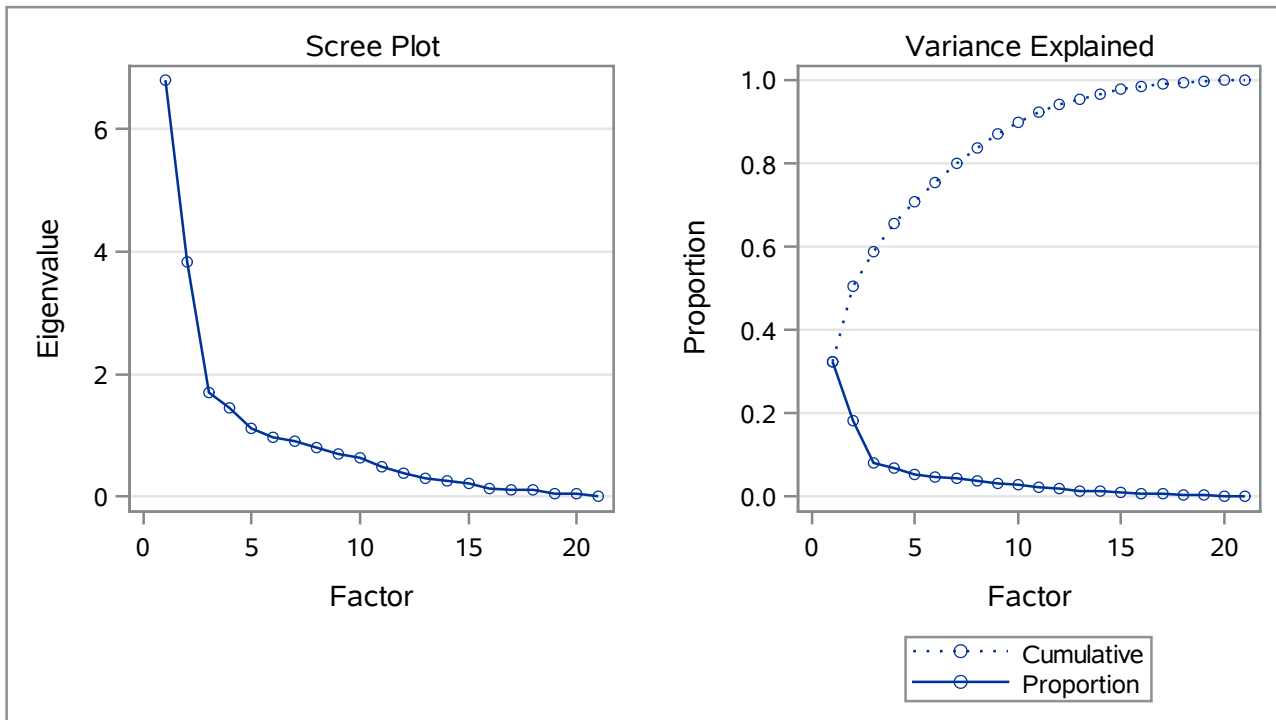
Prior Communality Estimates: ONE

Eigenvalues of the Correlation Matrix: Total = 21 Average = 1				
	Eigenvalue	Difference	Proportion	Cumulative
1	6.79900631	2.97380066	0.3238	0.3238
2	3.82520566	2.12580310	0.1822	0.5059
3	1.69940256	0.25015915	0.0809	0.5868
4	1.44924341	0.33784725	0.0690	0.6559
5	1.11139616	0.13821774	0.0529	0.7088
6	0.97317841	0.05946943	0.0463	0.7551
7	0.91370898	0.12276746	0.0435	0.7986
8	0.79094152	0.09608320	0.0377	0.8363
9	0.69485832	0.06774738	0.0331	0.8694
10	0.62711094	0.14549361	0.0299	0.8992
11	0.48161733	0.09009578	0.0229	0.9222
12	0.39152155	0.09746197	0.0186	0.9408
13	0.29405958	0.02820400	0.0140	0.9548
14	0.26585558	0.05562579	0.0127	0.9675
15	0.21022979	0.07376666	0.0100	0.9775
16	0.13646313	0.01552054	0.0065	0.9840
17	0.12094258	0.01614773	0.0058	0.9897
18	0.10479486	0.04754142	0.0050	0.9947
19	0.05725343	0.00856401	0.0027	0.9975
20	0.04868943	0.04416898	0.0023	0.9998
21	0.00452044		0.0002	1.0000

4 factors will be retained by the NFACTOR criterion.

Average Ratio Sulfate to Chloride Concentrations by Season

The FACTOR Procedure Initial Factor Method: Principal Components



		Factor Pattern			
		Factor1	Factor2	Factor3	Factor4
temp	Temp	0.67457	-0.36528	0.11716	0.44873
cond25	Cond25	0.71886	-0.24379	0.36375	-0.03757
ph	pH	-0.38235	-0.63698	0.09371	0.10174
chla	Chla	0.42311	-0.35432	0.24538	0.36754
doc	DOC	0.49079	0.37361	-0.13222	0.35660
tdn	TDN	0.51752	0.73821	-0.13842	0.15460
fe	Fe	0.01474	0.30277	0.46017	0.24004
mg	Mg	0.79468	-0.32570	-0.06821	-0.19039
ca	Ca	0.24815	-0.09030	0.48875	-0.15184
k	K	0.85301	-0.41769	-0.07867	-0.03408
na	Na	-0.22468	0.29847	0.13350	-0.68576
so4	SO4	0.78104	-0.39765	-0.09183	-0.22397
cl	Cl	0.68136	-0.20033	-0.12806	-0.42339
d13c	d13C	-0.70156	-0.35679	0.09089	0.27520
dic	DIC	0.80033	0.14337	-0.37953	-0.02070
d18o	d18O	0.45212	-0.16641	0.17337	0.03190
dd	dD	0.70511	-0.42311	-0.05720	0.04074
rn222		0.16229	0.25321	0.44272	0.01765
nh4		0.48541	0.80235	-0.12864	0.12367
no2		0.28040	0.30551	0.73713	-0.18445
po4		0.52219	0.77008	0.04520	0.06097

Average Ratio Sulfate to Chloride Concentrations by Season

The FACTOR Procedure Initial Factor Method: Principal Components

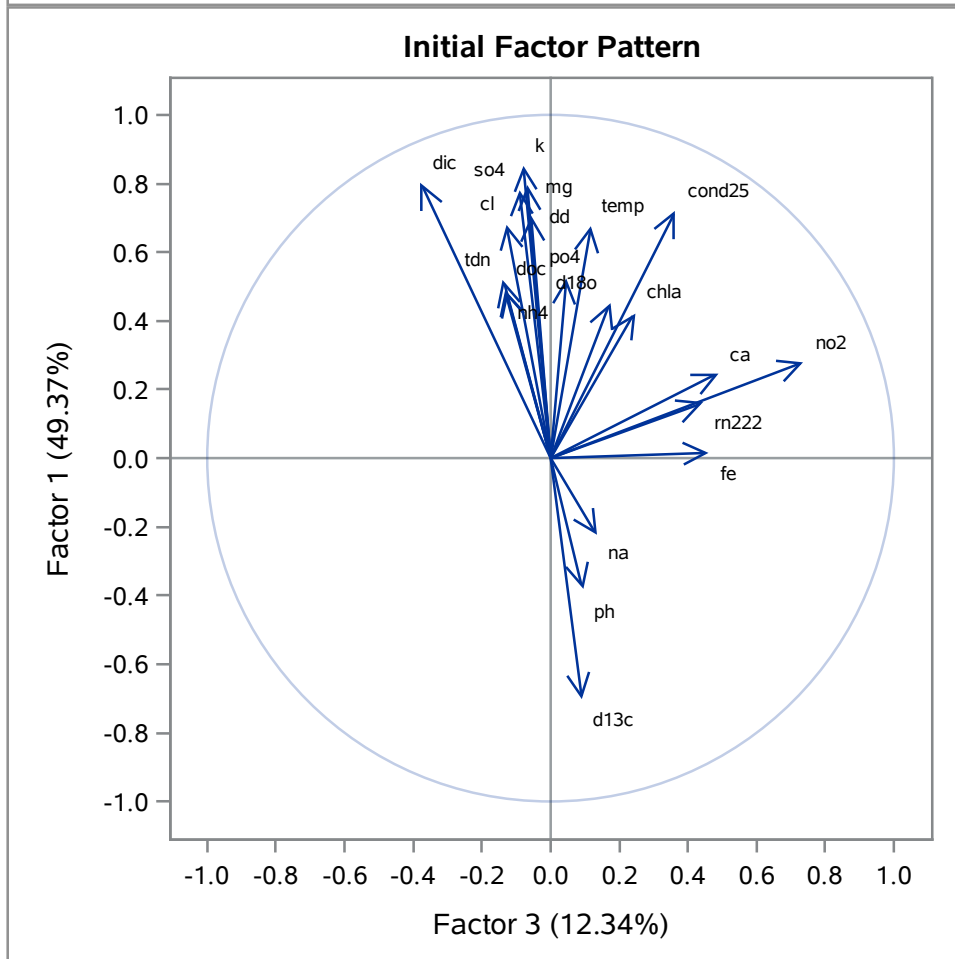
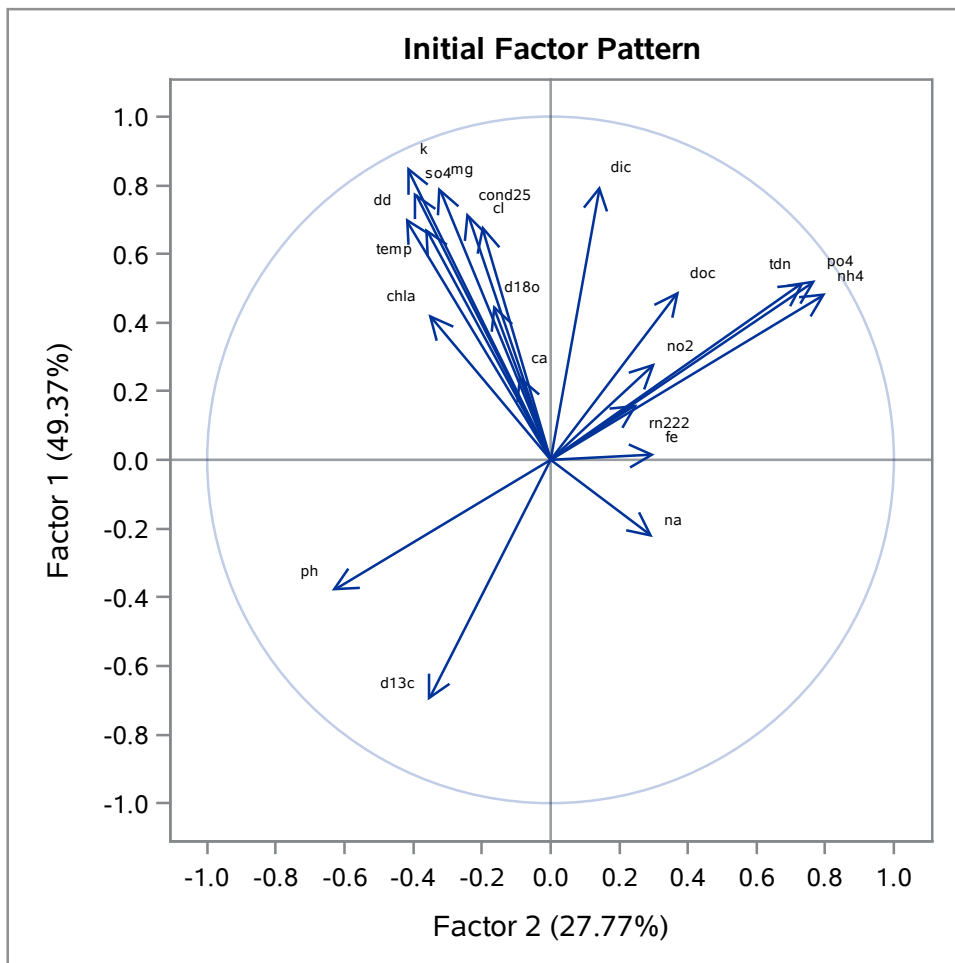
Variance Explained by Each Factor			
Factor1	Factor2	Factor3	Factor4
6.7990063	3.8252057	1.6994026	1.4492434

Final Community Estimates: Total = 13.772858							
temp	cond25	ph	chla	doc	tdn	fe	mg
0.80356826	0.70992388	0.57106384	0.49986395	0.52510522	0.85584644	0.36126402	0.77850327
ca	k	na	so4	cl	d13c	dic	d18o
0.33166474	0.90944138	0.62765652	0.82673665	0.70004677	0.70348178	0.80555887	0.26317997

dd	rn222	nh4	no2	po4
0.68113469	0.28676818	0.91124025	0.74934789	0.87146137

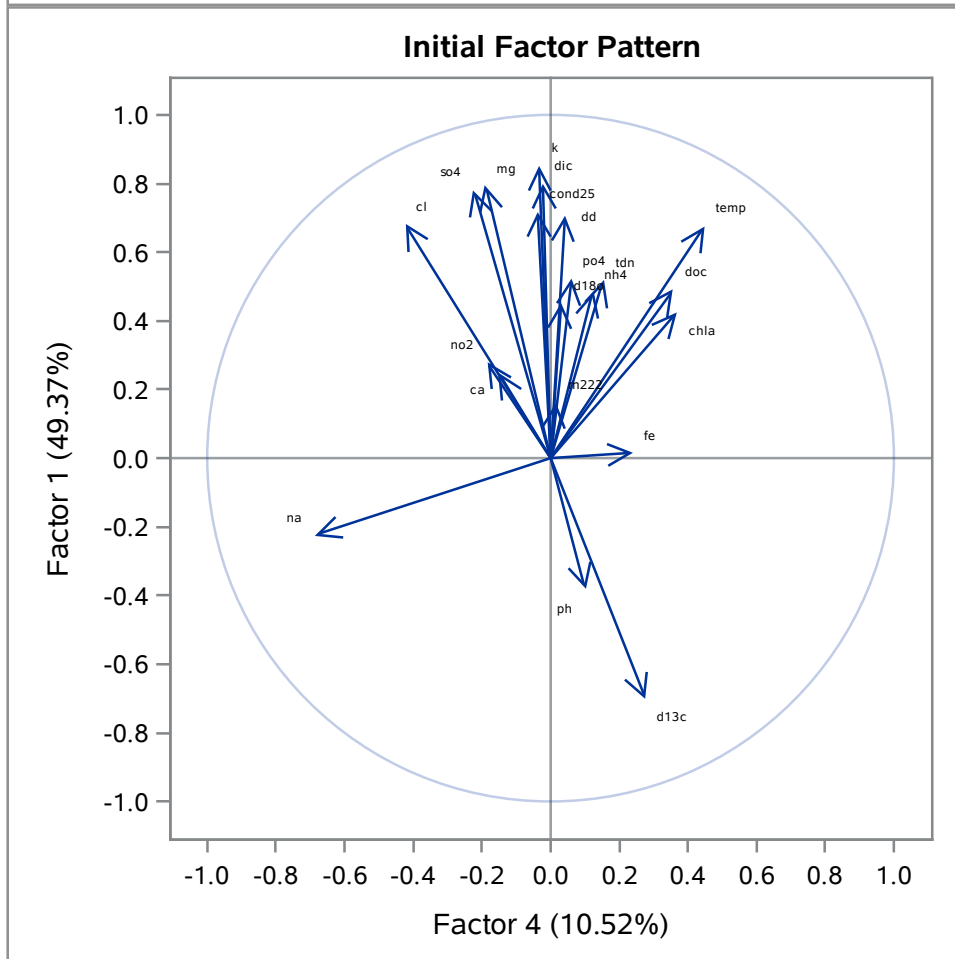
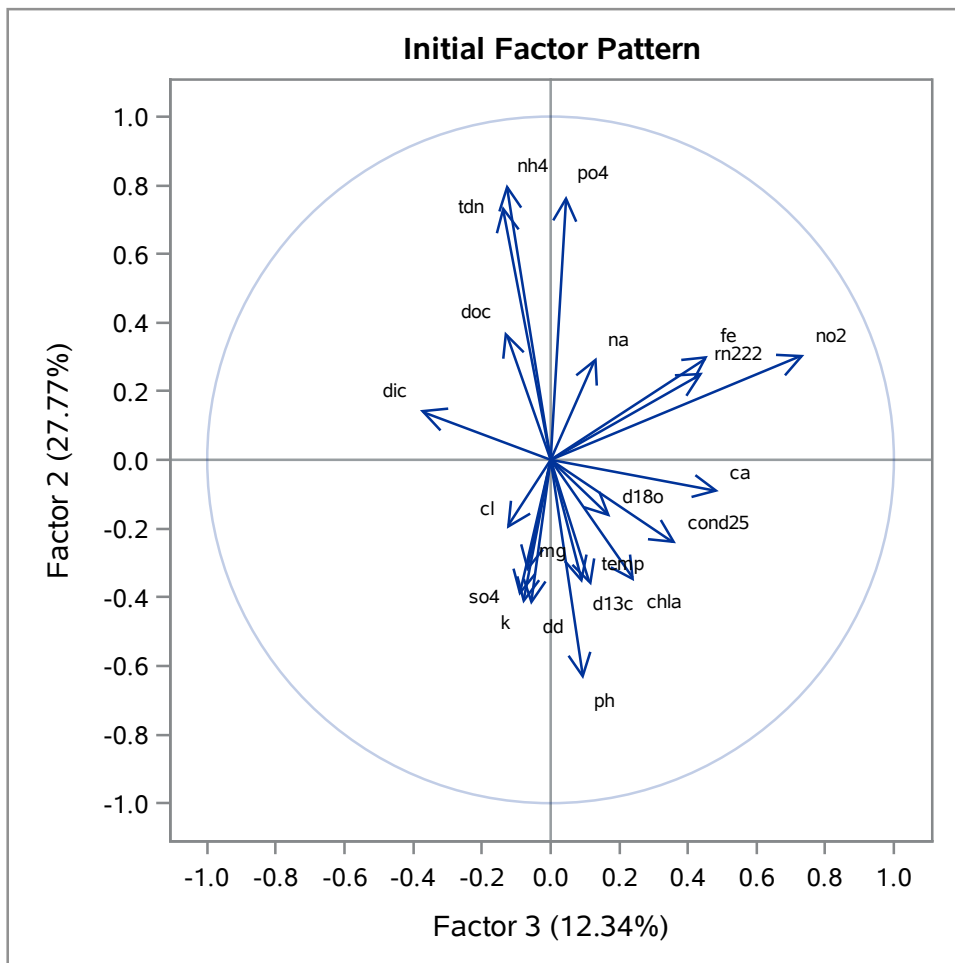
Average Ratio Sulfate to Chloride Concentrations by Season

The FACTOR Procedure Initial Factor Method: Principal Components



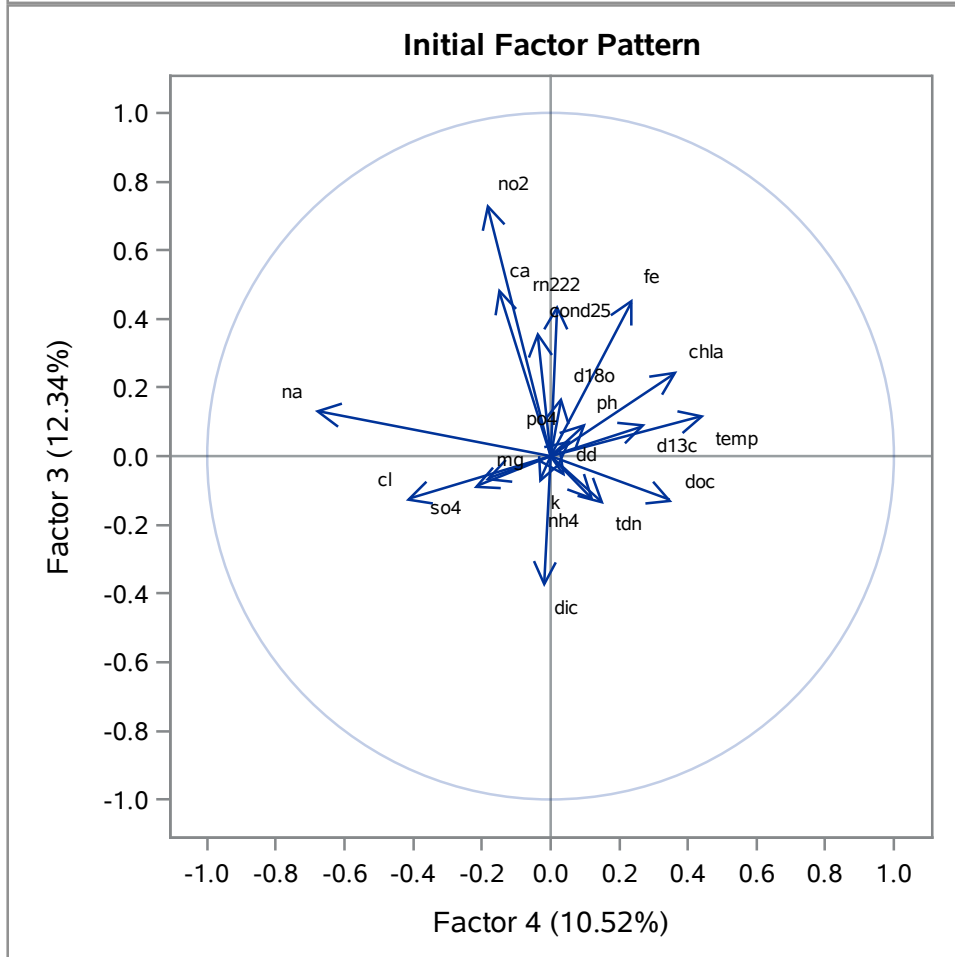
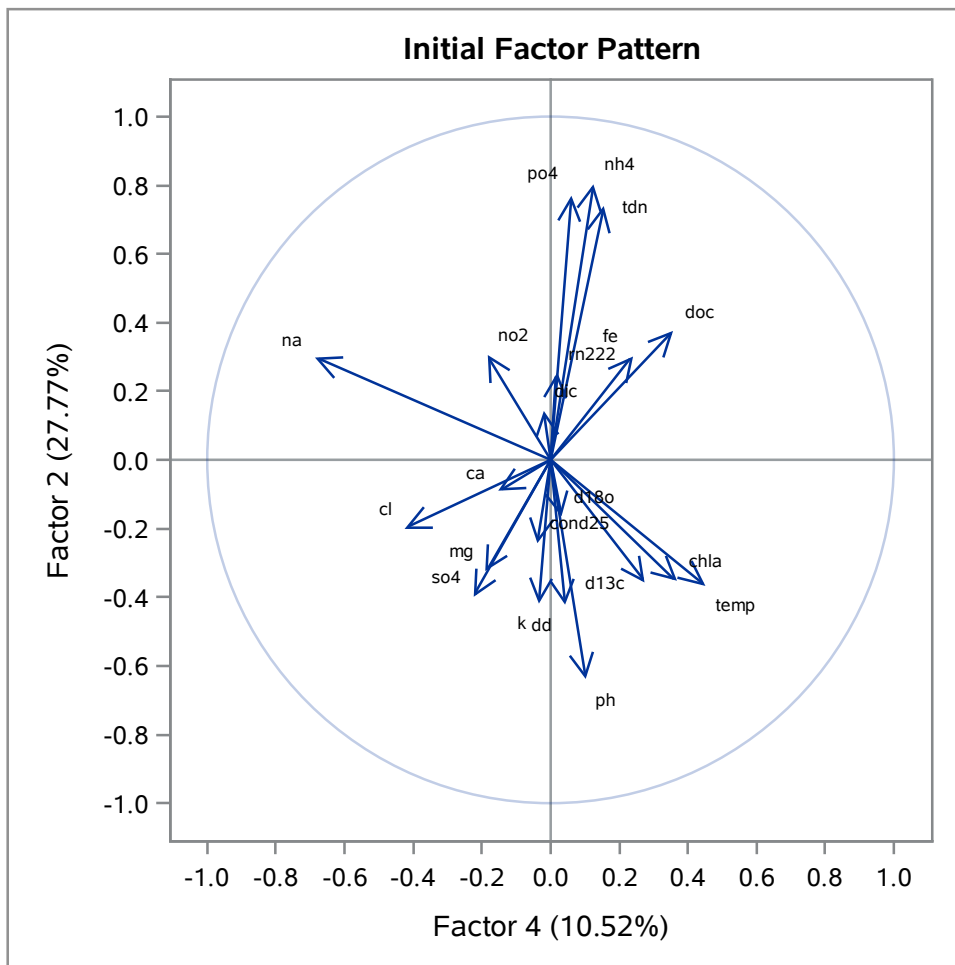
Average Ratio Sulfate to Chloride Concentrations by Season

The FACTOR Procedure
Initial Factor Method: Principal Components



Average Ratio Sulfate to Chloride Concentrations by Season

The FACTOR Procedure
Initial Factor Method: Principal Components



Average Ratio Sulfate to Chloride Concentrations by Season

The FACTOR Procedure
Rotation Method: Varimax

Orthogonal Transformation Matrix				
	1	2	3	4
1	0.81232	0.49274	0.25776	0.17582
2	-0.44848	0.82193	-0.29145	0.19585
3	-0.07758	-0.24921	0.06386	0.96322
4	-0.36468	0.13978	0.91899	-0.05413

Rotated Factor Pattern					
		Factor1	Factor2	Factor3	Factor4
temp	Temp	0.53906	0.06568	0.70020	0.13561
cond25	Cond25	0.67876	0.05793	0.24504	0.43105
ph	pH	-0.06929	-0.72108	0.18658	-0.10722
chla	Chla	0.34953	-0.09252	0.56576	0.22145
doc	DOC	0.11134	0.63171	0.33688	0.01280
tdn	TDN	0.04368	0.91787	0.05148	0.09387
fe	Fe	-0.24704	0.17499	0.16554	0.49215
mg	Mg	0.86633	0.11425	0.12043	0.02053
ca	Ca	0.25953	-0.09497	-0.01805	0.50494
k	K	0.89877	0.09184	0.30526	-0.00576
na	Na	-0.07664	0.00549	-0.76658	0.18466
so4	SO4	0.90159	0.04958	0.10552	-0.01689
cl	Cl	0.80766	0.14380	-0.16326	-0.01988
d13c	d13C	-0.51729	-0.62312	0.18187	-0.12058
dic	DIC	0.62282	0.60388	0.12125	-0.19567
d18o	d18O	0.41682	0.04726	0.20542	0.21216
dd	dD	0.75211	0.01961	0.33884	-0.01620
rn222		-0.02251	0.18022	0.01253	0.50361
nh4		-0.00064	0.94800	-0.00330	0.11188
no2		0.10084	0.17979	-0.13920	0.82914
po4		0.05308	0.88751	-0.03092	0.28287

Variance Explained by Each Factor			
Factor1	Factor2	Factor3	Factor4
5.4587310	4.3687663	2.0075139	1.9378468

Average Ratio Sulfate to Chloride Concentrations by Season

The FACTOR Procedure Rotation Method: Varimax

Final Communality Estimates: Total = 13.772858							
temp	cond25	ph	chla	doc	tdn	fe	mg
0.80356826	0.70992388	0.57106384	0.49986395	0.52510522	0.85584644	0.36126402	0.77850327

ca	k	na	so4	cl	d13c	dic	d18o
0.33166474	0.90944138	0.62765652	0.82673665	0.70004677	0.70348178	0.80555887	0.26317997

dd	rn222	nh4	no2	po4
0.68113469	0.28676818	0.91124025	0.74934789	0.87146137

Average Ratio Sulfate to Chloride Concentrations by Season

The FACTOR Procedure Rotation Method: Varimax

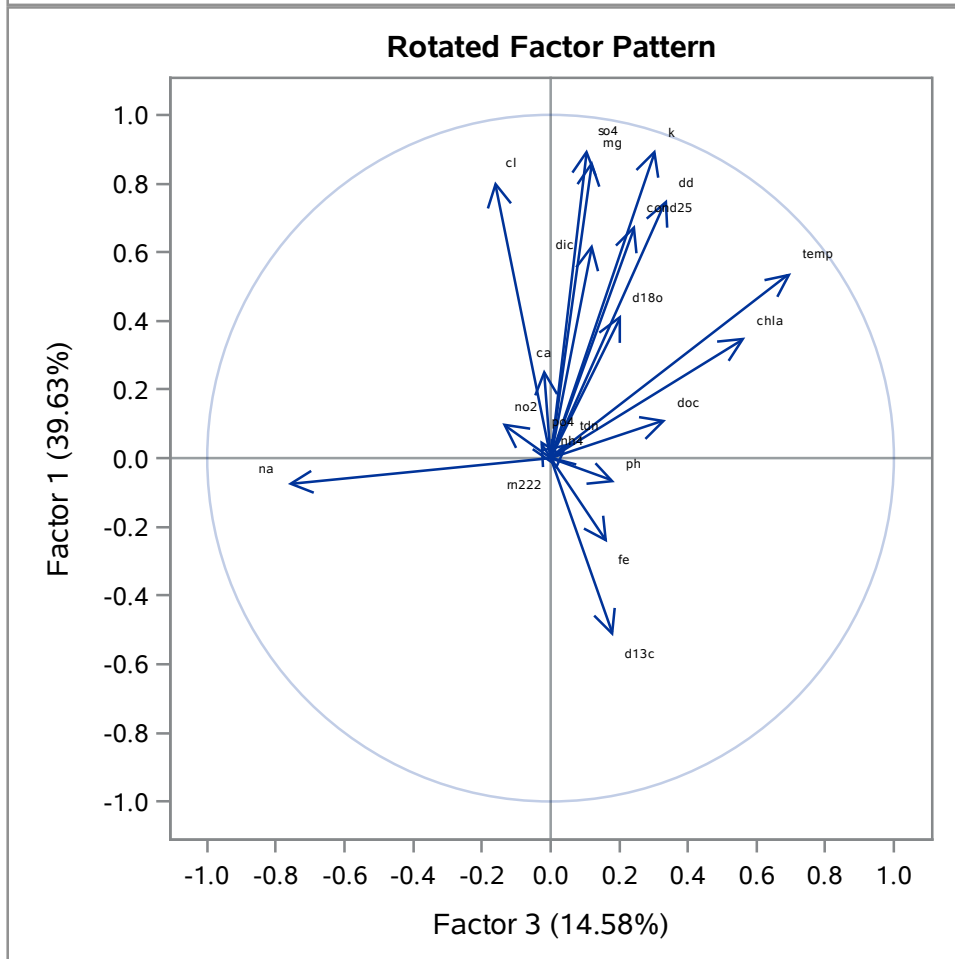
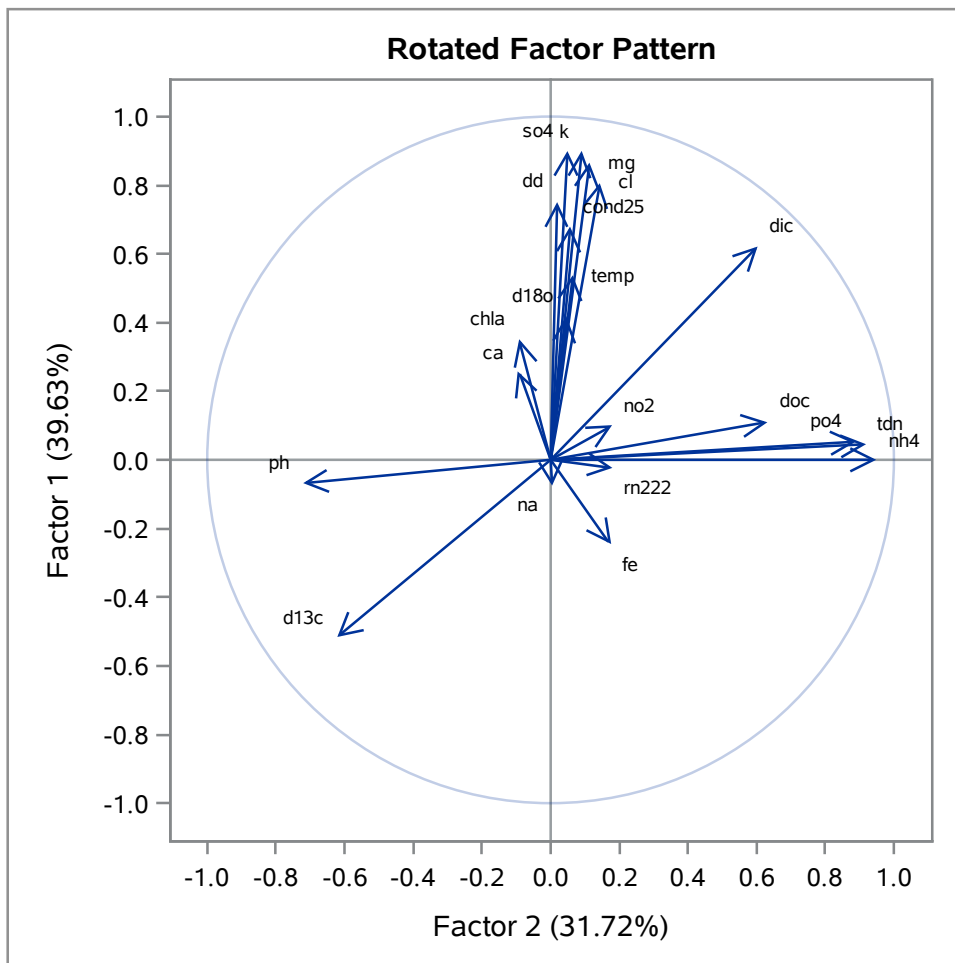
Scoring Coefficients Estimated by Regression

Squared Multiple Correlations of the Variables with Each Factor			
Factor1	Factor2	Factor3	Factor4
1.0000000	1.0000000	1.0000000	1.0000000

Standardized Scoring Coefficients					
		Factor1	Factor2	Factor3	Factor4
temp	Temp	0.00516	-0.00350	0.34236	0.04838
cond25	Cond25	0.10732	-0.05725	0.03567	0.21368
ph	pH	-0.00088	-0.16851	0.10207	0.00681
chla	Chla	-0.01159	-0.04600	0.28532	0.11815
doc	DOC	-0.06886	0.16963	0.21130	-0.05644
tdn	TDN	-0.05730	0.23134	0.05621	-0.03305
fe	Fe	-0.11514	0.02180	0.14700	0.26774
mg	Mg	0.18415	-0.02075	-0.06835	-0.02768
ca	Ca	0.05613	-0.08774	-0.06163	0.28449
k	K	0.16305	-0.01968	0.03959	-0.04264
na	Na	0.10463	-0.03787	-0.46110	0.11075
so4	SO4	0.20049	-0.03698	-0.08556	-0.04385
cl	Cl	0.21728	-0.01572	-0.23220	-0.04941
d13c	d13C	-0.11539	-0.11429	0.17851	0.00483
dic	DIC	0.10135	0.14247	-0.00797	-0.18631
d18o	d18O	0.05759	-0.02534	0.05656	0.10024
dd	dD	0.12621	-0.02750	0.08265	-0.03737
rn222		-0.03495	0.00295	0.01469	0.26744
nh4		-0.06132	0.23837	0.03085	-0.02390
no2		0.01045	-0.03992	-0.10191	0.44759
po4		-0.04530	0.20256	0.00149	0.07627

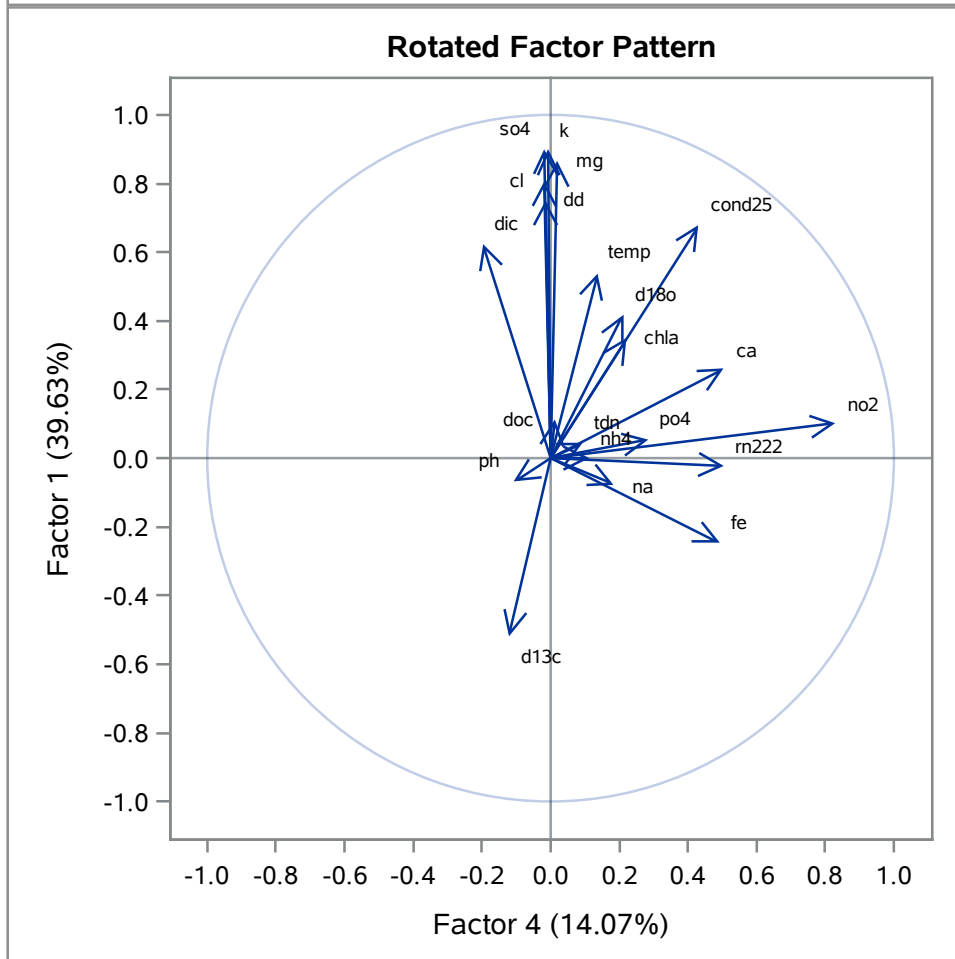
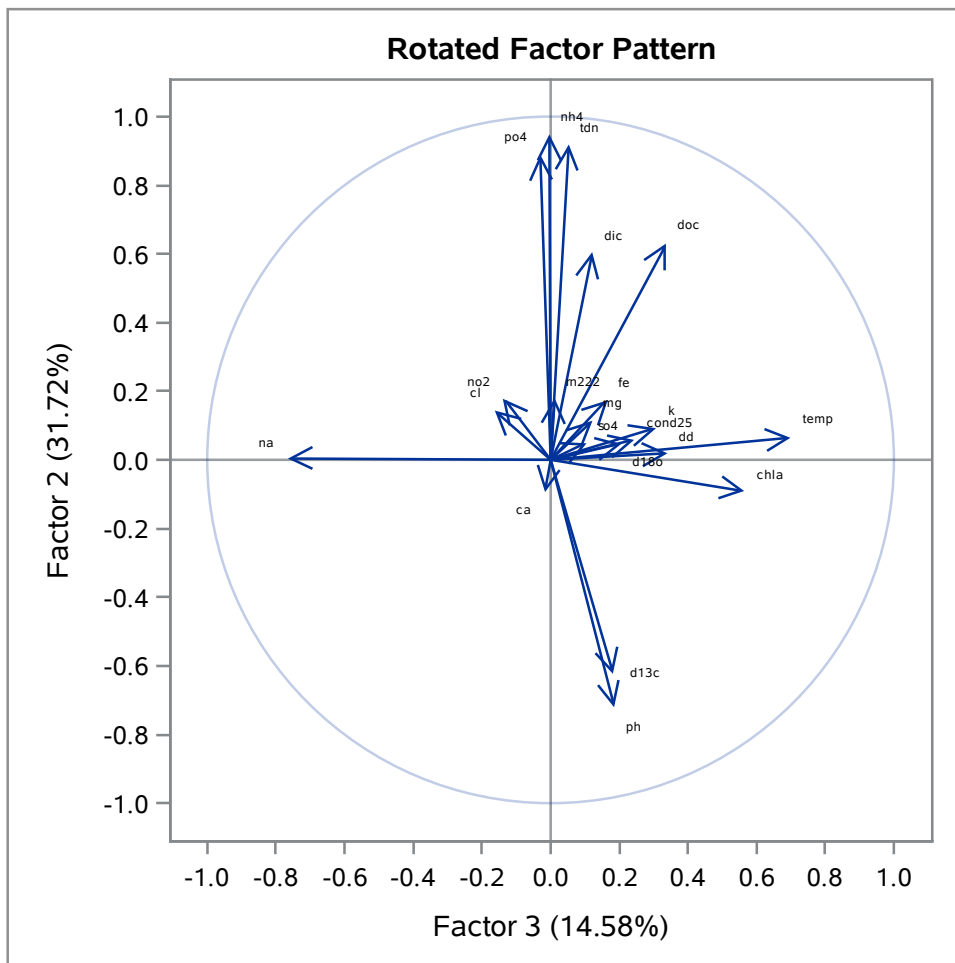
Average Ratio Sulfate to Chloride Concentrations by Season

The FACTOR Procedure
Rotation Method: Varimax



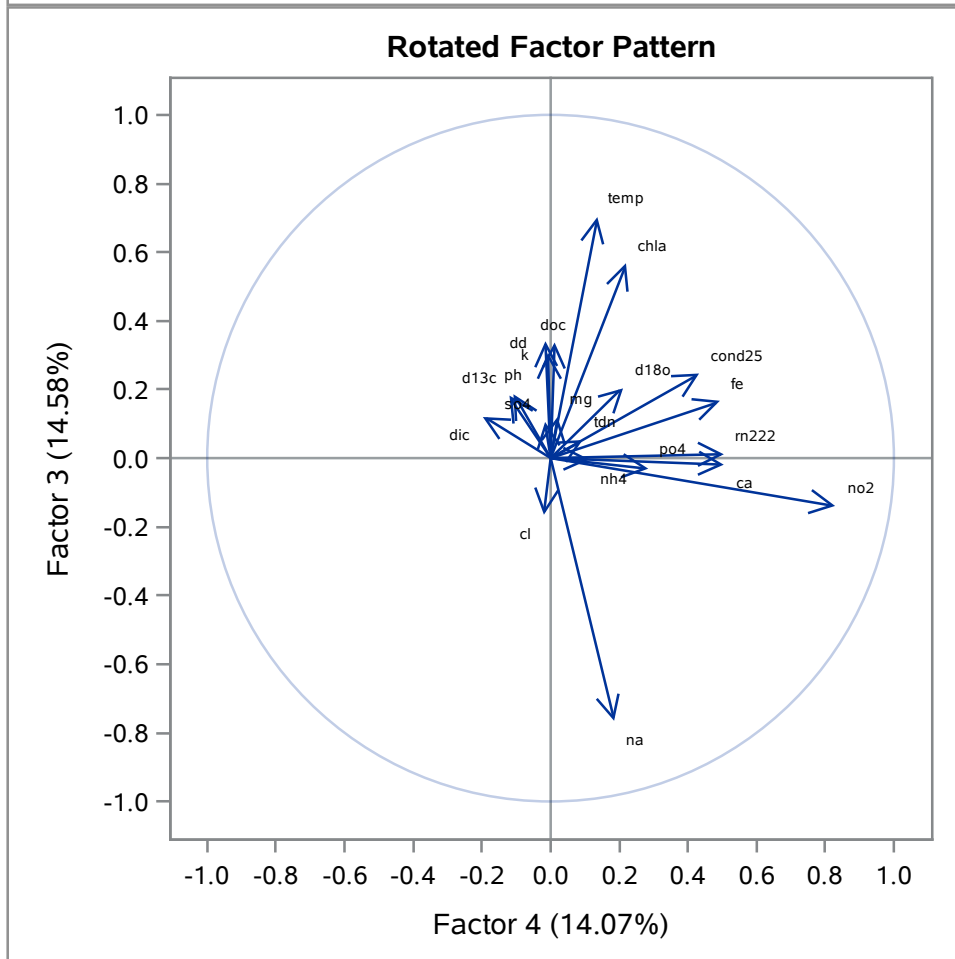
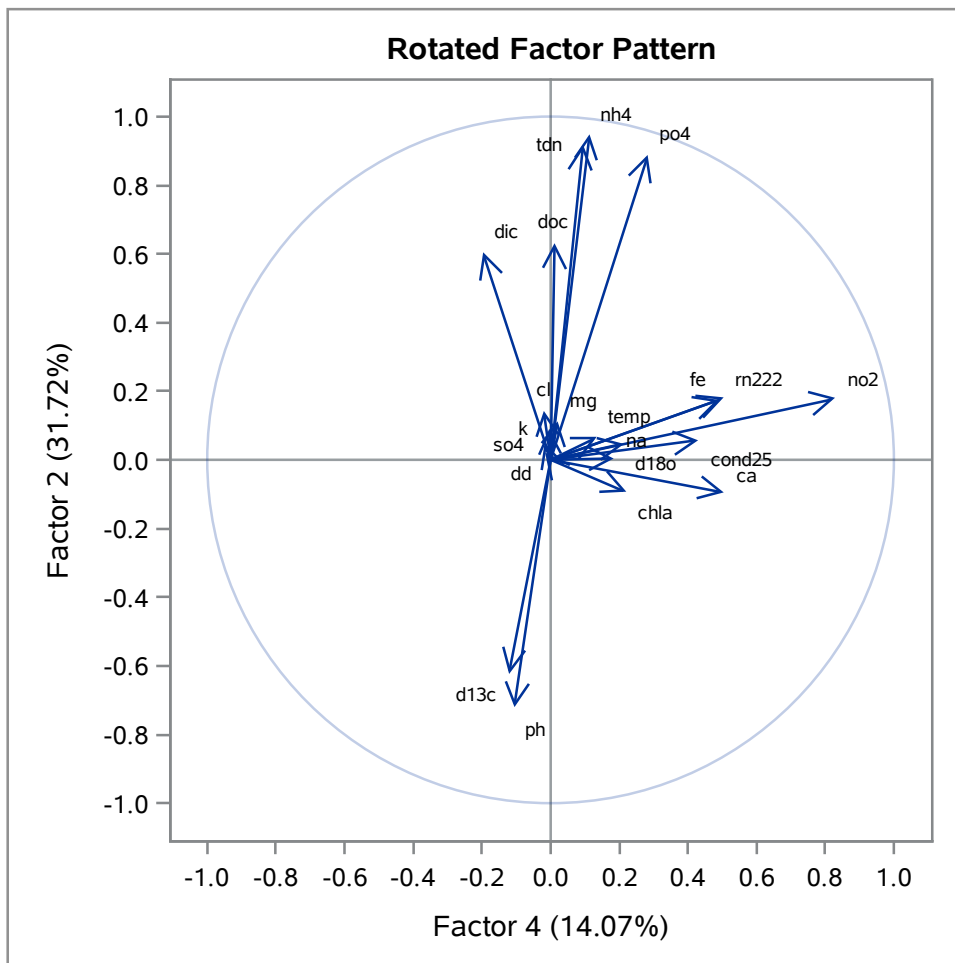
Average Ratio Sulfate to Chloride Concentrations by Season

The FACTOR Procedure
Rotation Method: Varimax

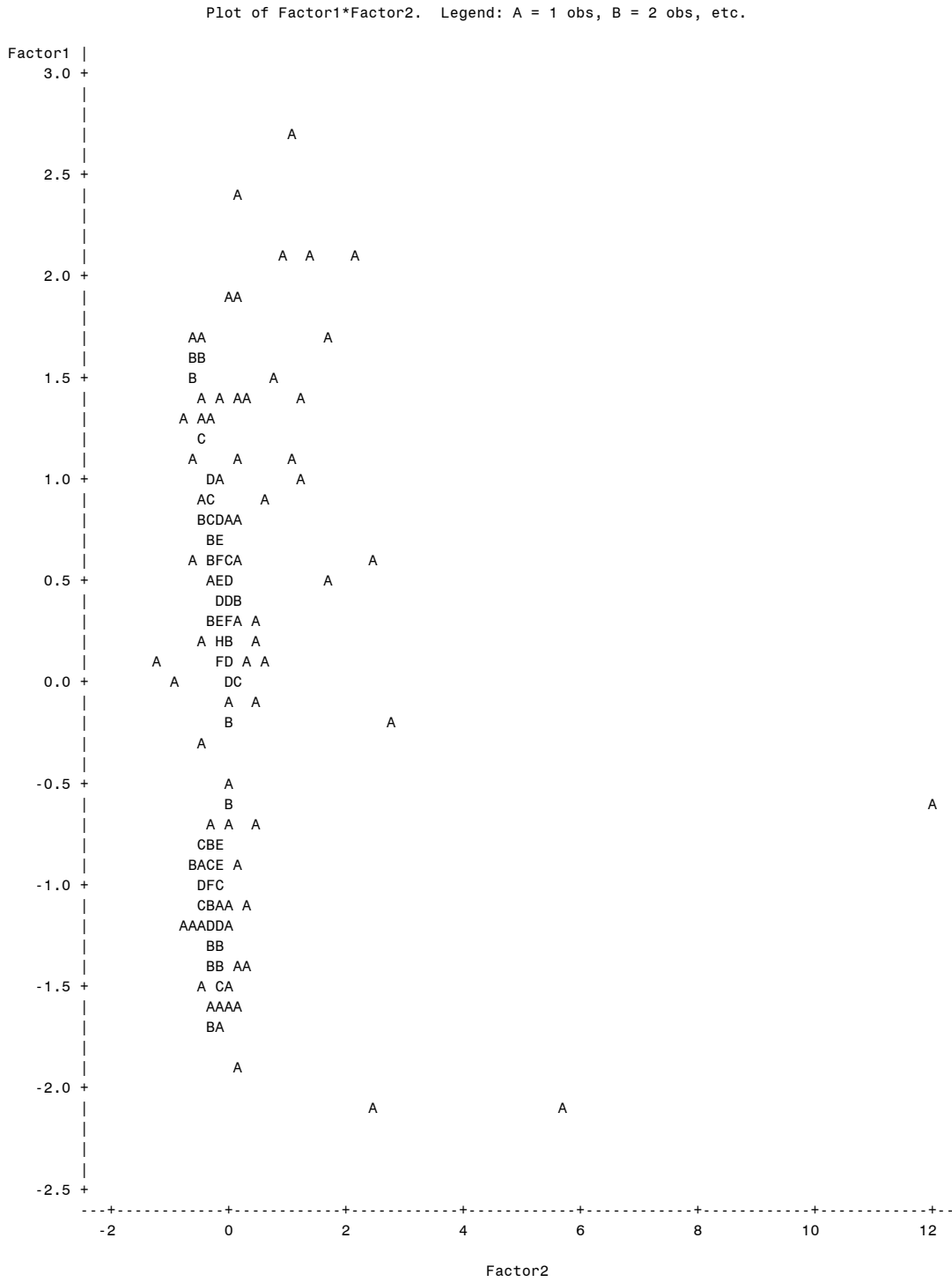


Average Ratio Sulfate to Chloride Concentrations by Season

The FACTOR Procedure
Rotation Method: Varimax

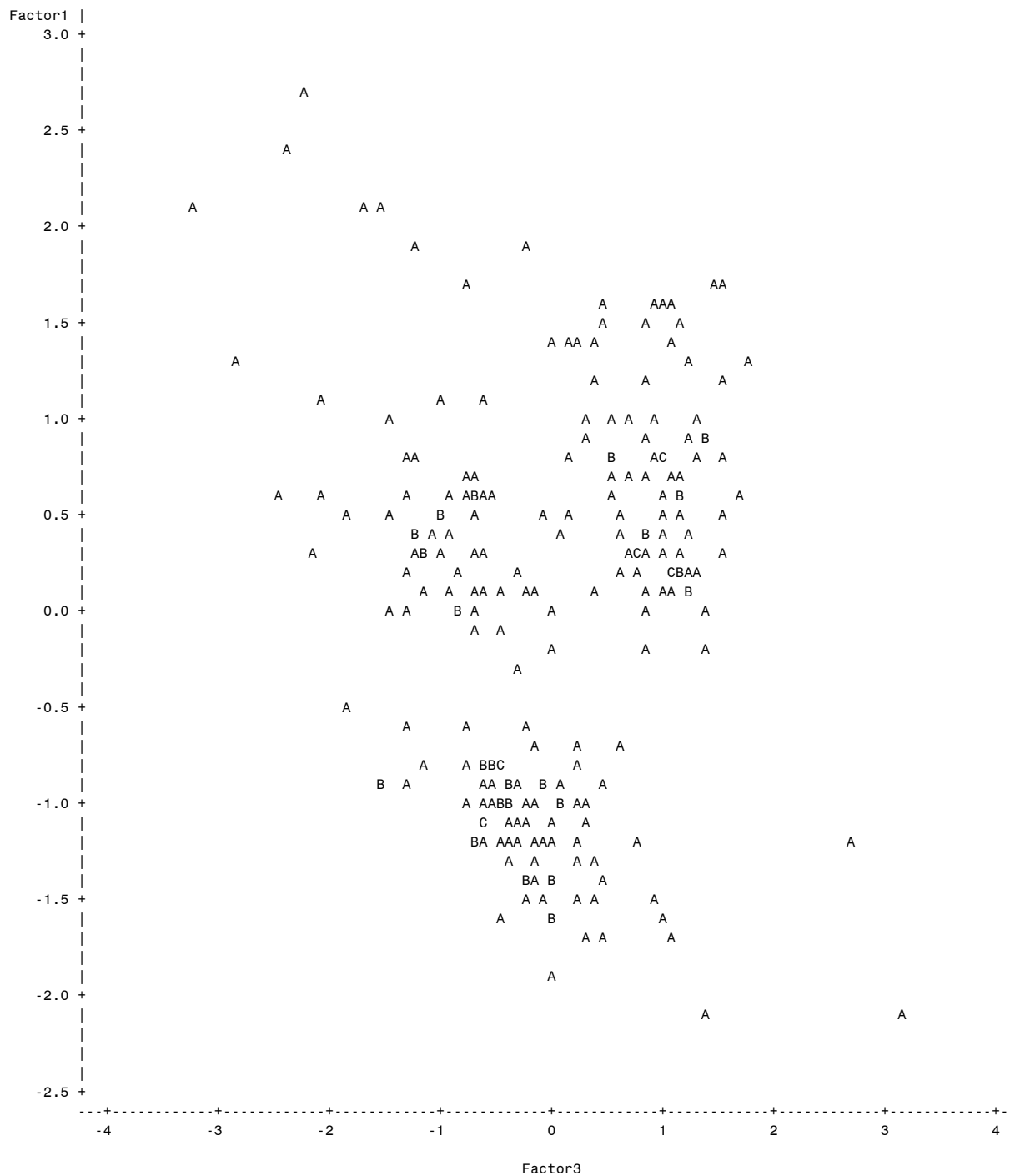


Average Ratio Sulfate to Chloride Concentrations by Season



Average Ratio Sulfate to Chloride Concentrations by Season

Plot of Factor1*Factor3. Legend: A = 1 obs, B = 2 obs, etc.



Average Ratio Sulfate to Chloride Concentrations by Season

The CORR Procedure

21 With Variables:	temp nh4	cond25 no2	ph po4	chla	doc	tdn	fe	mg	ca	k	na	so4	cl	d13c	dic	d18o	dd	rn222
3 Variables:	Factor1	Factor2	Factor3															

Simple Statistics							
Variable	N	Mean	Std Dev	Sum	Minimum	Maximum	Label
temp	236	19.88905	7.93417	4694	6.90000	31.60000	Temp
cond25	236	56832	6299	13412406	27794	83055	Cond25
ph	236	8.25552	0.25299	1948	7.04000	8.72000	pH
chla	236	5.41169	2.38469	1277	0.26000	18.03000	Chla
doc	236	453.36999	509.92860	106995	197.84419	6022	DOC
tdn	236	62.61709	158.81309	14778	18.09239	2236	TDN
fe	236	0.40533	0.61872	95.65820	0.02600	5.96380	Fe
mg	236	1325	203.89929	312682	545.66667	1896	Mg
ca	236	451.11563	91.75799	106463	312.46875	1314	Ca
k	236	555.61979	81.59286	131126	426.55313	740.25938	K
na	236	11260	3536	2657283	4712	26085	Na
so4	236	27.54629	5.47448	6501	0.26736	39.12289	SO4
cl	236	519.32169	92.79721	122560	1.06264	759.37289	Cl
d13c	236	-2.73061	2.79524	-644.42440	-22.07191	3.24557	d13C
dic	236	1514	1435	357321	0.19880	12507	DIC
d18o	236	1.07037	0.55003	252.60631	-2.40328	2.12764	d18O
dd	236	7.64726	3.29965	1805	3.26143	25.33762	dD
rn222	236	113.19502	308.40461	26714	0	3272	
nh4	236	25.47794	122.27983	6013	0.19450	1660	
no2	236	0.13484	0.16693	31.82170	0.02650	1.41500	
po4	236	0.95995	2.82255	226.54783	0.00300	30.34250	
Factor1	236	0	1.00000	0	-2.14381	2.71143	
Factor2	236	0	1.00000	0	-1.17389	11.99306	
Factor3	236	0	1.00000	0	-3.24788	3.12675	

Pearson Correlation Coefficients, N = 236 Prob > r under H0: Rho=0			
	Factor1	Factor2	Factor3
temp Temp	0.53906 <.0001	0.06568 0.3150	0.70020 <.0001
cond25 Cond25	0.67876 <.0001	0.05793 0.3757	0.24504 0.0001
ph pH	-0.06929 0.2891	-0.72108 <.0001	0.18658 0.0040
chla Chla	0.34953 <.0001	-0.09252 0.1565	0.56576 <.0001

Average Ratio Sulfate to Chloride Concentrations by Season

The CORR Procedure

Pearson Correlation Coefficients, N = 236 Prob > r under H0: Rho=0			
	Factor1	Factor2	Factor3
doc DOC	0.11134 0.0879	0.63171 <.0001	0.33688 <.0001
tdn TDN	0.04368 0.5042	0.91787 <.0001	0.05148 0.4312
fe Fe	-0.24704 0.0001	0.17499 0.0070	0.16554 0.0109
mg Mg	0.86633 <.0001	0.11425 0.0798	0.12043 0.0647
ca Ca	0.25953 <.0001	-0.09497 0.1458	-0.01805 0.7827
k K	0.89877 <.0001	0.09184 0.1596	0.30526 <.0001
na Na	-0.07664 0.2409	0.00549 0.9332	-0.76658 <.0001
so4 SO4	0.90159 <.0001	0.04958 0.4484	0.10552 0.1059
cl Cl	0.80766 <.0001	0.14380 0.0272	-0.16326 0.0120
d13c d13C	-0.51729 <.0001	-0.62312 <.0001	0.18187 0.0051
dic DIC	0.62282 <.0001	0.60388 <.0001	0.12125 0.0629
d18o d18O	0.41682 <.0001	0.04726 0.4700	0.20542 0.0015
dd dD	0.75211 <.0001	0.01961 0.7644	0.33884 <.0001
rn222	-0.02251 0.7308	0.18022 0.0055	0.01253 0.8482
nh4	-0.00064 0.9922	0.94800 <.0001	-0.00330 0.9598
no2	0.10084 0.1224	0.17979 0.0056	-0.13920 0.0326
po4	0.05308 0.4170	0.88751 <.0001	-0.03092 0.6365

Average Ratio Sulfate to Chloride Concentrations by Season**The FACTOR Procedure**

Input Data Type	Raw Data
Number of Records Read	143
Number of Records Used	143
N for Significance Tests	143

Average Ratio Sulfate to Chloride Concentrations by Season

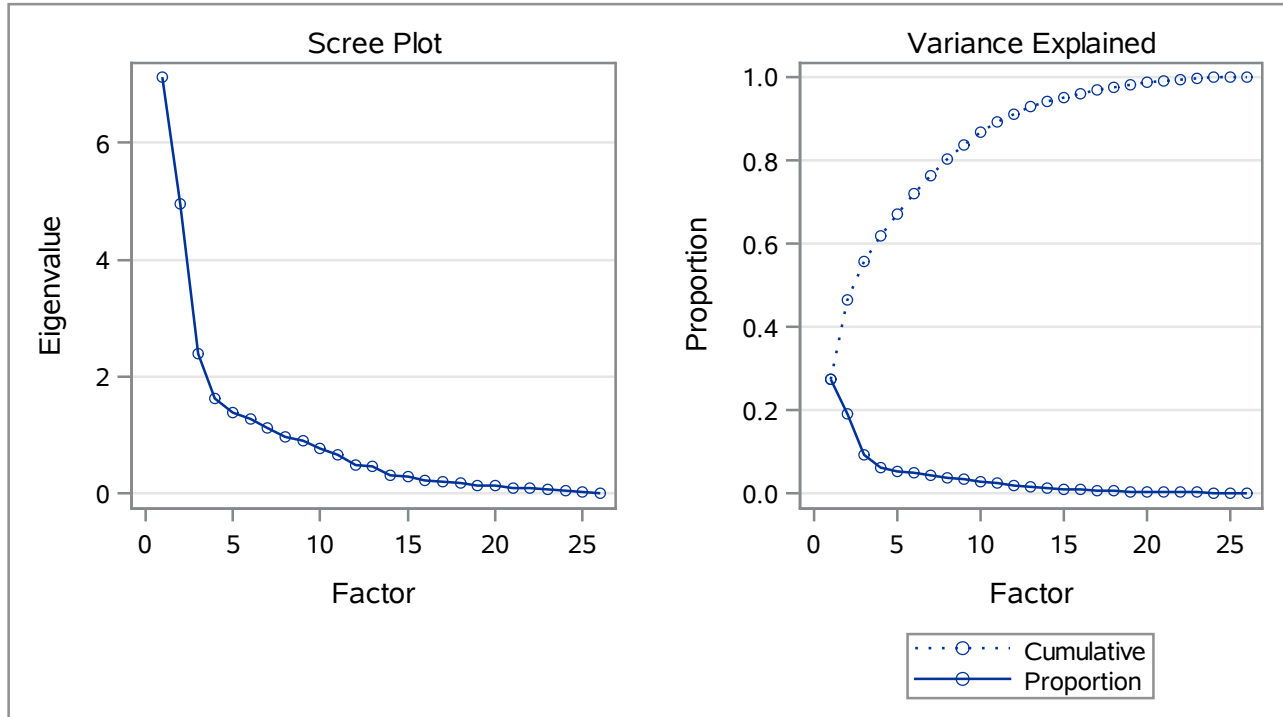
The FACTOR Procedure Initial Factor Method: Principal Components

Prior Communality Estimates: ONE

Eigenvalues of the Correlation Matrix: Total = 26 Average = 1				
	Eigenvalue	Difference	Proportion	Cumulative
1	7.12409695	2.16519576	0.2740	0.2740
2	4.95890118	2.56337452	0.1907	0.4647
3	2.39552667	0.77721783	0.0921	0.5569
4	1.61830884	0.23124578	0.0622	0.6191
5	1.38706306	0.11934175	0.0533	0.6725
6	1.26772130	0.13806901	0.0488	0.7212
7	1.12965229	0.15250601	0.0434	0.7647
8	0.97714628	0.06742161	0.0376	0.8022
9	0.90972466	0.13880243	0.0350	0.8372
10	0.77092223	0.11262773	0.0297	0.8669
11	0.65829451	0.17671033	0.0253	0.8922
12	0.48158418	0.01882437	0.0185	0.9107
13	0.46275981	0.15496536	0.0178	0.9285
14	0.30779445	0.02683457	0.0118	0.9404
15	0.28095988	0.04452328	0.0108	0.9512
16	0.23643660	0.02352360	0.0091	0.9603
17	0.21291300	0.02546290	0.0082	0.9685
18	0.18745010	0.04363249	0.0072	0.9757
19	0.14381761	0.01155704	0.0055	0.9812
20	0.13226057	0.02854483	0.0051	0.9863
21	0.10371574	0.01625776	0.0040	0.9903
22	0.08745798	0.01990509	0.0034	0.9936
23	0.06755289	0.00785021	0.0026	0.9962
24	0.05970268	0.02489540	0.0023	0.9985
25	0.03480728	0.03137800	0.0013	0.9999
26	0.00342928		0.0001	1.0000

5 factors will be retained by the NFACTOR criterion.

Average Ratio Sulfate to Chloride Concentrations by Season

The FACTOR Procedure
Initial Factor Method: Principal Components

		Factor Pattern				
		Factor1	Factor2	Factor3	Factor4	Factor5
temp	Temp	0.25648	0.64433	-0.56352	0.17584	-0.08107
cond25	Cond25	0.40935	0.77766	0.14151	0.16155	-0.04800
ph	pH	-0.76901	0.30643	-0.04487	0.19371	-0.11099
chla	Chla	0.23420	0.62466	-0.06850	0.29319	0.05263
doc	DOC	0.58248	-0.07762	-0.08455	0.37484	-0.00621
tdn	TDN	0.77332	-0.36070	0.12471	0.32941	-0.19781
fe	Fe	0.38321	-0.34371	-0.40147	0.01996	0.29243
mg	Mg	0.13934	0.48238	0.58508	0.19679	-0.23047
ca	Ca	0.35658	0.61616	0.01167	-0.24588	-0.22459
k	K	0.27904	0.85637	0.13332	0.11667	0.03645
na	Na	-0.01596	-0.32030	0.63603	-0.18383	0.18188
so4	SO4	0.21473	0.63965	0.35990	-0.29140	0.21348
cl	Cl	0.27754	0.28638	0.60795	-0.38973	0.22323
d13c	d13C	-0.70308	0.29920	-0.24599	0.18163	0.20384
dic	DIC	0.79150	-0.26137	0.17558	0.09758	-0.11377
d18o	d18O	0.15703	0.23738	-0.14708	-0.21848	-0.57136
dd	dD	0.15360	0.66171	0.13404	0.34191	0.43506
do_conc		-0.76068	-0.34207	0.33103	0.15971	-0.06888
mn_		0.64521	0.13437	-0.44385	-0.10421	0.33750
NN		-0.06385	-0.12386	0.24426	0.34103	0.11779
sio4		0.87604	-0.09528	0.04160	0.01705	0.00332
mmhg_		-0.06911	-0.38935	0.19127	0.40008	0.39511

Average Ratio Sulfate to Chloride Concentrations by Season

The FACTOR Procedure Initial Factor Method: Principal Components

Factor Pattern						
		Factor1	Factor2	Factor3	Factor4	Factor5
rn222		0.33498	-0.04716	-0.23128	-0.38874	0.33540
nh4		0.80179	-0.41196	0.11273	0.27378	-0.16869
no2		0.59204	-0.10770	-0.01642	-0.24228	0.06997
po4		0.87562	-0.33834	0.03884	-0.00748	-0.01834

Variance Explained by Each Factor				
Factor1	Factor2	Factor3	Factor4	Factor5
7.1240969	4.9589012	2.3955267	1.6183088	1.3870631

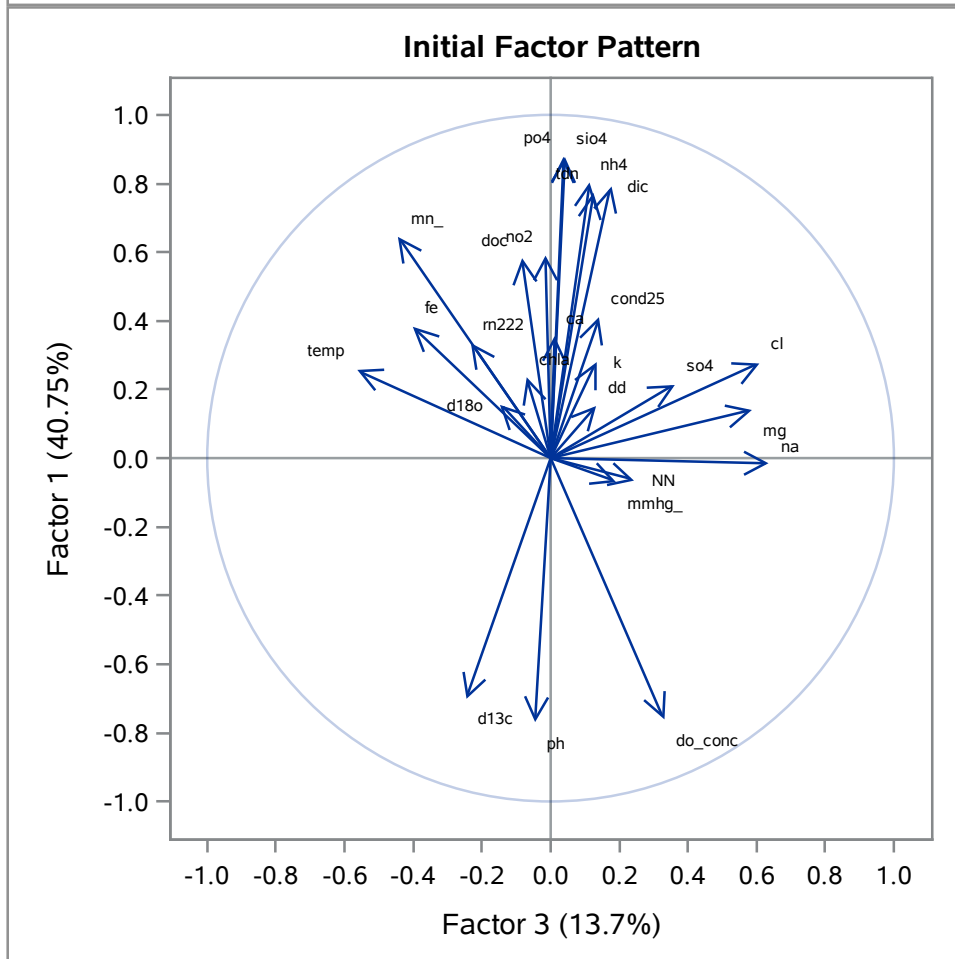
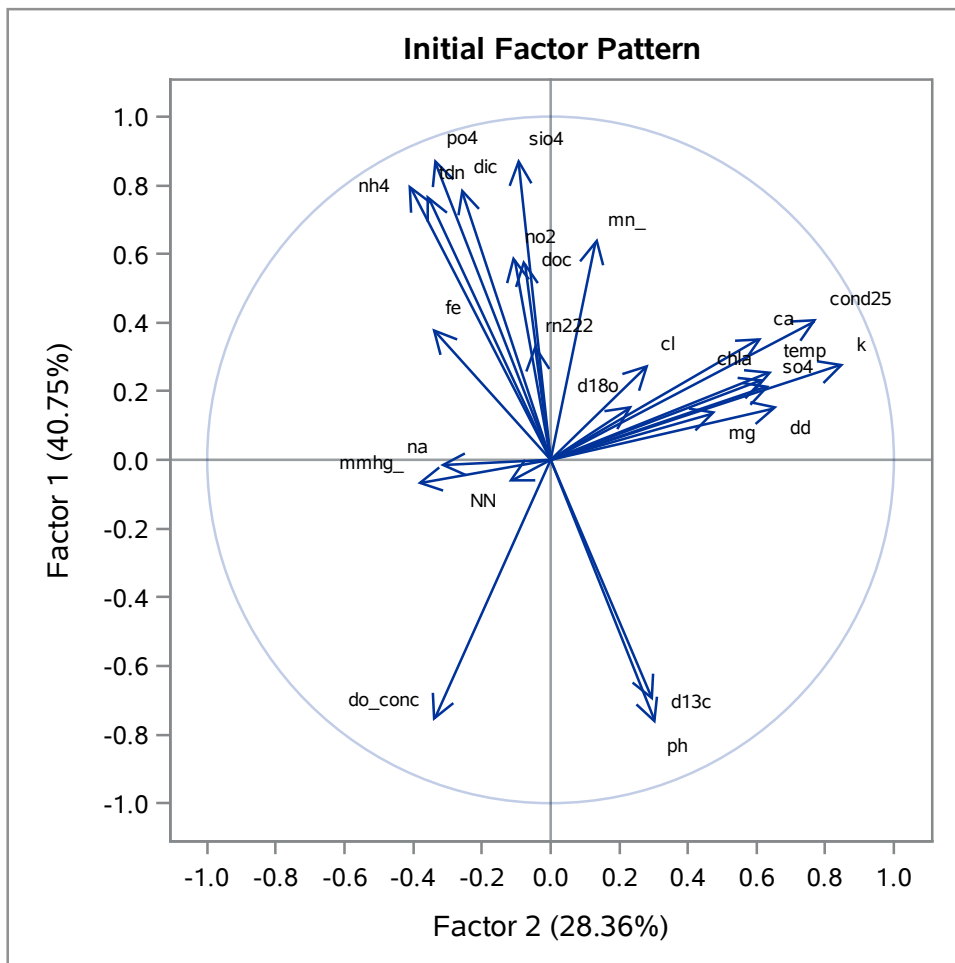
Final Community Estimates: Total = 17.483897								
temp	cond25	ph	chla	doc	tdn	fe	mg	ca
0.83599092	0.82074149	0.73712855	0.53847376	0.49300580	0.89132534	0.51208265	0.68627274	0.61782787

k	na	so4	cl	d13c	dic	d18o	dd	do_conc
0.84394284	0.57424799	0.71527430	0.73035983	0.71889276	0.74807863	0.47682689	0.78560520	0.83546505

mn_	NN	sio4	mmhg_	rn222	nh4	no2	po4
0.75612401	0.20925561	0.77855629	0.50913057	0.43153612	0.92870142	0.42597585	0.88307420

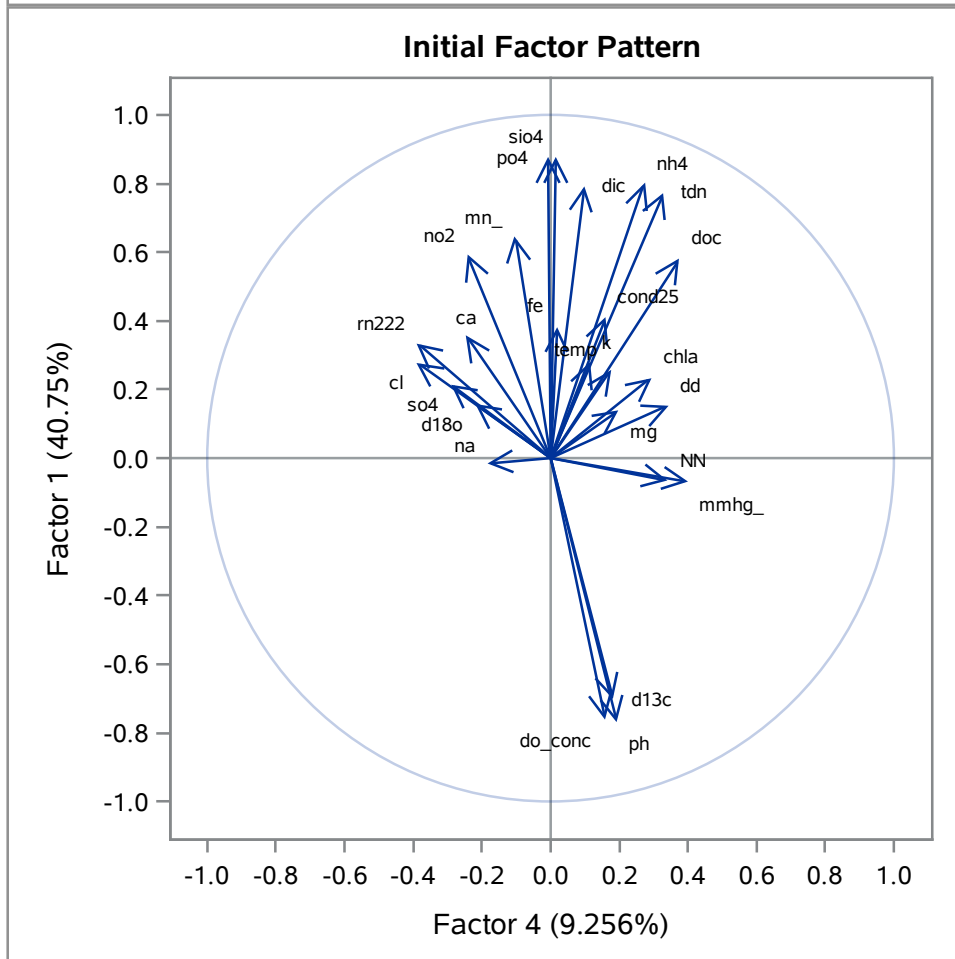
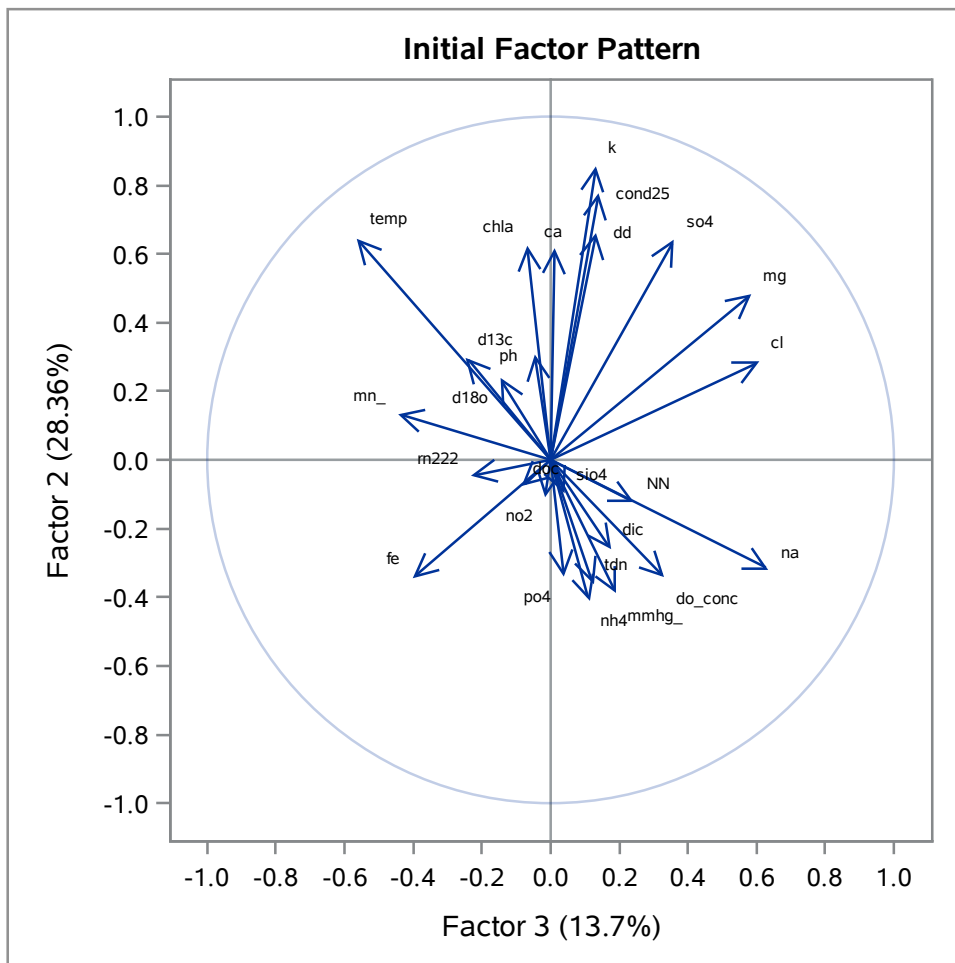
Average Ratio Sulfate to Chloride Concentrations by Season

The FACTOR Procedure Initial Factor Method: Principal Components



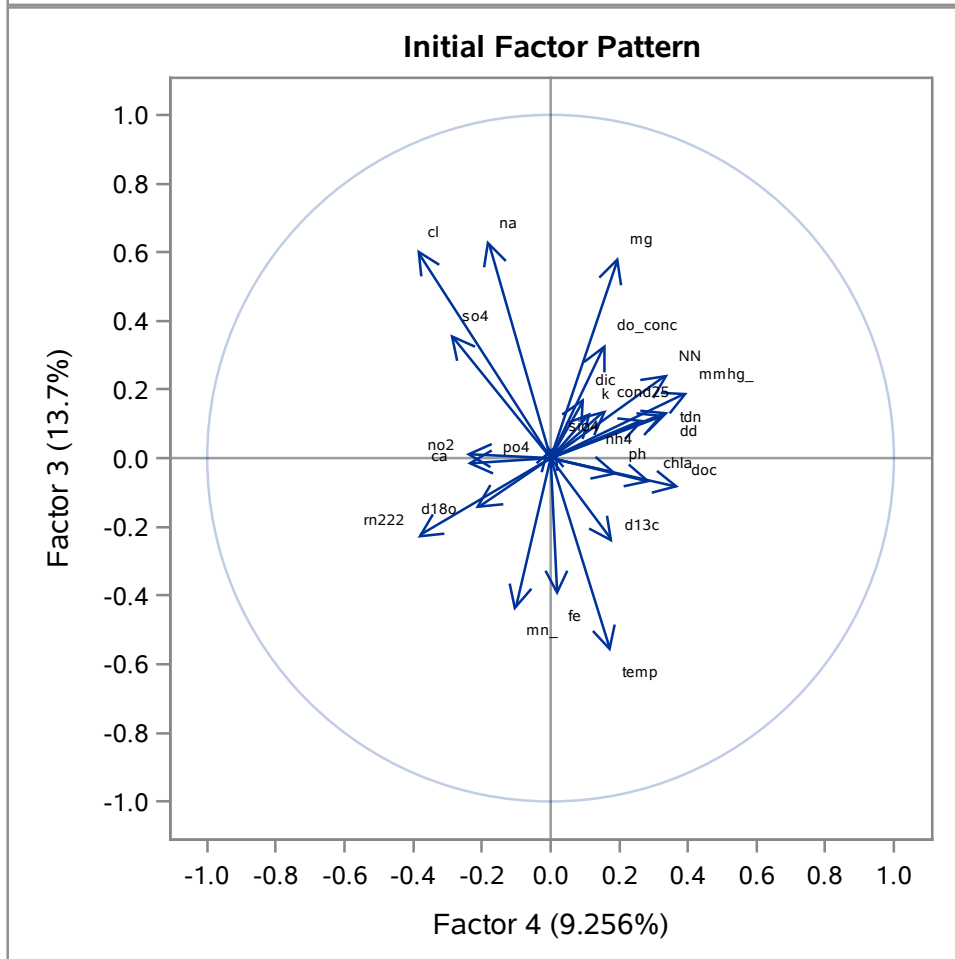
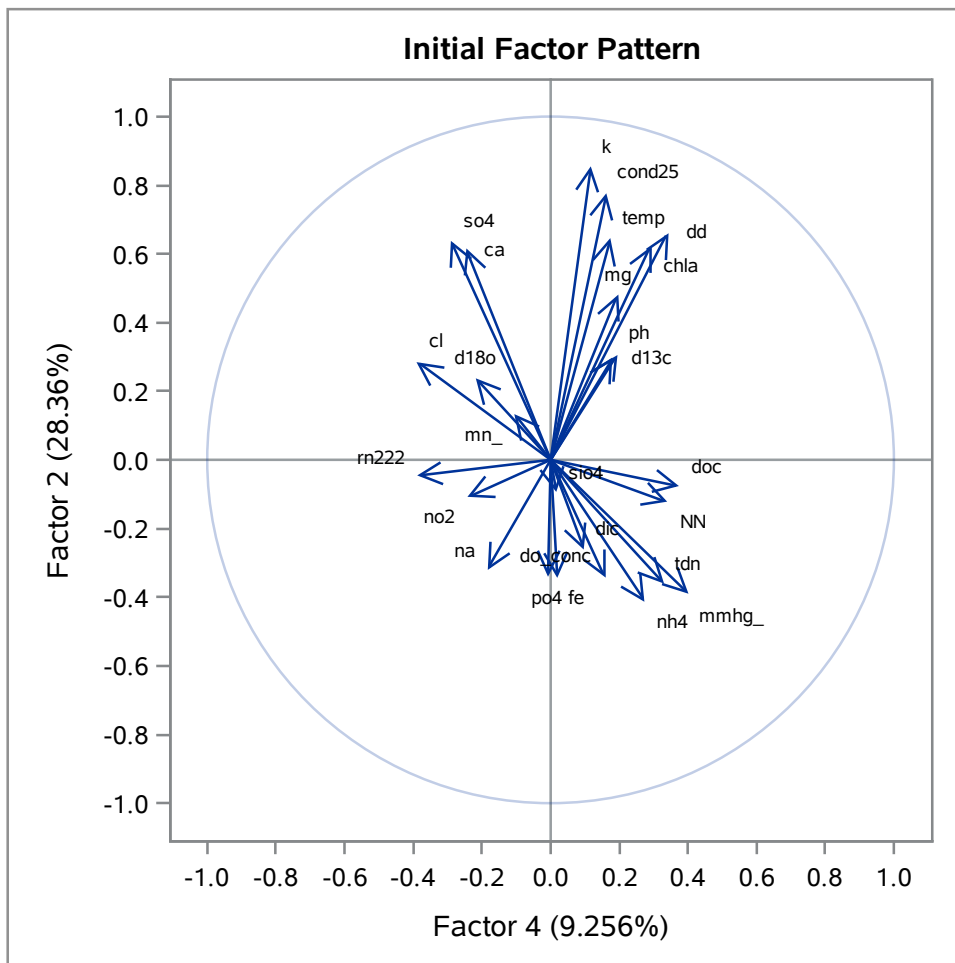
Average Ratio Sulfate to Chloride Concentrations by Season

The FACTOR Procedure
Initial Factor Method: Principal Components



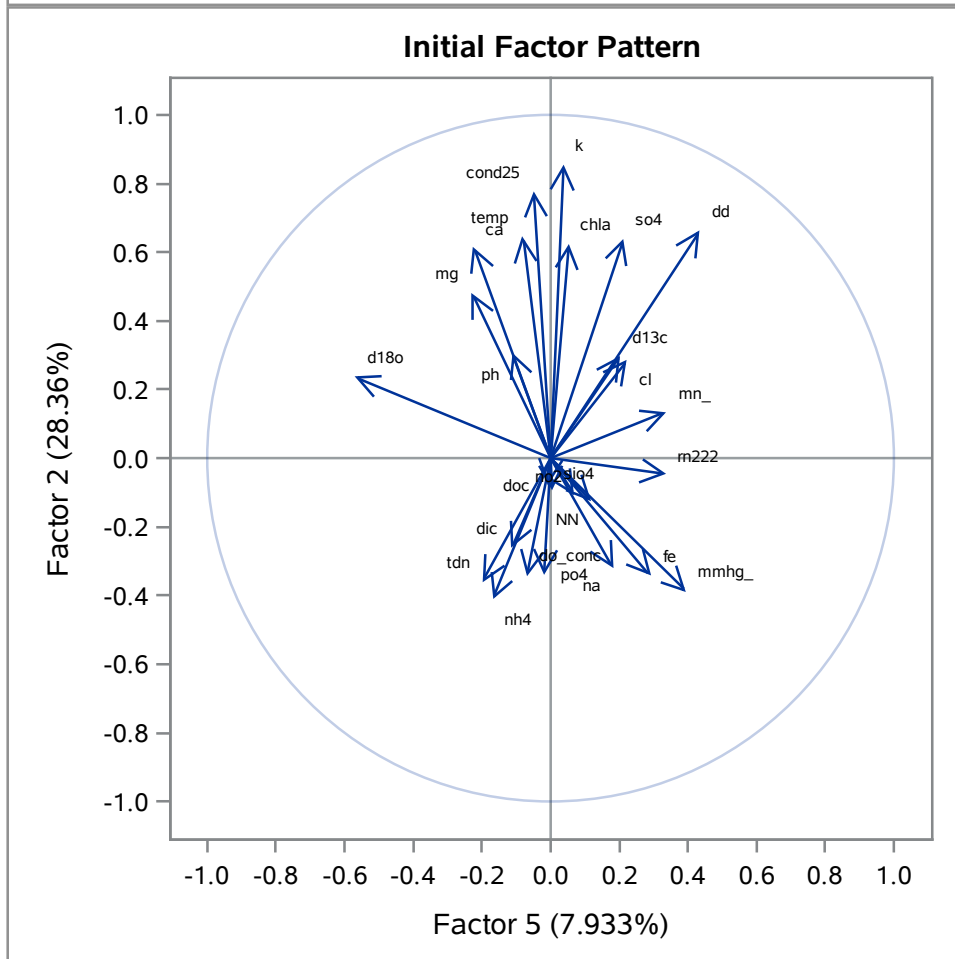
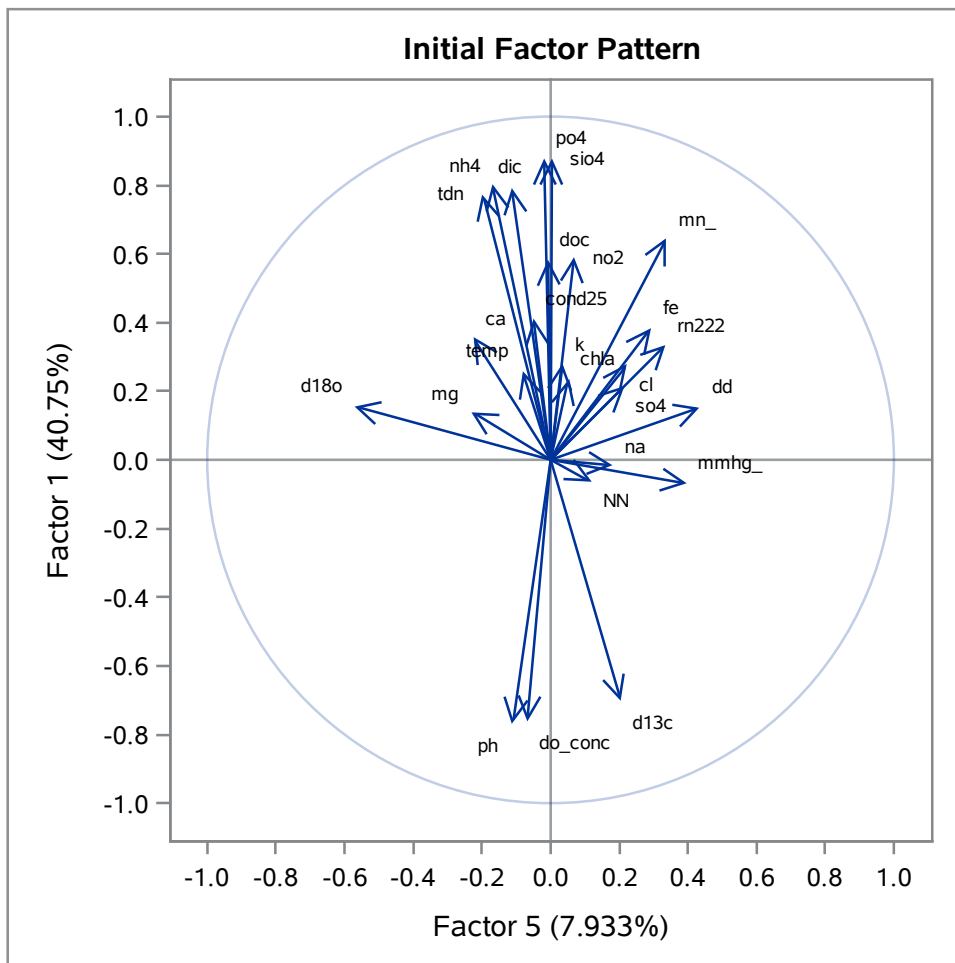
Average Ratio Sulfate to Chloride Concentrations by Season

The FACTOR Procedure
Initial Factor Method: Principal Components



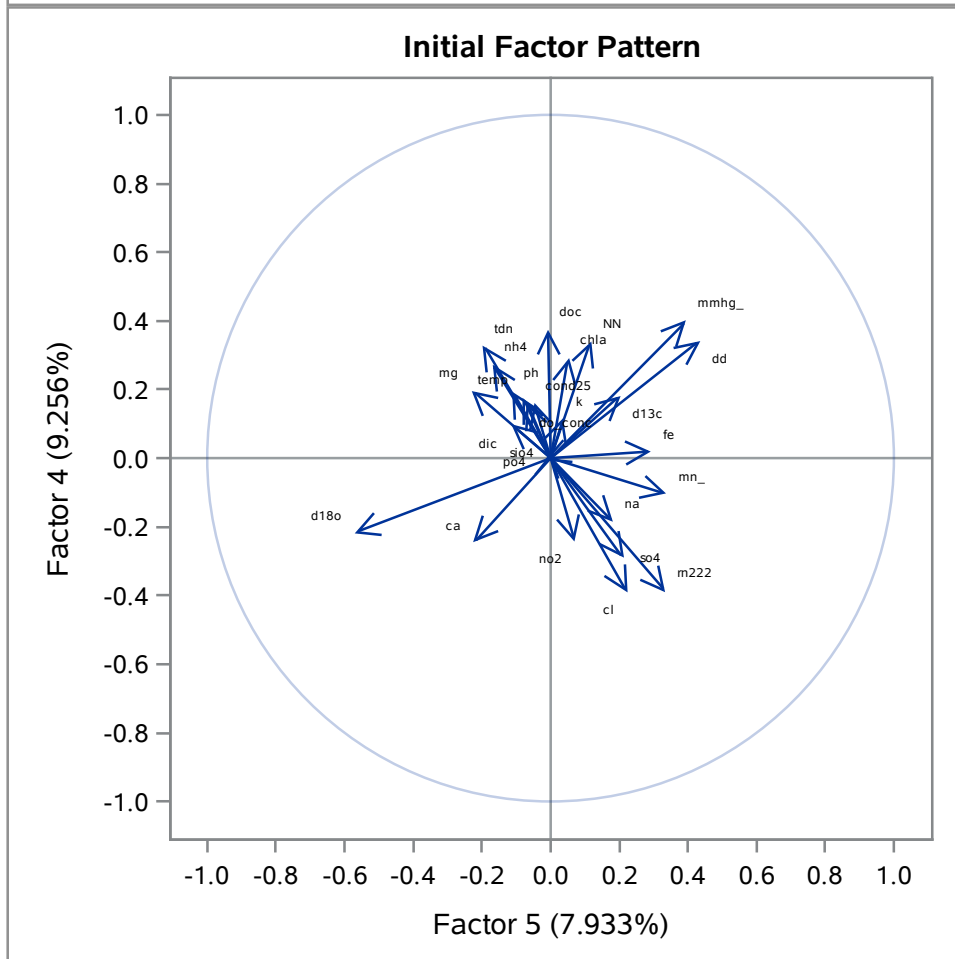
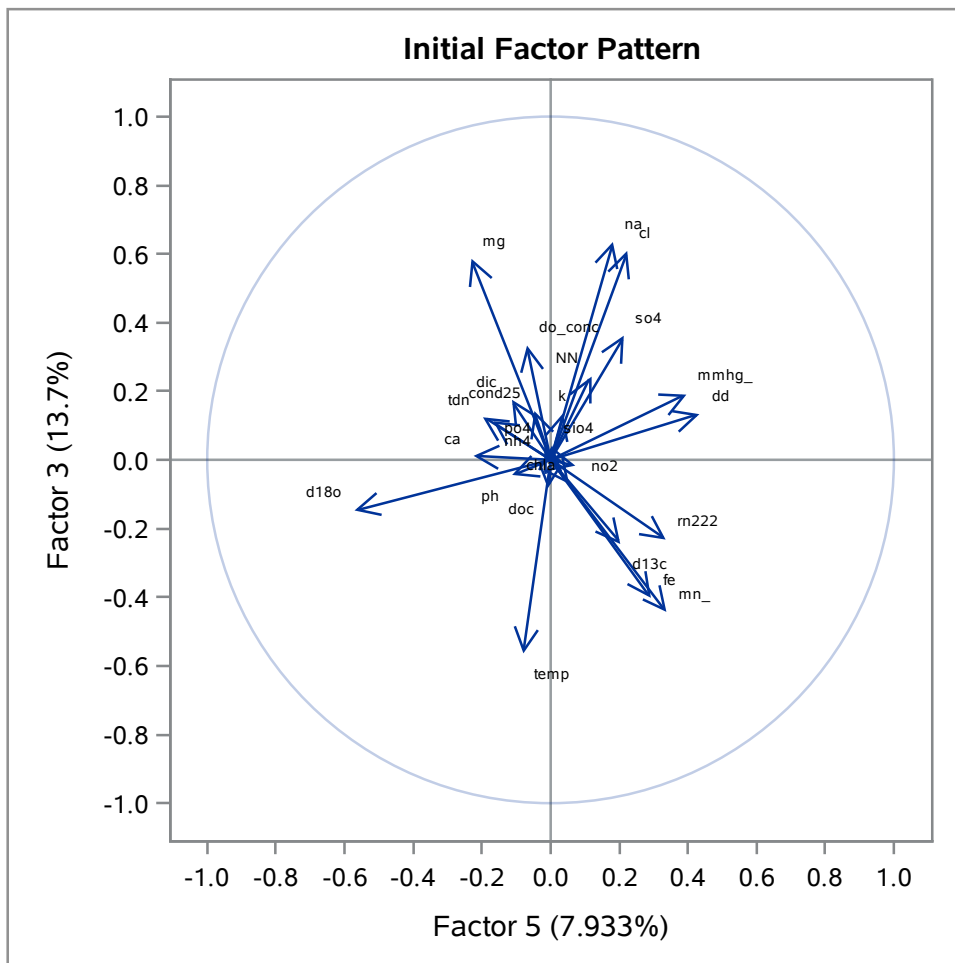
Average Ratio Sulfate to Chloride Concentrations by Season

The FACTOR Procedure
Initial Factor Method: Principal Components



Average Ratio Sulfate to Chloride Concentrations by Season

The FACTOR Procedure
Initial Factor Method: Principal Components



Average Ratio Sulfate to Chloride Concentrations by Season

The FACTOR Procedure Rotation Method: Varimax

Orthogonal Transformation Matrix					
	1	2	3	4	5
1	0.88267	0.30742	0.32199	0.06487	0.13601
2	-0.34700	0.87506	-0.03457	0.05048	0.33184
3	0.14955	0.08821	-0.54512	0.78060	-0.25173
4	0.18579	0.31200	-0.44391	-0.57045	-0.58794
5	-0.20881	0.18611	0.63318	0.24187	-0.67996

Rotated Factor Pattern						
		Factor1	Factor2	Factor3	Factor4	Factor5
temp	Temp	-0.03187	0.63274	0.23811	-0.51064	0.34230
cond25	Cond25	0.15267	0.86029	-0.07432	0.07250	0.21577
ph	pH	-0.73266	0.06757	-0.39002	-0.20679	-0.03003
chla	Chla	0.02320	0.71384	-0.00566	-0.16127	0.04822
doc	DOC	0.59937	0.21948	0.06600	-0.24746	-0.14142
tdn	TDN	0.92891	-0.00094	-0.07798	-0.10644	-0.10508
fe	Fe	0.34012	-0.15772	0.53042	-0.24653	-0.17146
mg	Mg	0.12779	0.53506	-0.52403	0.32210	0.07275
ca	Ca	0.10389	0.53131	0.05410	0.14928	0.54730
k	K	-0.01685	0.89010	-0.04114	0.10766	0.19519
na	Na	0.12005	-0.25259	-0.14402	0.62813	-0.28416
so4	SO4	-0.07732	0.60631	0.11537	0.54501	0.17704
cl	Cl	0.11750	0.30950	0.06241	0.78333	0.05709
d13c	d13C	-0.77002	0.11859	-0.05419	-0.27684	-0.17980
dic	DIC	0.85747	0.03936	0.05282	0.09203	-0.00330
d18o	d18O	0.11295	0.06852	-0.14226	-0.10620	0.65411
dd	dD	-0.10131	0.82573	0.07721	0.05818	-0.29011
do_conc		-0.45917	-0.46697	-0.52806	0.08402	-0.34736
mn_		0.36667	0.30708	0.70502	-0.15675	0.07586
NN		0.06191	0.02186	-0.22623	0.01422	-0.39187
sio4		0.81501	0.19554	0.25723	0.07557	0.06478
mmhg_		0.09453	-0.14672	-0.04048	-0.00749	-0.69063
rn222		0.13519	-0.01756	0.62050	0.14170	0.08863
nh4		0.95362	-0.05004	-0.01739	-0.07777	-0.10230
no2		0.49787	0.02374	0.35516	0.17528	0.14379
po4		0.89853	-0.02921	0.26418	0.06987	0.01390

Average Ratio Sulfate to Chloride Concentrations by Season

The FACTOR Procedure Rotation Method: Varimax

Variance Explained by Each Factor				
Factor1	Factor2	Factor3	Factor4	Factor5
6.3174431	4.6946680	2.3313892	2.1100455	2.0303509

Final Community Estimates: Total = 17.483897								
temp	cond25	ph	chla	doc	tdn	fe	mg	ca
0.83599092	0.82074149	0.73712855	0.53847376	0.49300580	0.89132534	0.51208265	0.68627274	0.61782787
k	na	so4	cl	d13c	dic	d18o	dd	do_conc
0.84394284	0.57424799	0.71527430	0.73035983	0.71889276	0.74807863	0.47682689	0.78560520	0.83546505

mn_	NN	sio4	mmhg_	rn222	nh4	no2	po4
0.75612401	0.20925561	0.77855629	0.50913057	0.43153612	0.92870142	0.42597585	0.88307420

Average Ratio Sulfate to Chloride Concentrations by Season

The FACTOR Procedure Rotation Method: Varimax

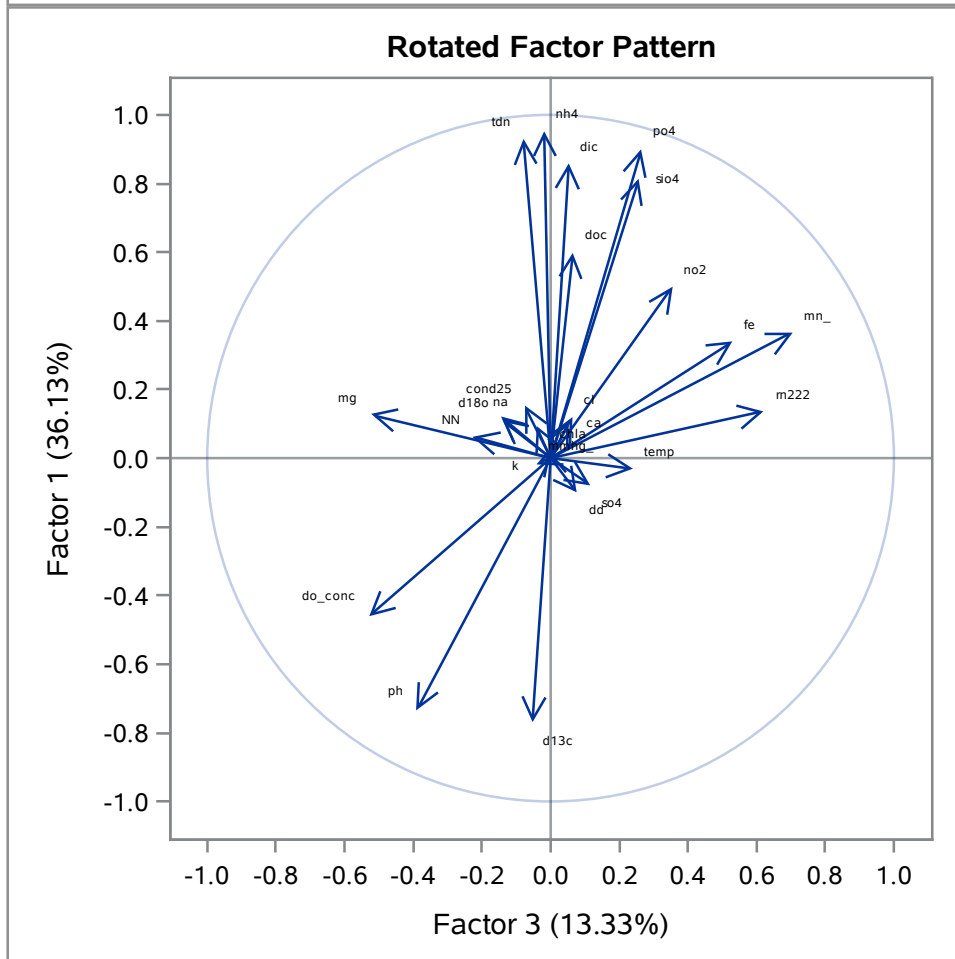
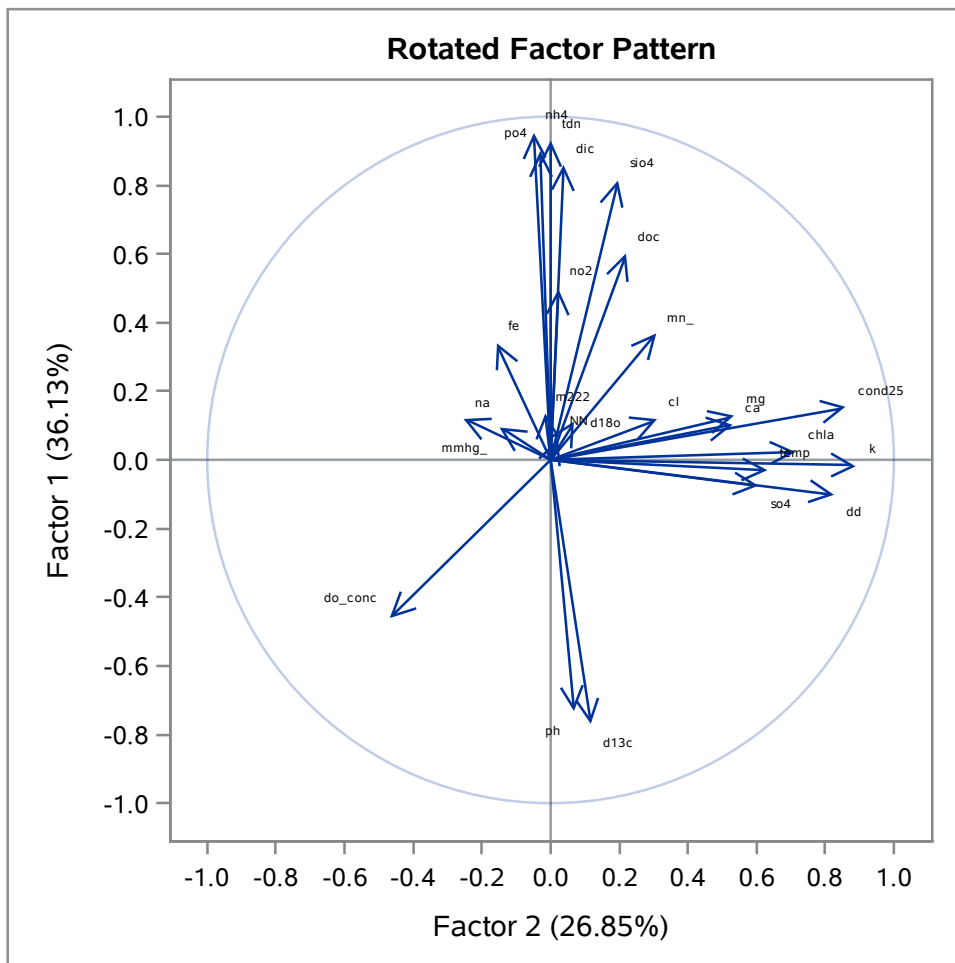
Scoring Coefficients Estimated by Regression

Squared Multiple Correlations of the Variables with Each Factor				
Factor1	Factor2	Factor3	Factor4	Factor5
1.0000000	1.0000000	1.0000000	1.0000000	1.0000000

Standardized Scoring Coefficients						
		Factor1	Factor2	Factor3	Factor4	Factor5
temp	Temp	-0.01610	0.12704	0.05009	-0.25085	0.08309
cond25	Cond25	0.03091	0.18481	-0.08535	-0.00756	0.00982
ph	pH	-0.08058	0.04169	-0.13049	-0.10614	-0.00543
chla	Chla	0.00677	0.18140	-0.03458	-0.10800	-0.07885
doc	DOC	0.11629	0.07976	-0.05955	-0.15625	-0.11833
tdn	TDN	0.19644	0.01128	-0.17157	-0.10660	-0.04519
fe	Fe	0.00474	-0.01581	0.23909	-0.08687	-0.12410
mg	Mg	0.07732	0.11970	-0.28939	0.08727	0.01494
ca	Ca	0.00737	0.04701	-0.02591	0.06083	0.24624
k	K	-0.00912	0.19545	-0.03906	0.01993	-0.01163
na	Na	0.01166	-0.04483	-0.00977	0.30036	-0.11095
so4	SO4	-0.06128	0.10786	0.10073	0.26568	0.01030
cl	Cl	-0.02605	0.03971	0.08101	0.37985	-0.00726
d13c	d13C	-0.13324	0.07577	0.06534	-0.11199	-0.13346
dic	DIC	0.15565	-0.00196	-0.08106	0.00752	-0.00051
d18o	d18O	0.05459	-0.07554	-0.16198	-0.06670	0.39380
dd	dD	-0.04515	0.25263	0.07664	0.00715	-0.30436
do_conc		-0.02094	-0.05945	-0.18257	0.02915	-0.09645
mn_		-0.01994	0.06040	0.31188	-0.04180	-0.05963
NN		0.03743	0.06594	-0.09738	-0.02192	-0.21681
sio4		0.11926	0.02625	0.02763	0.01513	-0.00184
mmhg_		0.01707	0.06550	0.02668	-0.01440	-0.38651
rn222		-0.06475	-0.03233	0.32784	0.12272	0.00436
nh4		0.19203	-0.00380	-0.13865	-0.08608	-0.04088
no2		0.04152	-0.03138	0.12964	0.09655	0.05954
po4		0.13649	-0.02439	0.02678	0.01662	0.00170

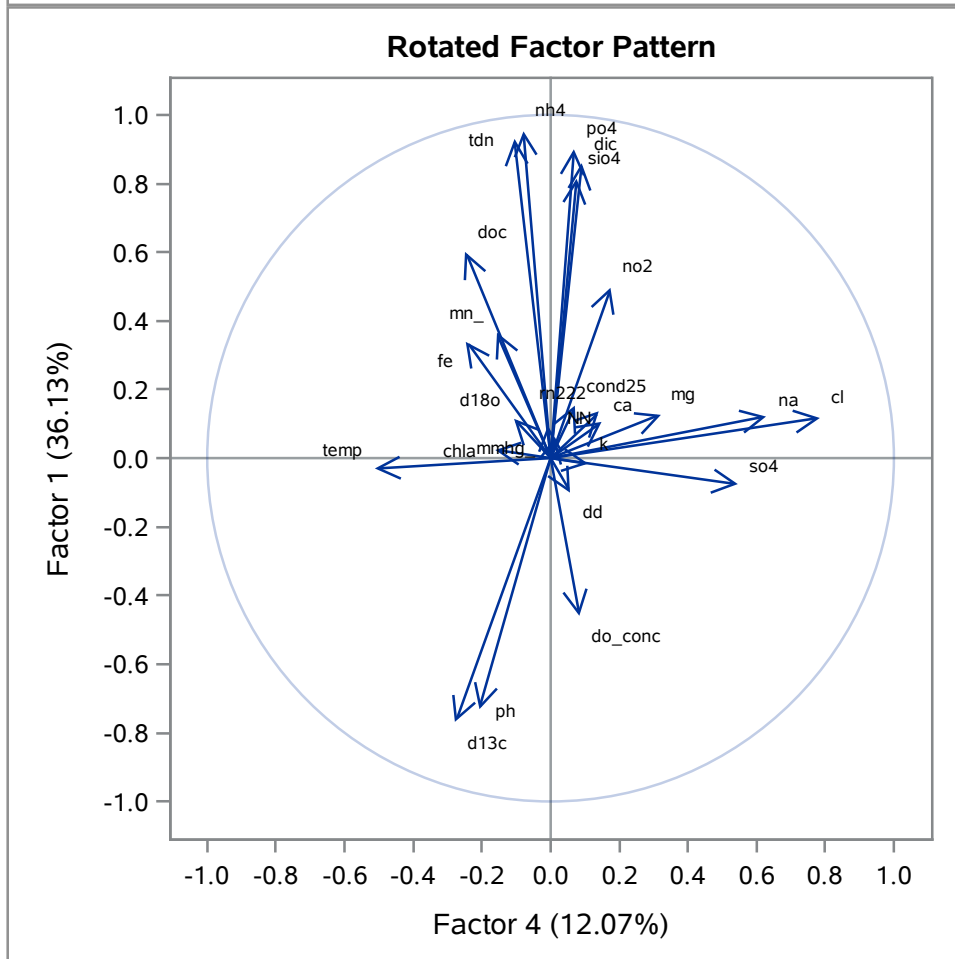
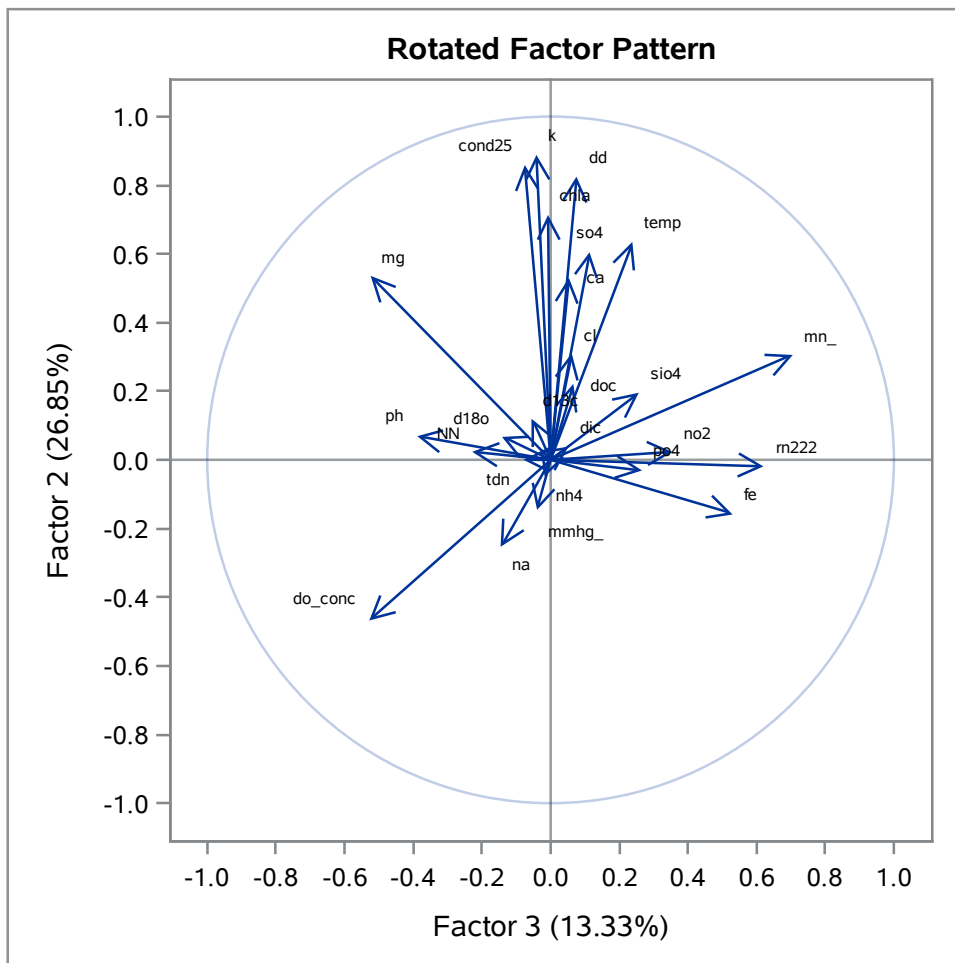
Average Ratio Sulfate to Chloride Concentrations by Season

The FACTOR Procedure
Rotation Method: Varimax



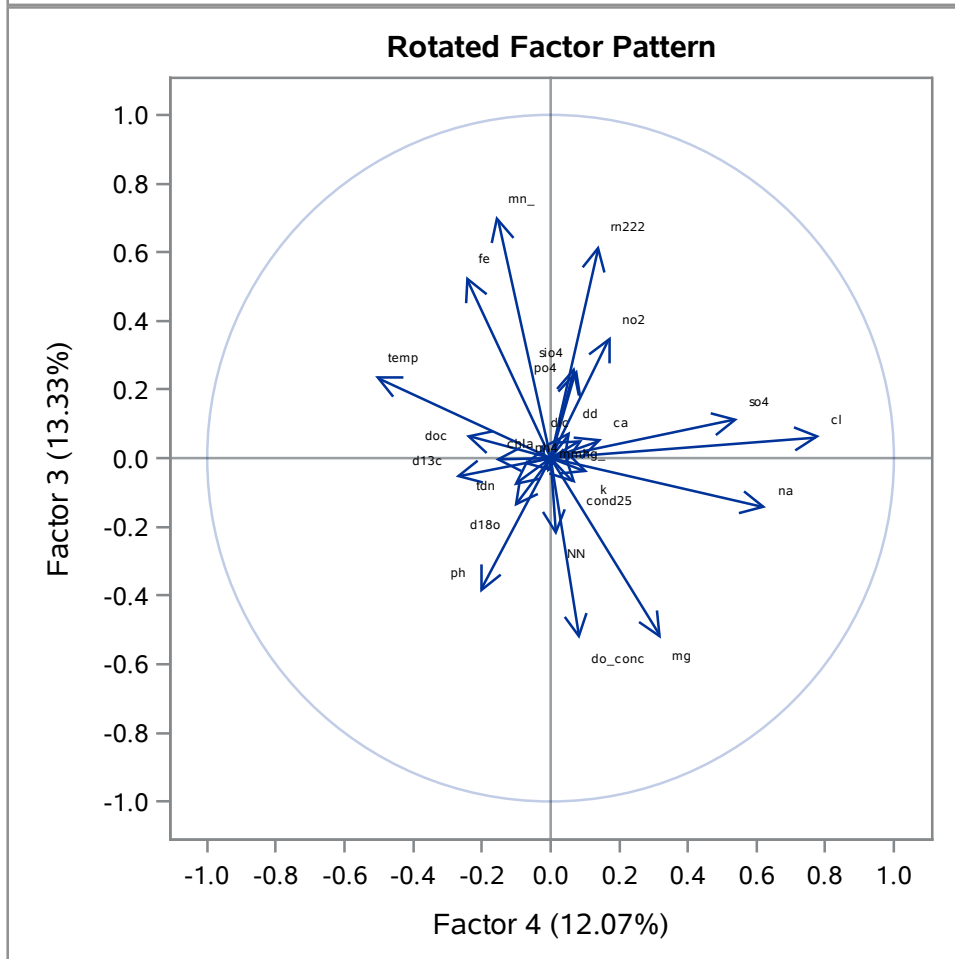
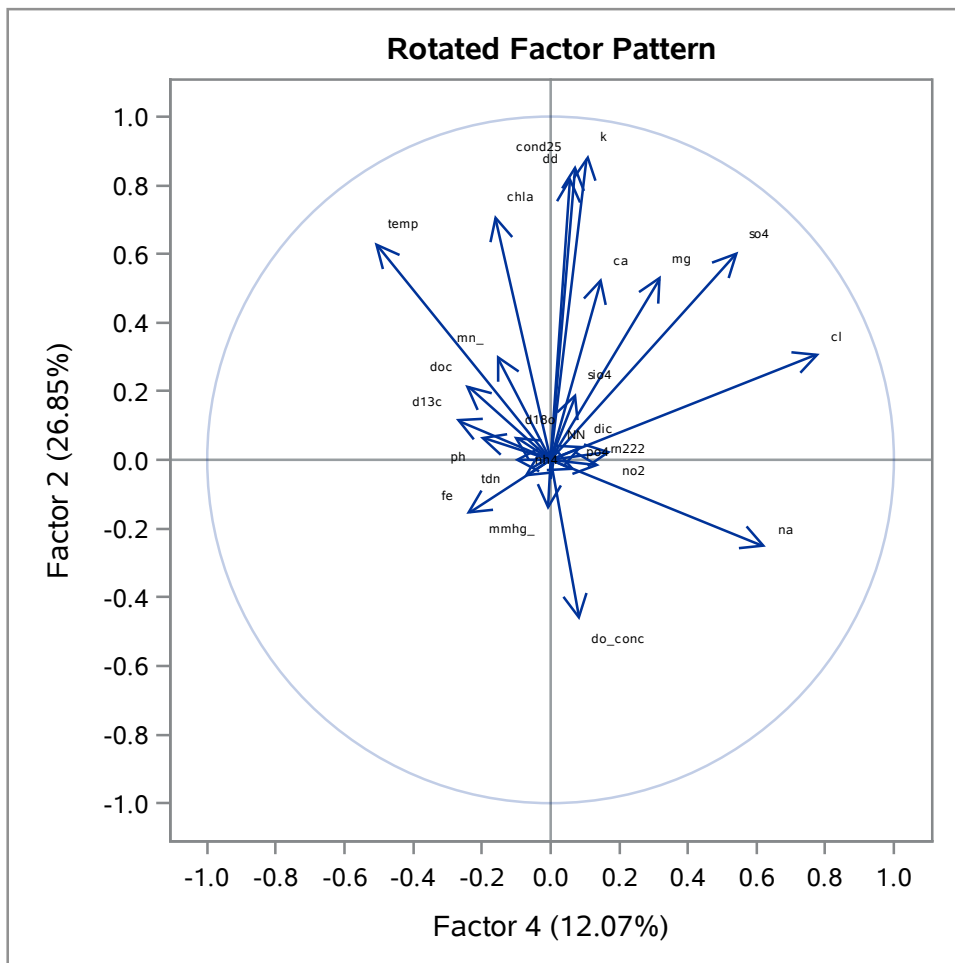
Average Ratio Sulfate to Chloride Concentrations by Season

The FACTOR Procedure
Rotation Method: Varimax



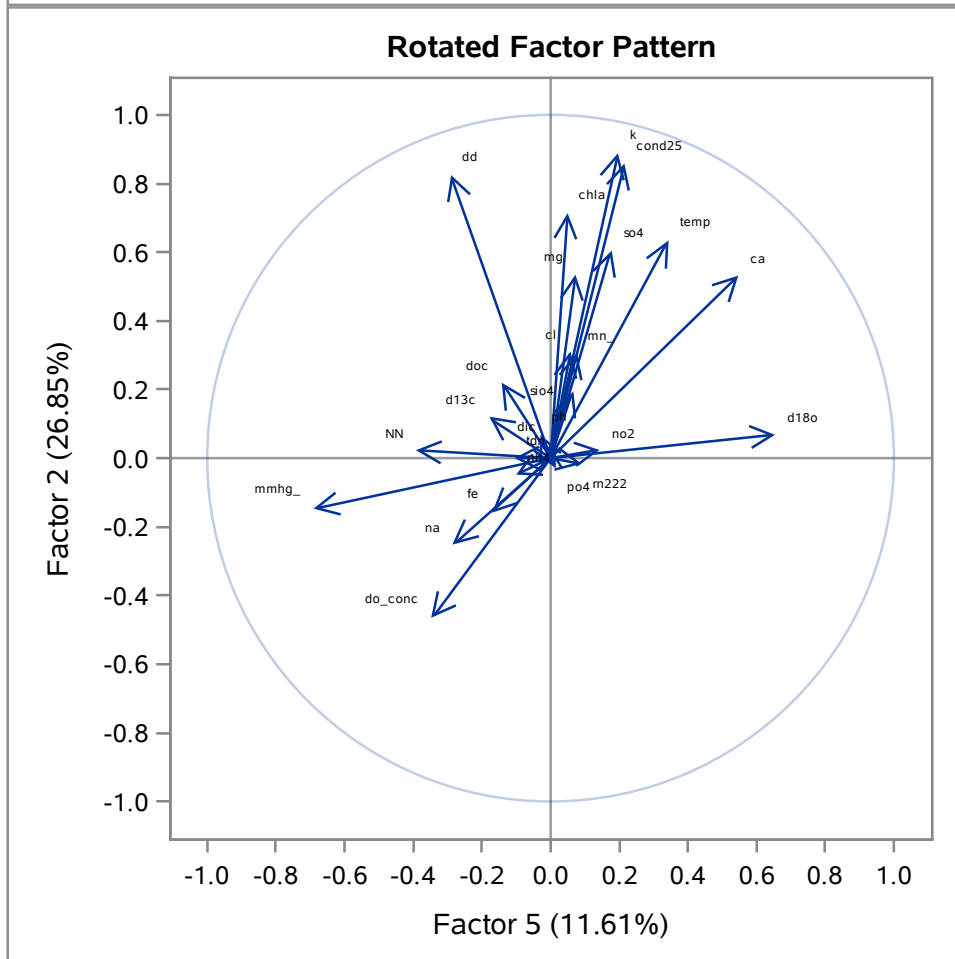
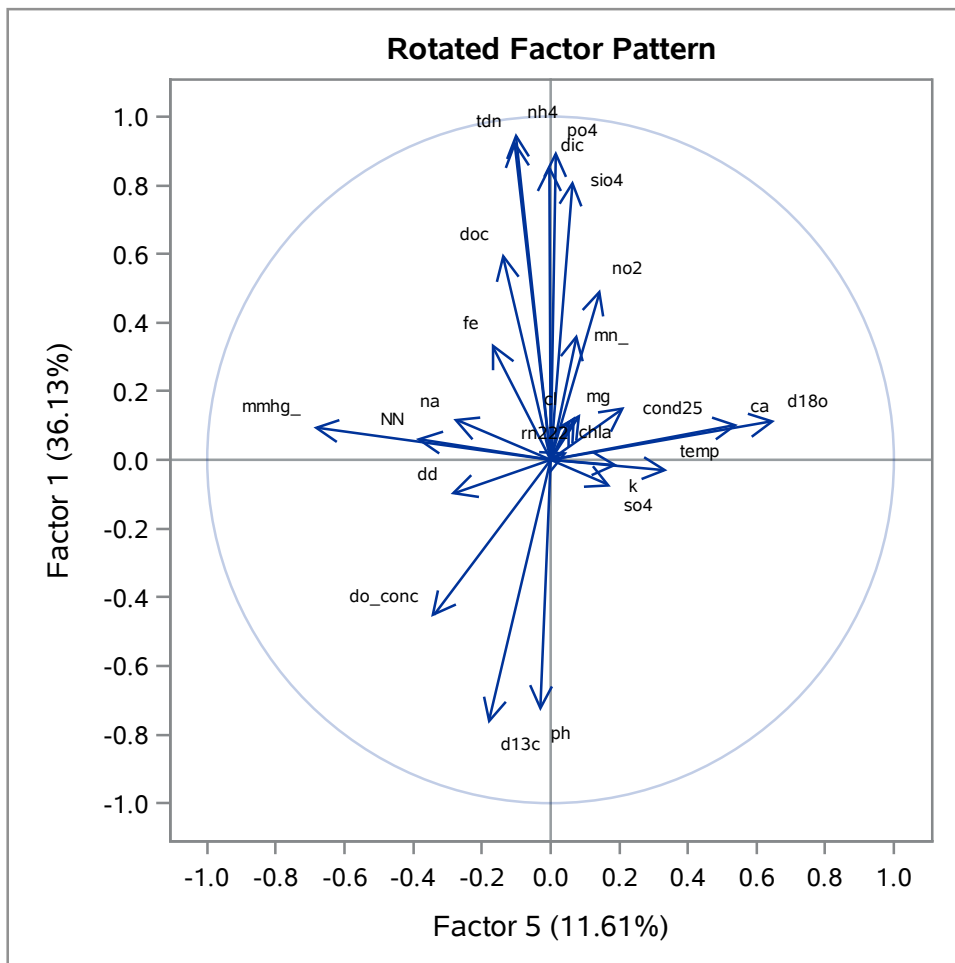
Average Ratio Sulfate to Chloride Concentrations by Season

The FACTOR Procedure
Rotation Method: Varimax



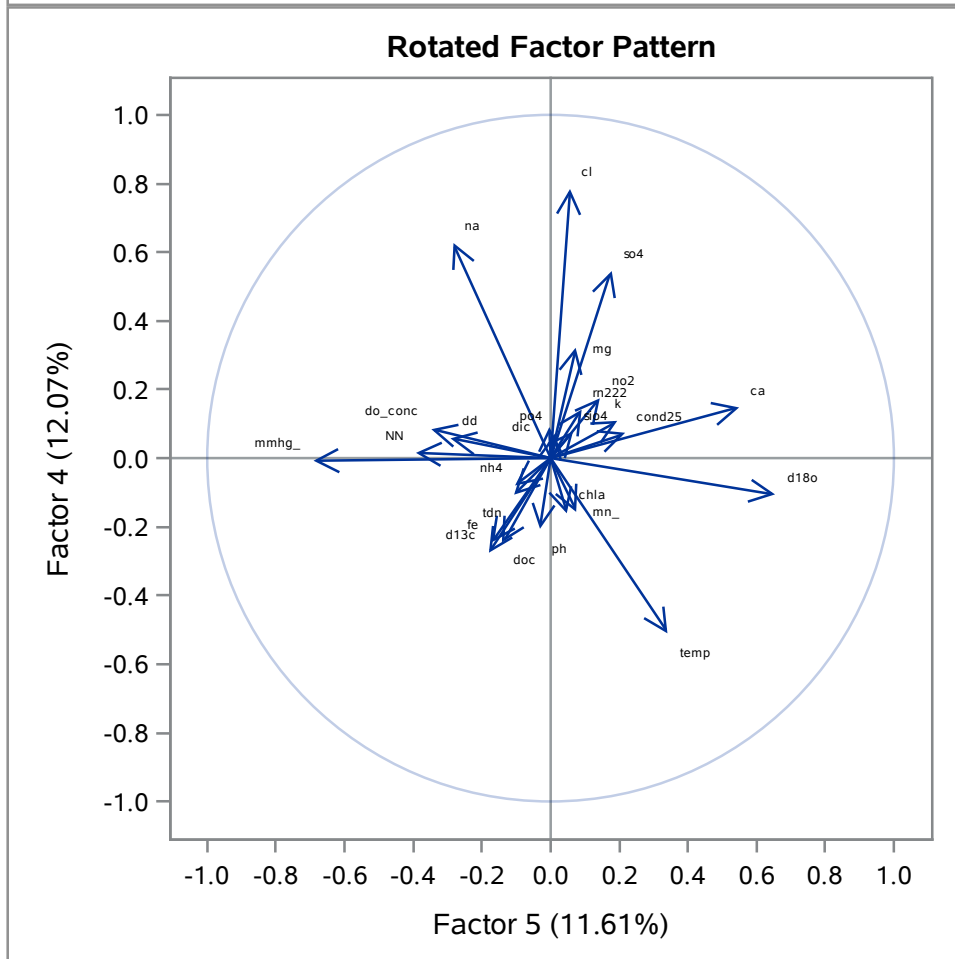
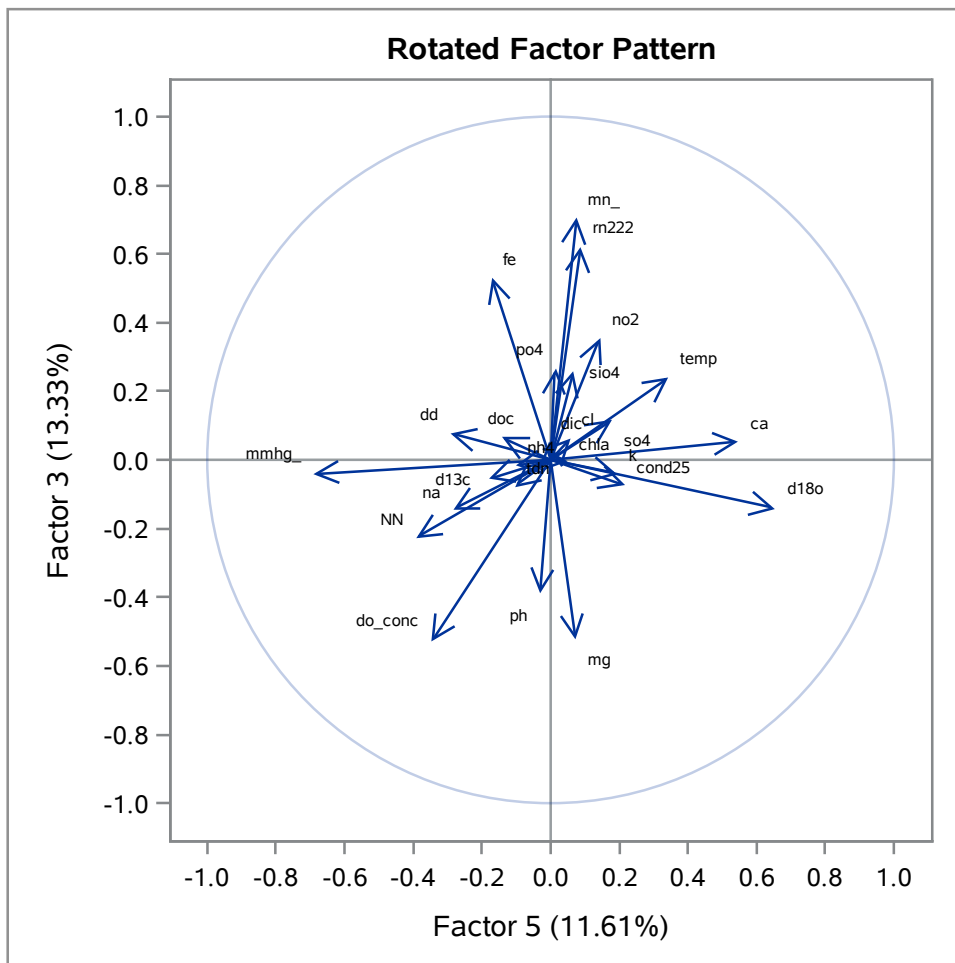
Average Ratio Sulfate to Chloride Concentrations by Season

The FACTOR Procedure
Rotation Method: Varimax



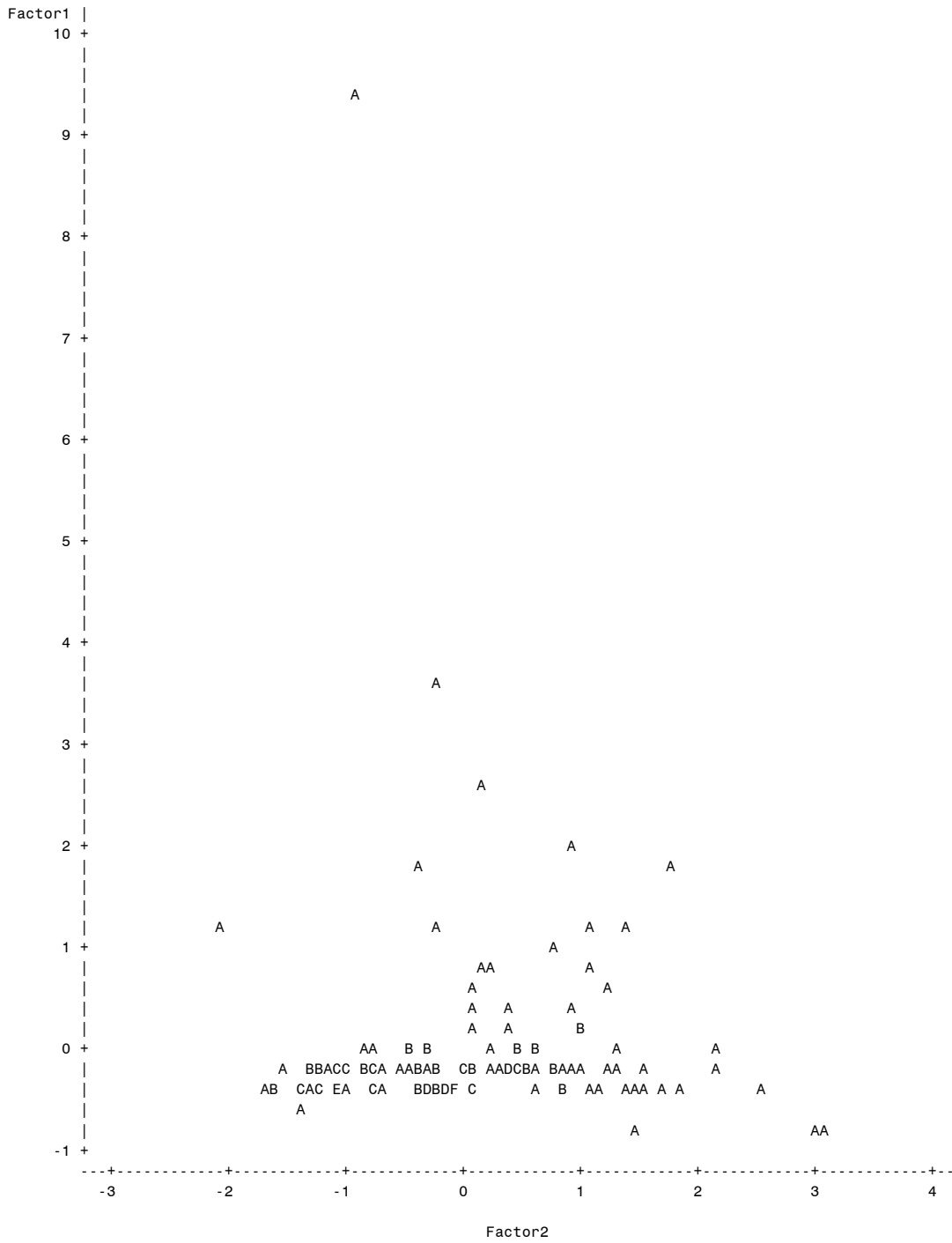
Average Ratio Sulfate to Chloride Concentrations by Season

The FACTOR Procedure
Rotation Method: Varimax



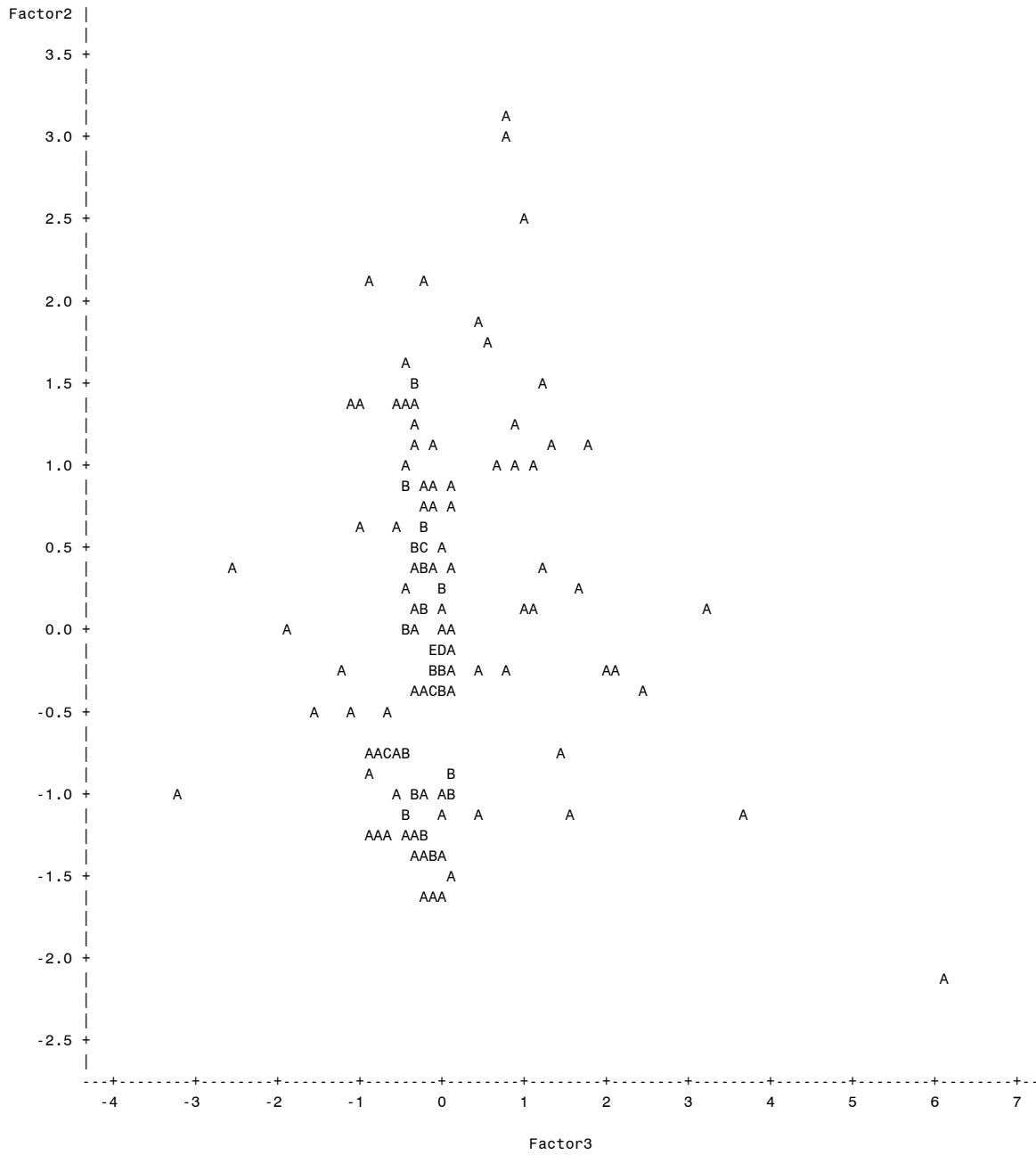
Average Ratio Sulfate to Chloride Concentrations by Season

Plot of Factor1*Factor2. Legend: A = 1 obs, B = 2 obs, etc.



Average Ratio Sulfate to Chloride Concentrations by Season

Plot of Factor2*Factor3. Legend: A = 1 obs, B = 2 obs, etc.



Average Ratio Sulfate to Chloride Concentrations by Season

The CORR Procedure

26 With Variables:	temp mn_	cond25 NN	ph sio4	chla mmhg_	doc rn222	tdn nh4	fe no2	mg po4	ca	k	na	so4	cl	d13c	dic	d18o	dd	do_conc
3 Variables:	Factor1 Factor2 Factor3																	

Simple Statistics							
Variable	N	Mean	Std Dev	Sum	Minimum	Maximum	Label
temp	143	23.66127	7.68896	3384	9.60000	31.60000	Temp
cond25	143	58960	4729	8431287	38454	71453	Cond25
ph	143	8.23444	0.30419	1178	7.04000	8.72000	pH
chla	143	6.00517	2.60402	858.73987	0.26000	18.03000	Chla
doc	143	566.69440	630.63939	81037	239.56302	6022	DOC
tdn	143	78.21597	197.67026	11185	18.80521	2236	TDN
fe	143	0.34037	0.36552	48.67356	0.02600	2.80900	Fe
mg	143	1447	138.82390	206973	545.66667	1896	Mg
ca	143	445.99136	69.68426	63777	312.46875	680.15625	Ca
k	143	612.42972	42.96099	87577	511.92188	740.25938	K
na	143	10380	3741	1484277	4712	26085	Na
so4	143	30.80500	3.93197	4405	0.26736	38.06600	SO4
cl	143	562.87592	83.44254	80491	1.06264	759.37289	Cl
d13c	143	-3.82487	2.59031	-546.95617	-22.07191	-0.98671	d13C
dic	143	2445	1095	349674	1585	12507	DIC
d18o	143	1.23843	0.63390	177.09594	-2.40328	2.12764	d18O
dd	143	9.44008	3.10394	1350	4.56419	25.33762	dD
do_conc	143	5.55437	2.69086	794.27437	0.13000	10.91000	
mn_	143	0.14092	0.14077	20.15184	0.03000	0.92000	
NN	143	0.32762	1.14197	46.84945	0	11.26100	
sio4	143	54.19299	79.05641	7750	2.41850	576.02500	
mmhg_	143	763.90915	3.08227	109239	751.40000	770.70000	
rn222	143	107.87211	356.15525	15426	0	3272	
nh4	143	33.41609	153.35289	4779	0.19450	1660	
no2	143	0.11647	0.09939	16.65541	0.04650	0.72000	
po4	143	1.23468	3.48814	176.55926	0.00300	30.34250	
Factor1	143	0	1.00000	0	-0.83215	9.46522	
Factor2	143	0	1.00000	0	-2.08222	3.10122	
Factor3	143	0	1.00000	0	-3.19421	6.09734	

Average Ratio Sulfate to Chloride Concentrations by Season

The CORR Procedure

Pearson Correlation Coefficients, N = 143 Prob > r under H0: Rho=0			
	Factor1	Factor2	Factor3
temp Temp	-0.03187 0.7055	0.63274 <.0001	0.23811 0.0042
cond25 Cond25	0.15267 0.0687	0.86029 <.0001	-0.07432 0.3777
ph pH	-0.73266 <.0001	0.06757 0.4227	-0.39002 <.0001
chla Chla	0.02320 0.7833	0.71384 <.0001	-0.00566 0.9465
doc DOC	0.59937 <.0001	0.21948 0.0084	0.06600 0.4335
tdn TDN	0.92891 <.0001	-0.00094 0.9911	-0.07798 0.3546
fe Fe	0.34012 <.0001	-0.15772 0.0599	0.53042 <.0001
mg Mg	0.12779 0.1283	0.53506 <.0001	-0.52403 <.0001
ca Ca	0.10389 0.2169	0.53131 <.0001	0.05410 0.5211
k K	-0.01685 0.8417	0.89010 <.0001	-0.04114 0.6256
na Na	0.12005 0.1533	-0.25259 0.0023	-0.14402 0.0862
so4 SO4	-0.07732 0.3587	0.60631 <.0001	0.11537 0.1700
cl Cl	0.11750 0.1622	0.30950 0.0002	0.06241 0.4590
d13c d13C	-0.77002 <.0001	0.11859 0.1584	-0.05419 0.5203
dic DIC	0.85747 <.0001	0.03936 0.6407	0.05282 0.5310
d18o d18O	0.11295 0.1792	0.06852 0.4162	-0.14226 0.0901
dd dD	-0.10131 0.2286	0.82573 <.0001	0.07721 0.3594
do_conc	-0.45917 <.0001	-0.46697 <.0001	-0.52806 <.0001
mn_	0.36667 <.0001	0.30708 0.0002	0.70502 <.0001
NN	0.06191 0.4626	0.02186 0.7955	-0.22623 0.0066
sio4	0.81501 <.0001	0.19554 0.0193	0.25723 0.0019
mmhg_	0.09453 0.2614	-0.14672 0.0804	-0.04048 0.6312
rn222	0.13519 0.1074	-0.01756 0.8351	0.62050 <.0001
nh4	0.95362 <.0001	-0.05004 0.5528	-0.01739 0.8367

Average Ratio Sulfate to Chloride Concentrations by Season**The CORR Procedure**

Pearson Correlation Coefficients, N = 143 Prob > r under H0: Rho=0			
	Factor1	Factor2	Factor3
no2	0.49787 <.0001	0.02374 0.7784	0.35516 <.0001
po4	0.89853 <.0001	-0.02921 0.7291	0.26418 0.0014

Average Ratio Sulfate to Chloride Concentrations by Season

The GLM Procedure

Class Level Information		
Class	Levels	Values
Event	3	JAN2014 JUL2014 NOV2014

Data for Analysis of ra224	
Number of Observations Read	236
Number of Observations Used	25

Data for Analysis of ra226	
Number of Observations Read	236
Number of Observations Used	35

Note: Variables in each group are consistent with respect to the presence or absence of missing values.

Average Ratio Sulfate to Chloride Concentrations by Season

The GLM Procedure

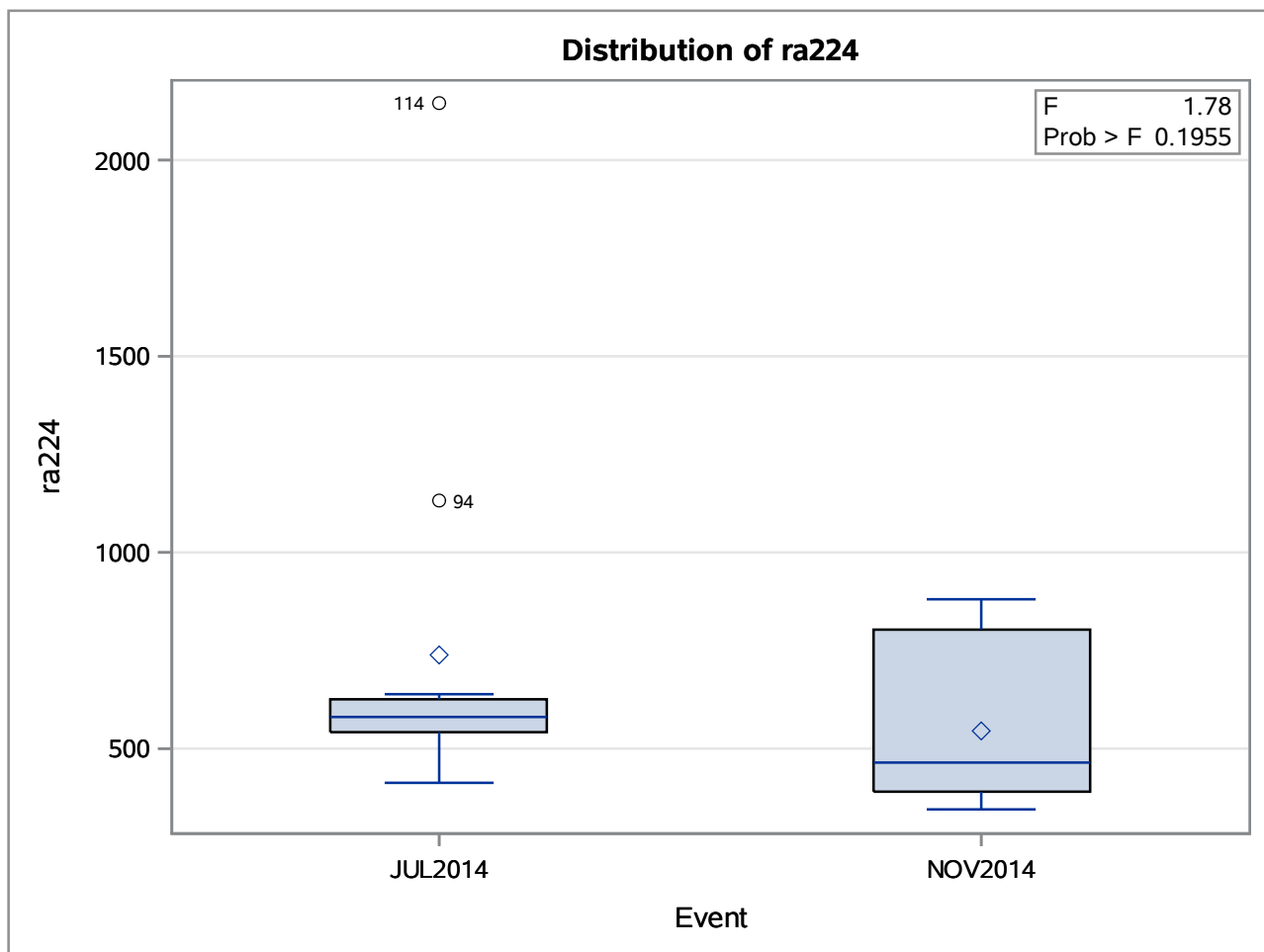
Dependent Variable: ra224

Source	DF	Sum of Squares	Mean Square	F Value	Pr > F
Model	1	233510.446	233510.446	1.78	0.1955
Error	23	3021956.089	131389.395		
Corrected Total	24	3255466.535			

R-Square	Coeff Var	Root MSE	ra224 Mean
0.071729	56.79217	362.4768	638.2512

Source	DF	Type I SS	Mean Square	F Value	Pr > F
Event	1	233510.4463	233510.4463	1.78	0.1955

Source	DF	Type III SS	Mean Square	F Value	Pr > F
Event	1	233510.4463	233510.4463	1.78	0.1955



Average Ratio Sulfate to Chloride Concentrations by Season

The GLM Procedure

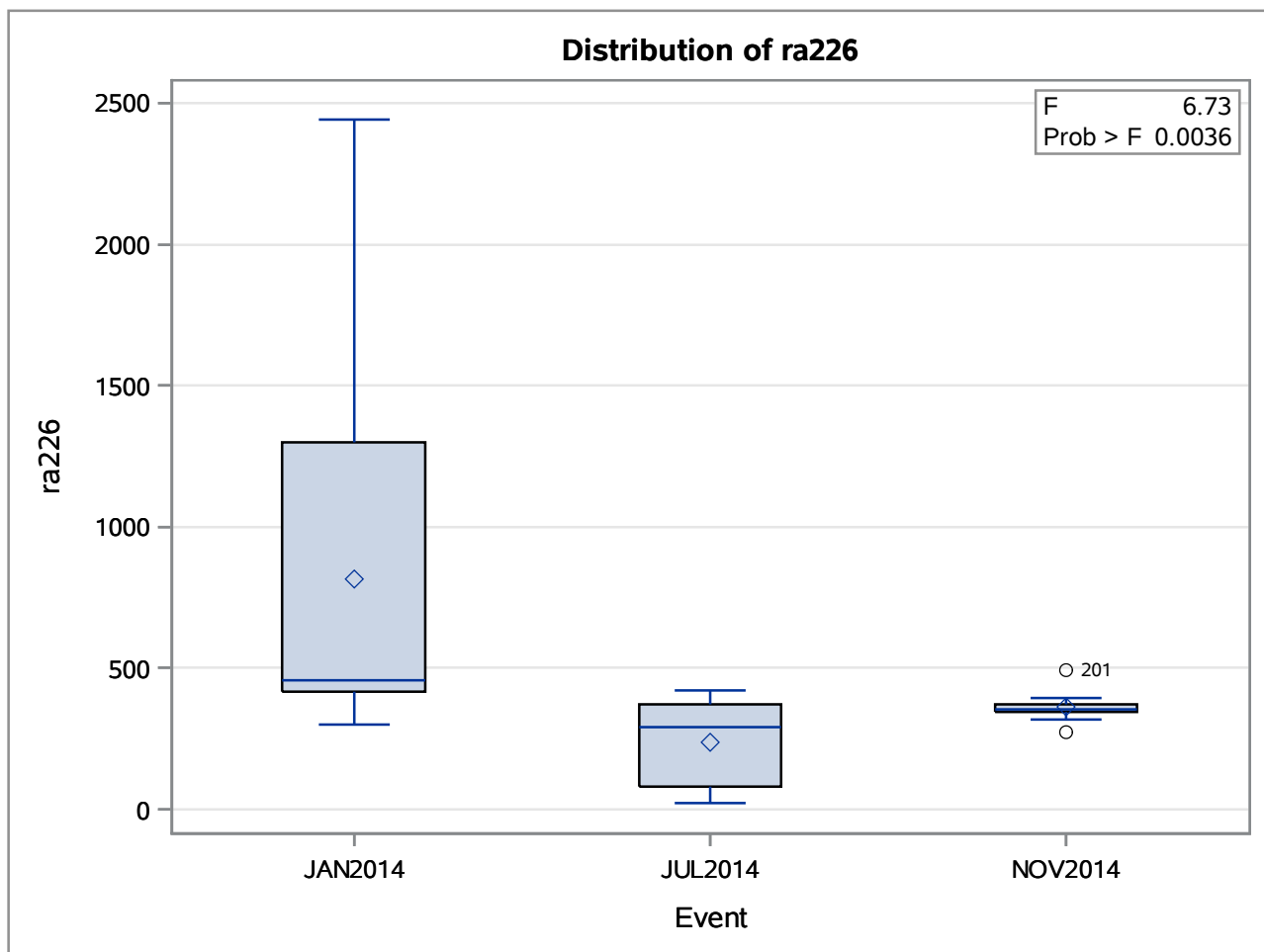
Dependent Variable: ra226

Source	DF	Sum of Squares	Mean Square	F Value	Pr > F
Model	2	1985868.181	992934.091	6.73	0.0036
Error	32	4719295.322	147477.979		
Corrected Total	34	6705163.504			

R-Square	Coeff Var	Root MSE	ra226 Mean
0.296170	85.40737	384.0286	449.6434

Source	DF	Type I SS	Mean Square	F Value	Pr > F
Event	2	1985868.181	992934.091	6.73	0.0036

Source	DF	Type III SS	Mean Square	F Value	Pr > F
Event	2	1985868.181	992934.091	6.73	0.0036



Average Ratio Sulfate to Chloride Concentrations by Season

The GLM Procedure

Class Level Information		
Class	Levels	Values
Transect	5	1 2 3 4 5

Data for Analysis of ra224	
Number of Observations Read	236
Number of Observations Used	25

Data for Analysis of ra226	
Number of Observations Read	236
Number of Observations Used	35

Note: Variables in each group are consistent with respect to the presence or absence of missing values.

Average Ratio Sulfate to Chloride Concentrations by Season

The GLM Procedure

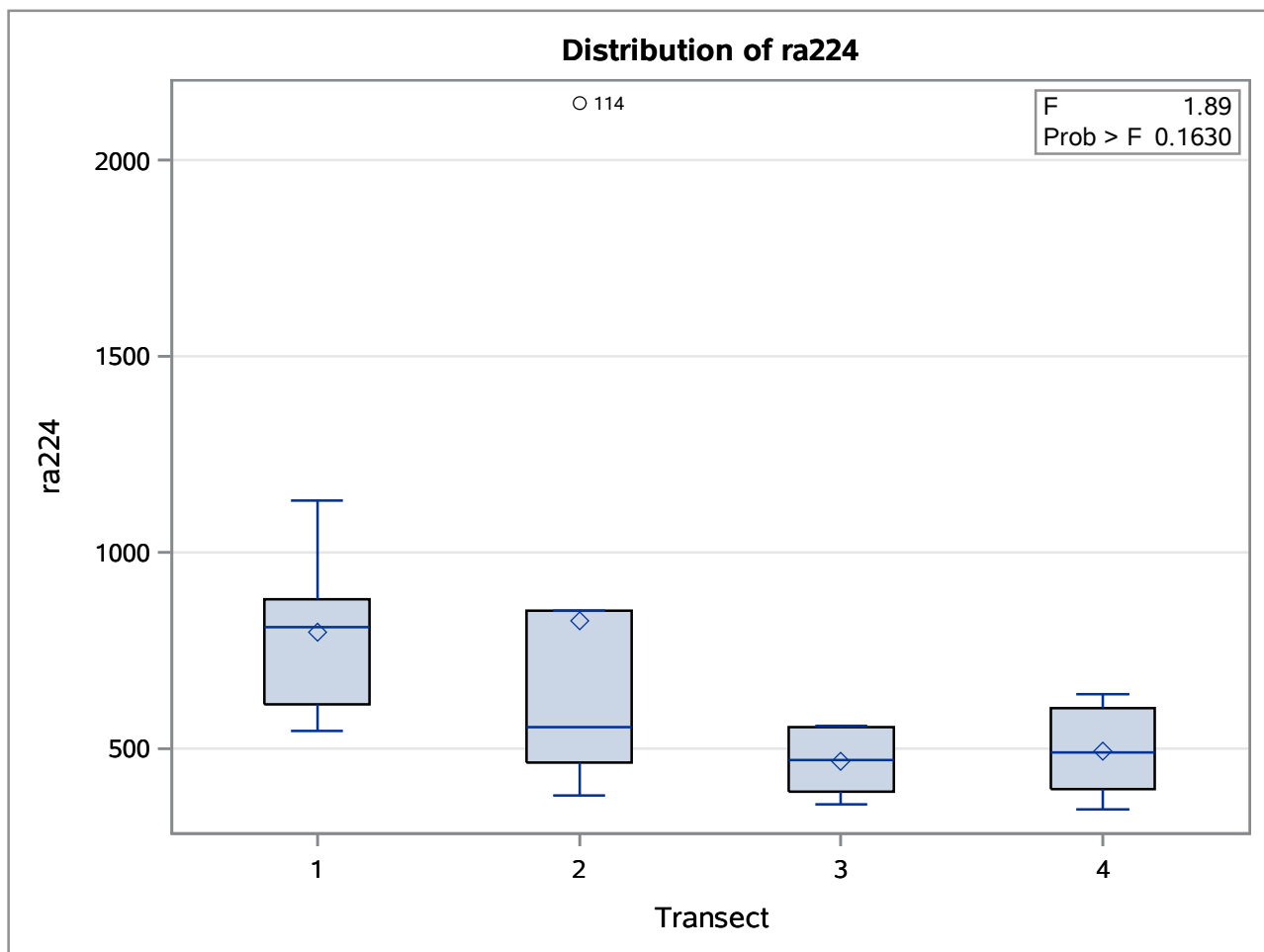
Dependent Variable: ra224

Source	DF	Sum of Squares	Mean Square	F Value	Pr > F
Model	3	690753.068	230251.023	1.89	0.1630
Error	21	2564713.467	122129.213		
Corrected Total	24	3255466.535			

R-Square	Coeff Var	Root MSE	ra224 Mean
0.212183	54.75428	349.4699	638.2512

Source	DF	Type I SS	Mean Square	F Value	Pr > F
Transect	3	690753.0683	230251.0228	1.89	0.1630

Source	DF	Type III SS	Mean Square	F Value	Pr > F
Transect	3	690753.0683	230251.0228	1.89	0.1630



Average Ratio Sulfate to Chloride Concentrations by Season

The GLM Procedure

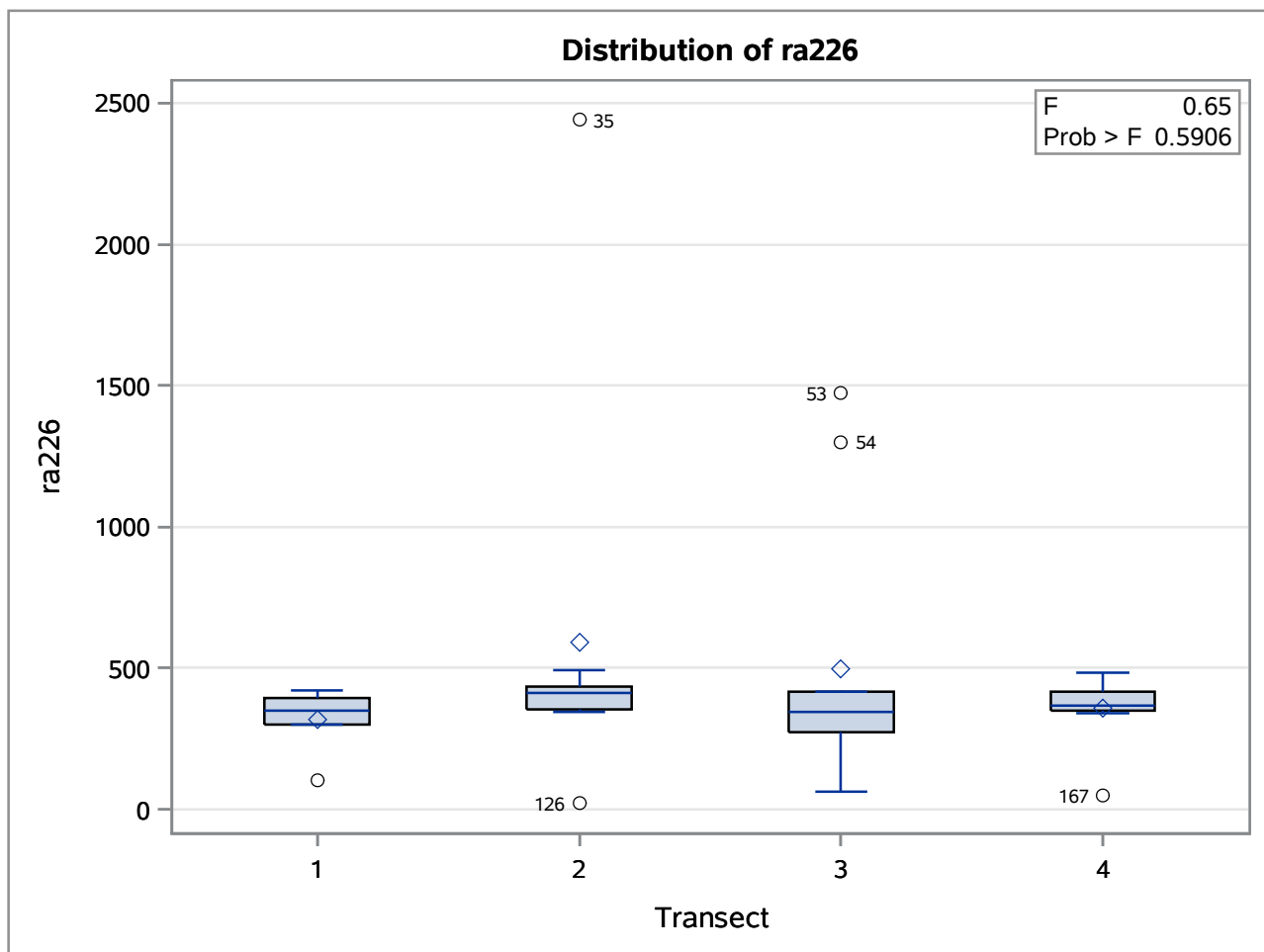
Dependent Variable: ra226

Source	DF	Sum of Squares	Mean Square	F Value	Pr > F
Model	3	395216.135	131738.712	0.65	0.5906
Error	31	6309947.368	203546.689		
Corrected Total	34	6705163.504			

R-Square	Coeff Var	Root MSE	ra226 Mean
0.058942	100.3376	451.1615	449.6434

Source	DF	Type I SS	Mean Square	F Value	Pr > F
Transect	3	395216.1353	131738.7118	0.65	0.5906

Source	DF	Type III SS	Mean Square	F Value	Pr > F
Transect	3	395216.1353	131738.7118	0.65	0.5906



Average Ratio Sulfate to Chloride Concentrations by Season**The GLM Procedure**

Class Level Information		
Class	Levels	Values
Level	4	B M P S

Data for Analysis of ra224	
Number of Observations Read	236
Number of Observations Used	25

Data for Analysis of ra226	
Number of Observations Read	236
Number of Observations Used	35

Note: Variables in each group are consistent with respect to the presence or absence of missing values.

Average Ratio Sulfate to Chloride Concentrations by Season

The GLM Procedure

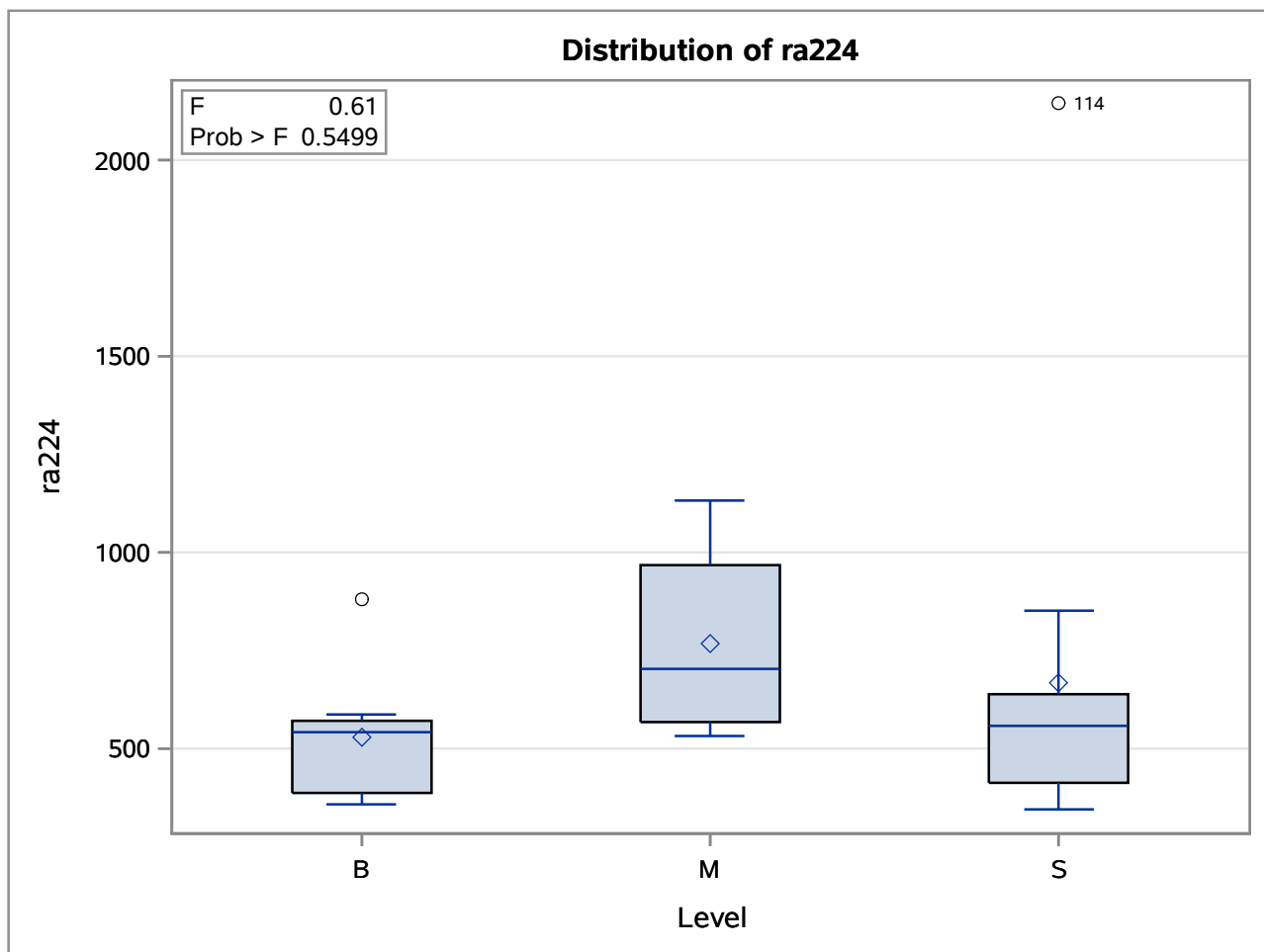
Dependent Variable: ra224

Source	DF	Sum of Squares	Mean Square	F Value	Pr > F
Model	2	172274.384	86137.192	0.61	0.5499
Error	22	3083192.152	140145.098		
Corrected Total	24	3255466.535			

R-Square	Coeff Var	Root MSE	ra224 Mean
0.052918	58.65395	374.3596	638.2512

Source	DF	Type I SS	Mean Square	F Value	Pr > F
Level	2	172274.3835	86137.1918	0.61	0.5499

Source	DF	Type III SS	Mean Square	F Value	Pr > F
Level	2	172274.3835	86137.1918	0.61	0.5499



Average Ratio Sulfate to Chloride Concentrations by Season

The GLM Procedure

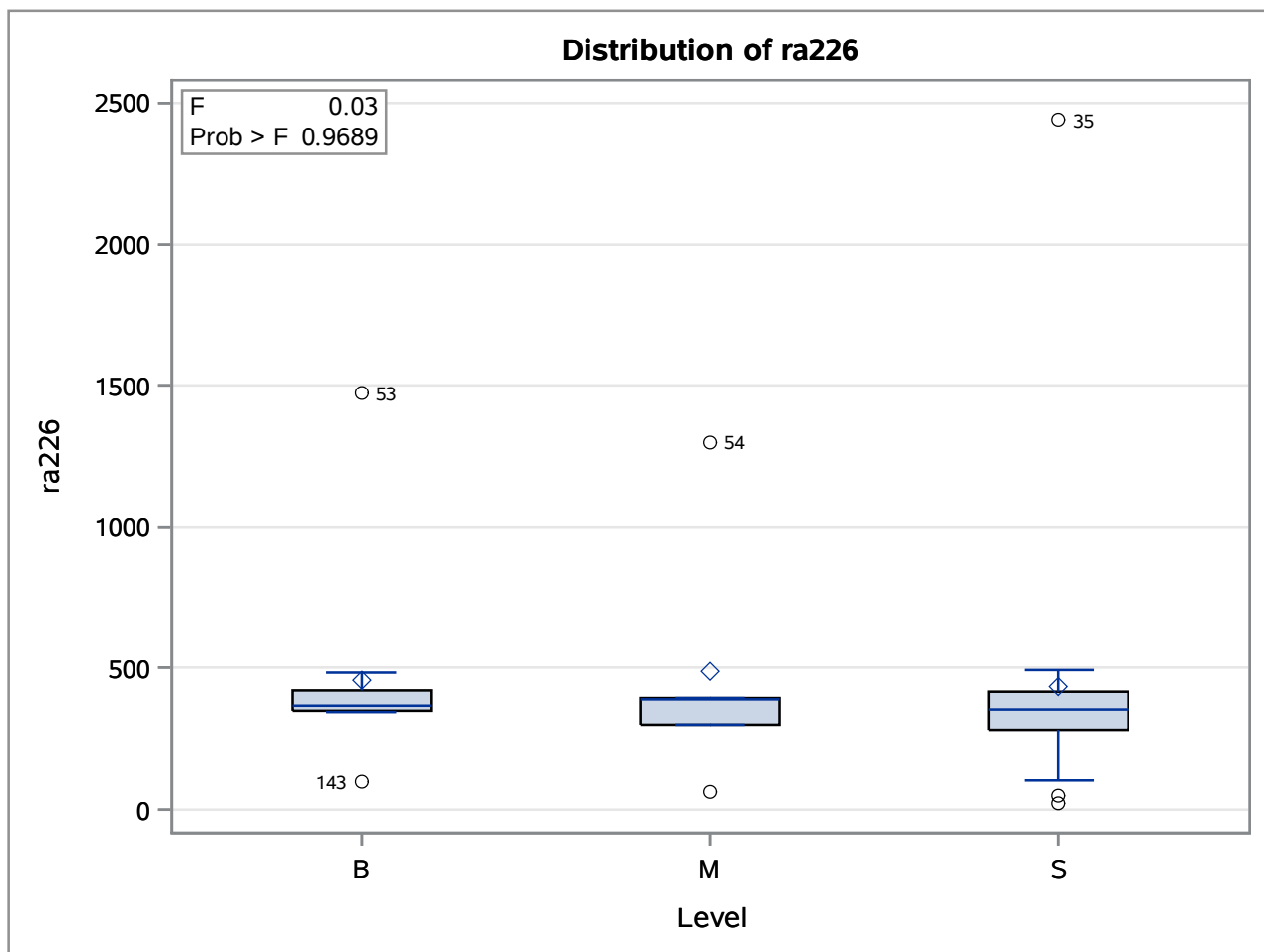
Dependent Variable: ra226

Source	DF	Sum of Squares	Mean Square	F Value	Pr > F
Model	2	13234.404	6617.202	0.03	0.9689
Error	32	6691929.099	209122.784		
Corrected Total	34	6705163.504			

R-Square	Coeff Var	Root MSE	ra226 Mean
0.001974	101.7027	457.2994	449.6434

Source	DF	Type I SS	Mean Square	F Value	Pr > F
Level	2	13234.40443	6617.20221	0.03	0.9689

Source	DF	Type III SS	Mean Square	F Value	Pr > F
Level	2	13234.40443	6617.20221	0.03	0.9689



Average Ratio Sulfate to Chloride Concentrations by Season**The GLM Procedure**

Class Level Information		
Class	Levels	Values
Event	3	JAN2014 JUL2014 NOV2014
Level	4	B M P S

Data for Analysis of temp ph	
Number of Observations Read	236
Number of Observations Used	210

Data for Analysis of do_conc	
Number of Observations Read	236
Number of Observations Used	192

Data for Analysis of sal	
Number of Observations Read	236
Number of Observations Used	179

Data for Analysis of chla	
Number of Observations Read	236
Number of Observations Used	142

Data for Analysis of nh4	
Number of Observations Read	236
Number of Observations Used	228

Data for Analysis of no2	
Number of Observations Read	236
Number of Observations Used	228

Data for Analysis of po4	
Number of Observations Read	236
Number of Observations Used	223

Data for Analysis of sio4	
Number of Observations Read	236
Number of Observations Used	186

Average Ratio Sulfate to Chloride Concentrations by Season

The GLM Procedure

Data for Analysis of rn222	
Number of Observations Read	236
Number of Observations Used	222

Note: Variables in each group are consistent with respect to the presence or absence of missing values.

Average Ratio Sulfate to Chloride Concentrations by Season

The GLM Procedure

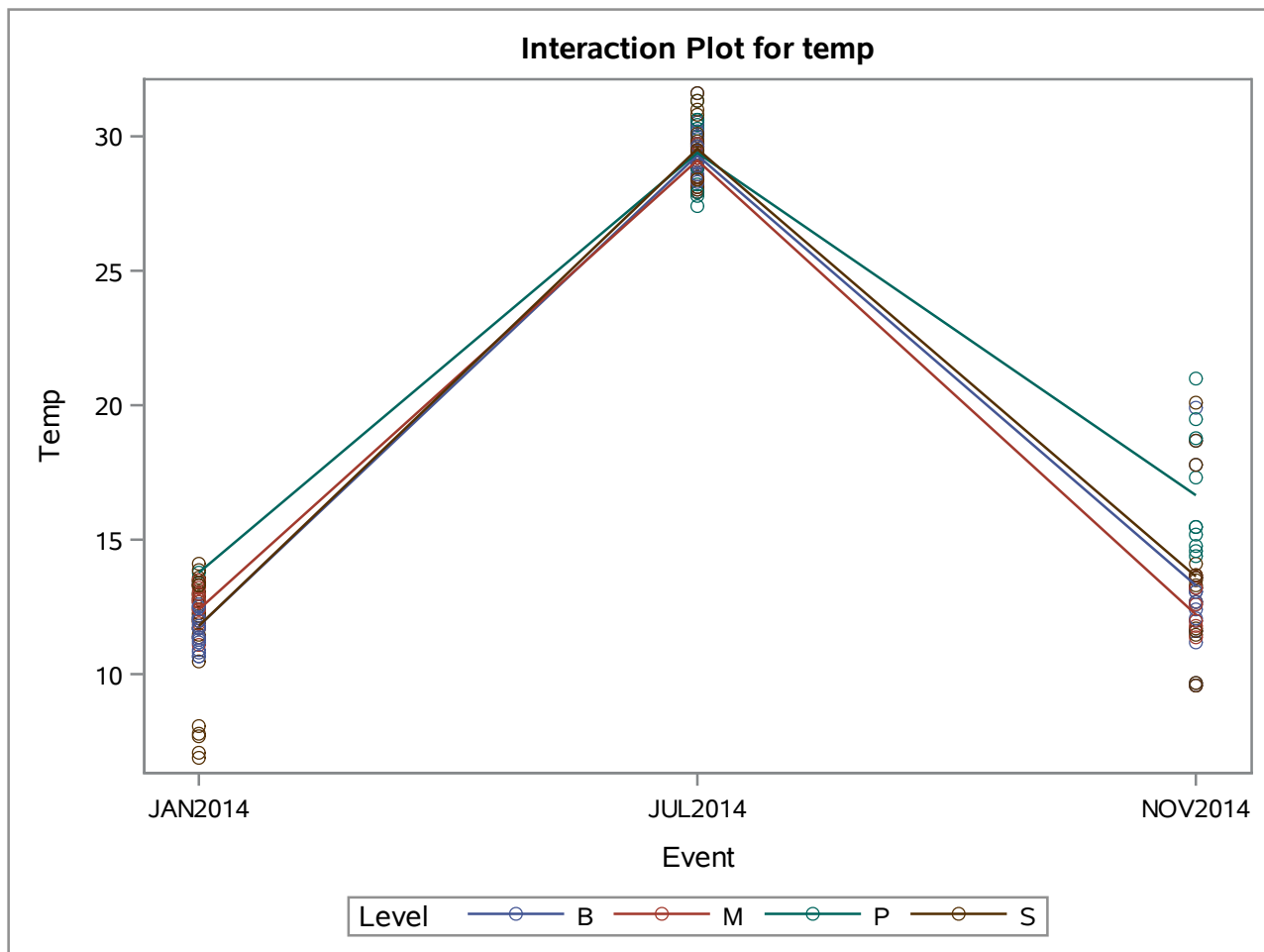
Dependent Variable: temp Temp

Source	DF	Sum of Squares	Mean Square	F Value	Pr > F
Model	11	14249.49090	1295.40826	471.50	<.0001
Error	198	543.99391	2.74744		
Corrected Total	209	14793.48481			

R-Square	Coeff Var	Root MSE	temp Mean
0.963227	8.333941	1.657542	19.88905

Source	DF	Type I SS	Mean Square	F Value	Pr > F
Event	2	14128.50995	7064.25498	2571.21	<.0001
Level	3	45.06373	15.02124	5.47	0.0012
Event*Level	6	75.91723	12.65287	4.61	0.0002

Source	DF	Type III SS	Mean Square	F Value	Pr > F
Event	2	8948.476117	4474.238058	1628.51	<.0001
Level	3	28.318419	9.439473	3.44	0.0180
Event*Level	6	75.917227	12.652871	4.61	0.0002



Average Ratio Sulfate to Chloride Concentrations by Season

The GLM Procedure

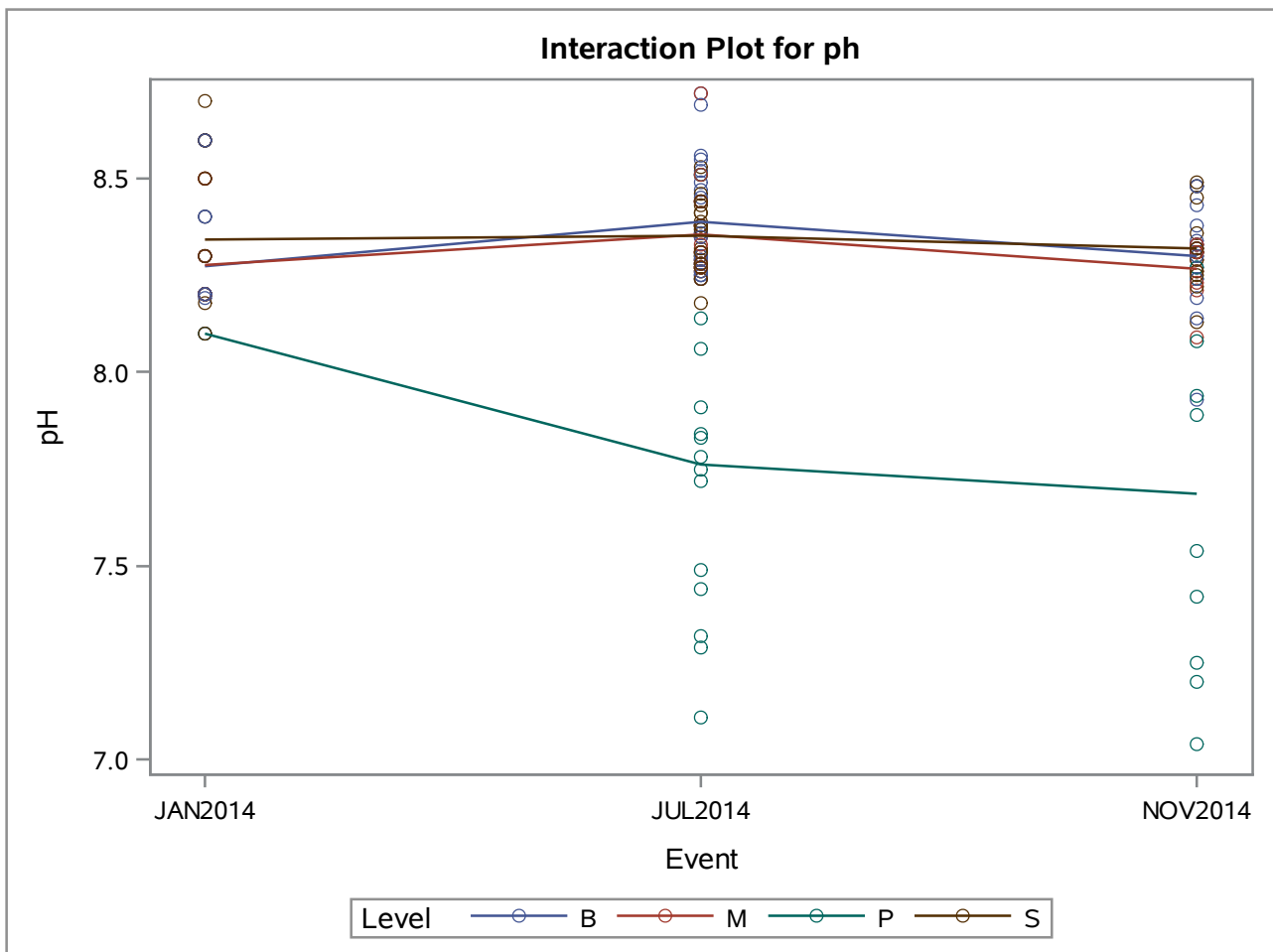
Dependent Variable: ph pH

Source	DF	Sum of Squares	Mean Square	F Value	Pr > F
Model	11	8.16053679	0.74186698	21.35	<.0001
Error	198	6.88065559	0.03475079		
Corrected Total	209	15.04119238			

R-Square	Coeff Var	Root MSE	ph Mean
0.542546	2.258071	0.186416	8.255524

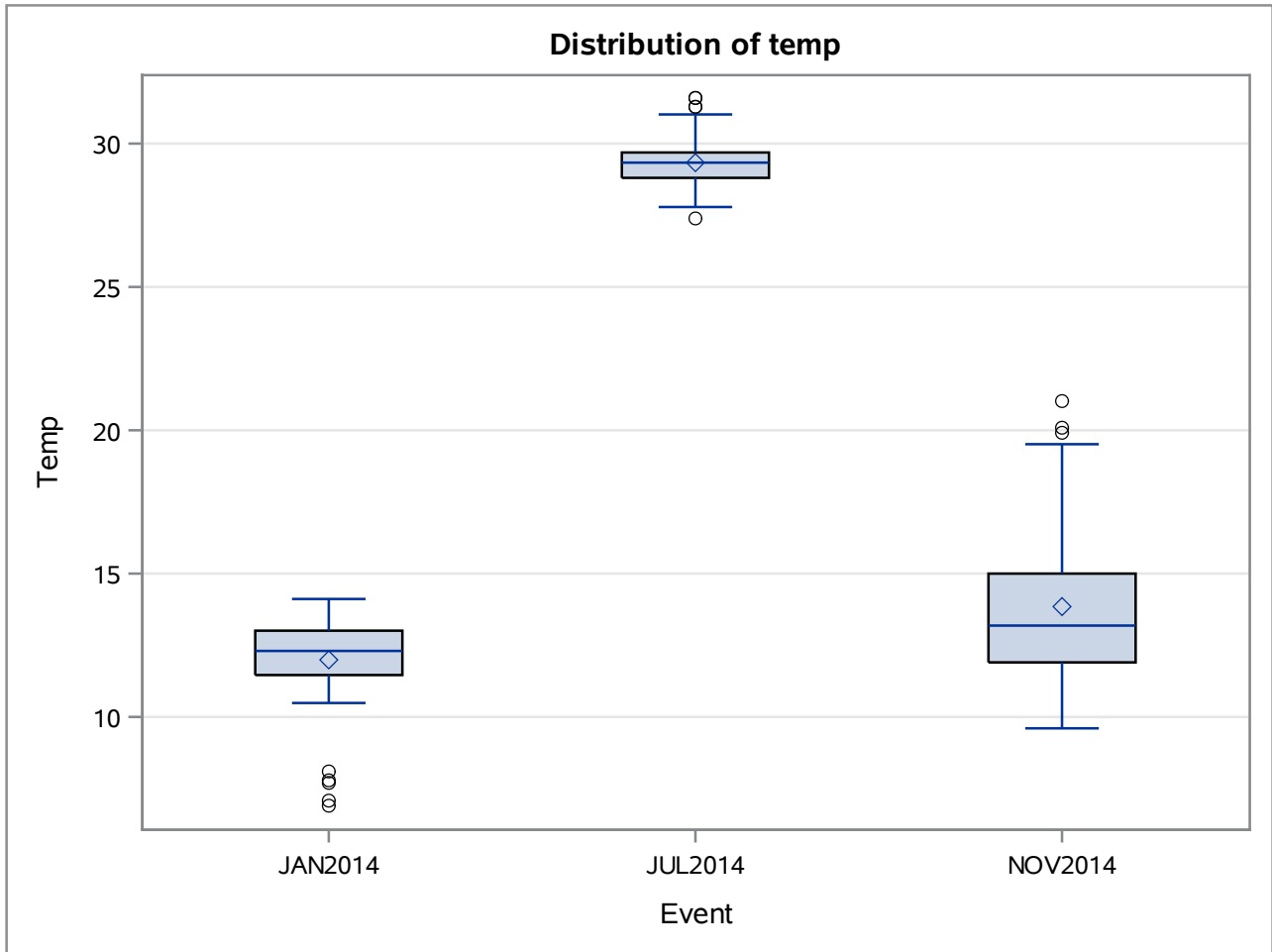
Source	DF	Type I SS	Mean Square	F Value	Pr > F
Event	2	0.42457869	0.21228935	6.11	0.0027
Level	3	7.50381129	2.50127043	71.98	<.0001
Event*Level	6	0.23214681	0.03869113	1.11	0.3558

Source	DF	Type III SS	Mean Square	F Value	Pr > F
Event	2	0.20270397	0.10135199	2.92	0.0564
Level	3	1.68430802	0.56143601	16.16	<.0001
Event*Level	6	0.23214681	0.03869113	1.11	0.3558



Average Ratio Sulfate to Chloride Concentrations by Season

The GLM Procedure



Average Ratio Sulfate to Chloride Concentrations by Season

The GLM Procedure

Tukey's Studentized Range (HSD) Test for temp

Note: This test controls the Type I experimentwise error rate, but it generally has a higher Type II error rate than REGWQ.

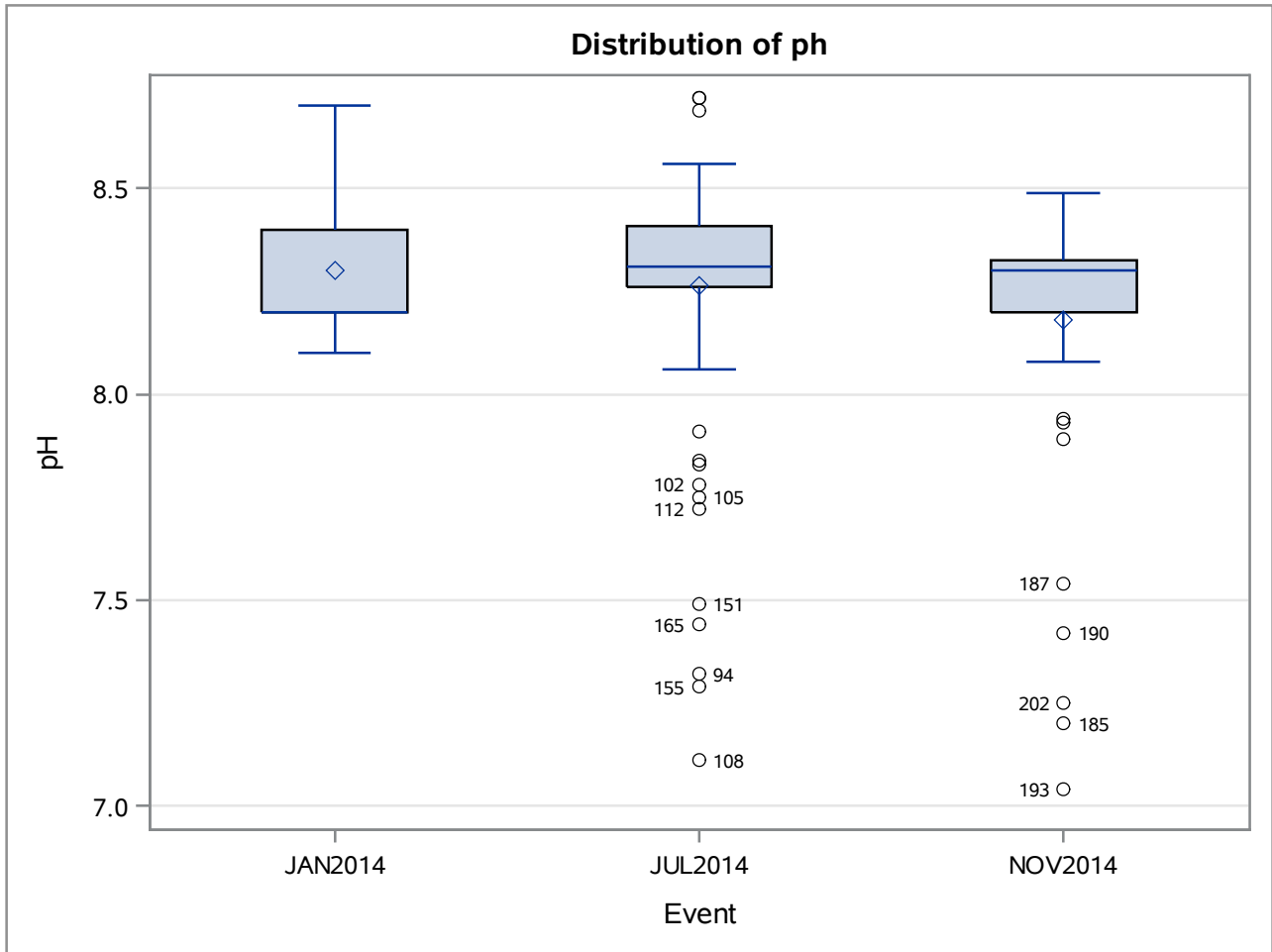
Alpha	0.05
Error Degrees of Freedom	198
Error Mean Square	2.747444
Critical Value of Studentized Range	3.33963
Minimum Significant Difference	0.6783
Harmonic Mean of Cell Sizes	66.59598

Note: Cell sizes are not equal.

Means with the same letter are not significantly different.			
Tukey Grouping	Mean	N	Event
A	29.3267	90	JUL2014
B	13.8558	52	NOV2014
C	12.0118	68	JAN2014

Average Ratio Sulfate to Chloride Concentrations by Season

The GLM Procedure



Average Ratio Sulfate to Chloride Concentrations by Season

The GLM Procedure

Tukey's Studentized Range (HSD) Test for ph

Note: This test controls the Type I experimentwise error rate, but it generally has a higher Type II error rate than REGWQ.

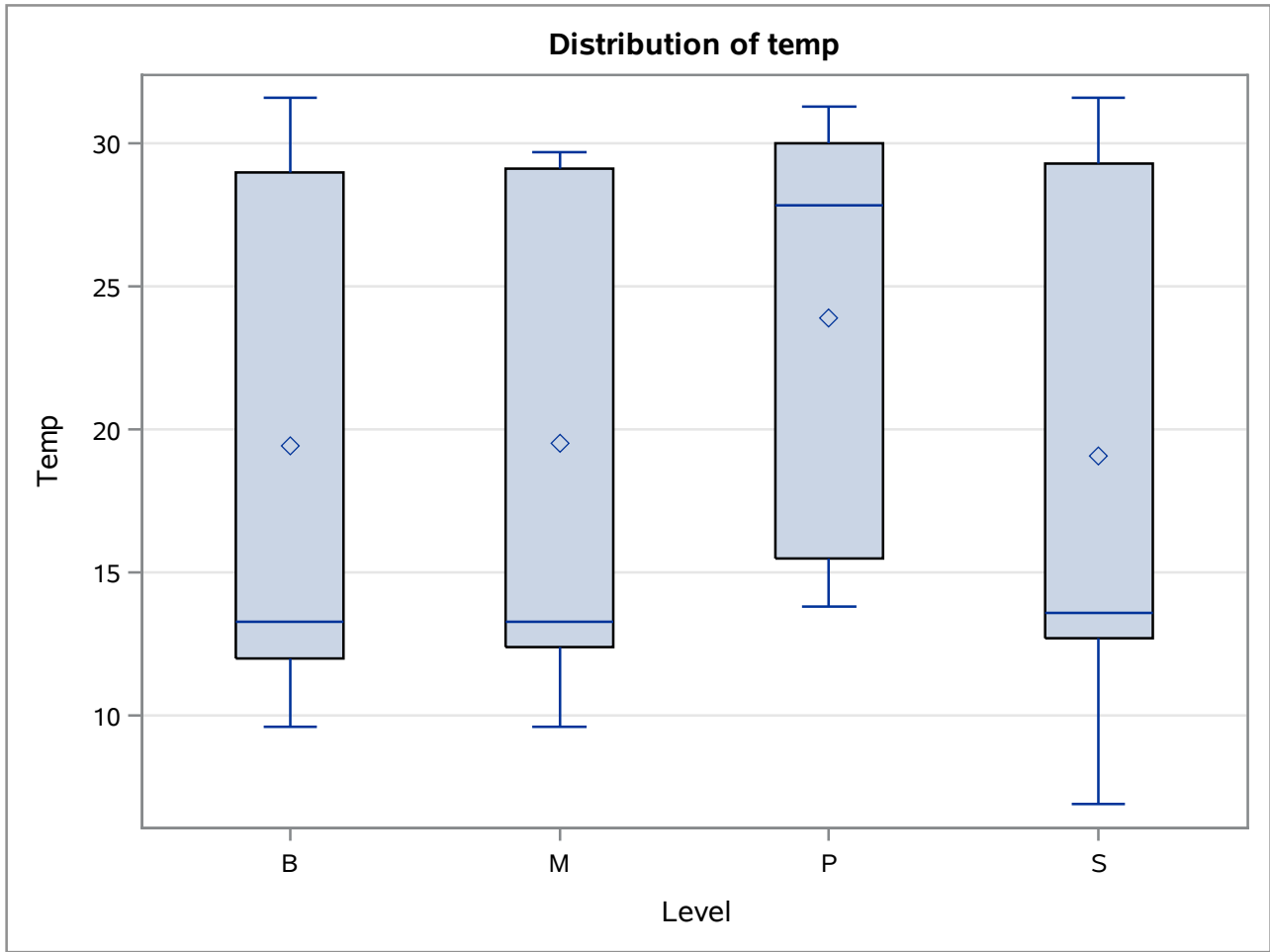
Alpha	0.05
Error Degrees of Freedom	198
Error Mean Square	0.034751
Critical Value of Studentized Range	3.33963
Minimum Significant Difference	0.0763
Harmonic Mean of Cell Sizes	66.59598

Note: Cell sizes are not equal.

Means with the same letter are not significantly different.			
Tukey Grouping	Mean	N	Event
A	8.29956	68	JAN2014
A			
A	8.26500	90	JUL2014
B	8.18154	52	NOV2014

Average Ratio Sulfate to Chloride Concentrations by Season

The GLM Procedure



Average Ratio Sulfate to Chloride Concentrations by Season

The GLM Procedure

Tukey's Studentized Range (HSD) Test for temp

Note: This test controls the Type I experimentwise error rate, but it generally has a higher Type II error rate than REGWQ.

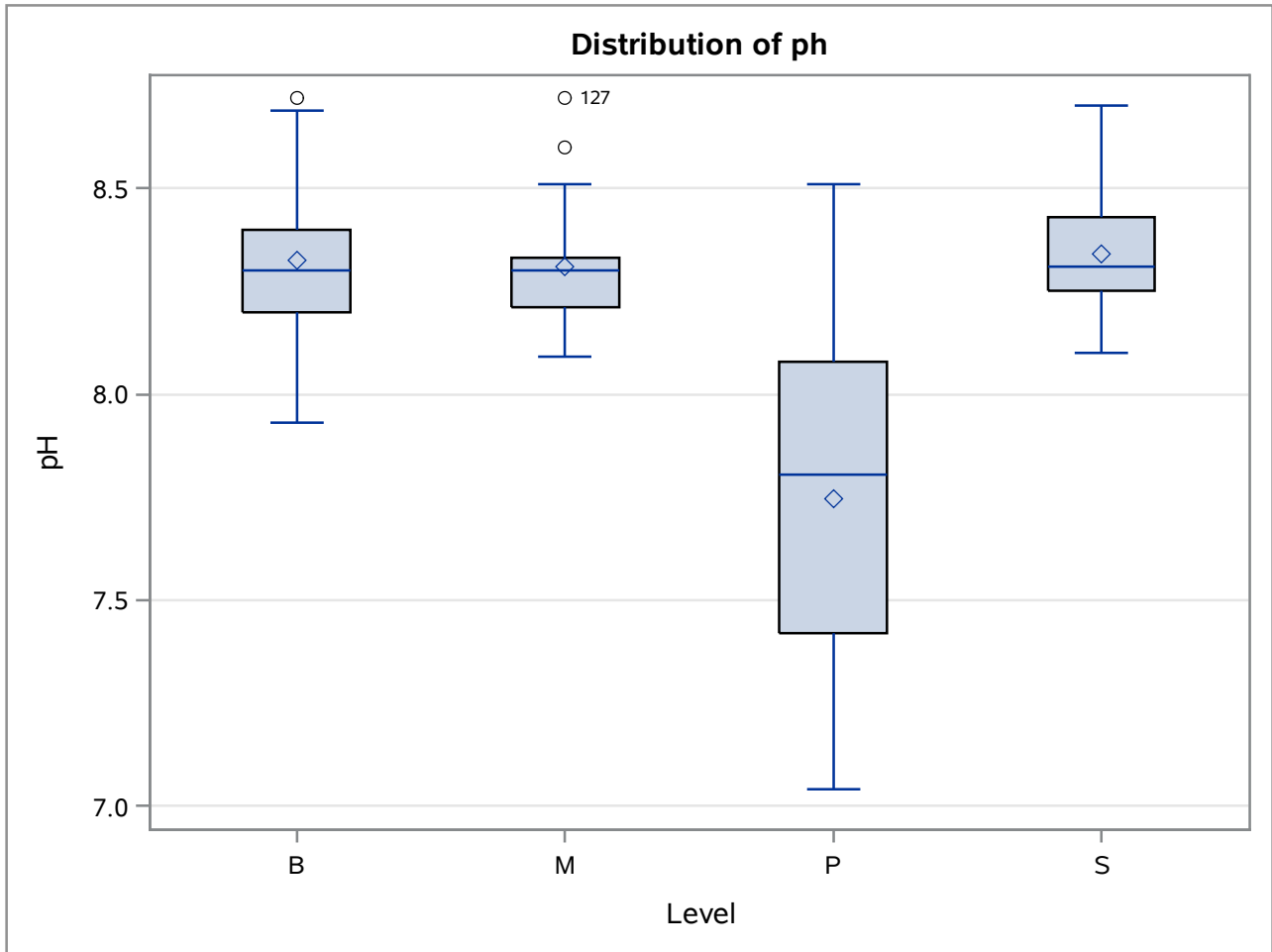
Alpha	0.05
Error Degrees of Freedom	198
Error Mean Square	2.747444
Critical Value of Studentized Range	3.66420
Minimum Significant Difference	0.9036
Harmonic Mean of Cell Sizes	45.1773

Note: Cell sizes are not equal.

Means with the same letter are not significantly different.			
Tukey Grouping	Mean	N	Level
A	23.8846	26	P
B	19.5286	49	M
B			
B	19.4415	65	B
B			
B	19.0729	70	S

Average Ratio Sulfate to Chloride Concentrations by Season

The GLM Procedure



Average Ratio Sulfate to Chloride Concentrations by Season

The GLM Procedure

Tukey's Studentized Range (HSD) Test for ph

Note: This test controls the Type I experimentwise error rate, but it generally has a higher Type II error rate than REGWQ.

Alpha	0.05
Error Degrees of Freedom	198
Error Mean Square	0.034751
Critical Value of Studentized Range	3.66420
Minimum Significant Difference	0.1016
Harmonic Mean of Cell Sizes	45.1773

Note: Cell sizes are not equal.

Means with the same letter are not significantly different.			
Tukey Grouping	Mean	N	Level
A	8.34129	70	S
A			
A	8.32662	65	B
A			
A	8.30898	49	M
B	7.74615	26	P

Average Ratio Sulfate to Chloride Concentrations by Season

The GLM Procedure

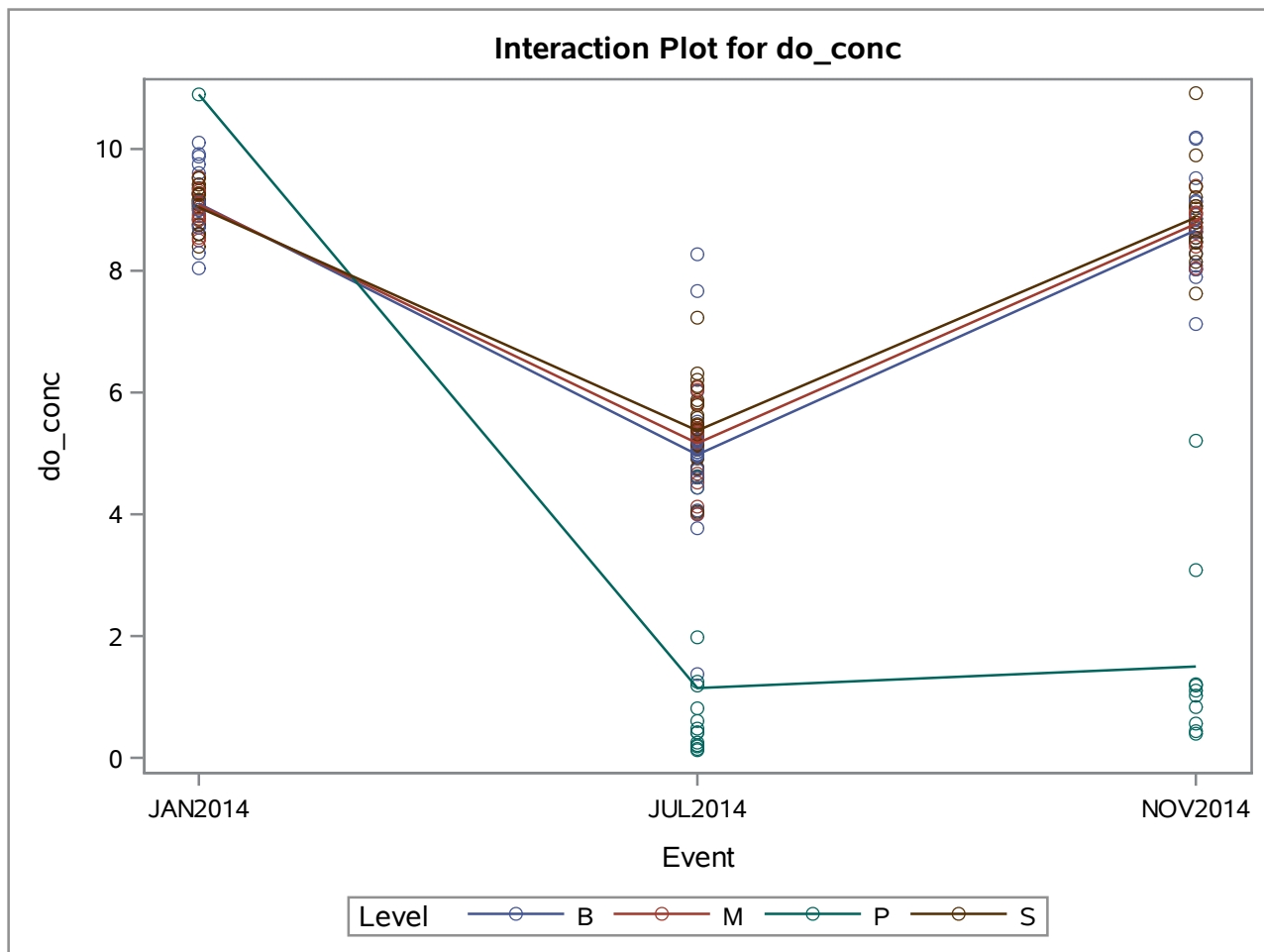
Dependent Variable: do_conc

Source	DF	Sum of Squares	Mean Square	F Value	Pr > F
Model	11	1373.891975	124.899270	168.96	<.0001
Error	180	133.062206	0.739234		
Corrected Total	191	1506.954181			

R-Square	Coeff Var	Root MSE	do_conc Mean
0.911701	13.26896	0.859787	6.479688

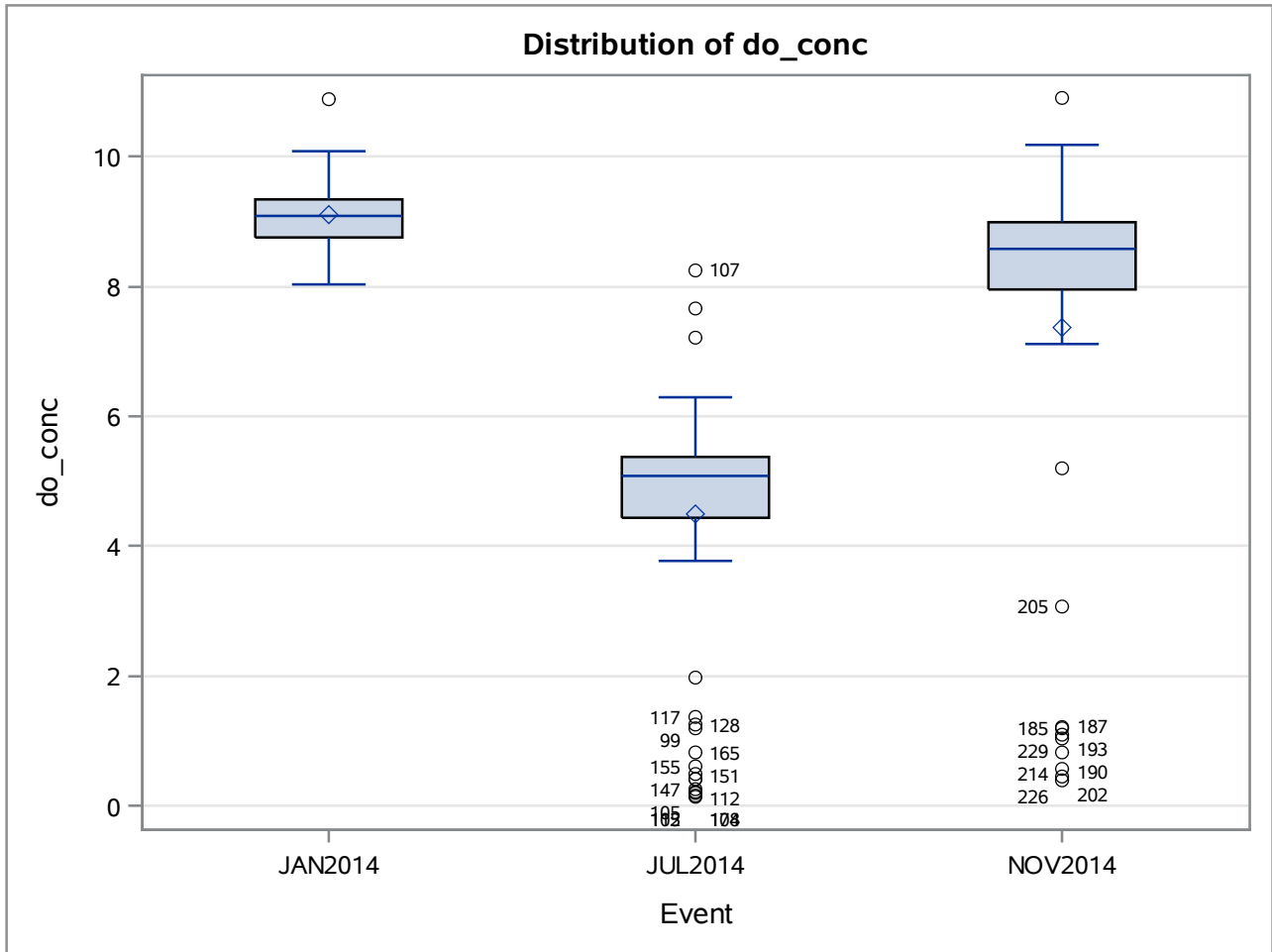
Source	DF	Type I SS	Mean Square	F Value	Pr > F
Event	2	739.0625600	369.5312800	499.88	<.0001
Level	3	535.1482122	178.3827374	241.31	<.0001
Event*Level	6	99.6812031	16.6135338	22.47	<.0001

Source	DF	Type III SS	Mean Square	F Value	Pr > F
Event	2	473.3533986	236.6766993	320.16	<.0001
Level	3	74.3707739	24.7902580	33.54	<.0001
Event*Level	6	99.6812031	16.6135338	22.47	<.0001



Average Ratio Sulfate to Chloride Concentrations by Season

The GLM Procedure



Average Ratio Sulfate to Chloride Concentrations by Season

The GLM Procedure

Tukey's Studentized Range (HSD) Test for do_conc

Note: This test controls the Type I experimentwise error rate, but it generally has a higher Type II error rate than REGWQ.

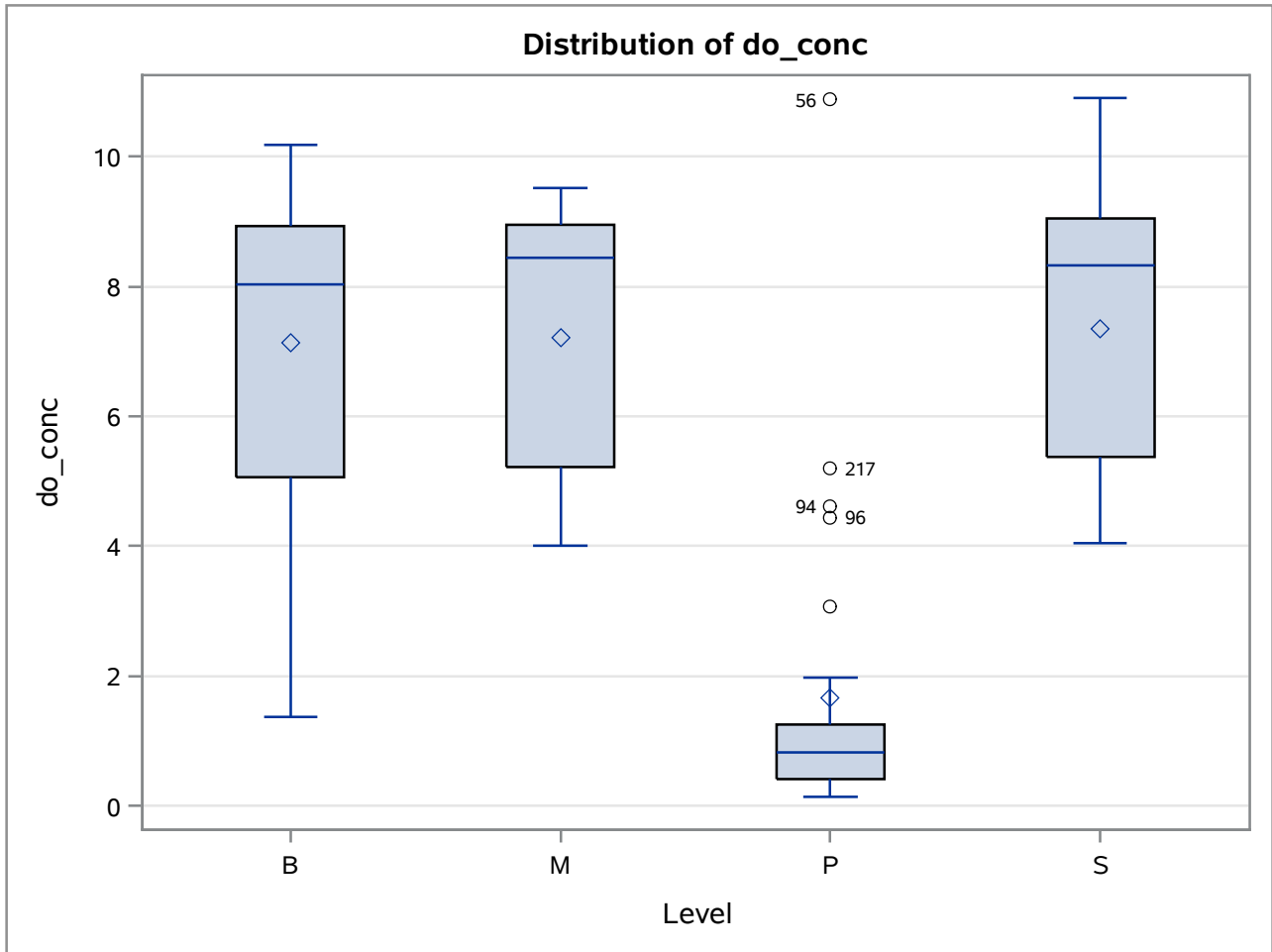
Alpha	0.05
Error Degrees of Freedom	180
Error Mean Square	0.739234
Critical Value of Studentized Range	3.34216
Minimum Significant Difference	0.3722
Harmonic Mean of Cell Sizes	59.59253

Note: Cell sizes are not equal.

Means with the same letter are not significantly different.			
Tukey Grouping	Mean	N	Event
A	9.1076	50	JAN2014
B	7.3758	52	NOV2014
C	4.5020	90	JUL2014

Average Ratio Sulfate to Chloride Concentrations by Season

The GLM Procedure



Average Ratio Sulfate to Chloride Concentrations by Season

The GLM Procedure

Tukey's Studentized Range (HSD) Test for do_conc

Note: This test controls the Type I experimentwise error rate, but it generally has a higher Type II error rate than REGWQ.

Alpha	0.05
Error Degrees of Freedom	180
Error Mean Square	0.739234
Critical Value of Studentized Range	3.66733
Minimum Significant Difference	0.4822
Harmonic Mean of Cell Sizes	42.7652

Note: Cell sizes are not equal.

Means with the same letter are not significantly different.			
Tukey Grouping	Mean	N	Level
A	7.3473	60	S
A			
A	7.2176	46	M
A			
A	7.1353	60	B
B	1.6588	26	P

Average Ratio Sulfate to Chloride Concentrations by Season

The GLM Procedure

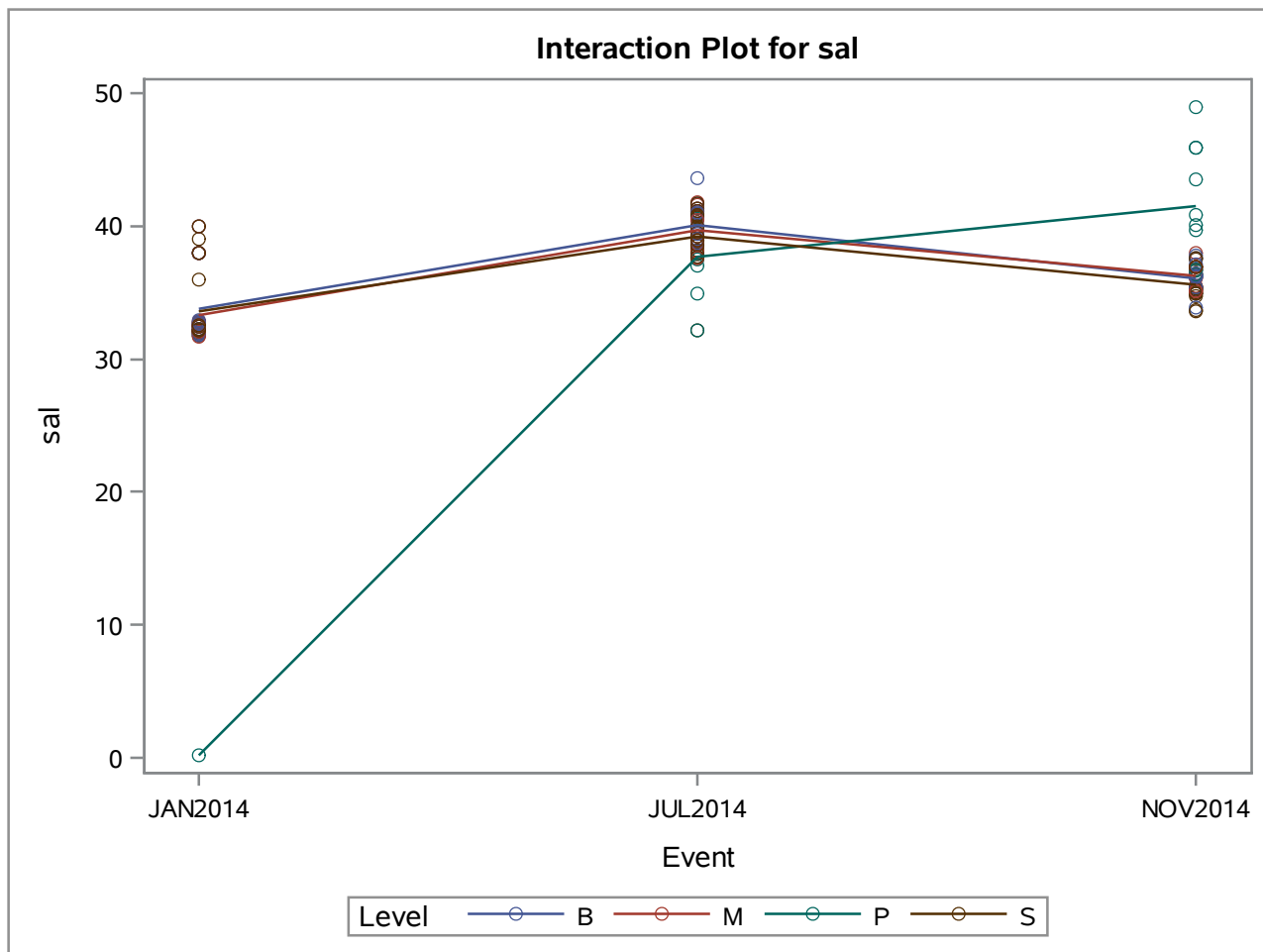
Dependent Variable: sal

Source	DF	Sum of Squares	Mean Square	F Value	Pr > F
Model	11	2693.085419	244.825947	48.42	<.0001
Error	167	844.323961	5.055832		
Corrected Total	178	3537.409380			

R-Square	Coeff Var	Root MSE	sal Mean
0.761316	6.165333	2.248518	36.47034

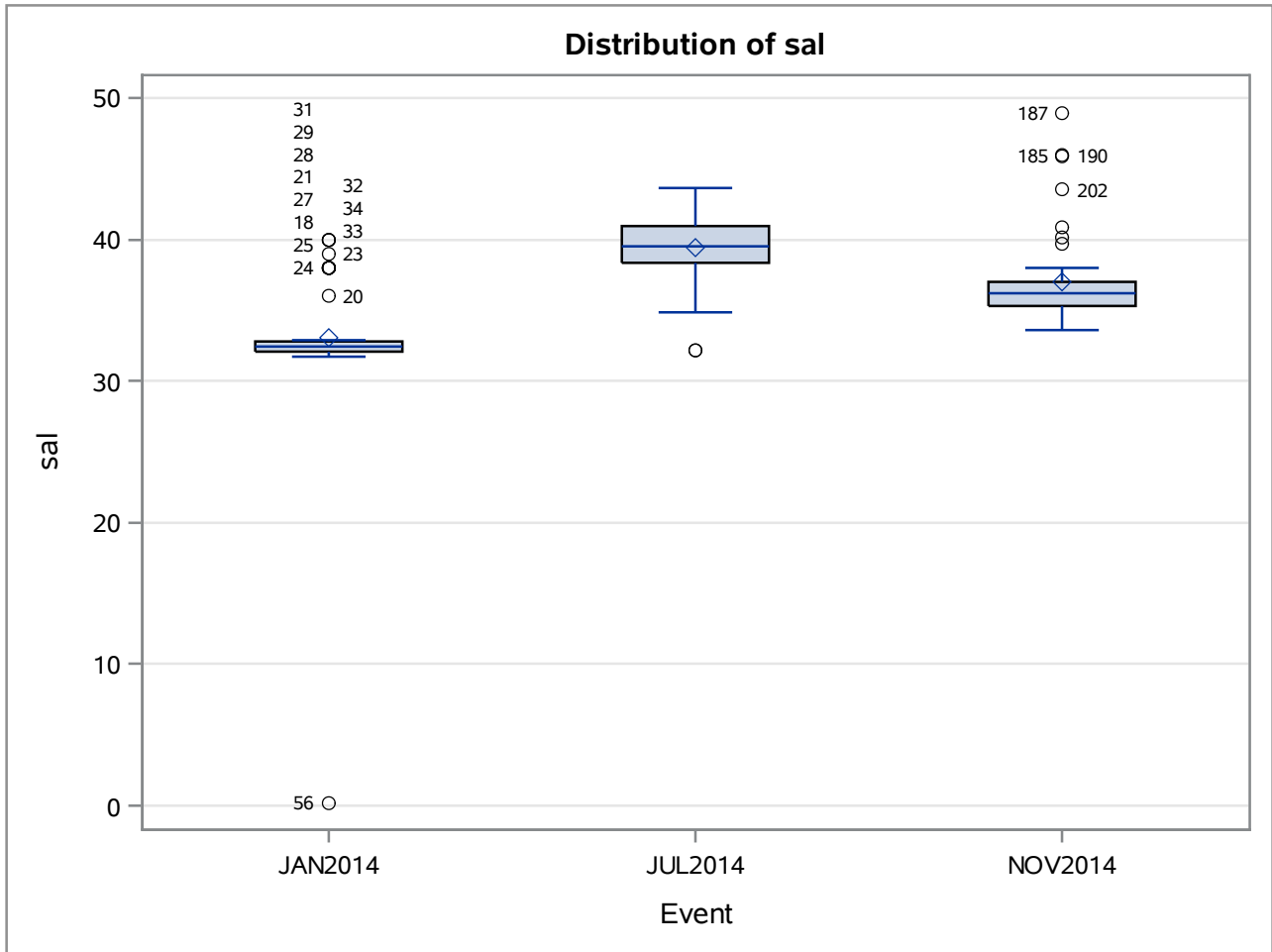
Source	DF	Type I SS	Mean Square	F Value	Pr > F
Event	2	1312.383811	656.191906	129.79	<.0001
Level	3	6.775001	2.258334	0.45	0.7200
Event*Level	6	1373.926606	228.987768	45.29	<.0001

Source	DF	Type III SS	Mean Square	F Value	Pr > F
Event	2	2177.981837	1088.990919	215.39	<.0001
Level	3	690.258010	230.086003	45.51	<.0001
Event*Level	6	1373.926606	228.987768	45.29	<.0001



Average Ratio Sulfate to Chloride Concentrations by Season

The GLM Procedure



Average Ratio Sulfate to Chloride Concentrations by Season

The GLM Procedure

Tukey's Studentized Range (HSD) Test for sal

Note: This test controls the Type I experimentwise error rate, but it generally has a higher Type II error rate than REGWQ.

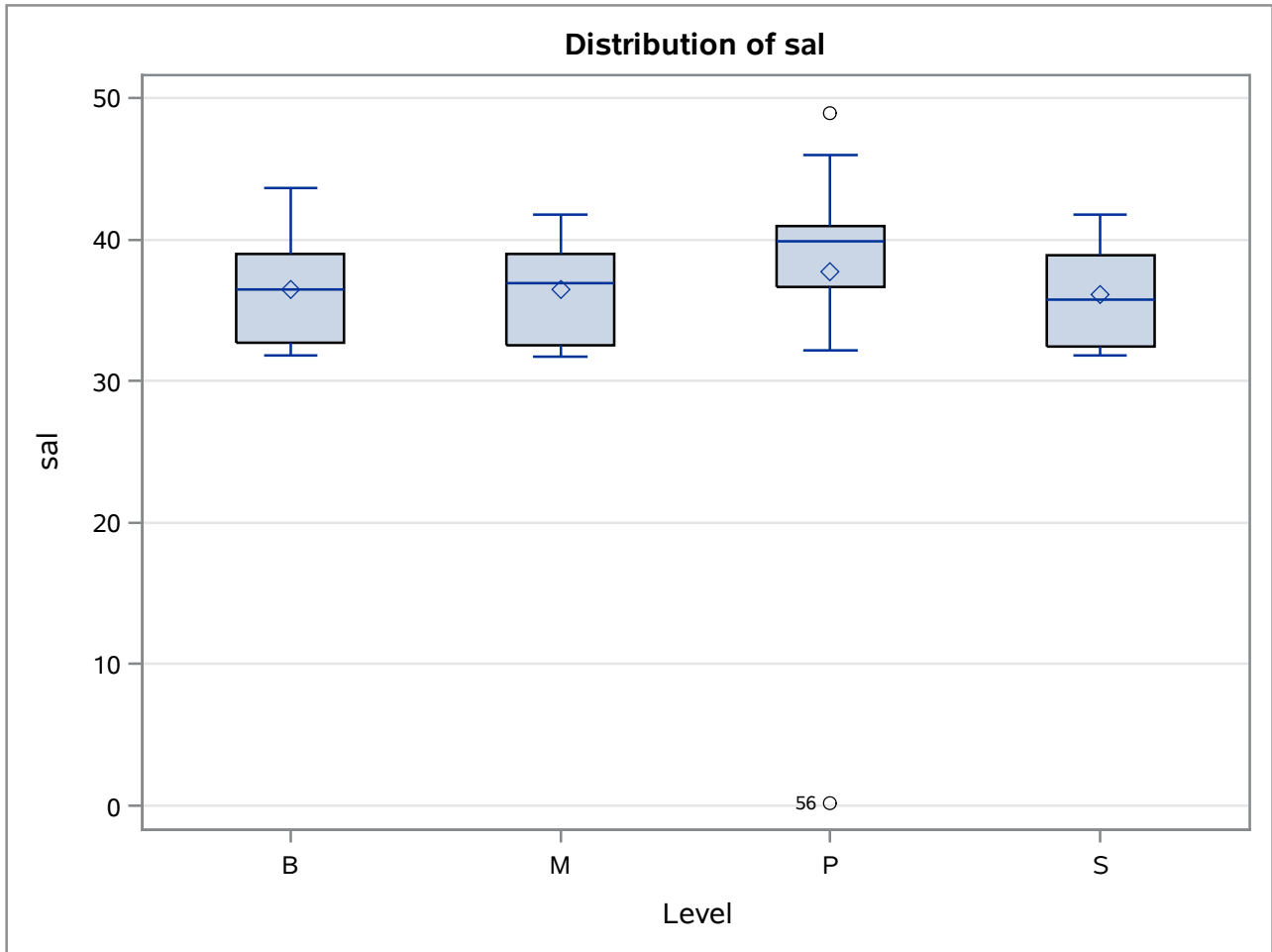
Alpha	0.05
Error Degrees of Freedom	167
Error Mean Square	5.055832
Critical Value of Studentized Range	3.34433
Minimum Significant Difference	0.9778
Harmonic Mean of Cell Sizes	59.13802

Note: Cell sizes are not equal.

Means with the same letter are not significantly different.			
Tukey Grouping	Mean	N	Event
A	39.4294	64	JUL2014
B	36.9769	52	NOV2014
C	33.0462	63	JAN2014

Average Ratio Sulfate to Chloride Concentrations by Season

The GLM Procedure



Average Ratio Sulfate to Chloride Concentrations by Season

The GLM Procedure

Tukey's Studentized Range (HSD) Test for sal

Note: This test controls the Type I experimentwise error rate, but it generally has a higher Type II error rate than REGWQ.

Alpha	0.05
Error Degrees of Freedom	167
Error Mean Square	5.055832
Critical Value of Studentized Range	3.67001
Minimum Significant Difference	1.3813
Harmonic Mean of Cell Sizes	35.68882

Note: Cell sizes are not equal.

Means with the same letter are not significantly different.				
Tukey Grouping		Mean	N	Level
	A	37.6956	18	P
	A			
B	A	36.4993	57	B
B	A			
B	A	36.4535	46	M
B				
B		36.0750	58	S

Average Ratio Sulfate to Chloride Concentrations by Season

The GLM Procedure

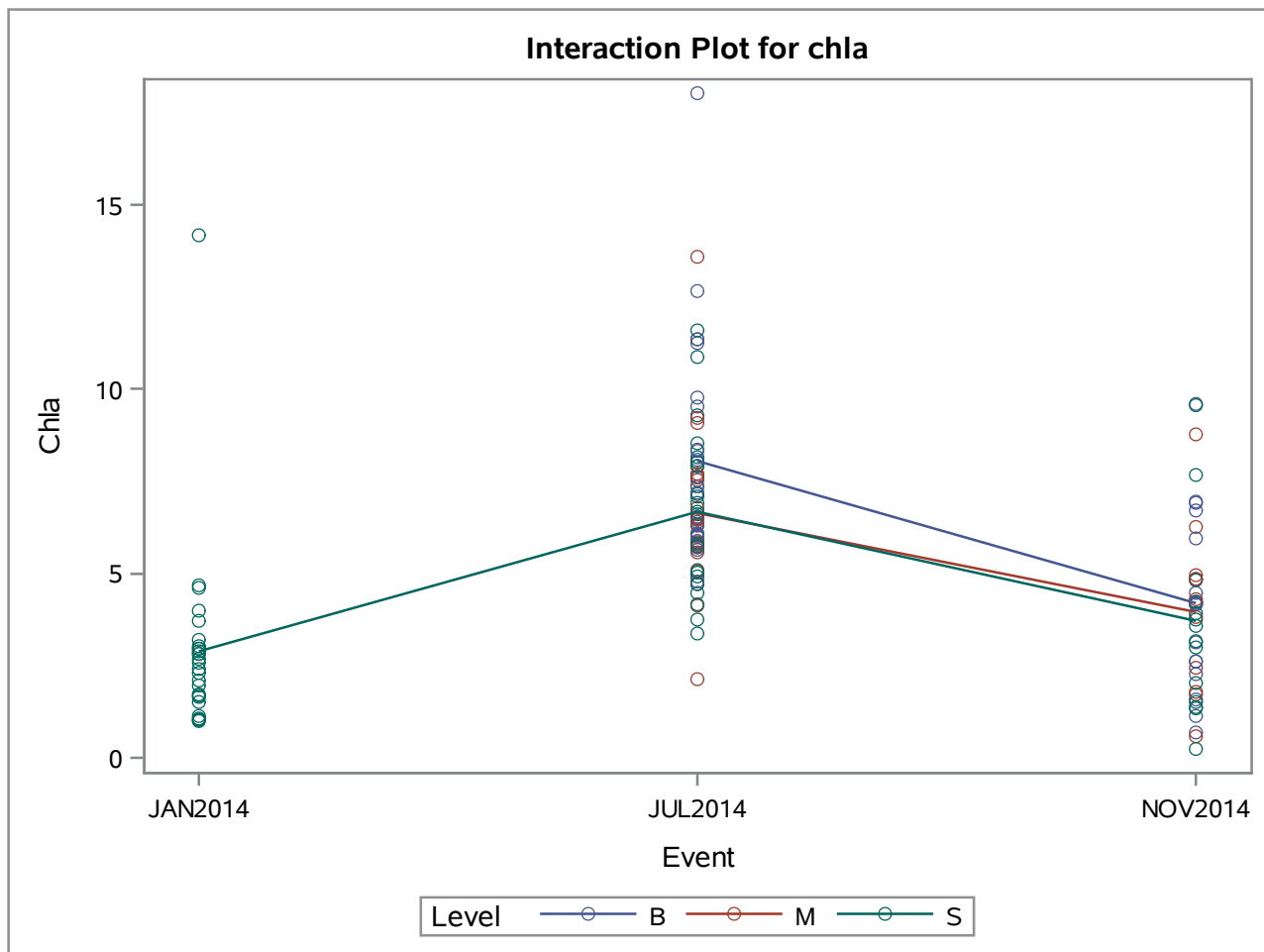
Dependent Variable: chla Chla

Source	DF	Sum of Squares	Mean Square	F Value	Pr > F
Model	6	525.399325	87.566554	14.58	<.0001
Error	135	810.988120	6.007319		
Corrected Total	141	1336.387444			

R-Square	Coeff Var	Root MSE	chla Mean
0.393149	45.29053	2.450983	5.411690

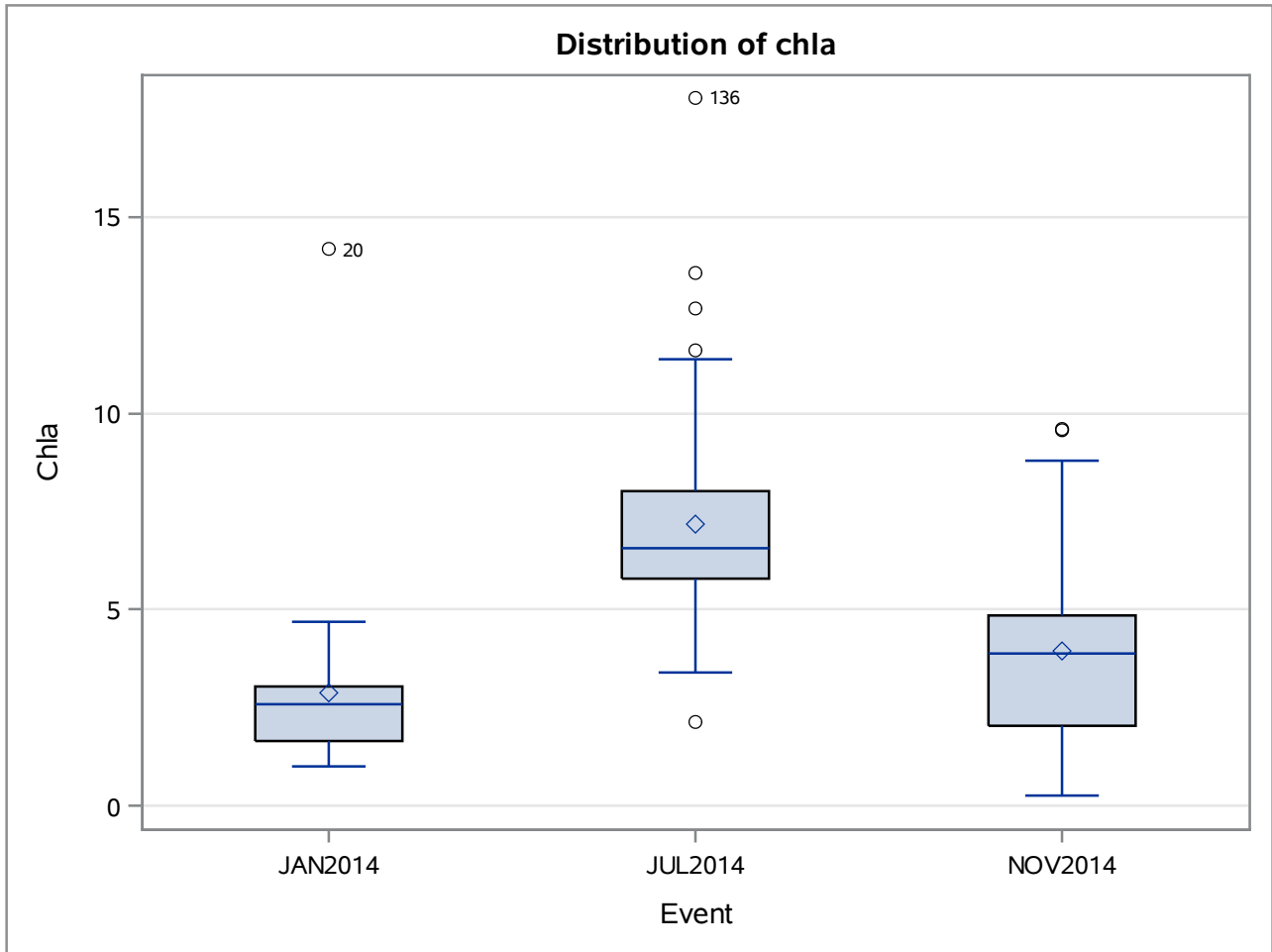
Source	DF	Type I SS	Mean Square	F Value	Pr > F
Event	2	490.4871131	245.2435565	40.82	<.0001
Level	2	28.4232480	14.2116240	2.37	0.0978
Event*Level	2	6.4889634	3.2444817	0.54	0.5840

Source	DF	Type III SS	Mean Square	F Value	Pr > F
Event	2	372.4050767	186.2025384	31.00	<.0001
Level	2	20.2016122	10.1008061	1.68	0.1900
Event*Level	2	6.4889634	3.2444817	0.54	0.5840



Average Ratio Sulfate to Chloride Concentrations by Season

The GLM Procedure



Average Ratio Sulfate to Chloride Concentrations by Season

The GLM Procedure

Tukey's Studentized Range (HSD) Test for chla

Note: This test controls the Type I experimentwise error rate, but it generally has a higher Type II error rate than REGWQ.

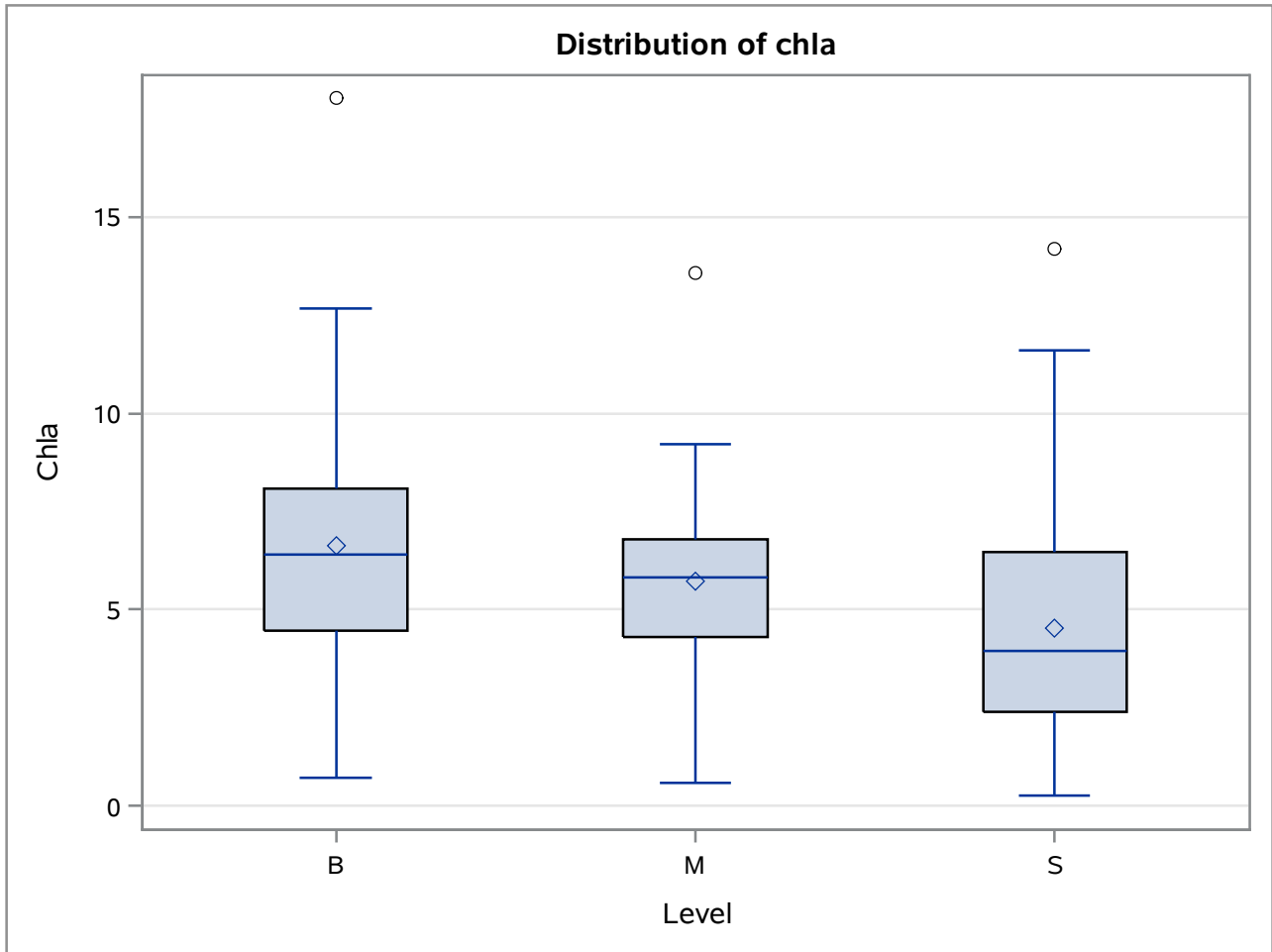
Alpha	0.05
Error Degrees of Freedom	135
Error Mean Square	6.007319
Critical Value of Studentized Range	3.35147
Minimum Significant Difference	1.2949
Harmonic Mean of Cell Sizes	40.24404

Note: Cell sizes are not equal.

Means with the same letter are not significantly different.			
Tukey Grouping	Mean	N	Event
A	7.1834	73	JUL2014
B	3.9574	42	NOV2014
B			
B	2.8839	27	JAN2014

Average Ratio Sulfate to Chloride Concentrations by Season

The GLM Procedure



Average Ratio Sulfate to Chloride Concentrations by Season

The GLM Procedure

Tukey's Studentized Range (HSD) Test for chla

Note: This test controls the Type I experimentwise error rate, but it generally has a higher Type II error rate than REGWQ.

Alpha	0.05
Error Degrees of Freedom	135
Error Mean Square	6.007319
Critical Value of Studentized Range	3.35147
Minimum Significant Difference	1.2728
Harmonic Mean of Cell Sizes	41.65262

Note: Cell sizes are not equal.

Means with the same letter are not significantly different.				
Tukey Grouping		Mean	N	Level
	A	6.6256	43	B
	A			
B	A	5.7226	29	M
B				
B		4.5372	70	S

Average Ratio Sulfate to Chloride Concentrations by Season

The GLM Procedure

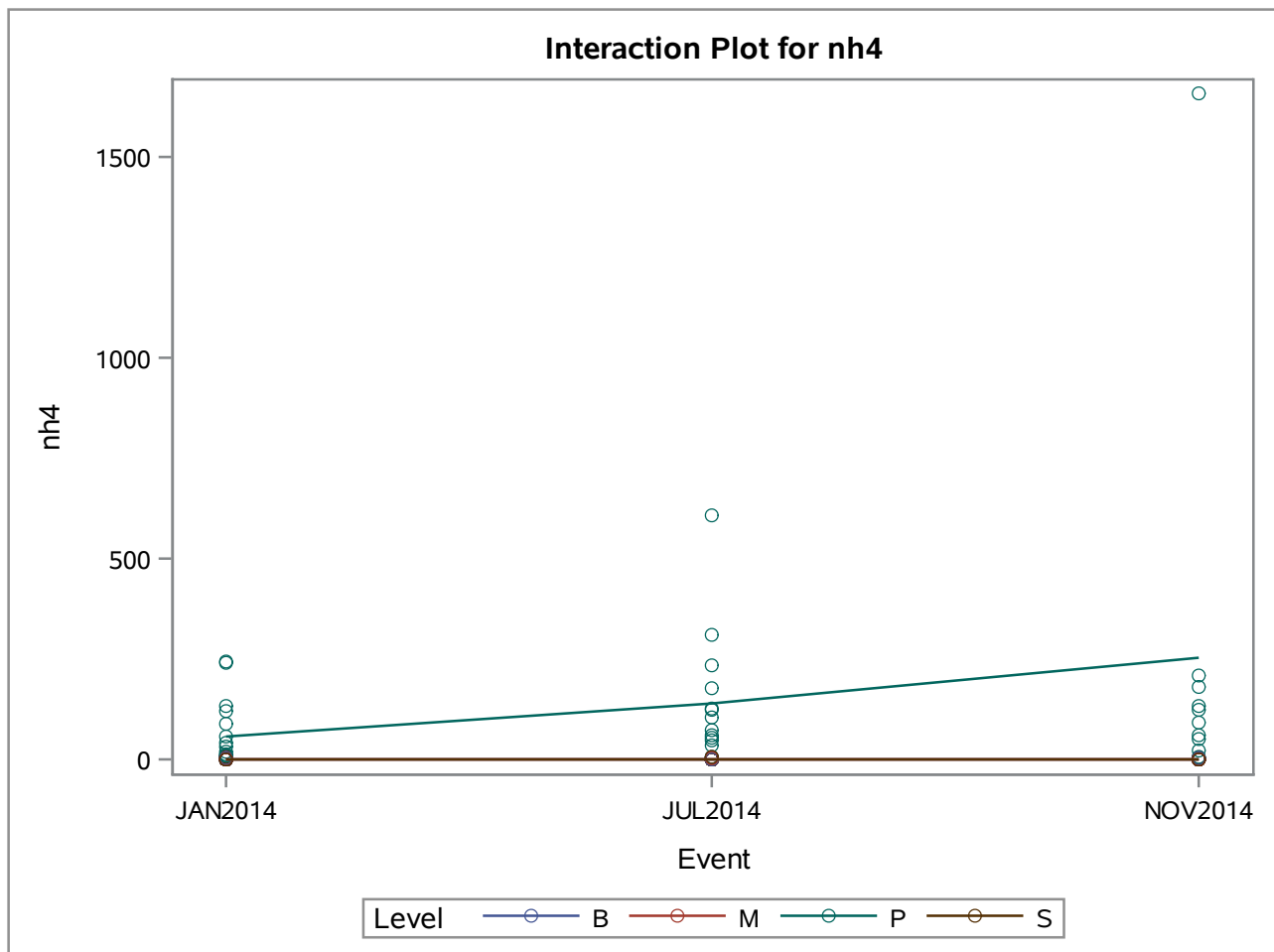
Dependent Variable: nh4

Source	DF	Sum of Squares	Mean Square	F Value	Pr > F
Model	11	836698.788	76063.526	6.14	<.0001
Error	216	2677105.122	12394.005		
Corrected Total	227	3513803.910			

R-Square	Coeff Var	Root MSE	nh4 Mean
0.238118	436.9599	111.3284	25.47794

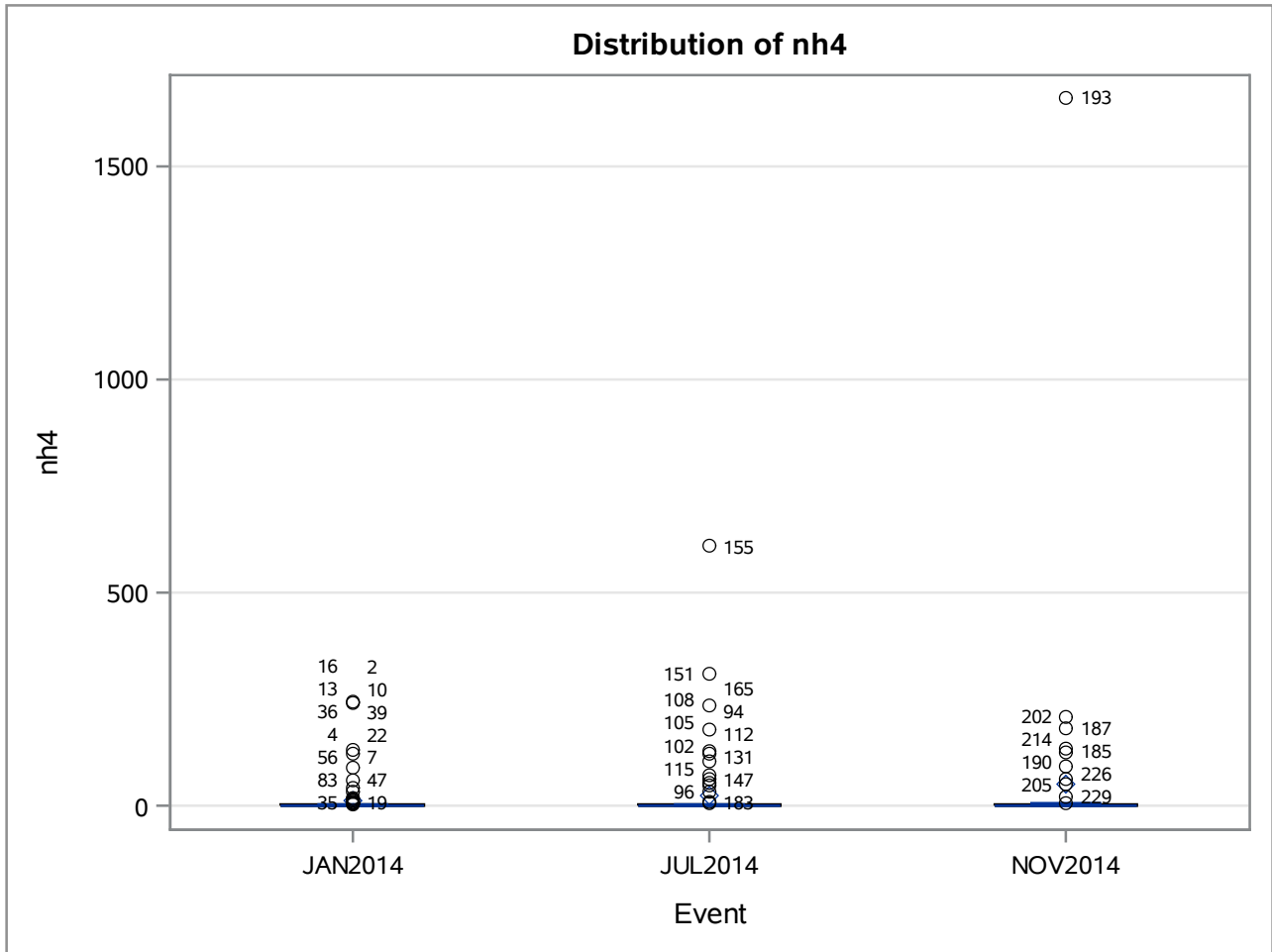
Source	DF	Type I SS	Mean Square	F Value	Pr > F
Event	2	45720.5355	22860.2677	1.84	0.1606
Level	3	588307.9600	196102.6533	15.82	<.0001
Event*Level	6	202670.2926	33778.3821	2.73	0.0143

Source	DF	Type III SS	Mean Square	F Value	Pr > F
Event	2	76257.7316	38128.8658	3.08	0.0482
Level	3	721099.5496	240366.5165	19.39	<.0001
Event*Level	6	202670.2926	33778.3821	2.73	0.0143



Average Ratio Sulfate to Chloride Concentrations by Season

The GLM Procedure



Average Ratio Sulfate to Chloride Concentrations by Season

The GLM Procedure

Tukey's Studentized Range (HSD) Test for nh4

Note: This test controls the Type I experimentwise error rate, but it generally has a higher Type II error rate than REGWQ.

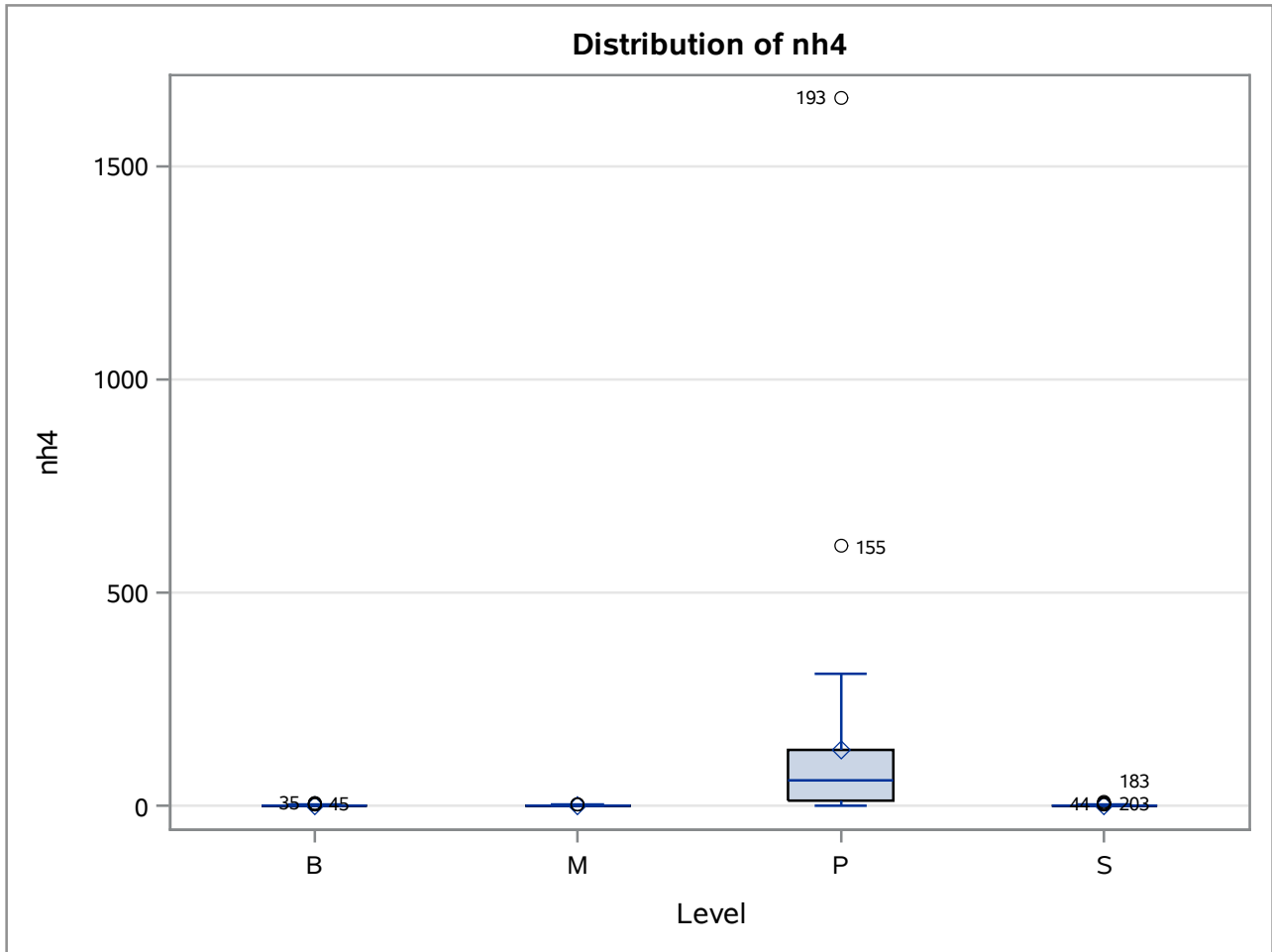
Alpha	0.05
Error Degrees of Freedom	216
Error Mean Square	12394.01
Critical Value of Studentized Range	3.33752
Minimum Significant Difference	43.942
Harmonic Mean of Cell Sizes	71.5

Note: Cell sizes are not equal.

Means with the same letter are not significantly different.			
Tukey Grouping	Mean	N	Event
A	50.04	52	NOV2014
A			
A	23.59	88	JUL2014
A			
A	12.85	88	JAN2014

Average Ratio Sulfate to Chloride Concentrations by Season

The GLM Procedure



Average Ratio Sulfate to Chloride Concentrations by Season

The GLM Procedure

Tukey's Studentized Range (HSD) Test for nh4

Note: This test controls the Type I experimentwise error rate, but it generally has a higher Type II error rate than REGWQ.

Alpha	0.05
Error Degrees of Freedom	216
Error Mean Square	12394.01
Critical Value of Studentized Range	3.66160
Minimum Significant Difference	55.226
Harmonic Mean of Cell Sizes	54.4838

Note: Cell sizes are not equal.

Means with the same letter are not significantly different.			
Tukey Grouping	Mean	N	Level
A	132.03	42	P
B	1.57	69	B
B			
B	1.40	68	S
B			
B	1.23	49	M

Average Ratio Sulfate to Chloride Concentrations by Season

The GLM Procedure

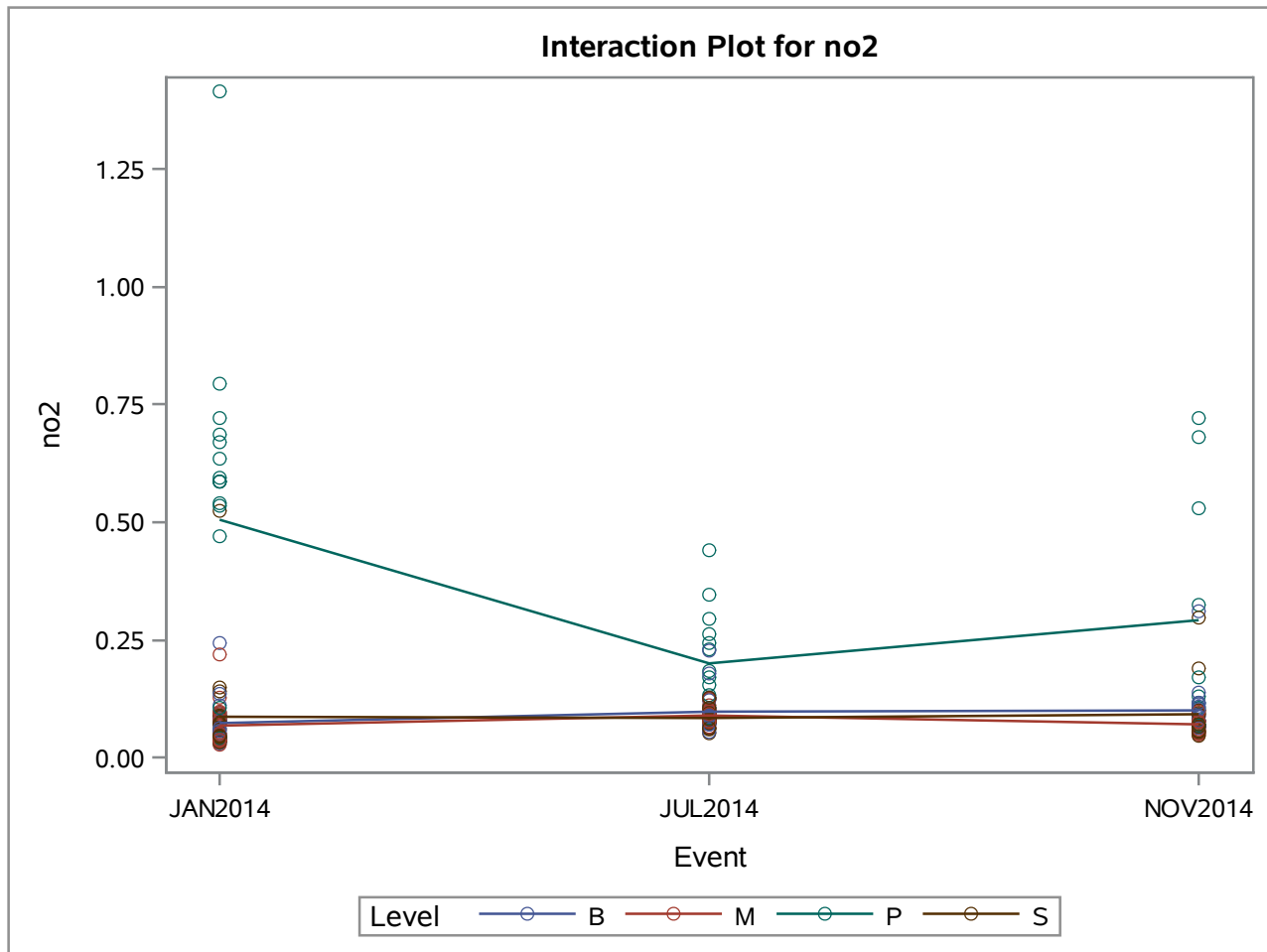
Dependent Variable: no2

Source	DF	Sum of Squares	Mean Square	F Value	Pr > F
Model	11	3.25285116	0.29571374	19.38	<.0001
Error	216	3.29566334	0.01525770		
Corrected Total	227	6.54851450			

R-Square	Coeff Var	Root MSE	no2 Mean
0.496731	91.60795	0.123522	0.134838

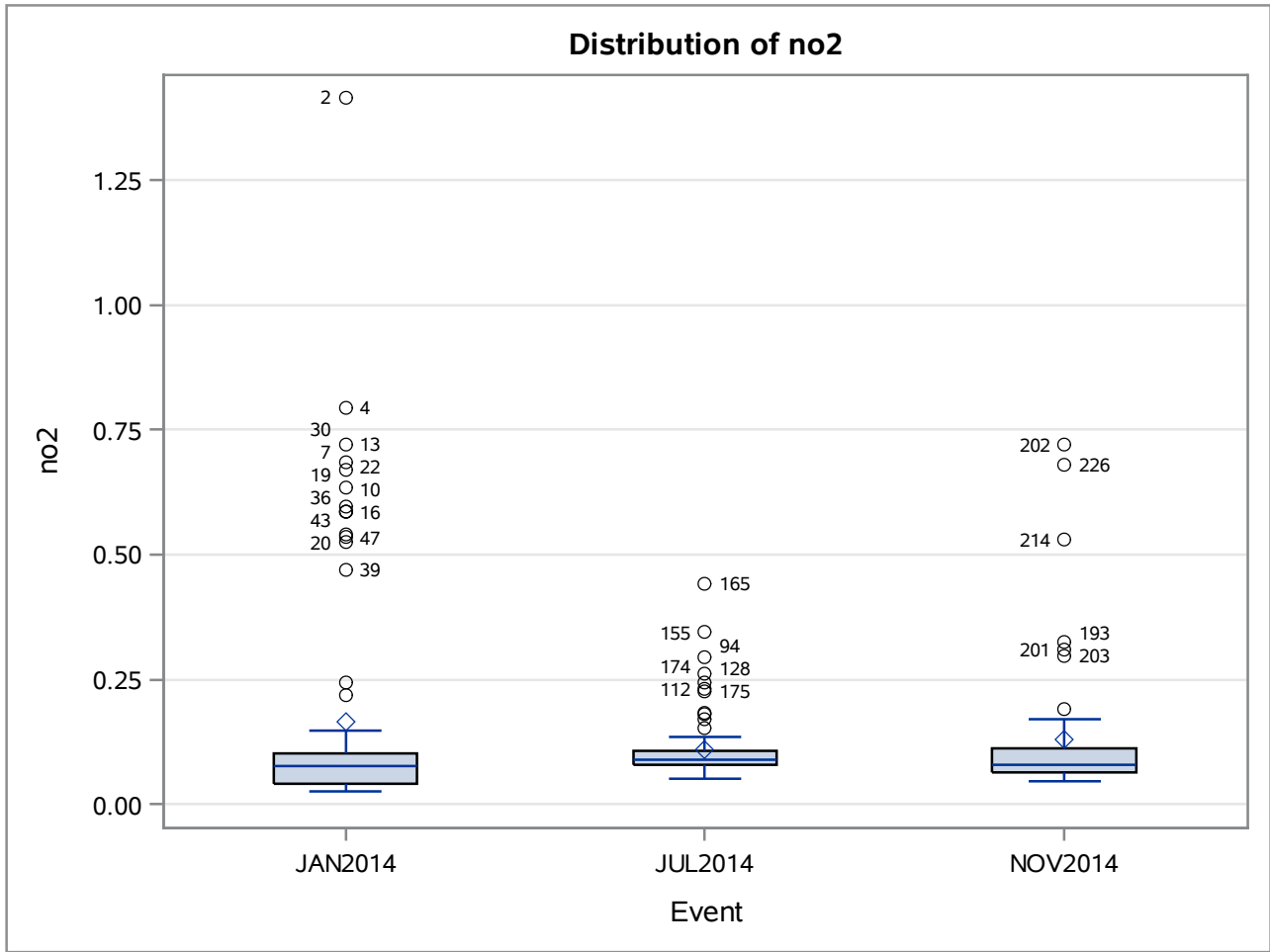
Source	DF	Type I SS	Mean Square	F Value	Pr > F
Event	2	0.13631504	0.06815752	4.47	0.0126
Level	3	2.38950269	0.79650090	52.20	<.0001
Event*Level	6	0.72703343	0.12117224	7.94	<.0001

Source	DF	Type III SS	Mean Square	F Value	Pr > F
Event	2	0.18714654	0.09357327	6.13	0.0026
Level	3	1.99615249	0.66538416	43.61	<.0001
Event*Level	6	0.72703343	0.12117224	7.94	<.0001



Average Ratio Sulfate to Chloride Concentrations by Season

The GLM Procedure



Average Ratio Sulfate to Chloride Concentrations by Season

The GLM Procedure

Tukey's Studentized Range (HSD) Test for no2

Note: This test controls the Type I experimentwise error rate, but it generally has a higher Type II error rate than REGWQ.

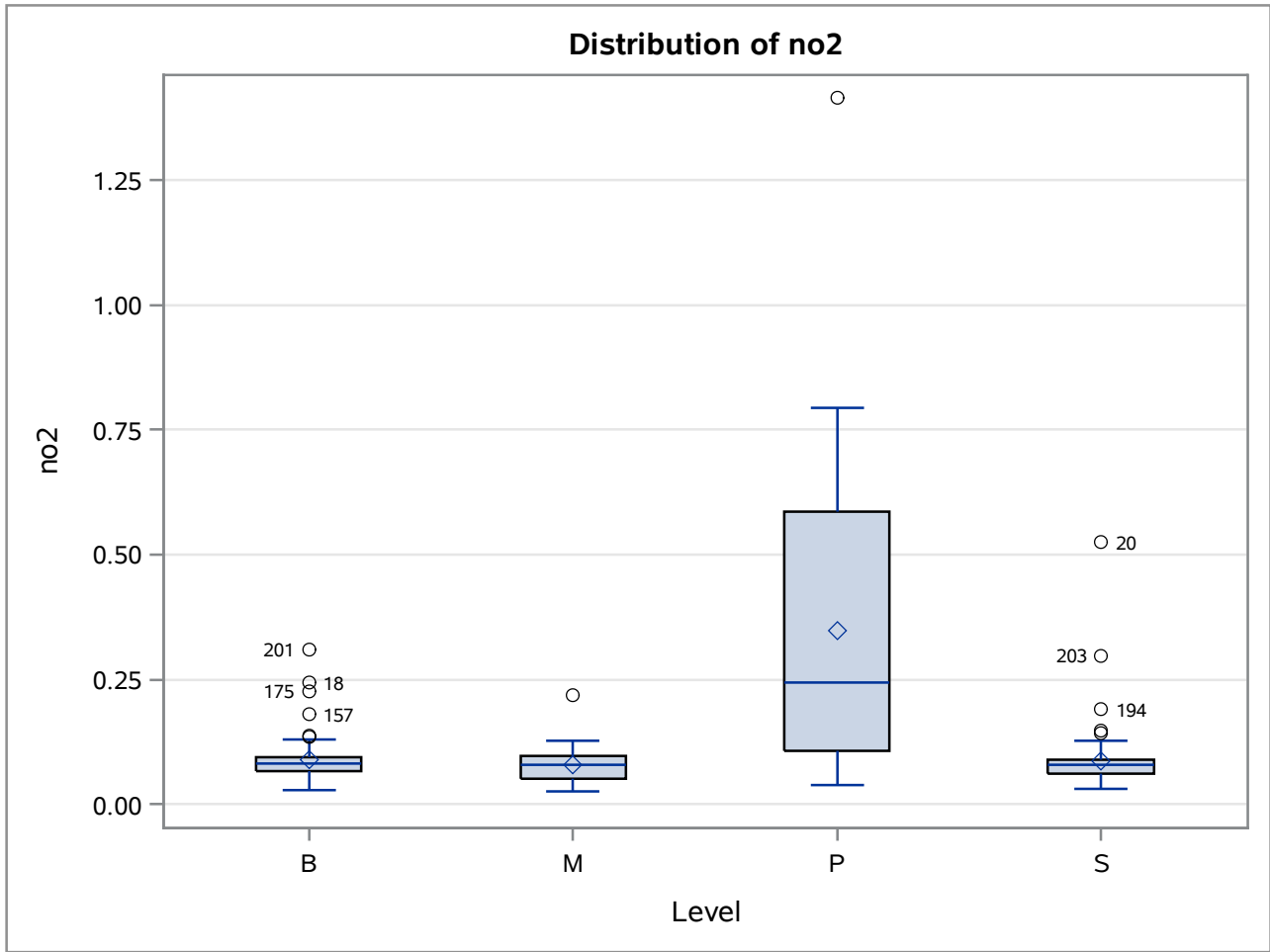
Alpha	0.05
Error Degrees of Freedom	216
Error Mean Square	0.015258
Critical Value of Studentized Range	3.33752
Minimum Significant Difference	0.0488
Harmonic Mean of Cell Sizes	71.5

Note: Cell sizes are not equal.

Means with the same letter are not significantly different.				
Tukey Grouping		Mean	N	Event
	A	0.16406	88	JAN2014
	A			
B	A	0.12946	52	NOV2014
B				
B		0.10880	88	JUL2014

Average Ratio Sulfate to Chloride Concentrations by Season

The GLM Procedure



Average Ratio Sulfate to Chloride Concentrations by Season

The GLM Procedure

Tukey's Studentized Range (HSD) Test for no2

Note: This test controls the Type I experimentwise error rate, but it generally has a higher Type II error rate than REGWQ.

Alpha	0.05
Error Degrees of Freedom	216
Error Mean Square	0.015258
Critical Value of Studentized Range	3.66160
Minimum Significant Difference	0.0611
Harmonic Mean of Cell Sizes	54.73296

Note: Cell sizes are not equal.

Means with the same letter are not significantly different.			
Tukey Grouping	Mean	N	Level
A	0.34874	43	P
B	0.08909	69	B
B			
B	0.08641	67	S
B			
B	0.07777	49	M

Average Ratio Sulfate to Chloride Concentrations by Season

The GLM Procedure

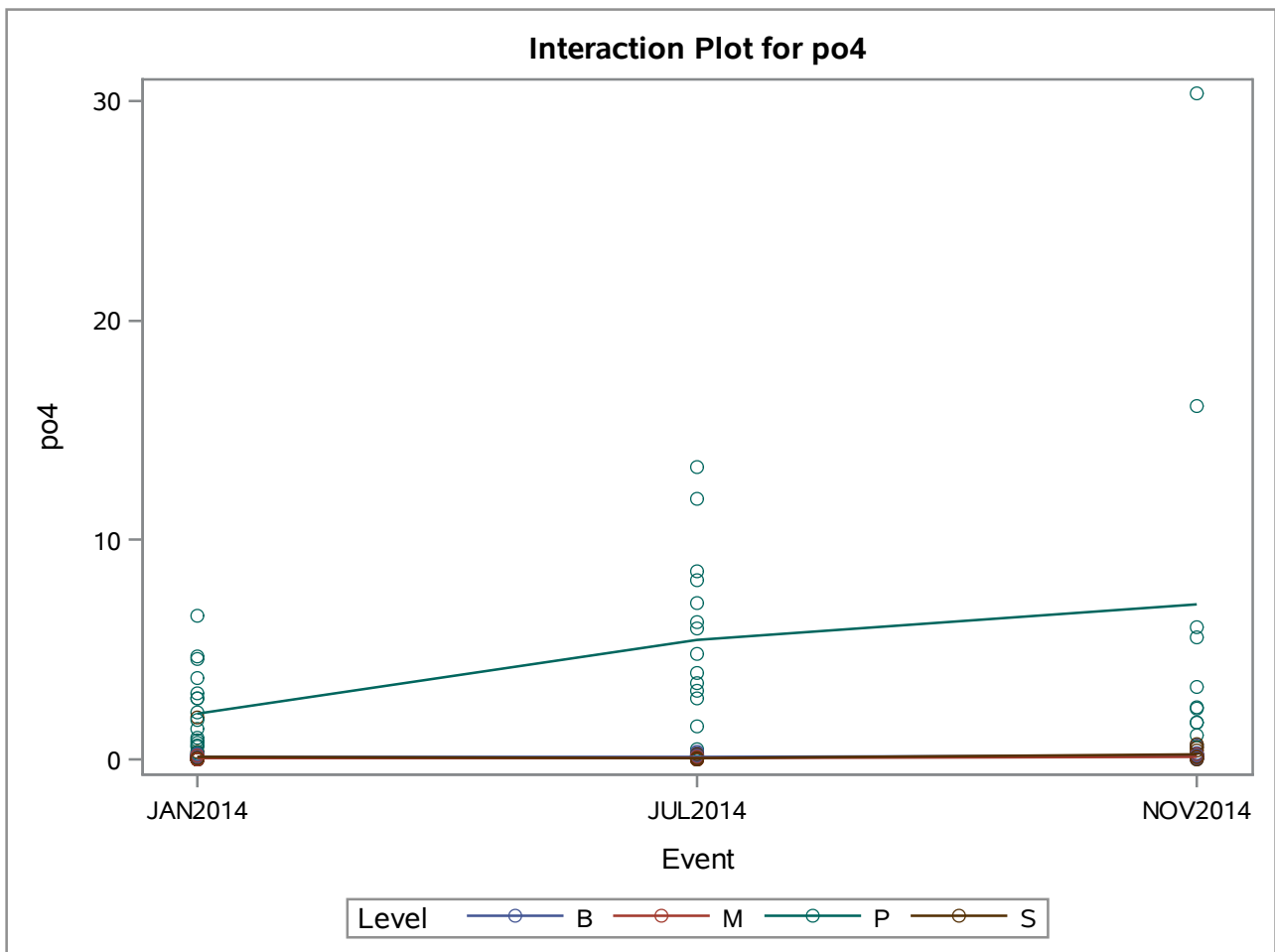
Dependent Variable: po4

Source	DF	Sum of Squares	Mean Square	F Value	Pr > F
Model	11	818.950447	74.450041	14.91	<.0001
Error	211	1053.244654	4.991681		
Corrected Total	222	1872.195102			

R-Square	Coeff Var	Root MSE	po4 Mean
0.437428	232.7424	2.234207	0.959948

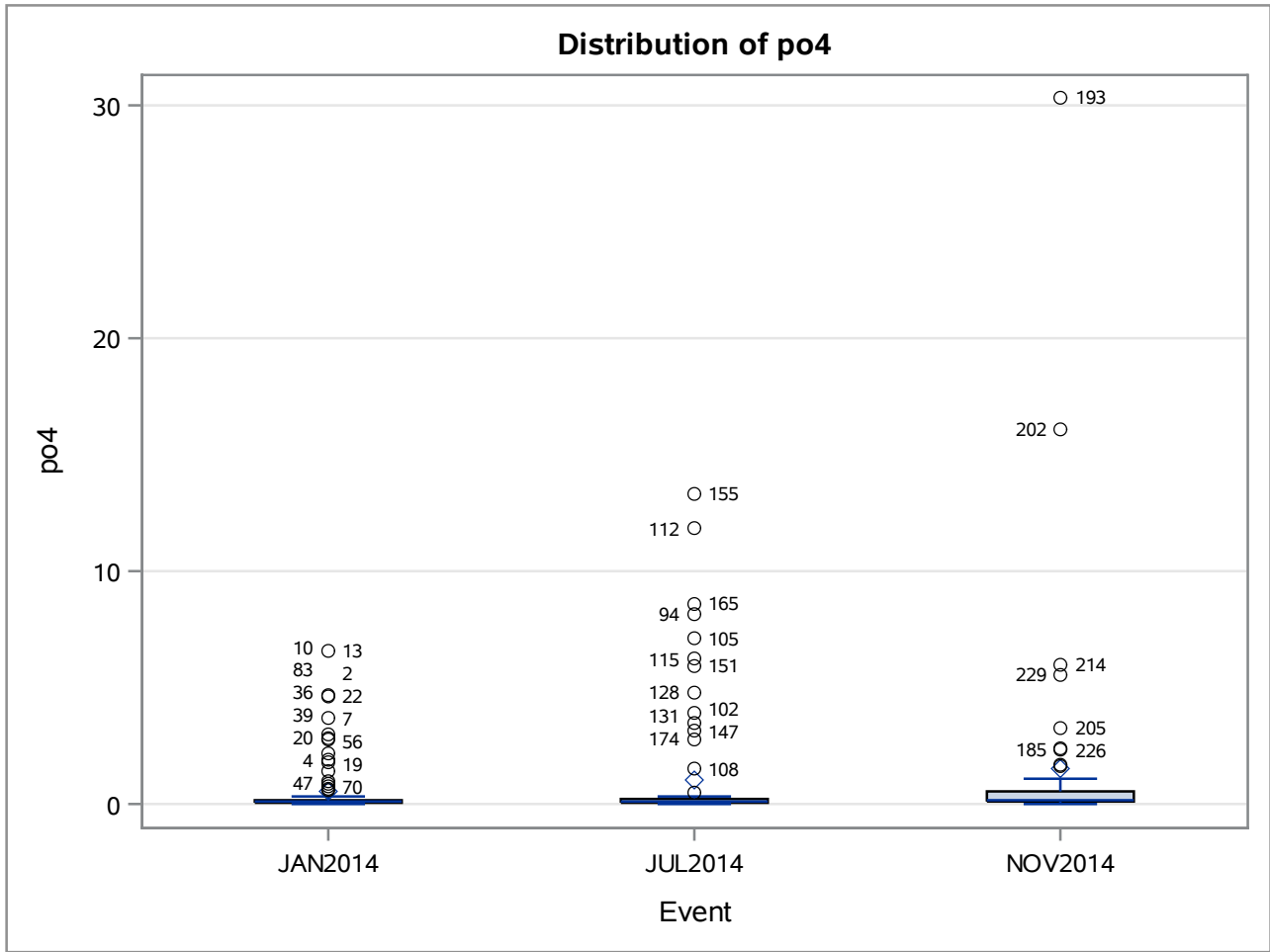
Source	DF	Type I SS	Mean Square	F Value	Pr > F
Event	2	32.6161299	16.3080649	3.27	0.0401
Level	3	644.1094848	214.7031616	43.01	<.0001
Event*Level	6	142.2248325	23.7041388	4.75	0.0001

Source	DF	Type III SS	Mean Square	F Value	Pr > F
Event	2	57.9694455	28.9847227	5.81	0.0035
Level	3	730.4199082	243.4733027	48.78	<.0001
Event*Level	6	142.2248325	23.7041388	4.75	0.0001



Average Ratio Sulfate to Chloride Concentrations by Season

The GLM Procedure



Average Ratio Sulfate to Chloride Concentrations by Season

The GLM Procedure

Tukey's Studentized Range (HSD) Test for po4

Note: This test controls the Type I experimentwise error rate, but it generally has a higher Type II error rate than REGWQ.

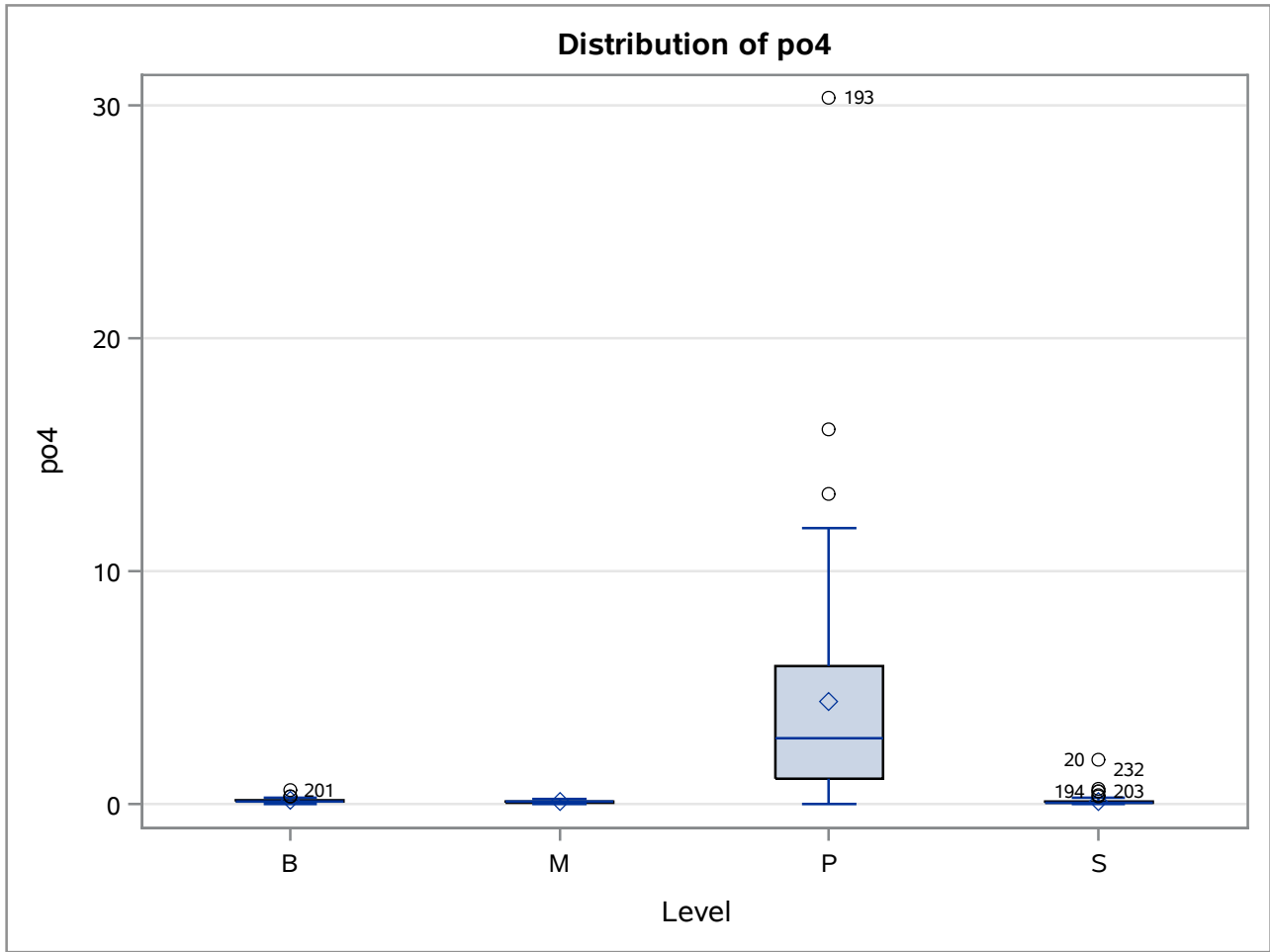
Alpha	0.05
Error Degrees of Freedom	211
Error Mean Square	4.991681
Critical Value of Studentized Range	3.33807
Minimum Significant Difference	0.889
Harmonic Mean of Cell Sizes	70.37333

Note: Cell sizes are not equal.

Means with the same letter are not significantly different.				
Tukey Grouping		Mean	N	Event
	A	1.5083	52	NOV2014
	A			
B	A	1.0653	84	JUL2014
B				
B		0.5305	87	JAN2014

Average Ratio Sulfate to Chloride Concentrations by Season

The GLM Procedure



Average Ratio Sulfate to Chloride Concentrations by Season

The GLM Procedure

Tukey's Studentized Range (HSD) Test for po4

Note: This test controls the Type I experimentwise error rate, but it generally has a higher Type II error rate than REGWQ.

Alpha	0.05
Error Degrees of Freedom	211
Error Mean Square	4.991681
Critical Value of Studentized Range	3.66228
Minimum Significant Difference	1.1175
Harmonic Mean of Cell Sizes	53.61262

Note: Cell sizes are not equal.

Means with the same letter are not significantly different.			
Tukey Grouping	Mean	N	Level
A	4.4199	43	P
B	0.1472	67	B
B			
B	0.1426	66	S
B			
B	0.1008	47	M

Average Ratio Sulfate to Chloride Concentrations by Season

The GLM Procedure

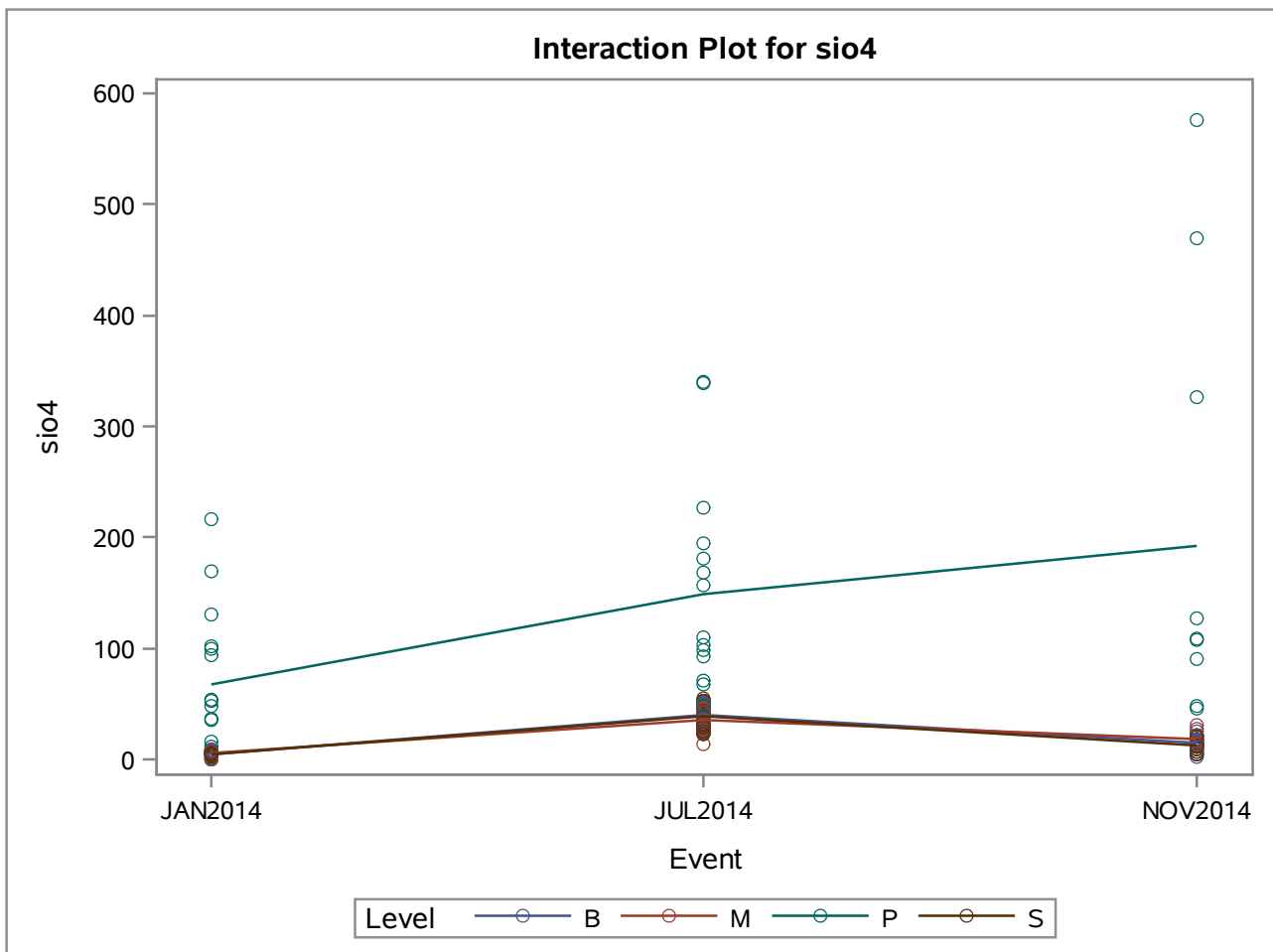
Dependent Variable: sio4

Source	DF	Sum of Squares	Mean Square	F Value	Pr > F
Model	11	474768.080	43160.735	13.96	<.0001
Error	174	537841.564	3091.043		
Corrected Total	185	1012609.644			

R-Square	Coeff Var	Root MSE	sio4 Mean
0.468856	116.5376	55.59715	47.70747

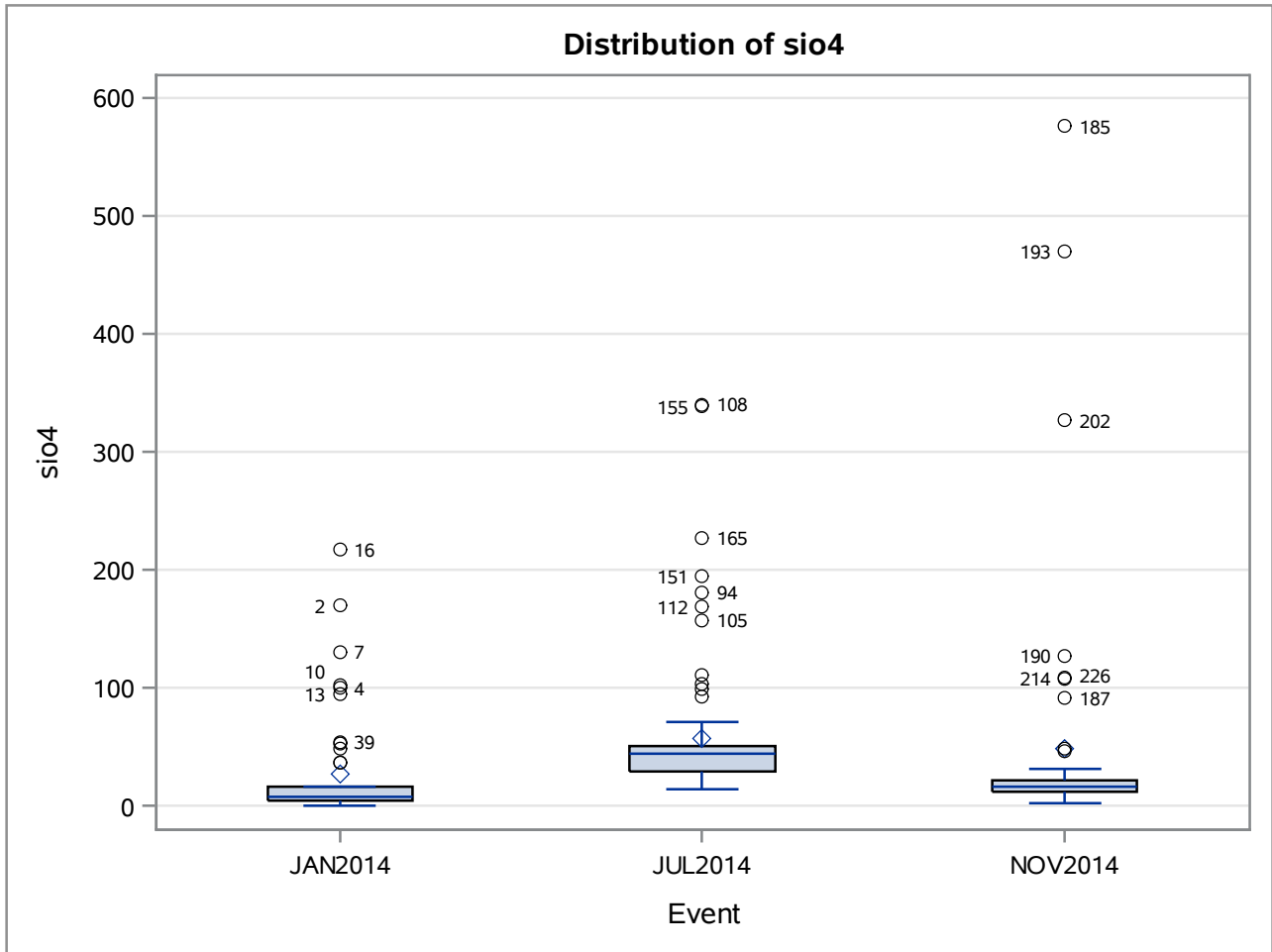
Source	DF	Type I SS	Mean Square	F Value	Pr > F
Event	2	26761.8270	13380.9135	4.33	0.0146
Level	3	387859.6260	129286.5420	41.83	<.0001
Event*Level	6	60146.6274	10024.4379	3.24	0.0048

Source	DF	Type III SS	Mean Square	F Value	Pr > F
Event	2	60251.3074	30125.6537	9.75	<.0001
Level	3	408454.4122	136151.4707	44.05	<.0001
Event*Level	6	60146.6274	10024.4379	3.24	0.0048



Average Ratio Sulfate to Chloride Concentrations by Season

The GLM Procedure



Average Ratio Sulfate to Chloride Concentrations by Season

The GLM Procedure

Tukey's Studentized Range (HSD) Test for sio4

Note: This test controls the Type I experimentwise error rate, but it generally has a higher Type II error rate than REGWQ.

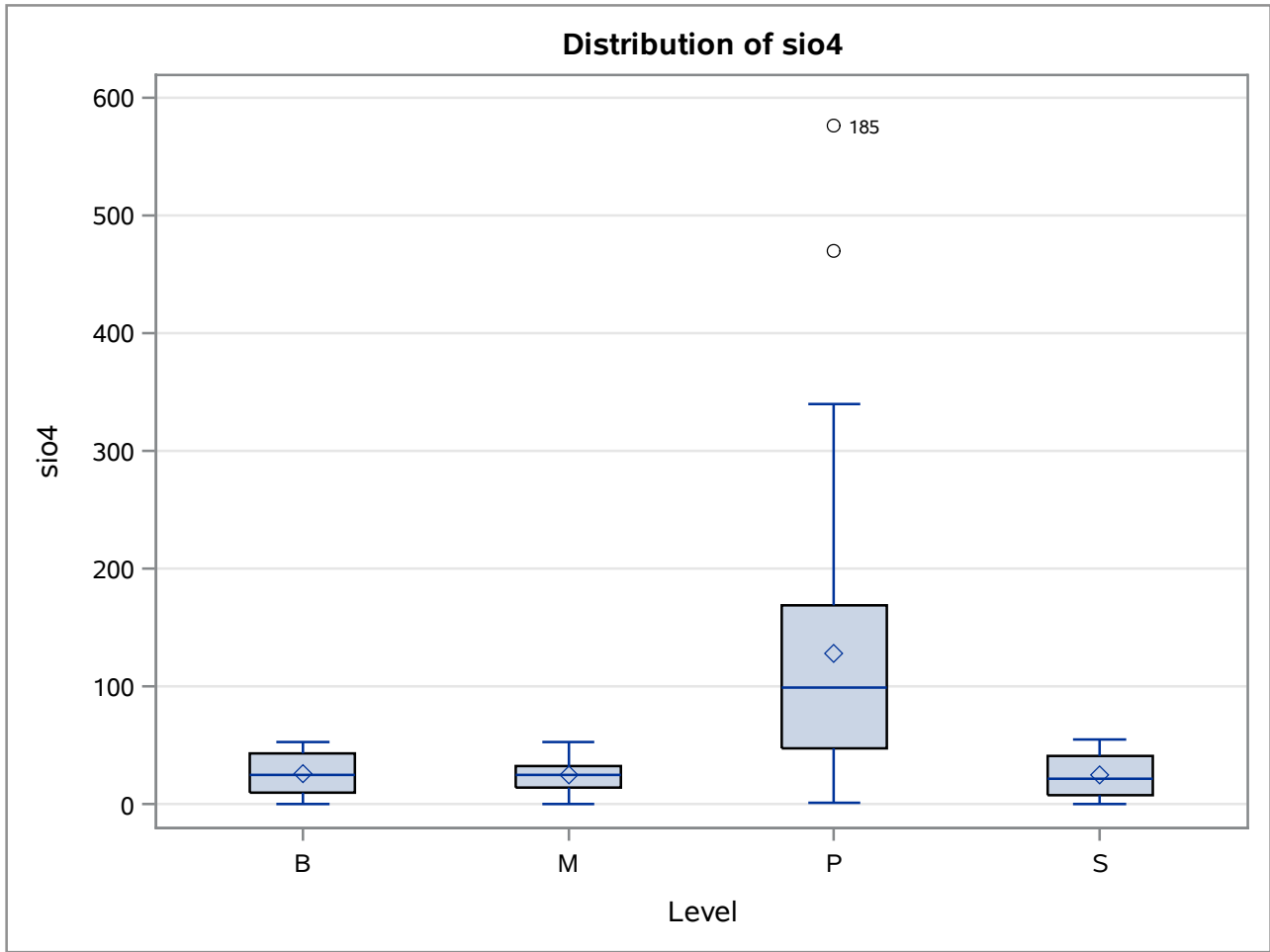
Alpha	0.05
Error Degrees of Freedom	174
Error Mean Square	3091.043
Critical Value of Studentized Range	3.34312
Minimum Significant Difference	24.632
Harmonic Mean of Cell Sizes	56.93794

Note: Cell sizes are not equal.

Means with the same letter are not significantly different.				
Tukey Grouping		Mean	N	Event
	A	57.25	89	JUL2014
	A			
B	A	48.97	52	NOV2014
B				
B		27.39	45	JAN2014

Average Ratio Sulfate to Chloride Concentrations by Season

The GLM Procedure



Average Ratio Sulfate to Chloride Concentrations by Season

The GLM Procedure

Tukey's Studentized Range (HSD) Test for sio4

Note: This test controls the Type I experimentwise error rate, but it generally has a higher Type II error rate than REGWQ.

Alpha	0.05
Error Degrees of Freedom	174
Error Mean Square	3091.043
Critical Value of Studentized Range	3.66851
Minimum Significant Difference	30.268
Harmonic Mean of Cell Sizes	45.40683

Note: Cell sizes are not equal.

Means with the same letter are not significantly different.			
Tukey Grouping	Mean	N	Level
A	127.96	41	P
B	25.81	53	B
B			
B	24.72	38	M
B			
B	24.44	54	S

Average Ratio Sulfate to Chloride Concentrations by Season

The GLM Procedure

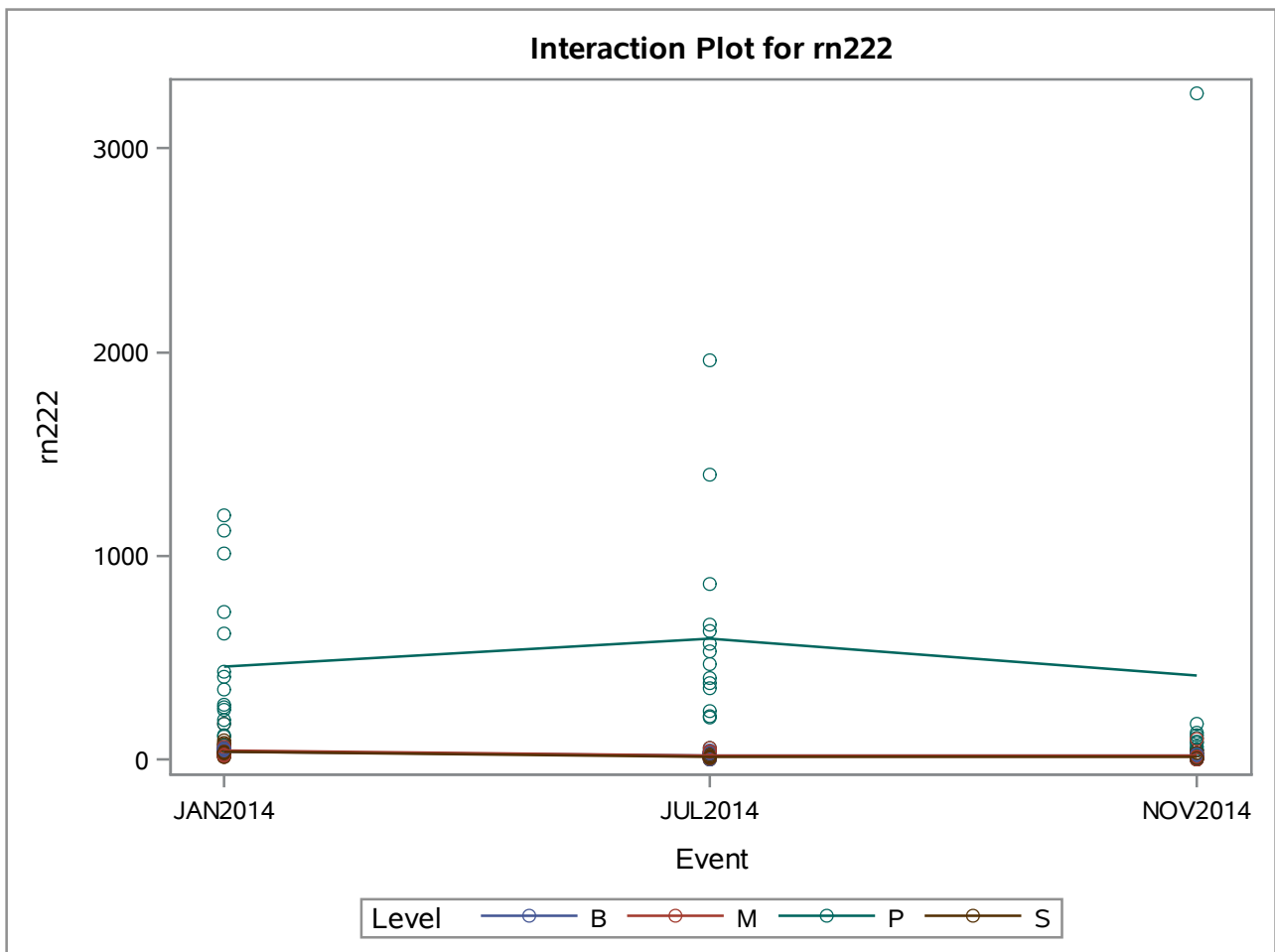
Dependent Variable: rn222

Source	DF	Sum of Squares	Mean Square	F Value	Pr > F
Model	11	7646547.23	695140.66	9.93	<.0001
Error	210	14705102.33	70024.30		
Corrected Total	221	22351649.56			

R-Square	Coeff Var	Root MSE	rn222 Mean
0.342102	233.7745	264.6210	113.1950

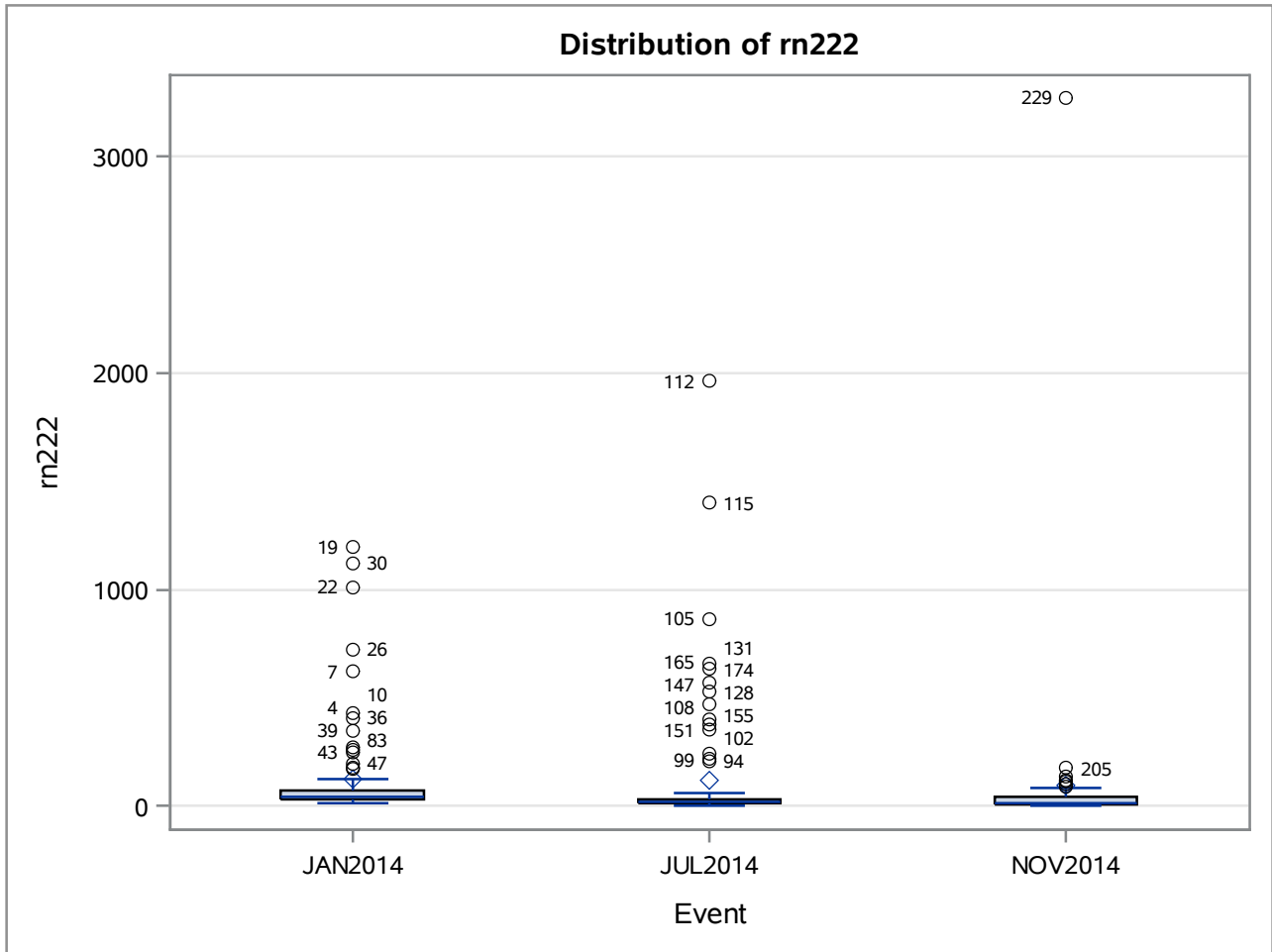
Source	DF	Type I SS	Mean Square	F Value	Pr > F
Event	2	29804.623	14902.312	0.21	0.8085
Level	3	7392607.861	2464202.620	35.19	<.0001
Event*Level	6	224134.746	37355.791	0.53	0.7825

Source	DF	Type III SS	Mean Square	F Value	Pr > F
Event	2	72369.451	36184.726	0.52	0.5972
Level	3	6813614.997	2271204.999	32.43	<.0001
Event*Level	6	224134.746	37355.791	0.53	0.7825



Average Ratio Sulfate to Chloride Concentrations by Season

The GLM Procedure



Average Ratio Sulfate to Chloride Concentrations by Season

The GLM Procedure

Tukey's Studentized Range (HSD) Test for rn222

Note: This test controls the Type I experimentwise error rate, but it generally has a higher Type II error rate than REGWQ.

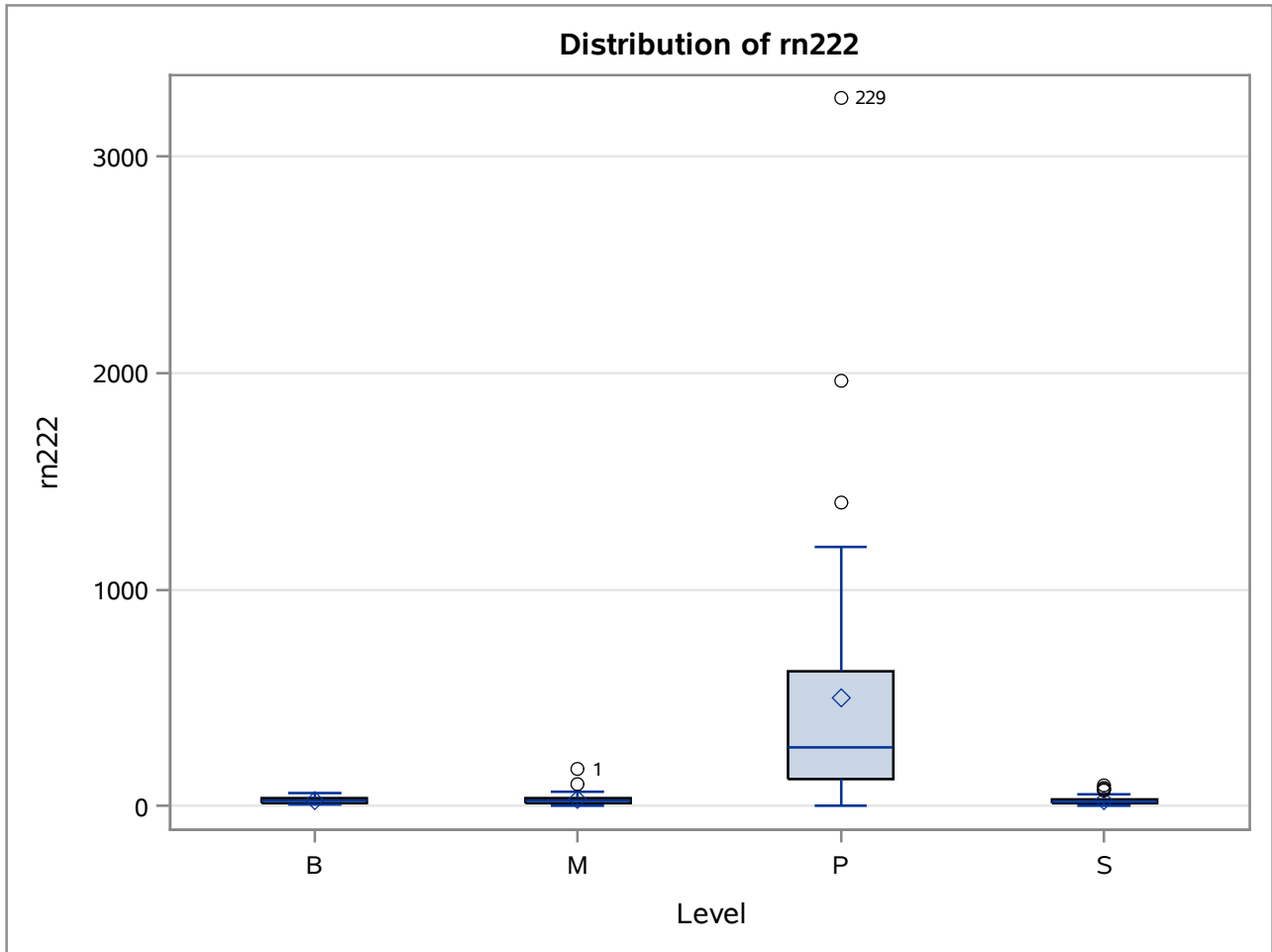
Alpha	0.05
Error Degrees of Freedom	210
Error Mean Square	70024.3
Critical Value of Studentized Range	3.33818
Minimum Significant Difference	105.53
Harmonic Mean of Cell Sizes	70.07315

Note: Cell sizes are not equal.

Means with the same letter are not significantly different.			
Tukey Grouping	Mean	N	Event
A	122.46	81	JAN2014
A			
A	116.71	89	JUL2014
A			
A	92.74	52	NOV2014

Average Ratio Sulfate to Chloride Concentrations by Season

The GLM Procedure



Average Ratio Sulfate to Chloride Concentrations by Season

The GLM Procedure

Tukey's Studentized Range (HSD) Test for rn222

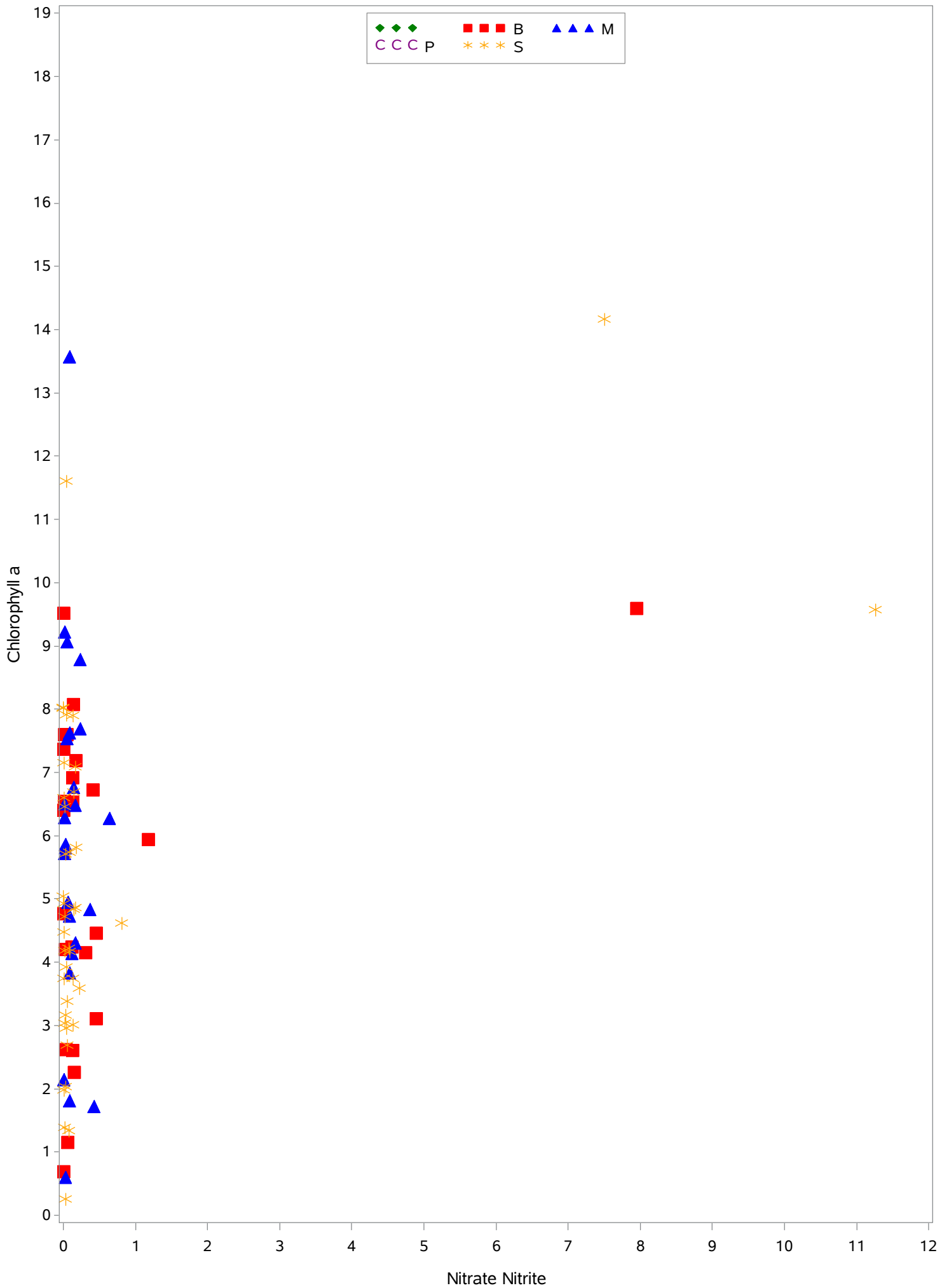
Note: This test controls the Type I experimentwise error rate, but it generally has a higher Type II error rate than REGWQ.

Alpha	0.05
Error Degrees of Freedom	210
Error Mean Square	70024.3
Critical Value of Studentized Range	3.66242
Minimum Significant Difference	133.38
Harmonic Mean of Cell Sizes	52.79787

Note: Cell sizes are not equal.

Means with the same letter are not significantly different.			
Tukey Grouping	Mean	N	Level
A	496.29	41	P
B	28.39	46	M
B			
B	27.10	67	B
B			
B	24.41	68	S

Average Ratio Sulfate to Chloride Concentrations by Season



Average Ratio Sulfate to Chloride Concentrations by Season

